

Size Effects in the Fatigue Behaviour of Tubular Bridge Joints

THÈSE N° 4142 (2008)

PRÉSENTÉE LE 14 AOÛT 2008

À LA FACULTE ENVIRONNEMENT NATUREL, ARCHITECTURAL ET CONSTRUIT
LABORATOIRE DE LA CONSTRUCTION MÉTALLIQUE
PROGRAMME DOCTORAL EN STRUCTURES

ÉCOLE POLYTECHNIQUE FÉDÉRALE DE LAUSANNE

POUR L'OBTENTION DU GRADE DE DOCTEUR ÈS SCIENCES

PAR

Luís António COSTA BORGES

M.Sc. in Civil Engineering, University of Coimbra, Portugal
et de nationalité portugaise

acceptée sur proposition du jury:

Prof. T. Keller, président du jury
Dr A. Nussbaumer, directeur de thèse
Prof. R. Connor, rapporteur
Dr A. Schumacher, rapporteur
Prof. I.F.C. Smith, rapporteur



ÉCOLE POLYTECHNIQUE
FÉDÉRALE DE LAUSANNE

Suisse
2008

Abstract

A critical aspect in the design of tubular bridges is the fatigue performance of the structural joints. Economic viability depends on it. Lower fatigue strength for joints with thicker failing members was observed in welded joints typical to the bridge application. Different approaches to this phenomenon, called size effect, have been suggested, all based on the thickness correction for welded plate joints first proposed by Gurney. For the welded tubular joints, few studies on the size effects have been carried out; most of the existing investigations refer to geometries typical to petroleum industry offshore structures. In contrast to offshore structures, bridge structures have different absolute sizes and different member proportions (in particular lower chord radius to thickness ratios, γ). Tubular joints are far more complex than welded plate joints, multiple parameters are needed to describe the geometry ($\alpha, \beta, \gamma, \tau, \zeta$) and there are several load scenarios. For these reasons, the fatigue behaviour analysis of such joints is a complex task. Current design recommendations combine the use of the structural (hot-spot) stress at the weld toe with a correction factor to take into account the wall thickness of the failing member. This approach oversimplifies the problem and can be very penalising, in particular for joints composed of thicker tubes, as is commonly the case for bridges. Furthermore, the truss member sizes that result from static design are likely to fall out of the validity range of current recommendations. This thesis focuses on a case of commonly used tubular joints: welded steel K-joint made out of circular hollow section (CHS).

The main goals of this research are to understand the fatigue behaviour of as-welded CHS K-joints and to clarify the influences/effects of the different geometric parameters on their fatigue strength. In order to carry out a thorough study on the geometric size effects in CHS K-joints for bridges, fatigue tests were conducted for large-scale specimens with crack depth measurements and an advanced 3-D crack propagation model was developed.

The first chapters of this thesis provide an introduction and a brief review of the main concepts in tubular joint fatigue and size effects on fatigue behaviour. The experimental tests of two tubular trusses under fatigue loading are then outlined. Crack growth in selected truss joints is monitored using the Alternating Current Potential Drop (ACPD) system.

An advanced 3-D modelling of welded K-joint with surface crack is implemented using the boundary element method (BEM). A crack propagation model, based on Linear Elastic Fracture Mechanics (LEFM), is then developed using a step-wise incremental crack growth strategy. This model allows for fatigue strength and life estimations. Furthermore, it considers the influence of all geometric parameters that define CHS K-joints in a realistic way. The validation of the crack propagation model is made by comparisons with experimental data at different levels (i.e. member and joint strains and stresses, ACPD crack growth data).

A parametric study is then carried out on joint geometries typical for a bridge application (low chord radius to thickness ratio) considering three basic load cases. Examples of results are shown and analysed on a "geometry cause"/"effect over the stress intensity factor and fatigue strength" basis. Parametric study results are then analysed, highlighting the case where the joint is proportionally scaled. The geometry correction factor, Y , is introduced as a function of the relative crack depth that is common to homothetic joints. The influence of the absolute size of the joint, also known as thickness effect, is determined for the three basic load cases.

Parametric results are finally explored bringing to light the effect of non-proportional scaling. It is shown that size correction factors for fatigue strength can be expressed as a function of the non-dimensional geometrical parameters β , γ and τ , chord thickness, T , and different load cases. A new fatigue design method is proposed for welded (CHS) K-joints, based on LEFM and accounting for geometric size effects.

Keywords: tubular bridges, steel, fatigue, crack propagation, size effect, thickness effect, scale effect, welded joints, circular hollow section, CHS K-joints, LEFM, boundary element model, large-scale tests, crack depth measurement, ACPD system.

Résumé

Lors de la conception de ponts tubulaires, des ingénieurs ont montré que la performance en fatigue des joints constitue un aspect critique qui peut avoir une influence importante sur la viabilité économique de ces structures. Au niveau des nœuds soudés, on a pu observer une diminution de la résistance à la fatigue avec l'augmentation de l'épaisseur du tube fissuré. Afin de tenir compte de ce phénomène, appelé effet de taille, différentes méthodes de calcul ont été proposées; toutes sont basées sur la correction d'épaisseur, proposée en premier par Gurney pour les assemblages de plaques. Dans le cas des nœuds tubulaires soudés, il existe peu d'études sur l'effet de taille et la plupart de celles effectuées concernent des géométries typiques de l'industrie pétrolière offshore. La structure porteuse des ponts tubulaires présente des différences par rapport aux structures offshore tant au niveau de la taille des éléments qu'au niveau des proportions entre les éléments qui la constituent (en particulier pour le rapport rayon/épaisseur de la membrure). Les nœuds tubulaires sont plus complexes que les assemblages de plaques: de nombreux paramètres sont nécessaires pour définir la géométrie ($\alpha, \beta, \gamma, \tau, \zeta$) et les nœuds peuvent être chargés de différentes manières. Ces raisons rendent l'analyse du comportement à la fatigue de ces nœuds difficile. Les recommandations actuelles en fatigue combinent l'utilisation de la contrainte structurale (hot-spot) au pied de cordon avec un facteur de correction qui tient compte de l'épaisseur du tube qui fissure. Cette approche simplifie de façon trop importante le problème et peut se révéler très pénalisante, en particulier pour les nœuds composés de tubes à forte épaisseur, fréquemment utilisés pour les ponts. De plus, il est fort possible que les tailles nécessaires des tubes composant le treillis résultant des calculs statiques se situent hors des limites de validité des recommandations actuelles. Ce travail de thèse se concentre sur le cas particulier de nœud rencontré le plus couramment dans les structures de pont: les nœuds en K réalisés à partir de sections creuses circulaires (CHS).

Les principaux objectifs de l'étude présentée ici sont de comprendre le comportement à la fatigue des nœuds soudés en K composés de tubes à section circulaire, et de clarifier les influences/effets des différents paramètres géométriques sur leur résistance à la fatigue. Afin d'étudier cette problématique, des essais en grandeur réelle sur des poutres à treillis, équipées d'un système de mesure de la profondeur de fissure, ainsi que des modèles numériques avec propagation tridimensionnelle de la fissuration ont été effectués.

Les premiers chapitres de cette thèse contiennent une introduction et un bref résumé de l'état des connaissances concernant les concepts majeurs dans les domaines de la fatigue des nœuds tubulaires et des effets de taille. Les essais de fatigue sur deux poutres à treillis tubulaires sont ensuite décrits. Les vitesses de propagation des fissures enregistrées au niveau des nœuds déterminants des treillis proviennent de mesures effectuées grâce à un système de chute de potentiel à courant alternatif (ACPD).

Un modèle numérique tridimensionnel d'un nœud tubulaire soudé en K avec une fissure de surface a été développé dans un logiciel utilisant la méthode des éléments frontières (BEM). Un modèle de propagation de la fissuration, basé sur la mécanique de la rupture linéaire-élastique (LEFM), a été ensuite développé en utilisant une procédure de calcul de la fissuration par incréments. Ce modèle permet une estimation de la durée de vie ainsi que de la résistance à la fatigue. De plus, il inclut d'une manière réaliste, l'influence de tous les paramètres géométriques qui définissent un nœud tubulaire en K de tubes CHS. La validation du modèle de propagation a été réalisée par comparaison avec différents résultats expérimentaux (déformations et contraintes dans les tubes et les nœuds, mesures de vitesses de propagation par ACPD).

Une étude paramétrique est ensuite effectuée sur des géométries typiques des nœuds de ponts (faibles rapports du rayon de la membrure inférieure sur son épaisseur), en considérant trois cas de charges de base. Les résultats sont ensuite présentés et analysés sur la base du rapport "cause géométrique"/"effet sur le facteur d'intensité de contrainte et résistance en fatigue". Les résultats de l'étude paramétrique sont ensuite analysés spécifiquement pour les cas des nœuds homothétiques

(dimensions augmentées de manière proportionnelle). Le facteur de correction géométrique, Y , est introduit comme une fonction de la profondeur relative de la fissure, puisque les nœuds sont homothétiques. L'influence de la taille absolue du nœud, aussi souvent appelée effet d'épaisseur, est déterminée pour les trois cas de charges de base.

Les résultats de l'étude paramétrique sont ensuite exploités différemment afin de mettre en lumière les effets non-proportionnels de taille. Des facteurs de correction de la résistance en fatigue pour la taille, exprimés en fonction des paramètres géométriques non-dimensionnels β , γ and τ , et de l'épaisseur de la membrure, T , sont proposés pour les différents cas de charges. Finalement, une proposition pour une nouvelle méthode de calcul pour les nœuds soudés en K de CHS, basée sur la LEFM et prenant en compte les effets de la taille et de la géométrie des nœuds, est proposée.

Mots-clés: ponts tubulaires, acier, fatigue, propagation de fissure, effet de taille, effet d'épaisseur, effet d'échelle, assemblages soudés, sections circulaires creuses (CHS), nœuds tubulaires en K, mécanique de la rupture linéaire, modèle aux éléments frontières, essais en vraie grandeur, mesure de profondeur de fissure, système à chute de potentiel.

Sumário

Um aspecto crucial no dimensionamento de pontes em treliça tubular é o comportamento à fadiga das ligações estruturais. Este comportamento desempenha um papel decisivo em termos da viabilidade económica da solução escolhida. Uma diminuição da resistência à fadiga foi observada em ligações entre elementos tubulares de maior espessura. Diferentes abordagens têm sido propostas para explicar este fenómeno, baseadas no factor de correcção proposto por Gurney para ligações de placas soldadas. Para as ligações tubulares soldadas poucos estudos foram realizados. A maior parte do trabalho de investigação efectuado neste domínio refere-se a geometrias típicas de estruturas da indústria petrolífera *offshore*. Comparadas com estas estruturas, as pontes exibem diferentes dimensões e esbeltezas dos elementos que constituem as cordas das treliças. A geometria das ligações tubulares é bastante mais complexa do que a correspondente a ligação de duas placas soldadas. Como consequência, são necessários vários parâmetros para descrever a geometria, adicionalmente existem vários cenários de carga possíveis. Por estes motivos, a análise do comportamento à fadiga destas ligações é complexa. As recomendações actuais combinam o uso do conceito de variação da tensão no *hot-spot* com um factor de correcção que tem em conta a espessura do elemento fissurado. Esta abordagem simplifica demasiado o problema e pode ser muito penalizadora, especialmente para as ligações compostas de tubos mais espessos como é normalmente o caso das pontes. Além disso, o resultado de um pré-dimensionamento das secções conduz frequentemente a geometrias que não são abrangidas pelo domínio de validade dos guias de dimensionamento actuais à fadiga. Esta tese concentra-se num caso particular de ligação tubular: ligação em K de perfis em secção circular oca (CHS).

Os principais objectivos desta investigação são: compreender o comportamento à fadiga das ligações tubulares soldadas e investigar as influências/efeitos dos diversos parâmetros geométricos na resistência à fadiga. Tendo em vista a realização de um estudo exaustivo sobre os efeitos de escala na fadiga, foram realizados ensaios a grande escala com monitorização das fissuras. Foi ainda desenvolvido um modelo avançado para simular a propagação das fissuras.

Os primeiros capítulos desta tese fornecem uma introdução e uma breve revisão dos principais conceitos relacionados com a fadiga de ligações tubulares e os efeitos de escala no comportamento à fadiga. Os ensaios experimentais de duas treliças tubulares sujeitas a uma carga de fadiga são de seguida descritos. A propagação de fissuras nos nós seleccionados é monitorizada usando um sistema de medida da variação de potencial num campo de corrente alterna (ACPD). Um modelo 3D, representando um nó K soldado, com uma fissura de superfície, foi implementado usando o método dos elementos fronteira (BEM). Foi desenvolvido um modelo de propagação de fissura, baseado na Teoria da Mecânica da Fractura Linear Elástica (MFLE), através da aplicação de uma estratégia incremental da propagação da fissura. Este modelo permite estimar a resistência à fadiga da ligação tendo em consideração a influência de todos os parâmetros geométricos que definem uma ligação deste tipo. A validação do modelo de propagação de fissura é feita por comparação com diversos resultados obtidos experimentalmente (tensões e extensões nos membros e ligação, dados de propagação de fissura obtidos com o sistema ACPD).

Este trabalho de investigação incluiu um estudo paramétrico para geometrias típicas de pontes (baixo valor da esbelteza das cordas, $\gamma < 12$) considerando três casos de carga básicos. Os resultados foram inicialmente analisados em termos de "causa geométrica"/"efeito nos factores de intensidade de tensão e resistência à fadiga". Estes resultados foram posteriormente analisados isolando os casos em que os nós são dimensionados de forma proporcional. O factor de correcção geométrico, Y , é introduzido como uma função da profundidade relativa da fissura e comum a uma família de nós homotéticos. A influência da dimensão absoluta do nó, também conhecida como efeito da espessura (*thickness effect*) foi determinada para três casos de carga básicos. Em seguida, os resultados do estudo paramétrico foram analisados tendo em vista clarificar o efeito de escala para transformações não

proporcionais. Estes efeitos são expressados em função dos parâmetros geométricos adimensionais β , γ , τ e da espessura da corda T para os três casos de carga considerados.

Finalmente, um novo método é proposto para o dimensionamento de nós tubulares em K, baseado na teoria da Mecânica da Fractura Linear Elástica levando em consideração os efeitos de escala geométricos.

Palavras-chave: pontes tubulares, aço, fadiga, propagação de fissura, efeito de escala, efeito de espessura, ligação soldada, secção circular oca, ligação K, Mecânica da Fractura Linear Elástica, modelo de elementos fronteira, ensaio de fadiga, medições de profundidade de fissura, ACPD

Acknowledgements

The research work presented herein was carried out at the Steel Structures Laboratory (ICOM) of the Swiss Federal Institute of Technology in Lausanne (EPFL). I would like to express my gratitude to Prof. Dr. Manfred A. Hirt for granting me the opportunity to work in an outstanding research environment and for his support, advice and encouragement. I am deeply grateful to Dr. Alain Nussbaumer, my thesis director, for his excellent guidance, patience and continuous support. The rich discussions we had provided me with very valuable help and were a source of many ideas.

I would like to acknowledge the support of the Swiss National Science Foundation that funded this thesis (grant no 200021-112014), Vallourec & Mannesmann Tubes, Germany who donated the tubes and Zwahlen & Mayr SA, Switzerland, which fabricated the test specimens.

I wish to express my gratitude to the members of the advisory committee for their periodic advice, guidance and valuable ideas. This committee consisted of Prof. Manfred A. Hirt, Dr. Stefan Herion, Dr. Ann Schumacher and Dr. Laurence Davaine. I would also like to thank the examining committee for the time spent to review my work. This committee included: Prof. Thomas Keller (chairman), Prof. Robert Connor, Dr. Ann Schumacher and Prof. Ian F. C. Smith. The valuable comments received have improved considerably the quality of this document.

The experimental work carried out was made possible thanks to the team led by Sylvain Demierre namely Hansjakob Reist, Roland Gysler, Patrice Gally, Gilles Guignet, Gilbert Pidoux, François Perrin. Their competence, assistance and humour made the time spent in the laboratory quite pleasant. I want to acknowledge the help I received from Odile, Olivier and Vincent who were doing projects or stages at ICOM on different tasks of the experimental tests. I am thankful to Esther von Arx and Claudio Leonardi for their valuable help with respectively administrative and multimedia issues.

I would like to thank my office mates: Matthias for his patience showing me so many computer related things; and Danijel for his permanent good mood, friendship and unconditional help. I would also like to thank Scott and Amy for helping me adapt during my first months in Lausanne and all the members of ICOM for their friendship and support: Jean-Paul Lebet and Michel Crisinel, Andreas, Michel, Senta, Scott, Thierry, Thomas, Yves, Rahel, Claire, Tamar and Dimitrios.

I will always be grateful to my many friends in Switzerland that made my stay very pleasant and for the good moments spent together: the Luso/Brazilian community (Marcelo, Montse, Pedro, Janina, Paulo, João C., Mário, Mónica, Bruno, Rui, Cátia, Kristijan, Pietro, Simona...) and also Aga, Amy, Bernard, Bernhard, Erika, João L., Juan, Matthias, Marta, Neven, Samo and many others.

I want to acknowledge the encouragement and help provided by Prof. Luís Simões da Silva from the University of Coimbra when four years ago I decided to apply to the EPFL doctoral school.

During the time spent in Lausanne my family and friends (Filipe, António, Carla...) in Portugal bridged the distance with their visits, contacts and "remote" support. I am immensely grateful to my parents and brother for their everyday love, encouragement and unconditional support.



Contents

Abstract	i
Resumé	ii
Sumário	iv
Acknowledgements	vii
Contents	ix
List of Figures	xv
List of Tables	xxi
Nomenclature	xxiv
Abbreviations	xxiv
Terminology	xxiv
1 Introduction	1
1.1 Background and motivation	1
1.2 Statement of the problem	2
1.3 Previous research on tubular joints at ICOM/EPFL	4
1.4 Objectives and scope of the research work	4
1.5 Organisation	5
2 Background and literature review	7
2.1 Introduction	7
2.2 Geometric parameters defining CHS-joints	8
2.3 Fatigue and factors influencing the fatigue behaviour of weldments	9
2.3.1 Generalities	9
2.3.2 Residual stresses and mean stress	10

2.4	Methods for fatigue analysis of welded details	11
2.4.1	Structural stress approaches	13
2.4.2	Fracture Mechanics approach	15
2.5	Numerical methods	16
2.5.1	Finite element method (FEM) and Boundary element method (BEM)	16
2.5.2	Boundary element method, BEM	17
2.6	Size effects	18
2.6.1	Size effects in fatigue	18
2.6.2	Historical review on size effects in fatigue	20
2.6.3	Size effect in existing recommendations for tubular joints	21
2.7	Recent research on the fatigue behaviour of tubular K-joints	23
2.8	Summary and conclusions	24
3	Experimental Investigation	25
3.1	Introduction	25
3.2	Description of test specimens	25
3.2.1	Material properties and dimensions	26
3.2.2	Specimen fabrication	26
3.2.3	Weld geometry	27
3.3	Test procedure and Measurements	28
3.3.1	Supports and load introduction	28
3.3.2	Static tests	28
3.3.3	Fatigue tests	31
3.4	Main results and discussion	34
3.4.1	Static tests	34
3.4.2	Fatigue tests	37
3.4.3	Crack initiation	42
3.4.4	Initial defect size	43
3.4.5	Crack shape	44
3.4.6	Coalescence	45
3.4.7	Residual stresses, compression cracks	45
3.5	Summary and conclusions	48
4	Numerical Investigation	49
4.1	Introduction	49
4.2	Boundary element model	49
4.2.1	Geometry definition	50
4.2.2	Material properties	54
4.2.3	Boundary conditions	54
4.2.4	Crack location and geometry	54
4.2.5	Meshing	54
4.2.6	Basic load cases and complex load case	57
4.2.7	Stress intensity factors	57
4.3	Fatigue crack growth model	58
4.4	Standard model for fatigue life computation	59
4.4.1	Initial crack size and location, crack increments and failure criterion	60
4.5	Model validation	60

4.5.1	Comparison to fatigue test results	61
4.5.2	BEASY - Accuracy evaluation	65
4.5.3	Model mesh convergence	67
4.6	Combining basic load cases	71
4.7	Summary and conclusions	72
5	Parametric study	73
5.1	Introduction	73
5.2	Scope of parametric study	73
5.2.1	Geometries	74
5.2.2	Varying β , γ , τ to resize the CHS joint	74
5.2.3	Load cases	78
5.3	Assumptions defining the parameters and estimation of effects	78
5.3.1	Eccentricity and gap size	78
5.3.2	Chord length between joints, L_{ch} , and truss height, H and diagonal angle, θ	79
5.3.3	Weld size	81
5.3.4	Initial crack size, a_i , and final crack depth, a_f	81
5.3.5	Paris-Erdogan constant, C	82
5.3.6	Crack shape, a/c	83
5.3.7	Crack angle	83
5.4	Results and discussion of Parametric Study	86
5.4.1	Introduction	86
5.4.2	τ - Thicknesses ratio	88
5.4.3	γ - Chord slenderness	90
5.4.4	β - Diameters ratio	92
5.4.5	T - Thickness effect	95
5.5	Summary and comparison with previous studies	97
5.6	Conclusions	97
6	Proportional scaling	101
6.1	Introduction	101
6.2	Separation between <i>Proportional geometry</i> and <i>Non-proportional crack size</i>	101
6.3	Defining Y , the geometry correction factor	102
6.4	Number of cycles to failure to homothetic joints	104
6.5	Thickness correction factor	105
6.5.1	Analogy with plates thickness effect	107
6.6	Generalisation for combined load case / Load case interaction	111
6.6.1	Graphical solution	111
6.6.2	Comparison with fatigue test results	111
6.7	Efficiency of proportionally scaled joints	112
6.8	Summary and conclusions	114
7	Non-proportional scaling	115
7.1	Introduction	115
7.2	Effect on the geometry correction factor, Y	115
7.2.1	Influence of thickness ratio, τ	116

7.2.2	Influence of chord slenderness, γ	116
7.2.3	Influence of diameters ratio β	117
7.3	Alternative approach for fatigue assessment of CHS joints	117
7.3.1	Principle	117
7.3.2	Single basic load cases	119
7.3.3	Combined load case	126
7.3.4	Validation/Example	128
7.4	Comparison $Y(a_r/T)$ and SCF	130
7.5	Efficiency of joint geometries	130
7.6	Conclusions	131
8	Summary, conclusions and future work	133
8.1	Summary	133
8.2	Conclusions	134
8.3	Future work	135
Appendices		137
A	Fatigue tests instrumentation	139
A.1	Map of gages - S5-1	140
A.2	Map of gages - S5-2	142
A.3	Metallography procedure	144
B	Fatigue tests results	145
B.1	Simplified bar model	146
B.2	ACPD results	147
B.2.1	ACPD results	147
B.2.2	ACPD results - Crack depth against number of cycles	149
B.2.3	ACPD results - Crack growth against number of cycles	151
B.2.4	ACPD results - SIF against number of cycles	151
B.2.5	ACPD results - Crack growth against number of cycles	152
C	Numerical model	153
D	Parametric study	155
D.1	Parametric table	155
D.2	Parametric results	160
D.3	Other effects	168
D.3.1	Chord length between joints, L_{ch} , and truss height, H and crack angle, θ	168
D.3.2	Truss height, H	169
D.3.3	Crack shape, a/c	170
D.3.4	Crack angle, ϕ_{crack}	171
E	Proportional scaling	173
E.1	Behaviour of function $p \left(\frac{a}{T}\right)^{q-1} + \left(\frac{a}{T}\right)^q$	173
E.2	Fatigue life function of load case	174

F Non-proportional scaling	181
F.1 Effect over fatigue strength, S	181
F.1.1 Influence of thickness ratio, τ	181
F.1.2 Influence of diameters ratio, β	181
F.1.3 Influence of chord slenderness, γ	182
References	183
Curriculum vitæ	189
Education	189
Professional experience	189
Publications	189
Professional affiliations	191

List of Figures

1	Hot-spot locations in a K-joint made of CHS.	xxvi
1.1	<i>Cais das Pedras</i> viaduct (1997, Porto - Portugal).	2
1.2	Simplified representation of geometrical size effect - plates.	3
1.3	Different combinations of joint geometries (though exhibiting the same chord thickness), load cases and load levels can present the same hot-spot stress, σ_{hs}	4
1.4	Thesis organisation.	6
2.1	Geometric dimensions defining K-joint made of CHS.	8
2.2	Extrapolated hot-spot stress as defined in (Zhao et al., 2000).	14
2.3	Reference detail to assess local stress produced by weld profile (from Xiao and Yamada (2004)).	15
2.4	One point crack opening displacement - coordinate system at crack front (from Wilde and Aliabadi (1999)).	18
2.5	Influence of plate thickness on fatigue strength, normalised to a thickness of 32mm. All tests at R=0 except where stated (from (Gurney, 2006)).	21
3.1	Tubular truss fatigue test setup.	26
3.2	Tubular truss and joints nomenclature.	26
3.3	Preparation of joint before welding, backing rings and bevel.	27
3.4	Detail of welded joint mould impression.	28
3.5	Comparison of different weld leg lengths on chord.	29
3.6	Fatigue test rig.	30
3.7	Example of joint instrumentation with uniaxial strain gages, S5-2 joint 1.	30
3.8	Strip strain gages and ACPD voltage probes in joint 1 - beam S5-2.	30
3.9	Alternating current potential drop theory and notation (adapted from Chiew et al. (2004)).	32
3.10	Alternating current potential drop system - field probe and crack voltage probes (left) and Acquisition box (up); AC 120W generator (down).	33
3.11	Alternating current potential drop probe locations for S5-1 and S5-2.	34
3.12	Comparison of strain measured by gages (j_i) placed in symmetrical positions in the truss beam, static test of S5-2.	35
3.13	Strip gages installed in joint 1 and joint 5N of specimen S5-2. Strain range at surface near the weld toe in joints of specimen S5-2.	36
3.14	Comparison of S5 results to previous similar tests.	38
3.15	Comparison of ICOM test results to CHS joint database.	38

3.16	3-D Crack depth (a), length ($2c$) and angle convention.	39
3.17	Fatigue cracks for beam S5-2, opened after 273000 cycles.	40
3.18	Schematic of the procedure to analyse ACPD results to determine SIFs experimentally. . .	42
3.19	Number of cycles vs. crack depth at probe location for series S5-2 joints - using filtered results	43
3.20	Crack growth rate vs. number of cycles - S5-1 and S5-2.	43
3.21	Stress intensity factors vs. number of cycles.	44
3.22	Stress intensity factor range ΔK vs. relative crack depth, d/T	44
3.23	Comparison of final crack and crack estimations using ACPD system (S5-1 joint 1)	44
3.24	Crack opened-up and cutting planes.	45
3.25	Cross-section photos after surface was treated with Nital. (CBM) Chord base metal; (HAZ) Heat affected zone; (WM) Welding material; (DBM) Diagonal base material.	46
3.26	Microscopic photo of the crack after Nital etching (S5-2-j5N).	46
3.27	Crack shape evolution using final crack and ink marks when available (a is measured in the crack plane).	47
3.28	Blue ink marks showing independent small cracks and coalescence.	47
3.29	Close view of the crack texture - joint S5-2 j2 - with transitions identified as A, B, C and D.	47
4.1	Weld geometry.	51
4.2	Dimensions needed to define weld geometry - left, crown toe and right, weld crown heel.	52
4.3	Weld footprint length comparison - AWS (AWS, 2000) recommended minimum, S5 BEM model and S5-2 j2 measured.	52
4.4	Tube intersection.	53
4.5	Stress concentration in the joint (σ_{xx}) - Series S5 fatigue test loading conditions.	54
4.6	Crack surface geometry.	55
4.7	Zoning of the boundary element model.	56
4.8	Zone 2 - refined mesh in zone where the surface crack is located.	57
4.9	Detail of auto-remeshed area near the crack.	58
4.10	Comparison of the ΔK for the three different crack opening modes for load case 1 ($\Delta\sigma_{nom} = 100\text{MPa}$, $\beta = 0.53$; $\gamma = 4.2$; $\tau = 0.4$; $T = 20\text{mm}$).	59
4.11	Schematic of the procedure used to carry-out a crack propagation analysis.	60
4.12	Truss model used to calculate forces and bending moment acting in the joint.	61
4.13	Model representing tested joint S5-2 j1 and the external forces applied.	62
4.14	Stresses in chord of joint S52-j1, calculated and measured.	63
4.15	Nominal and hot-spot stresses in brace of joint S52-j1, calculated and measured	63
4.16	Comparison of principal strains at Location 1 and 11 of joint S21, between validated Abaqus model (Schumacher, 2003), BEASY model and measured.	64
4.17	Comparison of ΔK values at different crack depths - BEASY and ACPD experimental measures (beam S5-2) (d is the crack depth at the probe location).	65
4.18	Stress error norm.	65
4.19	Models used for mesh convergence testing.	68
4.20	Convergence of K_I values along the crack front ($a = 0.15\text{mm}$) for load cases LC1, LC4 and LC5.	69
4.21	Convergence of K_I values along crack front ($a = 10\text{mm}$) for load cases LC1, LC4 and LC5.	70
4.22	Stress intensity factor results obtained for the basic load cases acting isolated and combined and corresponding complex load case	71
5.1	Non-dimensional parameters changing: τ , β , γ	77
5.2	Influence of the gap/eccentricity ($\beta = 0.53$; $\gamma = 4.2$; $\tau = 0.4$; for $\zeta = 0.38$, $\zeta = 0.23$, $\zeta = 0.17$ and $\zeta = 0.12$).	79

5.3	Influence of chord length L_{ch} ($\beta = 0.53$; $\gamma = 4.2$; $\tau = 0.4$; for $\alpha = 38.6$, $\alpha = 25.7$, $\alpha = 12.9$).	80
5.4	Influence of truss height, H ($\beta = 0.53$; $\gamma = 4.2$; $\tau = 0.4$; $T = 20$ mm; for $H = 900$ mm, $H = 1800$ mm, $H = 2700$ mm).	80
5.5	Side view of the diagonal to chord wall joint, definition of weld size.	81
5.6	Influence of weld size, W_1 ($\beta = 0.53$; $\gamma = 4.2$; $\tau = 0.4$; $T = 20$ mm; for $W_1 = 7.5$ mm and $W_1 = 15$ mm).	82
5.7	Influence of weld size, W_1 . ($\beta = 0.53$; $\gamma = 4.2$; $\tau = 0.4$; $T = 20$ mm; for $W_1 = 7.5$ mm, $W_1 = 15$ mm).	83
5.8	Influence of initial defect size, a_0 , on the number of cycles to failure or on the fatigue strength - S5 geometry ($\beta = 0.53$; $\gamma = 4.2$; $\tau = 0.4$; $T = 20$ mm).	83
5.9	Influence of the final crack size, a_f , in the fatigue strength, considering $a_0 = 0.15$ mm - S5 geometry ($\beta = 0.53$; $\gamma = 4.2$; $\tau = 0.4$; $T = 20$ mm).	84
5.10	Influence of Paris-Erdogan constant C , for $m=3$, on fatigue life or on the fatigue strength - S5 geometry ($\beta = 0.53$; $\gamma = 4.2$; $\tau = 0.4$; $T = 20$ mm).	84
5.11	Influence of crack shape.	85
5.12	Influence of crack angle, ϕ_{crack}	85
5.13	Fatigue strength at 2×10^6 cycles function of τ , β , γ	86
5.14	Fatigue strength in terms of hot-spot stress function of the chord thickness, T , for the three basic load cases.	87
5.15	Stress intensity factor (SIF) ranges due to balanced axial brace load.	88
5.16	Stress intensity factors (SIF) due to balanced axial chord load.	89
5.17	Stress intensity factors (SIF) due to in-plane chord bending.	89
5.18	Thickness ratio effect in terms of nominal fatigue strength, S_{nom} ($\beta = 0.53$; $\gamma = 4.2$; $T = 60.0$ mm).	89
5.19	Stress intensity factors (SIF) due to balanced axial brace load.	90
5.20	Stress intensity factors (SIF) due to balanced axial chord load.	90
5.21	Stress intensity factors (SIF) due to in-plane chord bending.	91
5.22	Effect of chord slenderness in terms of nominal fatigue strength, S_{nom} , $\beta = 0.53$; $\tau = 0.5$; $T = 30$; , - $\gamma = 4.2$; $\gamma = 7$; $\gamma = 8.5$	91
5.23	Stress intensity factors (SIF) due to balanced axial brace load.	92
5.24	Changes in β parameter.	92
5.25	Stress intensity factors (SIF) due to balanced axial brace load.	93
5.26	Stress intensity factors (SIF) due to in-plane chord bending.	93
5.27	Effect of β in terms of nominal fatigue strength, S_{nom}	94
5.28	Stress intensity factors (SIF) due to balanced axial brace load.	95
5.29	Stress intensity factors (SIF) due to balanced axial chord load.	95
5.30	Stress intensity factors (SIF) due to in-plane chord bending.	96
5.31	Thickness effect in terms of nominal fatigue strength, S_{nom}	96
6.1	Geometry factor Y equation for different crack depths and basic load cases in proportionally sized joints.	103
6.2	Geometry factor, Y , function of crack depth, for $\beta = 0.53$ and basic load cases LC1, LC4 and LC5.	108
6.3	Number of cycles to failure function of the thickness of the chord in proportionally scaled joints for load case 1 (and specific geometry $\beta = 0.53$; $\gamma = 4.2$; $\tau = 0.4$).	109
6.4	Reference number of cycles to half thickness crack depth, $N_{T/2}$, function of the combination of the three basic load cases, for $\Delta\sigma = 100$ N/mm ²	112
6.5	Comparison between experimental results and estimations obtained using procedure described in 6.6.1.	113

6.6	Comparison of static admissible force to admissible fatigue force range, calculated according to different hypotheses for proportionally scaled geometries.	113
7.1	Geometry correction factor, influence of the thickness ratio, τ	116
7.2	Geometry correction factor, influence of the chord slenderness, γ	116
7.3	Geometry correction factor, influence of the diameters ratio β	117
7.4	Schematic comparing 1-D hot-spot approach to 2-D Y approach.	118
7.5	$S_{a_r} - N$ lines resulting from plotting the Equation (7.2) as a function of $\Delta\sigma \cdot Y(a_r/T)$ for chord thicknesses $T = 16$ mm and $T = 60$ mm.	119
7.6	Relative error on the fatigue life when using the $a_{r_{\text{mean},T_i}}$ (obtained using expressions (7.4) and (7.5)) for the geometries in the parametric table, considering two absolute dimensions for each case: $T = 16$ mm (red dots) and $T = 50$ mm (blue dots) as defined by Equation (7.12).	122
7.7	Representative crack depth, a_r , for basic load cases 1 and 4, as a function of non-dimensional parameters γ and τ (Dark red surface: $\beta = 0.53$; Blue surface: $\beta = 0.63$). The absolute size corresponds to a chord thickness of $T = 16$ mm.	123
7.8	Relative error on the fatigue life when using the representative depth $a_{r_{\beta,\gamma,\tau,T_i}}$ (obtained using expressions (7.8) and (7.9)) for the geometries in the parametric table, considering two absolute dimensions for each case: $T = 16$ mm (red dots) and $T = 50$ mm (blue dots).	123
7.9	Equivalent correction factor, Y_{a_r} , for basic load cases 1 and 4, as a function of non-dimensional parameters γ and τ (Dark red surface: $\beta = 0.53$; Blue surface: $\beta = 0.63$). The absolute size corresponds to a chord thickness of $T = 16$ mm.	125
7.10	Relative error of expressions obtained from regression.	125
7.11	Fatigue strength size correction factor as a function of the chord thickness and the non-dimensional parameters for LC1 and LC4.	126
7.12	Envelope of the relative error over the parametric matrix geometries for the combined case, considering different absolute sizes (represented by the chord thickness, T) and different combination ratios $\frac{\Delta\sigma_1}{\Delta\sigma_4}$	127
7.13	Application of the procedure described in Section 7.3.3 to fatigue tested series and geometries in parametric matrix. For the parametric table geometries two chord thicknesses ($T = 16$ mm and $T = 50$ mm) and three load cases are considered (100% LC1, 50%LC1 + 50% LC4, 100% LC5).	129
7.14	Comparison of SCF values and Y ($T = 16$ mm).	130
7.15	Force range the joint would resist, ΔF , against cross-sectional area of joined elements, $A_{\text{chord+diagonal}}$, considering basic load cases acting alone.	131
7.16	Force range the joint would resist, ΔF , against cross-sectional area of joined elements, $A_{\text{chord+diagonal}}$, considering a combined load case typical to bridge truss.	131
A.1	Tubular truss strain gages and displacement transducers map (S5-1).	141
A.2	Tubular truss strain gages and displacement transducers map (S5-1).	143
B.1	Simplified bar model - Axial force.	146
B.2	Simplified bar model - Bending moment.	146
B.3	ACPD results, S5-1, unfiltered.	147
B.4	ACPD results, S5-1, filtered.	147
B.5	ACPD results, S5-2, unfiltered.	148
B.6	ACPD results, S5-2, filtered.	148
B.7	Number of cycles vs. crack depth at probe location for series S5-1 joints.	149
B.8	Number of cycles vs. crack depth at probe location for series S5-1 joints - using filtered results.	149
B.9	Number of cycles vs. crack depth at probe location for series S5-2 joints.	150

B.10	Crack growth rate vs. number of cycles - S5-1.	151
B.11	Stress intensity factors vs. number of cycles.	151
B.12	Stress intensity factor range ΔK vs. relative thickness (d/T).	152
C.1	Comparison of the ΔK for the three different crack opening modes for load cases 4 and 5 ($\Delta\sigma_{nom} = 100$ MPa, $\beta = 0.53$; $\gamma = 4.2$; $\tau = 0.4$; $T = 20$ mm).	153
C.2	Available boundary elements in BEASY (from BEASY (2003)).	154
C.3	Joint deformation mode (Load case 1).	154
D.1	Influence of chord length L_{ch} ($\beta = 0.53$; $\gamma = 4.2$; $\tau = 0.4$; $\alpha = 38.6$); ($\beta = 0.53$; $\gamma =$ 4.2 ; $\tau = 0.4$; $\alpha = 25.7$); ($\beta = 0.53$; $\gamma = 4.2$; $\tau = 0.4$; $\alpha = 12.9$).	168
D.2	Influence of truss height, H	169
D.3	Influence of crack shape.	170
D.4	Influence of crack angle, ϕ_{crack}	171
E.1	Behaviour of function $p \left(\frac{a}{T}\right)^{q-1} + \left(\frac{a}{T}\right)^q$	173
E.2	Fatigue life function of load case and geometry.	175
E.3	Fatigue life function of load case and geometry.	176
E.4	Fatigue life function of load case and geometry.	177
E.5	Fatigue life function of load case and geometry.	178
E.6	Fatigue life function of load case and geometry.	179
E.7	Fatigue life function of load case and geometry.	180
F1	Fatigue strength, influence of the thicknesses ratio, τ	181
F2	Fatigue strength, influence of the diameters ratio, β	181
F3	Fatigue strength, influence of the chord slenderness, γ	182

List of Tables

2.1	Influencing parameters controlling each of the crack initiation and crack propagation periods in steels (adapted from Radaj (1996)).	10
2.2	Boundaries of extrapolation region for CHS joints (Zhao et al., 2000).	14
2.3	Thickness effect in existing standards.	22
3.1	Fatigue test series tested recently at ICOM.	27
3.2	ACPD systems characteristics.	33
3.3	Load and deflection results.	35
3.4	Nominal and hot-spot stresses for test joints.	37
3.5	Fatigue crack dimensions for beam S5-1 (final crack front after 169000 cycles).	39
3.6	Fatigue crack dimensions for beam S5-2 (final crack front after 273000 cycles).	40
4.1	Individual basic load cases and boundary conditions (adapted from Schumacher (2003)).	59
4.2	Geometric parameters of model used to compare with S5 fatigue test results.	61
4.3	Non-dimensional parameters of model used to compare with S5 fatigue test results.	61
4.4	Model accuracy report.	66
4.5	Models used for mesh convergence testing.	67
5.1	Summary of the parametric table ($\beta = 0.53$)	75
5.2	Summary of the parametric table ($\beta = 0.65$)	76
5.3	Basic load cases selected for the parametric study.	78
5.4	Comparison of <i>SIF</i> with Stress Concentration Factors, <i>SCF</i> (from Schumacher (2003)), and normalised stress intensity factor, <i>F</i> (from Shao and Tjhen (2005)), for the different load cases.	98
5.5	Range of parameters β , γ , τ and <i>T</i> used in parametric study.	98
5.6	Effects of changing β , γ and τ on the stress intensity factor.	98
5.7	Trends in the fatigue strength obtained from the sensitivity analysis.	99
6.1	<i>Y</i> regression parameter <i>p</i> , for different geometries and load cases.	104
6.2	<i>Y</i> regression parameter <i>q</i> , for different geometries and load cases.	105
6.3	<i>Y</i> regression goodness of fit R^2 , for different geometries and load cases.	106
6.4	Thickness correction factor exponents n_N , for CHS joint geometries proportionally sized and different basic load cases, in terms of number of fatigue life (f_N) ($T_{ref} = 16$ mm) . . .	109

6.5	Thickness correction factor exponents n_s , for CHS joint geometries proportionally sized and different basic load cases, in terms of number of fatigue resistance (f_S) ($T_{ref} = 16$ mm)	110
6.6	Comparison of thickness correction factor exponents for proportional scaling, using σ_{nom} .	110
7.1	Representative coordinate a_r [mm] for load cases LC1 and LC4, considering joints of three different absolute sizes.	120
7.2	Equivalent geometry correction value $Y(a_r/T)$ for load cases LC1 and LC4, considering joints of three different absolute sizes.	124
7.3	Example of application of the procedure to the fatigue tested joints.	128
7.4	Influence of the eccentricity/gap in the determination of representative crack depth $Y(a_r/T)$	129
D.1	Parametric cases ID.	155
D.2	Parametric table.	156
D.3	Parametric results.	161

Nomenclature

Latin Letters

a	crack depth at deepest point in the crack (measured in the crack plan)	[mm]
a_f	final crack size	[mm]
a_i	initial crack size	[mm]
$2c$	crack length	[mm]
m	material constant	[–]
D	chord outside diameter	[mm]
d	brace outside diameter	[mm]
d_i	crack depth at probe location i	[mm]
E	modulus of elasticity	[N/mm ²]
e	eccentricity between brace and chord axes intersection	[mm]
F	force	[N]
f_N	thickness correction factor for fatigue life	[–]
f_S	thickness correction factor for fatigue strength	[–]
g	gap distance	[mm]
g'	distance between weld toes	[mm]
H	truss height	[mm]
L_{ch}	chord length (between two nodes)	[mm]
C	material constant	[(mm/cycle)(N/mm ^{-3/2})]
M	moment	[N·m]
N	number of load cycles	[–]
n	size effect exponent	[–]
N_1	number of load cycles to a 15% change in strain near the crack initiation point	[–]
N_2	number of load cycles at detection of first crack	[–]
N_3	number of load cycles to through-thickness cracking	[–]
N_4	number of load cycles to complete loss of static joint strength	[–]
n_N	thickness correction factor exponent for fatigue life	[–]
n_S	thickness correction factor exponent for fatigue strength	[–]

$N_{T/2}$	number of load cycles to half thickness cracking, $a = T/2$	[–]
Q_{max}	minimum load	[kN]
Q_{min}	minimum load	[kN]
R	stress ratio	[–]
$S_{r,hs}$	hot-spot stress range	[N/mm ²]
$S_{r,nom}$	nominal stress range	[N/mm ²]
T	chord wall thickness	[mm]
t	brace wall thickness	[mm]
V_{2i}	potential difference measured with the probe i	[mV]
Y	geometry correction factor	[–]

Greek Letters

α	chord length slenderness, $2 \cdot L_{ch}/D$	[–]
β	brace-to-chord diameter ratio, d/D	[–]
$\Delta\sigma_{hs}$	hot-spot stress range	[N/mm ²]
$\Delta\sigma_{nom}$	nominal stress range	[N/mm ²]
ΔK_{th}	stress intensity factor range threshold	[N/mm ^{3/2}]
δ	deflection	[mm]
Δ_i	spacing between probe contacts i	[mm]
ϕ_{crack}	crack angle	[°]
γ	chord slenderness, $D/(2 \cdot T)$	[–]
ν	Poisson ratio	[–]
ψ	local dihedral angle	[°]
σ_{hs}	hot-spot stress	[N/mm ²]
σ_{max}	maximum stress	[N/mm ²]
σ_{min}	minimum stress	[N/mm ²]
τ	thickness ratio, t/T	[–]
θ_{br}	brace angle	[–]
a_r	representative crack depth at which, the geometry correction factor takes a through thickness equiva- lent value	[mm]
ζ	gap to chord diameter ratio	[–]

Abbreviations

ACPD	alternating current potential drop
BEM	boundary element method
CHS	circular hollow section
FEM	finite element method
hs	hot-spot
LC	load case
LEFM	linear elastic fracture mechanics
SCF	stress concentration factor
SIF	stress intensity factor

Terminology

- ◆ **Tubular connections:** connection in the portion of a structure that contains two or more

intersecting members, at least one of which is a tubular member; Connection geometry may be described in terms of the topology of the intersecting members - their size, shape, position, and orientation (Marshall, 1992a).

- ◆ **Tubular joint:** a welded joint at the interface created between members in a tubular connection, consisting of the weld deposit, heat-affected zone, and immediately adjacent base metal. In the literature "tubular joint" is often used to refer to tubular connections as well (Marshall, 1992a).
- ◆ **Nominal stress:** the maximum stress in a cross section calculated on the actual cross section by simple elastic theory. Nominal stress does not take into account the effect of geometrical discontinuities.
- ◆ **Stress range, $\Delta\sigma$:** the algebraic difference between the maximum stresses, σ_{max} , and minimum stresses, σ_{min} , in a stress cycle.

$$\Delta\sigma = \sigma_{max} - \sigma_{min} \quad (1)$$

The stress range can be based on the nominal stress, σ_{nom} , or the hot-spot stresses σ_{hs} .

- ◆ **Stress ratio, R :** the ratio between the maximum and the minimum stresses in a stress cycle of constant amplitude loading and taking account of the sign of the stress values.
- ◆ **Hot-spot stress, σ_{hs} :** also called geometric stress, is defined as the extrapolated principal stress at a specified location at the weld toe (see Figure 1). The extrapolation must be carried out from the region outside the influence of the effects of the weld geometry and discontinuities at the weld toe, but close enough to fall inside the zone of the stress gradient caused by the global geometrical effects of the joint. The extrapolation is to be carried out on the brace side and the chord side of each weld. Generally the geometric stress (or the hot-spot stress) can be determined by considering the stress normal to the weld toe since the orientation of the maximum principal stress is normal or almost normal to the weld toe.
- ◆ **Fatigue strength** (of a welded component): a stress range, which causes failure of the component after a specified number of cycles N , with a given level of safety.
- ◆ **Fatigue life:** is the number of cycles N to a defined failure criterion. Four failure criteria give rise to the four definitions of fatigue life that can be found in the literature:
 - ◇ N_1 : number of cycles to a 15% change in strain near the crack initiation point;
 - ◇ N_2 : number of cycles at detection of first crack;
 - ◇ $N_{T/2}$: number of cycles to half thickness cracking, $a = T/2$.
 - ◇ N_3 : number of cycles to through-thickness cracking (criterion for test end);
 - ◇ N_4 : number of cycles to complete loss of static joint strength;
- ◆ **Cut off limit:** is the stress range below which it is assumed that the stress ranges of a variable amplitude loading do not contribute to the fatigue damage. For Eurocode 3, for example, this value corresponds to 0.405 the fatigue strength at $2 \cdot 10^6$ cycles.
- ◆ **Fatigue limit:** is defined as the stress range below which it is assumed that no fatigue failure occurs for a constant amplitude loading, is known as the fatigue limit. For Eurocode 3 (EN 1993-1-1:2005) and the CIDECT recommendations (Zhao and Packer, 2000), for example, this is defined as $0.745 \cdot \Delta\sigma_c$ and corresponds to $N = 5 \times 10^6$ cycles.

- ◆ **Stress concentration factor, SCF ,** is the ratio between the hot spot stress, or geometric stress, excluding local effects, at a particular location in a joint and the nominal stress in the member due to a basic member load which causes this geometric stress.
- ◆ $S_{r_{hs}} - N_f$ **curve** or *Wöhler* line gives the relationship between the (hot-spot) stress range at constant amplitude and the number of cycles to failure.
- ◆ **Stress intensity factor, SIF:** is given by $K = Y \cdot \sigma \sqrt{\pi a}$.
- ◆ **Size effects:** phenomena due to which the nominal strength of a material, and as a consequence, the specimen made of it, depends on the specimen dimension.
- ◆ **Scaling effect:** proposed by Mashiri et al. (2007), includes complete proportional scaling, practical proportional scaling and non-proportional scaling effects.
- ◆ **Complete proportional scaling:** stands for the case where all the dimensions affecting fatigue are scaled proportionally.
- ◆ **Thickness effect (Complete):** is frequently associated with the concept of proportional scaling, when the thickness is the only parameter needed to describe the fatigue life difference between two joints.
- ◆ **Practical proportional effect:** happens when only the important dimensions are scaled proportionally.

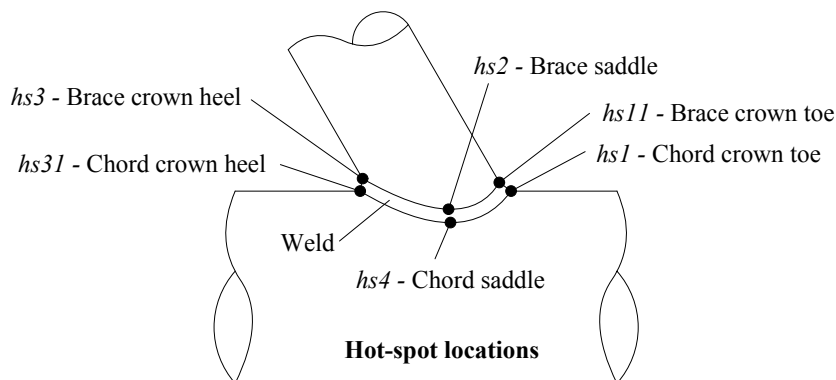


Figure 1: Hot-spot locations in a K-joint made of CHS.

Introduction

1.1 Background and motivation

Tubular sections have been recognised and used for a long time because of their excellent structural and mechanical properties; one of the first examples of tubular bridge design is the outstanding Firth of Forth Bridge in Scotland constructed in 1890. This bridge was built up from tubular members made out of rolled plates riveted together. Following World War II, remarkable progress related to manufacturing, end preparation and welding was achieved (Wardenier, 2001). Several advances in technological and production methods have emerged ever since, making it possible to roll longer and thinner walled tubes and allowing for new possibilities and design solutions.

The need for aesthetics and architectural transparency, in particular for improved passage of light, in urban areas, has impelled engineers and architects to search for innovative solutions. A rational use of hollow sections leads in general to cleaner and more spacious structures. This is also true for bridge designs (Eekhout, 1991). The relatively new concept of steel-concrete composite Circular Hollow Section (CHS) truss bridges presents the designer with new challenges, in particular with respect to the fatigue design of the CHS joints.

There is a wide variation in existing CHS bridges, from the structural system to the joint fabrication method. Presently, three main methods of joint fabrication can be found in existing bridges. For directly welded joints, the braces are cut to fit and welded to the continuous chord. A more conventional possibility consists of brace-to-chord connections using gusset plates. Cast steel nodes offer a third alternative whereby castings are employed to provide a smooth transition between the brace and chord members, which are welded to the casting stubs. Both solutions (directly welded and cast joints) present advantages, and have been extensively studied by the offshore industry (Marshall, 1992a).

Recent design and construction of welded tubular truss bridges in Switzerland (Lully (1997), Aarwangen (1997) and Dättwil (2001), (Schumacher et al., 2002b)) and abroad (Cais das pedras - Porto (1997) (P), Figure 1.1, Nesenbach Valley - Stuttgart (1999) (D)) have highlighted specific concerns about the behaviour of the CHS joints when subjected to fatigue loading.

During the design of the above cited bridges, it was found that existing fatigue specifications for bridges and tubular structures were not at all or only partially applicable to the types of joints found in bridges. Based on the static design of the bridge, the required joint dimensions fell out of the applicability range given by the codes (Schumacher et al., 2002b).

In comparison to offshore structures, bridges exhibit differences in member sizes, tube slenderness, fabrication techniques, etc. All these differences make the direct application of the current offshore knowledge to bridge design difficult, and demonstrate that the current behaviour models for welded joints and cast nodes subjected to fatigue are incomplete.

Concern over the size effect in fatigue arose from the difference between the welded joint sizes that were being tested in the laboratory and the much larger joints being used in civil engineering structures.



Figure 1.1: Cais das Pedras viaduct (1997, Porto - Portugal).

1.2 Statement of the problem

According to Gurney (2006), it has been known for a long time that plate thickness is a relevant parameter influencing the fatigue strength of specimens subjected to bending, due to steeper stress gradients in thinner specimens compared to thicker specimens.

Gurney (1977) also, recognised the effect of plate thickness even for welded joints under axial loading. One main reason is responsible for this phenomenon. It is well known that crack growth rate is predominantly a function of ΔK . ΔK is a function of the crack depth, a , and the stress range at the crack tip, $\Delta\sigma$, which is a function of a/T (Gurney, 2006). In thicker plates, for a similar crack depth, a , the stress at the crack tip is larger than that in thinner plates (see Figure 1.2).

Considering proportionally scaled joints under the same nominal stress, $\Delta\sigma_{nom}$, the same hot-spot stress range, $\Delta\sigma_{hs}$ is expected (as it is function of the nominal stress, $\Delta\sigma_{nom}$, and the non-dimensional stress concentration factor (SCF)). Making the reasonable assumption that the initial defect size is independent of the plate thickness, the crack growth rate is thus higher and, generally, fatigue strength is lower for thicker joints. This might not be the case for less aggressive details (lower SCF). The more aggressive the detail, the more pronounced the thickness effect.

For welded tubular joints, the size effect correction is based on a statistical study of a large database of tubular fatigue test results (van Wingerde et al., 1997). This database includes different joint types and load cases, and relies on the concept of hot-spot stress to take into consideration these differences.

Similarly to Gurney's correction factor, the thickness of the failed member was assumed to be the most important factor influencing the relative fatigue behaviour between different tubular joints. In the case of tubular joints however, instead of nominal stress, van Wingerde et al. (1997) employed the hot-spot stress at the weld toe. Indeed, a size effect correction factor was established, and is currently recommended by CIDECT (Zhao et al., 2000) and IIW (Zhao and Packer, 2000), for joints with a wall thickness other than 16 mm:

$$\frac{S_{r,hs,T}}{S_{r,hs,16}} = \left(\frac{T_{ref}}{T} \right)^n \quad (1.1)$$

where,

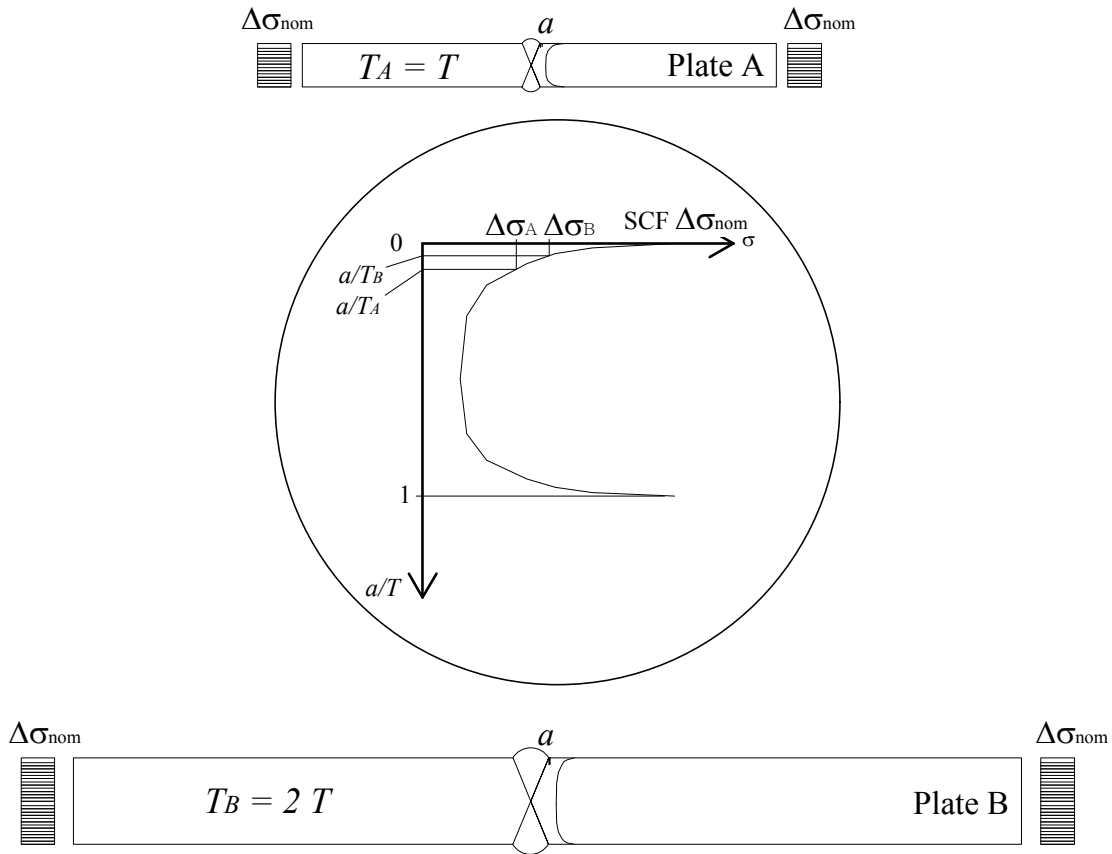


Figure 1.2: Simplified representation of geometrical size effect - plates.

- $S_{t,hs,T}$: (hot-spot) fatigue strength for a welded tubular joint of thickness T ;
- T_{ref} : reference thickness (16 mm);
- n : size correction exponent;

The exponent, n , is function of the fatigue life (defined as N_4 , see terminology), and thus of the stress range level, but independent of the geometry or load case. It varies from 0.24 (for 10^4 cycles) to 0.402 (for 5×10^6 cycles).

As the hot-spot is used, the concept of correction between "proportionally scaled" joints, as in the original work, is extended to both proportional and non-proportional scaling. The only parameters determining the fatigue strength of the joint, according to this method, are the hot-spot stress range and the thickness of the failing member. Compared to plates with a transverse attachment, tubular joints present more and different parameters defining geometry and load cases.

In order to show how the hot-spot method can oversimplify the problem, consider that, for a given chord thickness, it is possible to find multiple joints whose combinations of geometry parameters (τ, β, γ, e) and load cases conduct to the same surface hot-spot stress as shown in Figure 1.3. However, the stress gradient through thickness along the crack path will be different, and so will be the fatigue behaviour of each case. If we now scale up these joints, different correction factors would be expected for each one.

A major objective of the present work is to investigate how the simplified thickness correction, based on the hot-spot concept, can be extrapolated to tubular joint geometries typical for bridge application ($\gamma < 12$).

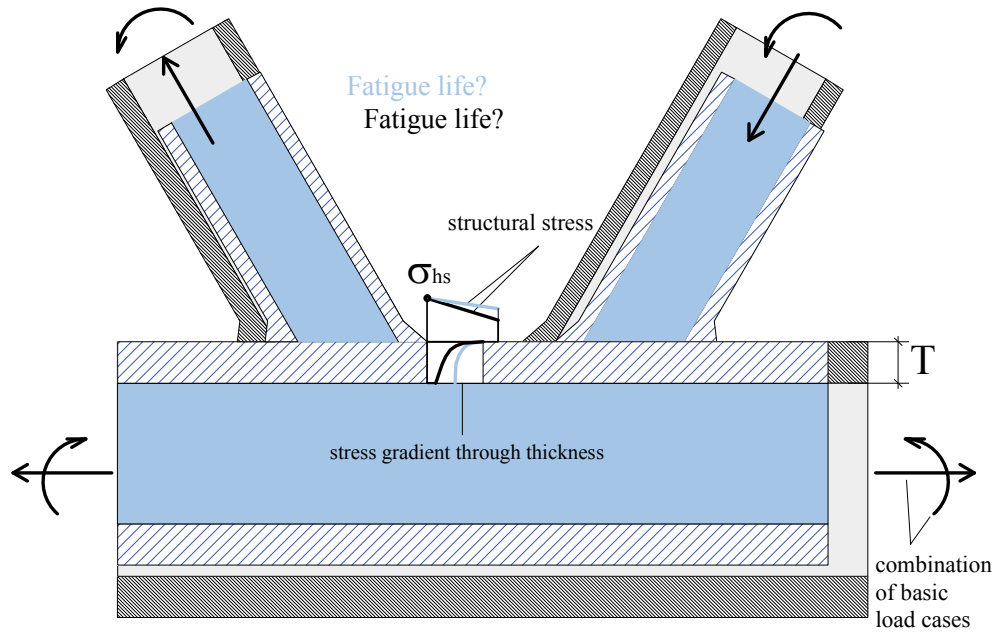


Figure 1.3: Different combinations of joint geometries (though exhibiting the same chord thickness), load cases and load levels can present the same hot-spot stress, σ_{hs} .

1.3 Previous research on tubular joints at ICOM/EPFL

The Steel Structures Laboratory (ICOM) at the EPFL has been active in the domain of fatigue of tubular joints since 1999. Schumacher (2003) carried out experimental and numerical studies to investigate two specific aspects of fatigue in welded K-joint for CHS bridge application: the joint stresses (hot-spot stresses and stress concentration factors) at fatigue-critical locations; and the influence of the size effect on the fatigue resistance of these joints using a statistical and an analytical approach, based on linear elastic fracture mechanics (LEFM). Schumacher found that the currently used exponent, n , (Equation (1.1)) was too conservative in many cases and not adapted for some combinations of geometry parameters.

Welded tubular joints are susceptible to fatigue problems due to a combination of stress concentration due to geometry discontinuity and defects caused by the welding process. Two different approaches can be taken to improve this situation. These were, recently, object of investigation at ICOM: to move the welds out of the area of high stress concentration (Haldimann-Sturm, 2005) or to improve the fatigue performance of the weld detail and the adjacent base metal (Walbridge, 2005).

The present research is made in the continuity of the work carried out by Schumacher. It is aimed at improving the knowledge on the effects of sizing the CHS joints on their fatigue behaviour.

1.4 Objectives and scope of the research work

The main objectives of this thesis are:

1. To define the terms (e.g., size, scale and thickness effects, proportional and non-proportional scaling) and the different parameters that contribute to the size effect associated with each of these terms.
2. To observe and measure fatigue crack growth (initiation and propagation) through large scale testing of two truss beams. The fatigue crack growth is monitored by adopting an Alternating Current Potential Drop (ACPD) system on the truss beams.

3. To develop an advanced numerical model in order to predict the fatigue behaviour of tubular joints.
4. To perform a parametric study on a range of Boundary Element models aiming to investigate in a deterministic manner the influence of geometry and basic load cases.
5. To understand the effect of size on the fatigue of tubular joints, distinguishing between proportional scaling and non-proportional scaling effects.

This investigation is limited to the study of:

- ◆ Non-overlapping, as-welded K-joints in uniplanar trusses with symmetrical braces;
- ◆ The most likely crack location in the joint (hot-spot 1);
- ◆ Geometry parameters typical to bridge application;
- ◆ In-phase and constant amplitude in-plane loading.

Crack propagation in an aggressive environment is not considered and neither are the fabrication effects, as they cannot be realistically accounted for using a deterministic approach. The investigation of welding residual stresses in CHS joints is out of the scope of this thesis.

Original contributions from this work include:

- ◆ Advanced 3-D modelling of cracked tubular K-joints in order to specifically address geometrical size effects.
- ◆ Experimental investigation of crack growth on large scale truss beams using the ACPD system.
- ◆ Calculation of geometry correction factors, Y , for K-joint geometries in the bridge application range and for the three main basic load cases.
- ◆ A new method to estimate fatigue crack propagation in tubular joints of different geometries, based on the value of the geometry correction factor at a representative crack depth.

1.5 Organisation

The thesis is divided into eight chapters.

Chapter 2 provides an introduction to key concepts and an overview of the current state-of-the-art in modelling the fatigue behaviour of CHS joints.

Chapter 3 details the experimental investigations carried-out on two large-scale tubular trusses. A description of the specimens, set-up instrumentation, and test procedures is presented. Results, especially alternating current potential drop (ACPD) data, are discussed and used to validate the numerical model developed in chapter 4.

Chapter 4 details the development of a numerical model to predict the fatigue behaviour of welded CHS joints. A 3-D boundary element model is built up to compute the Stress Intensity Factors (SIF) at different crack depths. The model is validated and standardised in order to be used in the parametric study described in Chapter 5.

Chapter 5 presents the parametric study. The principal assumptions and simplifications are justified and the main results are given. The results are presented in the form of stress intensity factors at different crack depths, fatigue life and fatigue strength.

Chapter 6 provides an analysis of the parametric study results, focusing specifically on the question of proportional scaling of the joints. The geometry correction factor Y is introduced and determined for the geometries in the parametric table and main basic load cases. Thickness correction factors are then computed for the different geometries and main basic load cases. A comparison between results obtained for K-joints and results existing in the literature for plates (thickness effect) is done.

Chapter 7 explores the parametric study results by bringing to light the effect of non-proportional scaling. Size correction factors for fatigue strength, as a function of the non-dimensional parameters, β , γ and τ , and chord thickness, T , are suggested for basic load cases 1 and 4. When the combined load case is considered, a size correction factor is proposed for fatigue life estimation. Ideas for an alternative design approach and recommendations are proposed.

Chapter 8 synthesises the main results and provides proposals for future work. Additional details on the work done, such as experimental data and detailed numerical results are presented in appendices at the end of the document.

The diagram in Figure 1.4 shows how this thesis is organised.

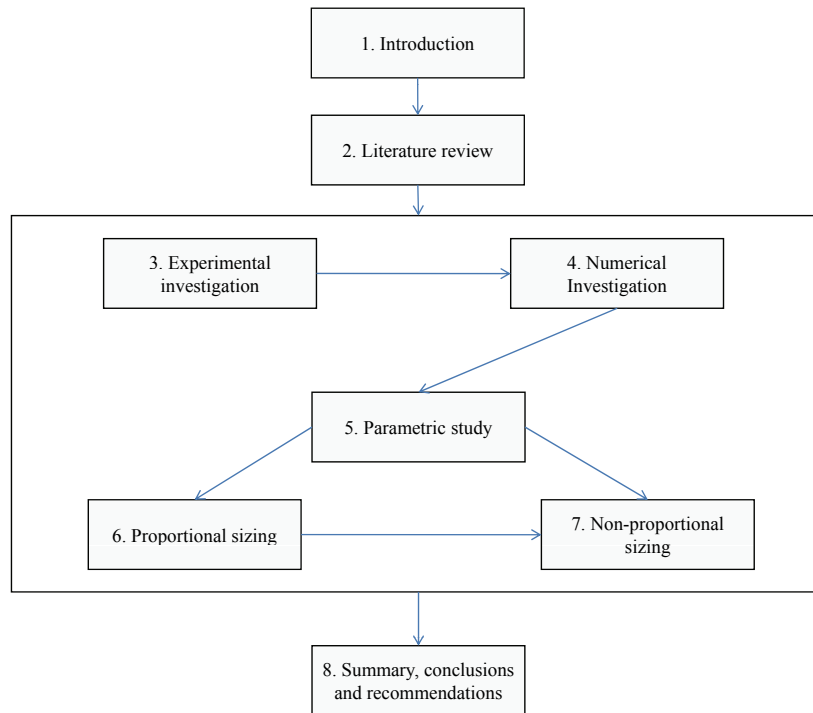


Figure 1.4: Thesis organisation.

Background and literature review

2.1 Introduction

The excellent mechanical properties of hollow sections, are greatly illustrated by the many examples that can be found in the nature, where the millenarian biology evolution corresponds, from an engineering optic, to a shape optimisation process. In fact, the efficient material distribution for either bending or buckling, closed shape (reduced area to protect) and lower drag coefficients if exposed to wind or water (particularly true in the case of circular shapes) make them an attractive profile to build tubular structures. Hollow sections are competitive and preferred, even though manufacturing costs are higher than other sections, to create structures in areas as different as architectural, civil (buildings and bridges), offshore, chemical, aeronautical, transport and agriculture (Wardenier, 2001). Hollow sections for structural applications are commonly designated as:

- ◆ structural hollow sections (SHS) - In Canada and the USA it is common to use Hollow Structural Sections (HSS) instead of (SHS) (*HSS* can however be confused with *High Strength Steel* or even with *Hot-Spot Stress* and will not be used in this thesis);
- ◆ circular hollow sections (CHS);
- ◆ rectangular hollow sections (RHS).

Detailed information on hollow section structures, is provided in the literature. A description of the manufacturing process, assembly, properties of sections and applications can be found, for example, in (Dutta et al., 1998, Eekhout, 1996, Wardenier, 2001), among others.

Tubular structures can be of all different types: beams and columns, trusses, tree shaped structures. Connections between hollow section members are usually made by welding one member directly to the others surface, and where possible, without stiffeners or connecting plates. In the structural design of tubular structures, tubular joints are critical for design both for static and fatigue actions.

The static behaviour of existing tubular joints configurations has been extensively studied and a great amount of literature has been produced (Marshall, 1992a). Studies on fatigue behaviour analysis of tubular joints have also been made but, due to complexity, less extensively. This is especially the case for joints with more complex geometry such as X, K, XX, or KK joints.

To date, most of the research work carried out on tubular joint fatigue has concentrated on T-joints (Beale and Toprac, 1967, Bowness and Lee, 1998) as the simple geometry configuration allows for easier experimental setup and load introduction. In practice, however, this type of joint is rarely found (either in offshore or bridge structures) and the stress concentration at the weld toe was found to be much higher, when compared to K-joints. These (K-joints), due to the two braces under

tension, respectively compression, exhibit a different stress state in the weld toe region, reducing stress concentration. K-joints are frequently preferred for offshore and bridge designs and became the focus of several fatigue behaviour investigations.

For K-joints made out of CHS, the intersection between the chord and each brace can only be described by a complex 3-D curve. When the weld profile is also considered, the geometry of the problem complexifies itself and so does the numerical analysis of the joint behaviour.

The objective of this chapter is to introduce a number of key concepts and to present a brief overview of the research in the domain of welded tubular joint fatigue - in particular for K-joints made of CHS.

In Section 2.2, the parameters commonly used to define the geometry of welded, non-overlapped joints made of CHS are presented. Section 2.3 gives a short introduction on the fatigue behaviour of weldments and the factors mostly influencing the different fatigue life periods, from crack initiation to crack propagation. Section 2.4 gives a description of the methods currently used for the assessment of the fatigue behaviour of welded joints. In section 2.5 a brief overview on the use of FEM and BEM methods in Linear Elastic Fracture Mechanics (LEFM) is given and then a description of basic concepts of the Boundary Elements Method (BEM) and its application to LEFM problems. Within Section 2.6, definitions on size effects are introduced, brief and non-exhaustive historical review on size effects in fatigue and the way this topic is covered in current design recommendations are given. Section 2.7 summarises the recent research on the fatigue behaviour of tubular joints. Finally, the main conclusions are listed in section 2.8.

2.2 Geometric parameters defining CHS-joints

The geometry of a single K-joint can be described by the diameters and thicknesses of chord and diagonals (respectively D, T, d, t , see Figure 2.1), the brace angle, θ_{br} , the chord length, L_{ch} , and the gap, g , or the eccentricity, e .

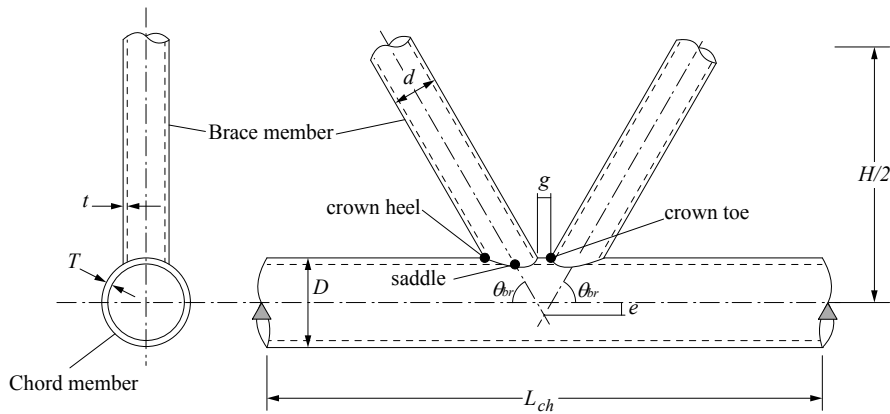


Figure 2.1: Geometric dimensions defining K-joint made of CHS.

Moreover, the following non-dimensional parameters are commonly used to characterise the joint:

$$\alpha = \frac{2L_{ch}}{D}; \beta = \frac{d}{D}; \gamma = \frac{D}{2T}; \tau = \frac{t}{T}; \zeta = \frac{g}{D} \quad (2.1)$$

where,

- d : brace outside diameter;
- D : chord outside diameter;
- t : brace wall thickness;
- T : chord wall thickness;
- g : gap distance;
- e : eccentricity;
- L_{ch} : distance between two nodes;
- H : truss height.

The non-dimensional parameters are commonly referred to as:

- ◆ γ - chord slenderness;
- ◆ β - diameters ratio;
- ◆ τ - thickness ratio.

2.3 Fatigue and factors influencing the fatigue behaviour of weldments

2.3.1 Generalities

Fatigue can be defined as a process in which damage accumulates due to the action of repetitive stresses that may be well below the yield point. Although this process and the many factors that influence it have been extensively investigated, it remains that the fatigue of materials is a very complex and still not completely understood process (Fricke, 2003).

According to Lawrence et al. (1996), the process of fatigue in weldments can be divided into three periods: crack nucleation, development and growth of a short crack (stage I) and the propagation of a dominant (long) crack to a length at which it either stops or causes fracture (stage II). Although the boundaries between these stages are not clearly defined, it is generally assumed that the total fatigue life of a weldment, N_T , is the sum of three life periods: fatigue crack nucleation, N_N , short crack (stage I) propagation, N_{p1} , and long crack (stage II) propagation, N_{p2} .

Crack initiation includes the moving dislocations and crack nucleation (N_N), the time it takes for crack creation and growth to a size longer than the size of several material grains. Crack propagation is then calculated ($N_{p1} + N_{p2}$).

Table 2.1 shows the influence parameters controlling the crack initiation and the crack propagation phases (Radaj, 1996).

The relative contribution of each of these periods to fatigue life is seen to depend on the geometry of the weld profile, size of the weld, nature of the residual stresses and severity of the weld discontinuities existing in the weldment. Two extreme kinds of weldments can be considered - one, where substantial weld discontinuities are present, and another, "ideal" weldment, which has blended weld toes and no weld discontinuity. The fatigue behaviour of these two different welded joints is greatly different.

In the case of "ideal" weldments free of discontinuities or post-weld treatment, the fatigue life of the welded joint can increase substantially, through increase in any or all of the life periods:

$$N_T = N_N + N_{p1} + N_{p2} \quad (2.2)$$

Stage II crack propagation generally dominates the fatigue life of a weldment, while crack nucleation and short crack growth periods are generally relatively short. A conservative assumption that

$$N_T \approx N_{p2} \quad (2.3)$$

can be made for domains where the failure criteria is a detectable crack (or the failure of the specimen), in presence of corrosion fatigue or when low quality welding procedures are used (Fisher et al., 1970, Gurney, 1979, Lawrence et al., 1996).

Table 2.1: Influencing parameters controlling each of the crack initiation and crack propagation periods in steels (adapted from Radaj (1996)).

	Crack initiation	Crack propagation
Material	type alloy grain size microstructure	type alloy* grain size* microstructure*
Component	shape size (technological, geometrical, statistical size effect)	shape size (technological, geometrical, statistical size effect)
Surface	roughness hardness σ_{res} significance of defects	significance of defects
Environment	temperature corrosion	temperature corrosion
Loading type	mean stress (+ σ_{res}) multiaxiality (phase angle)	crack opening mode mean stress multiaxiality
Loading course	amplitude spectrum amplitude sequence mean value sequence rest periods*	amplitude spectrum amplitude sequence mean value sequence rest periods
Crack	—	crack shape crack size

* parameter of secondary influence

2.3.2 Residual stresses and mean stress

Welding introduces tensile residual stresses, called short-range, local, residual stresses, which modify the mean stress in the welded joint under fatigue loading. Long-range, or reaction, residual stresses will also be introduced when welded members are connected together, due to imperfect fit-up. It is generally assumed that tensile residual stresses up to the yield strength of the material will be present in a welded structure. As a result, its fatigue life will be independent of mean stress and depend only on the applied stress range, even if this is compressive (Gurney, 1979). This is the reason why all the fatigue design recommendations rely on the use of the stress range, $\Delta\sigma$, regardless of whether it is tensile or compressive (Maddox, 2003).

Regarding the importance of the residual stress field on the fatigue life of welded details, it was long ago recognised (Gurney, 1979) that fatigue strength decreases with increasing dimensions of the testing specimens (with the same welded detail). As a result, to have a lower bound for the design S-N curves contained in design codes such as Eurocode 3, part 1-9 (prEN 1993-1-9:2003), only "large-scale" tests were included in the fatigue database used to define them. Recently, more sophisticated methods for measuring residual stresses (Synchrotron and neutron diffraction) have been used to improve the interpretation of the interaction between the above and fatigue performance (James et al., 2007), showing that this area however remains challenging. It was shown by several authors (ASTM, 1988)

that the modelling of the residual stress field effects on crack growth can be made using the concept of effective stress intensity factor range. Bremen (1989), Dubois (1994), Haagensen (1997) successfully applied this concept in a deterministic model of the crack propagation in specimens with welded attachments and subjected to different post-weld treatments, i.e. to welded joints with compressive residual stresses induced by treatments, which results in increasing fatigue lives. Fricke (2005) recently presented fatigue problems where the observed behaviour and shift of crack location in a welded detail is explained by the residual stress field, which can also be observed in tubular structures.

For tubular joints, an extensive review of available measured residual stress data in tubular joints was made by Stacey et al. (2000). In this reference, data is presented for a number of details applicable to tubular structures including: T-butt joints, pipe-to-endplate joints, tubular T- and Y-joints. It confirms that high tensile residual stresses are present in and near the welds, that residual stress distributions are highly variable, and the need to obtain further information on distributions in welded joints. Consideration for the uncertainties in the residual stress distributions due to welding can be found in (JCSS, 2001, Shetty and Baker, 1990). On this basis, Walbridge (Walbridge, 2005) modelled fatigue crack growth in tubular K-joints and considered uncertainties both in the residual stress distributions due to welding and post-weld treatment as two statistical variables, one for each stress type.

2.4 Methods for fatigue analysis of welded details

The estimation of the fatigue strength is an especially difficult task highly depending upon the geometrical or the technological stress raising effects and the resulting high variability in the stresses at the weld toe/root and their neighbourhoods (Tovo and Livieri, 2007). The fatigue strength describes a phenomenon which is not simply related to peak values of stresses but also to the mechanical behaviour of a structure sensible to the effect of a stress gradient.

The crack growth models used in mechanical, offshore and structural engineering domains to evaluate fatigue life are different as they usually concentrate on one of two main crack growth phases, namely: crack initiation or stable crack propagation. For crack initiation, most models are based on local notch strain approach (Dowling et al., 1977, Radaj et al., 1998). This approach utilises a strain-life relationship developed from the work of Basquin (1910), Coffin (1984), Manson (1953), Morrow (1965). Models based on local strain approach are able to take into account a number of load, geometry, material and environmental parameters. They can therefore be used to model size effects, but cannot account for the stable crack propagation phase.

For stable crack propagation, models are based on fracture mechanics (Lampman et al., 1996, Paris et al., 1998, Wang and Blom, 1991). These models can take into account all important geometry and loading parameters. In addition, they are capable of simulating several important aspects of fatigue crack propagation such as crack-closure effect (from the applied and residual stress fields), crack tip plasticity and fatigue threshold. They can therefore be used to model size effects, but cannot account for some material and microstructural aspects linked with the crack initiation stage. Some parameters have a large influence on crack initiation and little on stable crack propagation, and vice-versa.

Fatigue life of welded joints is frequently assessed by $S-N$ curve approach, using $S-N$ curves giving the design fatigue life for constant amplitude loading and using an appropriate damage accumulation law to consider the effect of variable amplitude loading.

Notches and stress gradients characterise welded structures, where often it is impossible to evaluate the maximum stress or strain due to geometrical discontinuities when a linear-elastic solution is adopted. Component $S-N$ data and a stress based approach are often used for design. Strain based approach is difficult to apply except where welds have well defined geometry and are of very high quality (free of crack-like defects).

To overcome these difficulties, several methodologies have been proposed (including nominal stress, hot-spot or structural stress approaches, etc.). Each of these methods suggests that a particular stress analysis is applicable to welded joints (Fricke, 2003, Poutiainen et al., 2004a, Radaj, 1995, Xiao

and Yamada, 2004):

1. The **Classification method**, or nominal stress approach, assigns different weld details with fatigue strength values largely based on experimental fatigue testing. Weld details with similar fatigue strength are then grouped into classes. The fatigue strength of a specific detail can be assessed by selecting the $S - N$ curve that represents a given safety or survival probability. Obvious drawbacks of this approach is that it can only deal with classified details and that it does not consider the size variations of a specific structural detail (Poutiainen et al., 2004b). As a consequence, detail category for K-joints (in EC3 (prEN 1993-1-9:2003)) is unusable for tubular bridge application due to the limits on the brace and chord thicknesses of 12.5 mm (Schumacher et al., 2002a). This method will not be further discussed here as it is well known from engineers.
2. The **Structural or hot-spot stress approaches**, sometimes also called geometric stress. Among the methods proposed in the literature to determine (numerically, experimentally or both) the structural stress range, the better known are the following:
 - ◆ Surface stress extrapolation method (hot-spot stress) - based on the stresses along the free surface. Extrapolation points are located in front of the weld toe, at distances defined according to weld plate thickness (see Section 2.4.1);
 - ◆ 1-mm stress - this method is based on the computed stress value 1-mm below the surface in the direction of the expected crack path (see Section 2.4.1);
 - ◆ Through thickness at the weld toe (TTWT) - the structural stress is calculated directly from the stresses in the cross-section of the weld toe. Although its distribution is non-linear, it is integrated first and then a linear distribution which produces the same membrane and bending force components is generated. The value of the linear function at the weld toe is the structural stress, according to this method (Poutiainen and Marquis, 2006);
 - ◆ Dong method - this method combines features of the through thickness and surface extrapolation procedures. This alternate structural hot-spot computation method is based on the equilibrium of nodal forces and claims to be a mesh-insensitive structural stress method. The stress state at a fatigue-critical location, the normal structural stress is presented in the form of membrane and bending components that satisfy equilibrium conditions (Dong, 2001, 2005);
3. The **Notch stress approach** needs information on the stress or strain distribution in the vicinity of the weld which can be obtained by FE analysis. The following variants of this approach exist in the literature:
 - ◆ Fictitious radius - where weld roots or toes are smoothed using a conventional value of the notch radius and strength is related to the stress value at the notch tip (Radaj and Sonsino, 1998);
 - ◆ Critical distance - where an effective stress is evaluated at a given distance from the tip and toes and roots are modelled as sharp notches (Susmel, 2008);
 - ◆ Average - where a mean value of stress, strain or energy is computed on a domain (line, area, volume) close to the notch tip (Livieri and Lazzarin, 2005);
 - ◆ Implicit gradient - the effective stress, weighted average of the stress, is computed by solving a second-order differential equation over all the component independently of its geometric shape. The solution is obtained by assuming the isotropic linear elastic constitutive law for the material and the maximum principal stress as equivalent stress (Tovo and Livieri, 2008);

Until now, nominal and hot-spot stresses have been preferred and are the most widely used approaches due to their simplicity. Due to advances in computer performances and 3-D modelling software it is likely that in a near future, 3-D solid modelling and methods based on the notch stress, or automatic crack growth based on LEFM, will be more extensively used in specific industry domains (automotive, machines,...). Two reasons are to explain for that: the design process is more and more done using semi-automatic 3-D modelling, thus simplifying structural engineers task to build solid models; the larger amount of DOFs generated by such models can now be managed by PCs in acceptable time. Secondly, the efficiency; as they are the only methods able to take into account all the geometric and loading aspects of the welded joint, they allow for easier identification of the potential critical crack initiation locations.

An alternative is the use of a **Linear Elastic Fracture Mechanics (LEFM)** approach based on the growth of the weld flaws modelled as cracks. This method uses a single parameter to characterise the stress state at the crack tip, the Stress Intensity Factor (SIF). The LEFM assumes that cracks, or crack like defects, are present in the structural detail at the very beginning of the fatigue life. Crack growth rates and crack sizes can be predicted at any life stage (Broek, 1986).

The methods that are used or referred to in this thesis work are further described in the following paragraphs.

2.4.1 Structural stress approaches

Structural stress approaches try to propose a stress solution excluding local effects from weld geometry. Dong (Dong, 2001) has proposed an alternative computation method for the structural stress that combines the through-thickness and surface extrapolation procedures. Poutiainen et al. (2004a) have proposed a new modified structural stress to better capture the stress state for thick plates or load-carrying welds. The methods from Dong and Marquis have been shown to better predict the size effect in welded joints than the current surface extrapolation method.

Xiao and Yamada (2004) have compared the stress concentration and its evolution in the through-thickness direction for different details under tension in order to separate the global and local stress concentration effects. On this basis, they have proposed to use the stress 1.0 mm below the surface as the stress parameter and shown by reanalysing the test results on cruciform joints that this parameter can predict well the size effect of plotted joints under tensile stress. This method could be promising but has not been applied to tubular joints yet.

Surface stress extrapolation

Surface extrapolation is based on the stresses along the free surface in the vicinity of the weld toe. Structural hot-spot surface stress, σ_{hs} , or geometric stress, includes all stress raising effects of a structural detail excluding all stress concentrations due to the local weld profile itself.

According to IIW - Fatigue Recommendations (XIII-1965-03/XV-1127-03 (Hobbacher, 2003), XIII-1819-00 (Niemi, 2000)), it can be extrapolated using FEM or experimental results and taking the stress values at different distances from the weld toe (see Figure 2.2).

For the specific case of CHS joints, the CIDECT (Zhao et al., 2000) suggests the use of extrapolation limits as shown in Table 2.2. Several different ways of determining the hot-spot do exist (a review on these methods can be found in (Maddox, 2001)).

The extrapolation method to use has been the object of several discussions (Romeijn, 1994, van Wingerde, 1992). In Schumacher (2003), in order to obtain comparable results, the extrapolation scheme proposed by Romeijn (1994) was followed. A second order polynomial is fitted to the strain data points in a region close to the weld toe, within the limits of extrapolation. A linear extrapolation to the weld toe is then carried out from the points corresponding to the fitted curve at extrapolation limits $L_{r,min}$ and $L_{r,max}$.

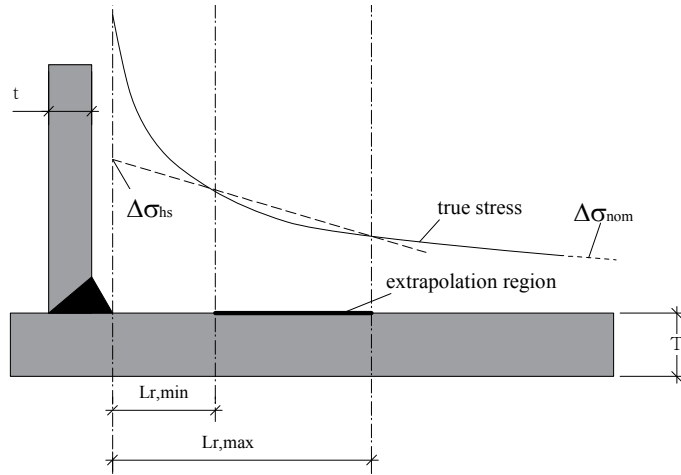


Figure 2.2: Extrapolated hot-spot stress as defined in (Zhao et al., 2000).

Table 2.2: Boundaries of extrapolation region for CHS joints (Zhao et al., 2000).

Dist. from weld toe	Chord		Brace	
	saddle	crown	saddle	crown
$L_{r,min}$		$0.4 \cdot T$		$0.4 \cdot t$
$L_{r,max}$	$0.09 \cdot D/2$	$0.4 \sqrt[4]{D/4 \cdot T \cdot d \cdot t}$	$0.65 \sqrt{d/2 \cdot t}$	
minimum value for $L_{r,min} = 4 \text{ mm}$				
minimum value for $L_{r,max} = L_{r,min} + 0.6 \cdot t$				

The stress concentration factor (*SCF*) is defined as the ratio between the hot-spot stress, σ_{hs} , and the nominal stress, σ_{nom} (away from stress rising singularity).

$$SCF = \frac{\sigma_{hs}}{\sigma_{nom}} \quad (2.4)$$

Through thickness - 1 mm stress method

A new method for evaluating the geometric or structural stress in welded connections was proposed by Xiao and Yamada (2004). This method is based on the computed stress value 1-mm below the surface in the direction of the expected crack path. It assumes the total stress distribution along the crack path to be the sum of the geometric stress caused by the structural geometry change and the highly non-linear local stress produced by the weld itself. This method considers that the stress concentration at weld toe is composed of two parts: the local peak stress due to weld profile and the geometric stress or hot-spot stress due to structural geometry change (e.g. a longitudinal attachment) as described by:

$$K_t = K_w \cdot K_s \quad (2.5)$$

where,

- K_t : the whole stress concentration at weld toe;
- K_w : the stress concentration due to weld profile;
- K_s : the structural geometry change stress.

The whole stress of a small size cruciform joint as represented in Figure 2.3 is thought to be equivalent to the local stress produced by the weld itself.

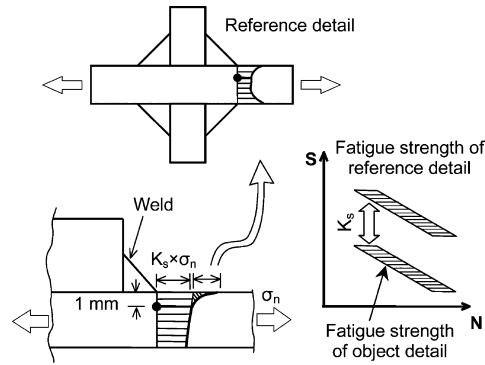


Figure 2.3: Reference detail to assess local stress produced by weld profile (from Xiao and Yamada (2004)).

In order to derive the structural stress, Xiao and Yamada propose to calculate the total stress and the stress produced by the local weld profile (obtained with a cruciform joint with the same weld toe geometry selected as a reference detail to express the local effect, Figure 2.3. The structural stress is then approximated by their ratio. At a depth of 1 mm, the following relationship can be written:

$$K_t(1\text{ mm}) = K_w(1\text{ mm}) \cdot K_s(1\text{ mm}) \quad (2.6)$$

Once the stress concentration due to the weld profile, $K_w(1\text{ mm})$, is approximately 1 at this depth, then $K_s(1\text{ mm}) \approx K_t(1\text{ mm})$. According to Xiao (Xiao and Yamada, 2004), a good correlation of crack propagation life can be established between studied detail and reference detail by using the geometric stress at a certain point along the crack path line. The following formula can be used to estimate the fatigue life of a detail based upon its structural stress at 1 mm in depth from the weld toe:

$$N_p = \frac{1}{(K_s(1\text{ mm}))^m} \cdot N_{pr} \quad (2.7)$$

where,

- N_p : life to propagate a crack from an initial size of 0.1 mm to a size of 10 mm;
- N_{pr} : life to propagate a crack from an initial size of 0.1 mm to a size of 10 mm for the reference detail;
- $K_s(1\text{ mm})$: structural stress at 1 mm in depth;
- C : material related parameter (Paris Crack Growth Law exponent);
- m : mechanical related parameter (Paris Crack Growth Law exponent (Paris, 1960)).

Note that the exact depth found was equal 1.3 mm, though, due to the flat stress gradient of geometric stress the stress at 1 mm in crack path results in a good correlation of fatigue propagation life. Since the studied detail and the reference detail may have different final or fracture crack length values the correlation might not be performed through the whole range of crack propagation. However, since most of the fatigue life is consumed when the crack is still small, the influence of the fracture value on fatigue life is not so significant.

2.4.2 Fracture Mechanics approach

In fatigue, Linear Elastic Fracture Mechanics (LEFM) is predominantly used. In this method, it is assumed that cracks or crack-like defects are present at the beginning of the fatigue life. LEFM focuses in describing the stress state in the vicinity of the tip of a crack. It has been shown by Irwin (Broek,

1986), that the stress state very close to the tip of a crack in a ductile material, as well as in a brittle one, can be described with a unique parameter under certain hypothesis (plane strain state). This parameter is referred to as the stress intensity factor (SIF) or K . Further, it has been shown (Paris, 1960) that the range of this parameter, $\Delta K = K_{max} - K_{min}$, can be used to characterise fatigue crack propagation. ΔK can be described by the following general expression:

$$\Delta K = Y \cdot \Delta \sigma \sqrt{\pi \cdot a} \quad (2.8)$$

where,

- a : crack depth;
- $\Delta \sigma$: stress range;
- Y : correction factor to adjust for free surface, finite thickness of the plate and non-uniform applied stress distribution.

In the case of constant amplitude loading, the applied stress intensity factor range can be related to the rate of crack growth using, in general, the Paris law:

$$\frac{da}{dN} = C \cdot \Delta K^m \quad (2.9)$$

where,

- a : crack depth;
- $\frac{da}{dN}$: crack propagation rate;
- C, m : constant and exponent of Paris law.

Several modifications to this relation are proposed in literature in order to include effects such as the crack closure, fatigue threshold, or residual stresses, in the ΔK parameter.

Integrating Paris law between initial and final crack sizes, permits the calculation of the fatigue life of a welded detail:

$$N_f = \int_{a_i}^{a_f} \frac{1}{C (\Delta K)^m} da \quad (2.10)$$

where,

- N_f : number of cycles needed to propagate a crack from a depth of a_i to a depth of a_f ;
- a_i : initial crack size;
- a_f : final crack size;

The determination of the stress intensity factor ranges, ΔK , depending on the complexity of the geometry and the existence, or not, of tables or equations, using numerical methods of structural analysis such as Finite Elements (FEM) or Boundary Elements (BEM) methods.

2.5 Numerical methods

2.5.1 Finite element method (FEM) and Boundary element method (BEM)

The estimation of a fatigue crack life using the theory of Linear Elastic Fracture Mechanics (LEFM) involves the calculation of stress intensity factors (SIF) at a number of discrete crack depths.

Different methods can be used to estimate SIFs. Most of them involve the use of expressions deduced from parametric studies on specific geometry ranges. A more complex way involves advanced modelling of the crack by finite element or boundary element codes.

The finite element method has been widely used in fracture mechanics applications. Recent investigations applied the finite element method to simulate the crack behaviour in CHS joints (Cao et al., 1998), (Shao, 2005). An intrinsic feature of the finite element method, common to all these formulations, is the need for continuous remeshing of the three-dimensional volume to follow the crack extension; this is a practical disadvantage of this method (Mellings et al., 2003).

In the boundary element method, only the boundary of the domain of interest is discretised (Portela et al., 1993). This is done using elements which are interconnected at discrete points called nodes. One disadvantage of this method is that it can only be used for linear elastic problems. However this is not an issue in modelling fatigue life in the long life region (the opposite from oligocyclic fatigue).

Hybrid approaches, combining both Finite Elements and Boundary Elements may couple the specific advantages of each method and eliminate disadvantages. They have been the focus of a number of investigations but are still under development and not available as ready to use packages for 3-D complex geometries (Forth and Staroselsky, 2005).

2.5.2 Boundary element method, BEM

The boundary element method is a solution technique for the well known coupling equation:

$$K_m \cdot u = f + p \quad (2.11)$$

where,

- K_m : stiffness matrix;
- u : displacements vector;
- f : support reactions vector;
- p : negative end fixing forces.

For a three-dimensional boundary element problem the mesh is two-dimensional. Because only the surface of the domain needs to be discretised, it is easier to use BEM than FEM. However, if interior data are required, the method becomes computationally costly. Also, for large geometries, as the matrix is full and unsymmetrical, the BEM is computationally expensive.

Application of the boundary element method to fracture mechanics problems is well described in literature. The direct solution of a crack problem is not possible using BEM in a single region. This is due to the coincidence of crack surfaces which creates a singular system of equations (Mi and Aliabadi, 1994). To overcome this problem, a dual boundary element method is used, incorporating two independent boundary integral equations, the displacement equation applied for collocation on one of the crack surfaces and the traction on the other. Detailed information can be found in (Mi and Aliabadi, 1994) and (Hartmann, 1989).

The model presented in the current investigation uses Boundary Element Method (BEM) commercial code (BEASY, 2003). This software was developed by *Computational Mechanics* in Southampton and its features can be summarised as follows:

BEASY uses the Dual Boundary Element Method (DBEM) to predict the stress field for cracked structures and hence to predict the stress intensity factors along the crack front. The analysis method implemented is based on the theoretical foundations developed for two-dimensional analysis by Portela, Aliabadi and Rooke (Portela et al., 1993) and for three-dimensional analysis by Mi and Aliabadi (Mi and Aliabadi, 1994). In the Dual Boundary Element method, the crack in a structure is represented by special "Dual" elements that allow the stress and displacement fields to be computed on both crack faces without the need to subdivide the body along the crack boundary. The Dual Boundary element method is a powerful solution tool for fracture mechanics, because it is a boundary only representation, it is highly accurate, and is able to represent the rapidly changing stress fields near the crack front. in (Mellings et al., 2003)

The stress intensity factors (SIF) for the three opening modes (K_I , K_{II} , K_{III}) are computed using crack opening displacement (COD) formulas, which are given, at crack front node Q (see Figure 2.4), by:

$$K_I^Q = \frac{E}{4(1-\nu^2)} \sqrt{\frac{\pi}{2r}} (\Delta u_b^P) \quad (2.12)$$

$$K_{II}^Q = \frac{E}{4(1-\nu^2)} \sqrt{\frac{\pi}{2r}} (\Delta u_n^P) \quad (2.13)$$

$$K_{III}^Q = \frac{E}{4(1+\nu)} \sqrt{\frac{\pi}{2r}} (\Delta u_t^P) \quad (2.14)$$

where,

- P : first node away from the crack front;
- r : vector from Q to P;
- n : unit normal at the crack front;
- Δu^P : displacement evaluated at point P;
- Δu_b^P : projections of Δu^P on the local binormal coordinate directions at the crack front;
- Δu_n^P : projections of Δu^P on the local normal coordinate directions at the crack front;
- Δu_t^P : projections of Δu^P on the local tangential coordinate directions at the crack front.

Further details can be found in Mi and Aliabadi (1994), Wilde and Aliabadi (1999).

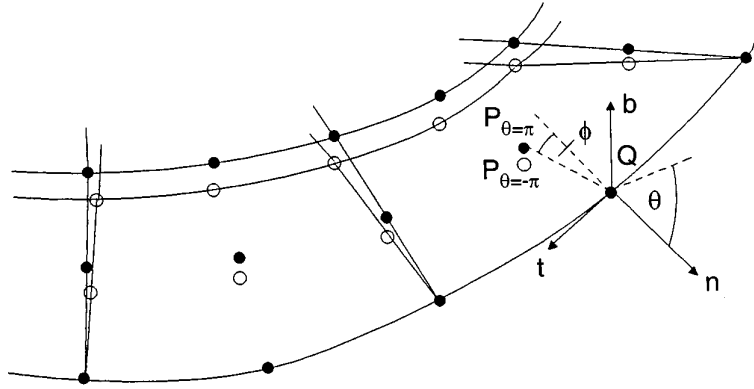


Figure 2.4: One point crack opening displacement - coordinate system at crack front (from Wilde and Aliabadi (1999)).

2.6 Size effects

2.6.1 Size effects in fatigue

Although there is a large amount of literature on "size effects", both related to static or fatigue behaviour of structures, the fact is that the terminology is confusing, there is a number of terms that are not always understood in the same way by different authors (Bazant, 1984, Carpinteri et al., 2001, Mashiri et al., 2007, van Wingerde, 1992). This section aims to clarify these and introduce a coherent terminology that will be used throughout this thesis work.

Definitions

◆ General:

- ◇ **Size effect:** generic term which deals with the consequences resulting from the modification of the dimensions of the sample (specimen) under study. Used in many domains: physics, engineering, finance, etc.
- ◇ **Structural size effect:** It is well-known from experimental evidence that the nominal strength of a material, and as a consequence the structure made of it, changes as a function of its dimensional size. Due to this phenomenon, called size effect, strength ceases to be a material constant. Various theories on size effect give interpretations of this experimental evidence and different models linking material strength with a characteristic structural size have been presented (Bazant, 1984, Carpinteri, 1994, Carpinteri et al., 2001, Weibull, 1939). A broad review on size effect on structural strength can be found in (Bazant, 1999).
- ◇ **Scaling effect:** particular case of sizing effect. As defined in Physics, the size modification is an homothety: all the proportions are conserved.

◆ Steel Tubes:

- ◇ **Scaling effect in tubular joints:** This concept was introduced by Mashiri et al. (2007). It includes, according to the authors, complete proportional, practical proportional and non-proportional scaling.
 - **Complete proportional scaling** states for the case where all the dimensions affecting fatigue are scaled proportionally (equivalent to a homothety). Associated with this concept, the so called "(complete) thickness effect", as the thickness is the only parameter needed to describe the relative fatigue life of two joints.
 - **Practical proportional scaling** happens when only the important dimensions are scaled proportionally.
 - **Non-proportional scaling** is the case where important factors influencing fatigue behaviour are not scaled proportionally.

◆ Metal fatigue:

- ◇ **Fatigue Size effect:** In the specific case of fatigue strength, three basic theoretical arguments are currently accepted (Dijkstra and van Straalen, 1997, Marshall, 1992b, Örjasäter, 1995, van Wingerde et al., 1997) when trying to interpret the size effect: statistical, technological and geometrical. These effects can be studied by comparing the fatigue behaviour of welded joints using a scaling effect. They are summarised here based on (Marshall, 1992a):
 - **statistical** The statistical size effect refers to the increased probability of having a larger variation in material properties and a larger flaw with an increase in stressed volume. This effect is also called volume effect. As the fatigue is a weakest link process, in the case for example of transverse attachment or built-up I sections, the length of the weld toe from which the cracks initiate is an influencing factor for fatigue strength.
 - **technological or metallurgical**
The technological or metallurgical size effect implies that an increased plate size (thickness) may result in a different grain structure (coarser), different surface roughness, lower yield strength, higher residual stresses (caused by welding in different plate thicknesses), welding processes, weld shape, increased probability of hydrogen cracking during fabrication and lower notch toughness.

- **geometrical** The geometrical size effect refers to the stress gradient that arises at geometrical discontinuities (e.g. notches, welded details) and/or due to bending stresses. Due to the presence of a steeper stress gradient, a unit volume of material at a geometrical discontinuity on or close to the surface of a thin specimen will experience a lower strain than the same unit volume of a thicker specimen, for the same stress at the surface. Geometrical size effect can be described as the resultant of three primary characteristics of the detail under consideration (Berge and Webster, 1987): The magnitude of the stress concentration at the weld toe; the gradient of the stress along the "plane", i.e. can also be a curved surface, of crack growth; the number of crack growth cycles needed to go through the steep stress gradient region, relative to the total number of cycles to failure.

2.6.2 Historical review on size effects in fatigue

The thickness effect phenomenon has been object of numerous investigations from as early as the 1950s to this day. These contributions have led to a better understanding of the influence of plate and or tube-wall thickness on fatigue strength of welded connections. A brief review is presented based on (Mashiri et al., 2007). Gurney (1979) pointed out that thickness effect could be demonstrated using both fracture mechanics theory and experimental work. This research led to the introduction of a thickness correction factor in the revised version of the UK Department of Energy Guidance Notes in 1984. Gurney (1989) also noted that a lot earlier than the introduction of the thickness effect on fatigue of welded connections, Phillips and Heywood (1951) had demonstrated the size dependence of fatigue strength of unwelded specimens. Gurney (1989) also pointed out that it had long been known that plate thickness was likely to be a relevant variable for fatigue strength under bending stresses, because the stress gradient through the thinner specimen would be steeper and therefore less damaging than that in thicker specimens. Gurney (1977) showed with the use of fracture mechanics theory, that fatigue strength of welded joints could be affected by plate thickness even when they were subjected to axial loading.

Using $S - N$ data for plate welds and for tubular joints, covering the range of plate thicknesses up to 50 mm, Gurney proposed an empirical thickness correction for fatigue strength.

Thickness influence is obtained by plotting the relative fatigue strength versus the thickness of the failing member. Gurney (1989) obtained the relationship between fatigue strength and thickness of member under failure by plotting the relative fatigue strength normalised to a thickness of 32 mm versus the thickness of different plate and tubular joints (see Figure 2.5 and Equation (2.15)).

A **thickness correction factor** can be used to predict the fatigue strength of wall thicknesses other than the reference thickness. According to Gurney, it can be described using the following expression:

$$S = S_{\text{ref}} \cdot \left(\frac{T_{\text{ref}}}{T} \right)^n \quad (2.15)$$

where,

- S : fatigue strength for plate thickness T ;
- S_{ref} : fatigue strength for reference plate thickness T_{ref} ;
- T_{ref} : reference plate thickness up to which the design rules are directly applicable without penalty;
- T : plate thickness;
- n : thickness correction factor exponent (for plates, $n = 0.25$).

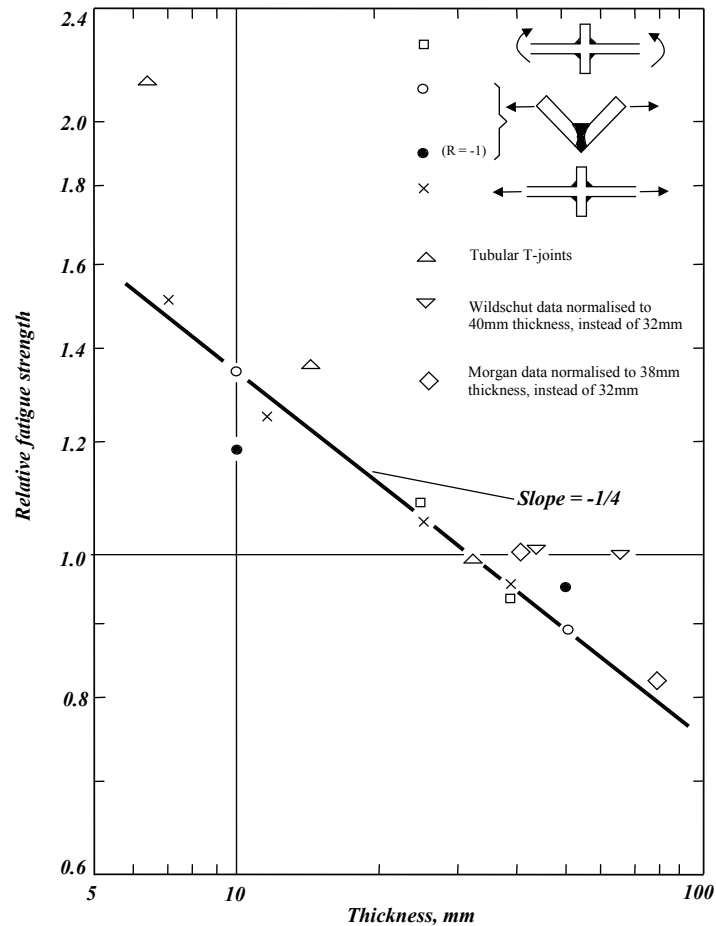


Figure 2.5: Influence of plate thickness on fatigue strength, normalised to a thickness of 32mm. All tests at $R=0$ except where stated (from (Gurney, 2006)).

It has been shown later that this "thickness" effect concept can be generalised by also allowing for the overall geometry of the joint, notably the attachment size (Maddox, 1987, 1995, Smith and Gurney, 1986), which means that this represents a size effect and not only a "thickness" effect anymore.

van Wingerde et al. (1997) analysed a large database containing fatigue test results on tubular joints. Through statistical analysis of this database, and taking the thickness of the failed member as the parameter influencing the most the fatigue behaviour, van Wingerde et al. (1997) determined a base $S_{r,hs} - N$ design curve for $T = 16$ mm, using the characteristic curve at $1.64 \cdot s_N$ of the dependent variable ($\log N$) below the mean and a forced slope of $m = 3$. The size correction (see Equation (2.16)) was established based on a maximum reduction of the scatter in the fatigue life (N_4). In the study by van Wingerde et al. (1997), the size correction is based on the hot-spot stress at the weld toe. This is a major difference when compared to Gurney, who based the size correction on the nominal stress away from the welded detail. The use of the hot-spot based $S - N$ design curve configures a size correction and, again, not anymore a thickness correction factor, since non-proportional scaling is included.

2.6.3 Size effect in existing recommendations for tubular joints

Various design guidelines are available and used around the world for the design of tubular structures. With respect to fatigue design, the American Petroleum Institute's (API, 2000) recommended practice, the American Welding Society's structural steel welding code (AWS, 2000) as well as the Eurocode 3 - Part 1.9 (prEN 1993-1-9:2003) and the CIDECT Design guide (Zhao et al., 2000) all recommend the use of both the classification method (based on nominal stress approach - and, as stated before, not

usable for tubular bridge applications) and the hot-spot stress method (Mashiri et al., 2008).

These hot-spot based $S - N$ curves, however, as the nominal $S - N$ curves before them, have been shown not to be able to correctly capture the size effect without a correction (Gurney, 1977, 1979, van Wingerde et al., 1997).

Thus, similar thickness correction factor expressions as Equations (2.15) and (2.16) have been included in EC3 (2003), the Australian Standard, AS4100-1998 (SAA 1998), BS7608 (BSI 1993), IIW recommendations (Hobbacher, 2003) and Department of Energy (1990) guidelines.

In current fatigue design guidelines for circular and rectangular hollow section joints such as IIW (2000) and the CIDECT Design guide (Zhao et al., 2000), the thickness effect has been incorporated into the hot-spot stress $S - N$ curves, resulting in shorter fatigue life for thicker walled tubular members under fatigue loading. The following expressions describe the size effect for the fatigue strength of CHS joints, as determined by van Wingerde et al. (1997):

$$\frac{S_{r,hs,T}}{S_{r,hs,16}} = \left(\frac{16}{T} \right)^n \quad (2.16)$$

$$n = 0.06 \cdot \log N_4 \text{ for } 10^3 < N_4 < 5 \times 10^6$$

$$n = 0.402 \text{ for } 5 \times 10^6 < N_4 < 10^8$$

where,

- $S_{r,hs,T}$: hot-spot stress range for tube thickness T ;
- $S_{r,hs,16}$: hot-spot stress range for reference tube wall thickness $T_{\text{ref}} = 16$ mm;
- T_{ref} : reference plate thickness up to which the design rules are directly applicable without penalty;
- T : thickness of failed member;
- n : size effect exponent;
- N_4 : number of cycles to failure (complete loss of strength).

The determination of the above expression is based on statistical analysis of all $S - N$ data on circular and rectangular hollow section joint types and loadings. Thus, many effects and joint parameters are included and fail to be distinguished.

In (HSE, 2001, Lotsberg and Larsen, 2001, Mashiri et al., 2008), reviews of the existing design guides for tubular joints are provided. Table 2.3 summarises the values of the thickness effect correction.

Table 2.3: Thickness effect in existing standards.

		EC3	API RP2A	IIW / CIDECT
Standard plate connection	T_{ref}	25	–	25
	n	0.25	–	0.1, 0.2 or 0.3
Tubular joints	T_{ref}	25	16, 25	16
	n	0.25	0.25	$0.06 \cdot \log N$

The thickness correction factor adopted by CIDECT Design Guide No. 8 and IIW has one of the most severe exponents ($n = 0.378$ at $N = 2 \times 10^6$ cycles). This thickness correction factor depends on the number of cycles to failure (N); the less the number of cycles, the less pronounced the thickness effect. Furthermore, these guides are currently limited to tube thicknesses between 4 mm and 50 mm inclusive (for circular tubes) and chord slenderness, $\gamma > 12$.

2.7 Recent research on the fatigue behaviour of tubular K-joints

In 2003, Schumacher, through experimental tests and numerical calculations, investigated the joint stresses at critical fatigue locations and the size effect on the fatigue resistance of CHS K-joints (Schumacher, 2003). Schumacher concentrated in joint geometries typical to bridge application ($\gamma < 12$). Sixteen tubular joint specimens were tested at the Steel Structures Laboratory (EPFL). The parameters covered by this study included member dimensions, fabrication methods and weld improvement.

For the directly welded joints, Schumacher (2003) carried out a total of 4 test series with 2 test specimens per series. Each test series examines a particular parameter: dimension, fabrication method or weld improvement. The non-dimensional parameters of the specimens were chosen to reflect actual CHS truss bridge parameters. Except for the weld-improved specimens, twelve out of the sixteen welded joints cracked at the same location and in the same manner. Cracks initiated in the chord gap region at the tension brace weld toe, referred to as Location 1 (Figure 3). This corresponded with the location of the highest measured hot-spot stress. Crack propagation occurred through the depth of the chord as well as along the weld toe.

Schumacher found that the measured hot-spot stresses at locations of fatigue cracking were lower than the hot-spot stresses calculated using current design guides. Different fatigue resistances were observed for joints of different sizes.

Tables and graphics providing stress concentration factor (SCF) values for the different hot-spot locations in a parametric range typical to bridge design can be found in (Schumacher et al., 2003).

Concerning the effects of joint size and scale, Schumacher underlines different points related to the fatigue test results database used as base for size correction definition: the inclusion of many different parameters and the large degree of scatter in the data and the lack of data for joint thicknesses typical relevant for bridge design. All these arguments highlight doubts regarding the correction factor for size effect that was obtained from this database and in particular its applicability to bridge joints.

Furthermore, Schumacher concludes that it does not seem justified to apply a size correction factor greater than the factor proposed by Gurney (1979) ($\left(\frac{T_{ref}}{T}\right)^{0.25}$), i.e. the size correction factor in current recommendations (Equation (2.16)) is too penalising. By means of statistical and analytical analysis, Schumacher (2003) questioned whether the correction factor for the size effect of tubular joints is a fair representation of the actual size effect problem, in particular for bridges.

The work carried out at the Nanyang Technological University, (Singapore) in recent years focused in tubular joint fatigue behaviour. This research work concentrated principally in numerical simulation (using FEM), crack meshing technics and has been validated using experimental tests of isolated joints, loaded in the braces, instrumented with ACPD system. Details can be found in a number of publications (Chiew et al., 2004, Lie et al., 2005a,b, 2004, Shao, 2005, 2007, Shao et al., 2008, Shao and Tjhen, 2005).

Of particular interest for the present work, Shao (2005) proposed a new modelling method for uni-planar tubular K-joints containing an arbitrary surface crack located along the chord weld toe. A FEM mesh generation technique was developed, according to which, the crack is defined first in a 2-D plane and then mapped onto a 3-D curved surface. The numerical model was validated by comparisons to two full-scale tubular joints. Shao modelled and analysed the stress intensity factors of K-joints containing a surface crack. An extensive parametric analysis served as basis for a database of SIF values. The parametric range of this study was taken from CIDECT (Zhao et al., 2000) ($\gamma \in [12, 30], \beta \in [0.3, 0.6], \tau \in [0.25, 1]$), thus not including low γ geometries typical to bridge design. The joint eccentricity was not considered. It included two loading situations: balanced axial load of the braces and balanced in-plane bending of braces. Shao proposed parametric equations for the determination of SIF values at different crack depths. He however did not study size effects in his original work. Afterwards, he studied the geometrical effect (non-dimensional parameters β, γ, τ and chord length ratio) on the stress distribution along the weld toe (Shao, 2007, Shao et al., 2008) (for T-

and K- joints), but no correlation between the stress concentration and the fatigue life or strength is made.

At the Monash University, the effect of thickness and joint type on fatigue performance of welded thin-walled joints has been studied. This research has concentrated mainly on thin-walled T-joints (CHS and RHS). Fatigue life for thin T-joints ($t < 4$ mm), tested in laboratory, was found to be below the expected CIDECT design $S_{r,hs} - N$ curves (Zhao et al., 2000). The greater negative impact of the weld toe defects such as undercut on the crack propagation life is responsible for this phenomenon which is contrary to the conventionally accepted size correction estimations, according to the authors.

2.8 Summary and conclusions

This chapter gives an introduction on the main concepts related to this thesis work. A brief overview of the fatigue behaviour of tubular joints is presented, namely: methods for fatigue assessment of welded joints, existing research on size effects, current design recommendations and recent research on tubular joint fatigue. This review resulted in the following conclusions:

- ◆ Multiple and sometimes confusing definitions exist in the literature to describe the size effect phenomenon in fatigue. Three terms are commonly employed to describe the effects under consideration and not always with the same meaning: scale effect, thickness effect and size effect. A concept for terminology clarification is presented.
- ◆ The Linear Elastic Fracture Mechanics method can be used to describe the fatigue behaviour of welded joints with complex geometries, taking in account the different dimension parameters by means of adequate computer simulations.
- ◆ The Boundary Element Method is an efficient method that can be used to calculate the stress intensity factors of surface cracks in CHS joints.
- ◆ The range of applicability of current fatigue specifications is limited and does not cover geometries typical to tubular bridge design. A lack of data for joint thicknesses typical to bridge applications and the scatter in the data related to the inclusion of many different parameters has been noticed.
- ◆ It does not seem justified, for CHS K-joints, to apply a size correction factor greater than the factor proposed by Gurney (1979) for plated joints (see Equation (2.16)).

Experimental Investigation

3.1 Introduction

Fatigue tests allow for a better understanding of the cracking process and the uncertainties resulting from the fabrication that may influence the fatigue life of the structure.

In our study, two uniplanar tubular truss beams were tested under fatigue loading. Each beam comprised 6 nodes are simultaneously tested nodes under different loading conditions resulting in a possible total of 12 data points. Also, several joints were equipped with a specific crack depth measuring system (Alternate Current Potential Drop, ACPD system) in order to get more information out of each test. The test beams were designed to augment the database comprising about 180 test results worldwide.

In Section 3.2, the test specimens are described regarding their dimensions, fabrication and material properties. In Section 3.3, the procedure and the instrumentation for static and fatigue tests are detailed. Measurements obtained during the tests are summarised and the main results are discussed in Section 3.4.

3.2 Description of test specimens

Two uni-planar CHS welded truss beams were tested under fatigue loading. These beams represent a fifth series, S5 (S5-1 and S5-2), which follows four series of similar specimens previously tested by Schumacher (2003).

Each one of the trusses consists of nine welded K-joints (see Figures A.1 and A.2 in Appendix). Four of them, namely j1, j2, j5N and j5S (see Figure 3.2) were selected to be studied in detail because of the respective loading conditions. Compared to the previously tested specimens, the S5 specimens are fabricated out of CHS tubes only, welded together (see Figure 3.1), while the previous series had an I-beam as the top chord, bolted onto the tubular joints. Table 3.1 shows the dimensions and geometry parameters of the series S5 and the series previously tested at ICOM (Schumacher and Nussbaumer, 2006). Series S1 to S4 were proportionally scaled, i.e. non-dimensional parameters remained constant. Series S5 represents a non-proportional scaling of the previous series (lower γ and τ). The non-dimensional parameters were: $\theta_{br} = 60^\circ$; $\beta = 0.53$; $\gamma = 4.21$, $\tau = 0.4$ and $e/D = 0.13$. These are parameters typical to CHS truss bridges.

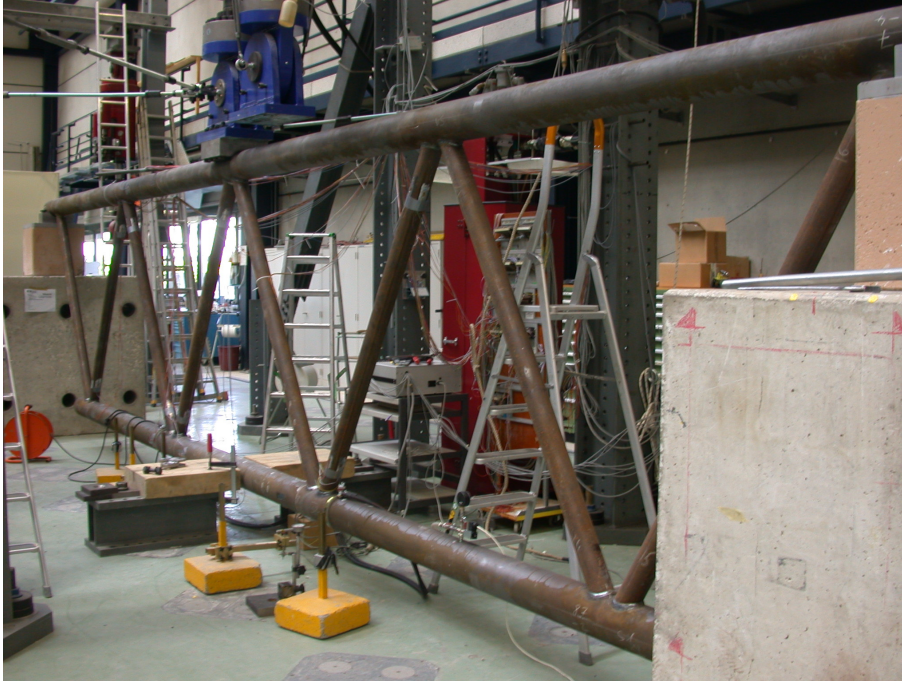


Figure 3.1: Tubular truss fatigue test setup.

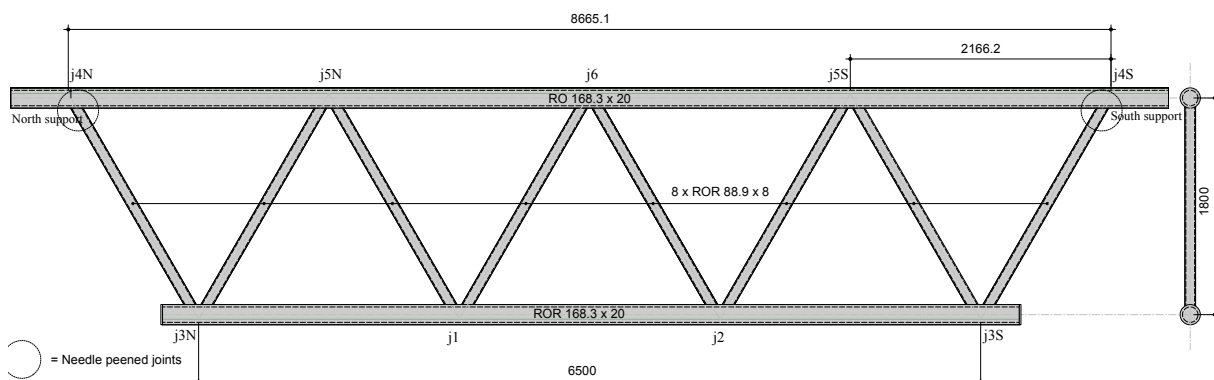


Figure 3.2: Tubular truss and joints nomenclature.

3.2.1 Material properties and dimensions

Truss members are made of steel S355 J2 H conforming to EN10210-1:1994 and EN10210-2:1997. This refers to a weldable steel with a minimum tensile yield stress, f_y , of 355 N/mm^2 (for nominal thicknesses $\leq 16 \text{ mm}$) or 345 N/mm^2 (for $16 \text{ mm} < \text{nominal thickness} \leq 40 \text{ mm}$), and a minimum ultimate tensile stress, f_u , between $490 - 630 \text{ N/mm}^2$ at 22% elongation. The minimum toughness of the steel is defined as 27 J at -20°C .

The diameters and thicknesses of the tubular members were measured. All measures meet the terms of the EN 10210-2:1997 tolerance requirements.

3.2.2 Specimen fabrication

Brace members were cut to fit the contour of the chord using computer controlled technology. Bevels were prepared at angles ranging from 30° to 45° . Backing-rings were used to facilitate the welder's task and make sure complete penetration of the weld is achieved (see Figure 3.3). In this way a fully penetrated weld could be applied continuously around the brace-chord intersection. A MAG cored

Table 3.1: Fatigue test series tested recently at ICOM.

ID	Nom. Dimensions [mm]			β	γ	τ	e/D	Weld	No. joints
	Bottom Chord	Top Chord	Brace						
S1*	273 × 20	I-beam	139.7 × 12.5	0.51	6.83	0.63	0.09	F, B	4
S2*	273 × 20	I-beam	139.7 × 12.5	0.51	6.83	0.63	0.19	F	4
S3*	168.3 × 12.5	I-beam	88.9 × 8	0.53	6.73	0.64	0.20	F, B	4
S4*	273 × 20	I-beam	139.7 × 12.5	0.51	6.83	0.63	0.20	F, B, W	4
S5	168.3 × 20	168.3 × 20	88.9 × 8	0.53	4.21	0.4	0.13	F, B	8

*(Schumacher, 2003)

F : Full penetration weld

B : Backing ring

W : Weld improved

metal arc welding with active gas shield (process 136) using covered electrodes in accordance with AWS A5.20:E71 T-1 was used.

Non destructive testing controls of the welds were done by the fabricator following SIA 263/1 code (SIA 263) (requirement weld quality B: 100% VT + 50% UT).

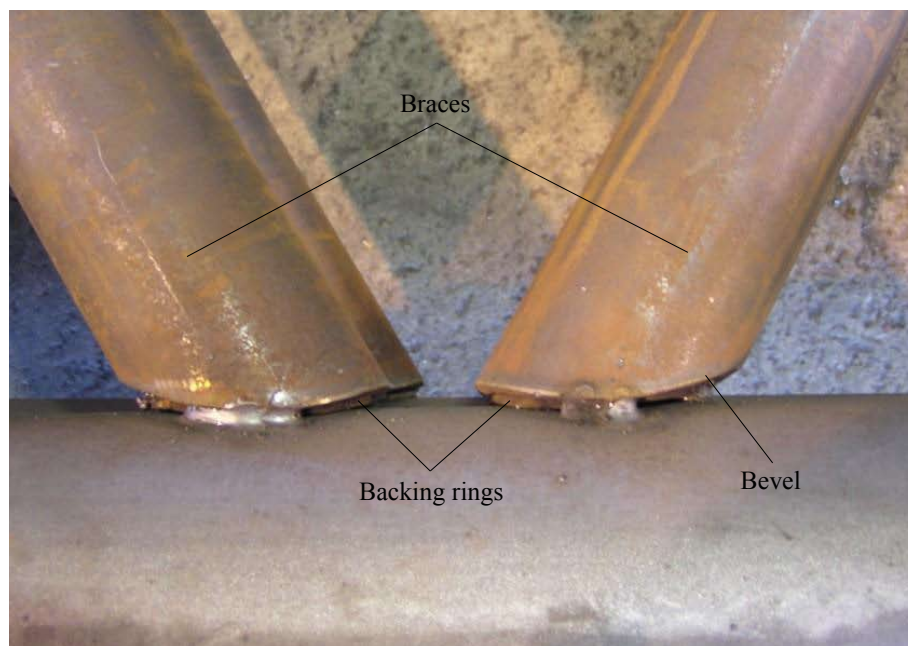


Figure 3.3: Preparation of joint before welding, backing rings and bevel.

Two plates were welded at the bottom chord extremities so that this tube could be put under air pressure (2 bar) and thus through depth cracks detected by depressurisation, a technique already used by Schumacher.

3.2.3 Weld geometry

Weld size has an important effect on the stress concentration at the weld toes of tubular joints. In order to measure the weld size of joints, a mould impression of the welds was done using *Rhodorsil RTV 3535* (Chimie, 2002). This modeling material presents a very low shrinkage, fast hardening and easiness for application (Figure 3.4).

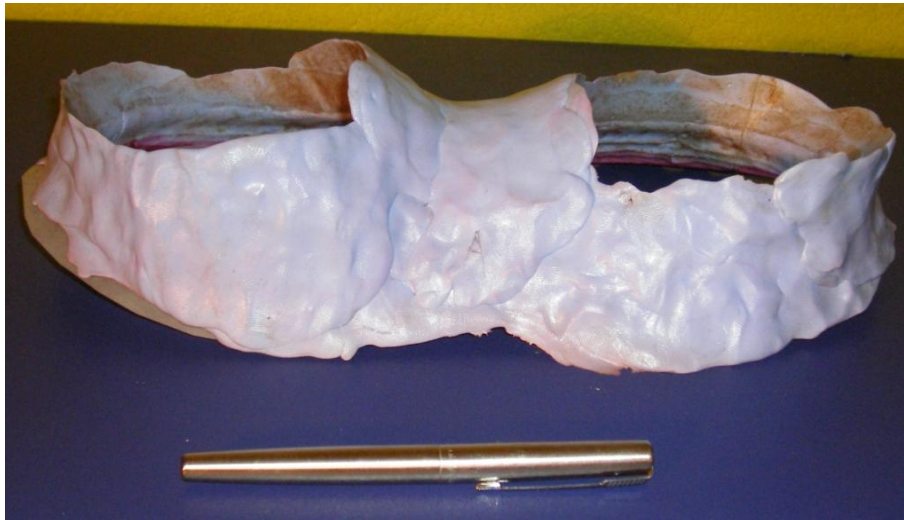


Figure 3.4: Detail of welded joint mould impression.

Real weld dimensions were then compared to the American Welding Society (AWS) recommendations (see Figure 3.5). AWS recommendations are globally fulfilled for both joints S5-j1 and S5-j2 and actual weld size is found to be normally much larger than AWS minimum recommendation but consistent.

3.3 Test procedure and Measurements

3.3.1 Supports and load introduction

The truss beam was simply supported at its extremities (with an eccentricity of about 70 mm to 90 mm) and the load introduced at mid-span (Figure 3.6). Three steel blocks were machined to fit the top chord circular shape with the support blocks thus allowing a proper introduction of the load at mid-span.

For the sake of safety, and to prevent possible instability, blocks with a *Teflon* layer were put in place on each side of the bottom chord to provide lateral support.

3.3.2 Static tests

Static tests were carried-out in order to: verify the linearity of the loading/unloading response, check symmetry, verify that the out-of-plane bending remains negligible, determine the nominal stress in the joints and evaluate the hot-spot stresses (for S5-2). Nominal stresses and hot-spot stresses were then used to validate the numerical model.

Before the fatigue test started, preliminary static tests were carried out, with the maximum force being increased stepwise up to approximatively the maximum required in the fatigue test (≈ 600 kN) and unloaded back to the minimum load in the fatigue test (≈ 60 kN). Static tests were then repeated about every 60000 cycles. The lateral displacements were not significant.

Deflection and load measurements

The load and deflection of the beam were measured during both static and fatigue tests. They were taken from the previously calibrated hydraulic jack output. In addition, an external Linear Variable Displacement Transducer (LVDT) was installed at mid-span under the bottom chord.

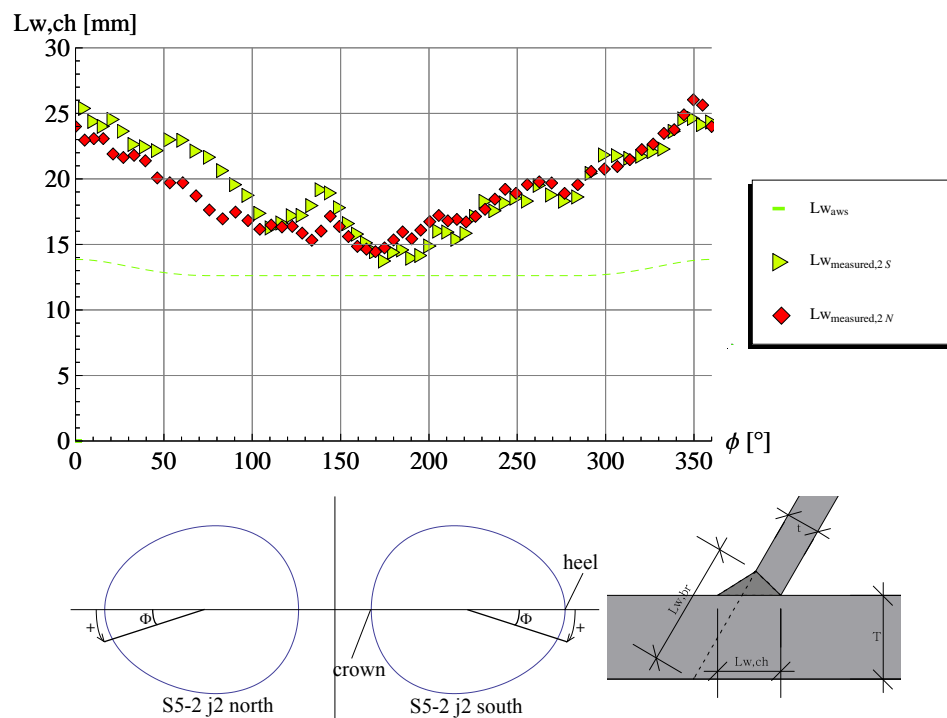


Figure 3.5: Comparison of different weld leg lengths on chord.

Strain measurements on members

Strains were measured on truss members during the static tests using uniaxial electrical resistance strain gages (HBM LY11-10/120) glued to brace and chord members. Gages were positioned in pairs, at two or four points around tube cross section following the same procedure taken for similar fatigue tests carried-out by Schumacher (2003).

The location of the gages changed from beam S5-1 to S5-2. Figure 3.7 shows strain gages placed at distances corresponding to $1.9D$ (chord) and $2.2d$ (brace) from the joints. Figures A.1 and A.2, in appendix, provide strain gages position drawings.

Strain measurements in joints

Strains in the vicinity of brace-chord welds were measured with uni-axial strip gages (TML FXV-1-11, 5-element 2 mm grid length) on specimen S5-2 for joints j1 and j5N. The strains measured were then linearly extrapolated to the weld toe to determine the hot-spot strain.

Due to the small gap between diagonals it was not possible to measure in this location, instead two strip gages were positioned perpendicular to the weld toe and at an angle of 30° with the longitudinal direction, on each side of the gap (see Figure 3.8).

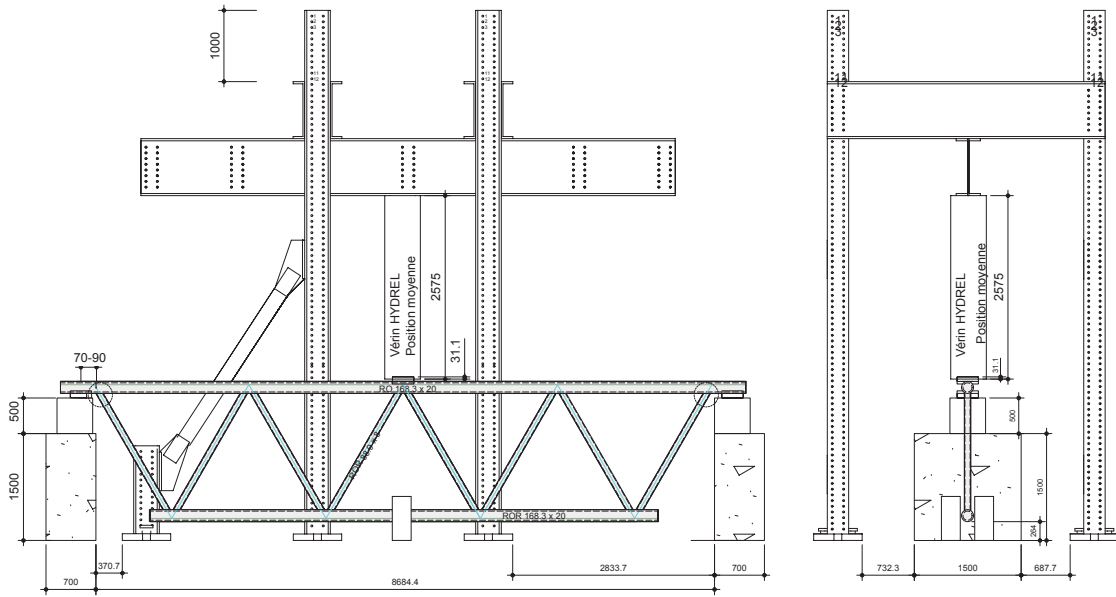


Figure 3.6: Fatigue test rig.

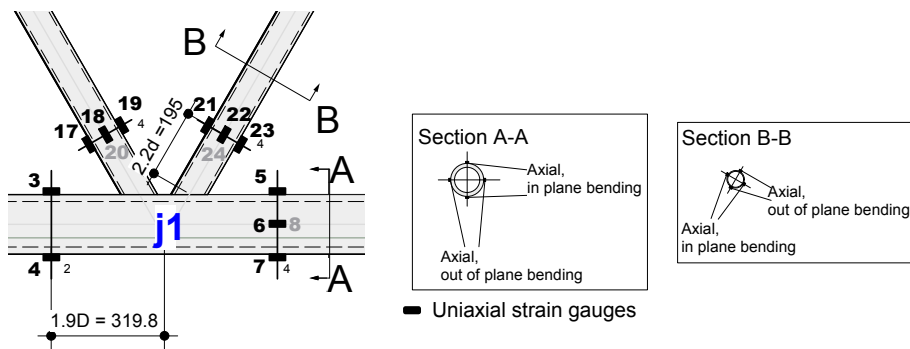


Figure 3.7: Example of joint instrumentation with uniaxial strain gauges, S5-2 joint 1.

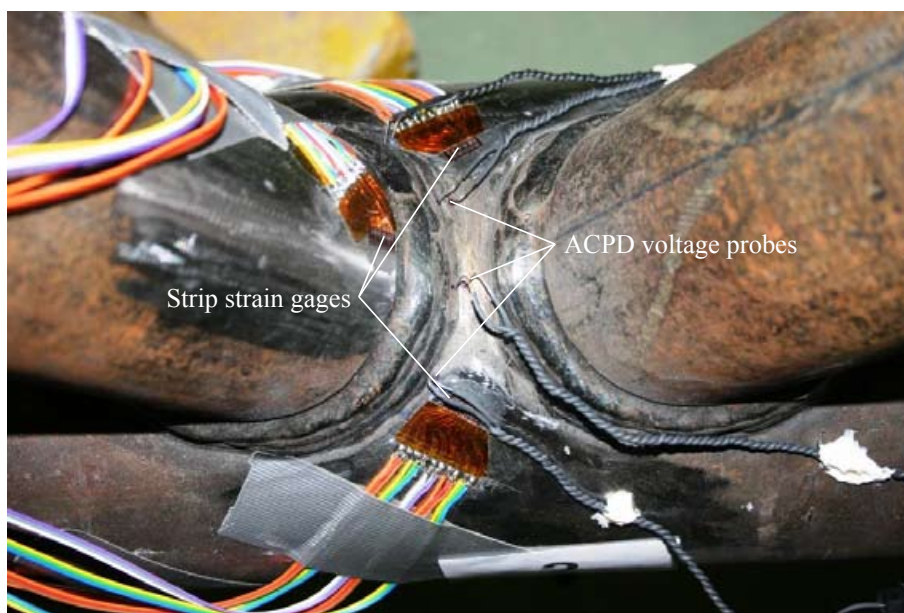


Figure 3.8: Strip strain gauges and ACPD voltage probes in joint 1 - beam S5-2.

3.3.3 Fatigue tests

Following the preliminary adjustments (actuator and beam aligning, precise determination of minimum and maximum actuator loads) and verifications (linearity and symmetry of response), the fatigue tests were then conducted. Constant amplitude load cycles were applied in order to investigate the initiation and propagation of the fatigue cracks. Several methods for monitoring fatigue cracks in small or large scale tubular joints exist for many years and are described in literature (Marsh et al., 1991). In order to monitor crack growth whenever possible, the following techniques were used:

- ◆ Ink marking;
- ◆ Beach-marking by applying a different stress amplitude for a limited number of cycles;
- ◆ Alternating current potential drop (ACPD) method, indirect method providing continuous information at discrete points along surface crack.

These techniques do not change the subsequent crack growth in a significative way. However, the risk exists that the crack starts at probe wires in the case of ACPD. Ink marking may induce corrosion at crack tip and thus induce subsequent modification in the crack growth rate. Furthermore, it is normally difficult to distinguish 2 different ink marks in the same crack surface.

Loading

A single *Hydrel* 1200 kN (static capacity) actuator under load control was used to apply a sinusoidal fatigue load at a frequency of about 0.7 Hz. The load ratio ($R = \frac{Q_{min}}{Q_{max}}$) was $R = 0.1$. The prescribed force range, ΔQ ($Q_{min} = 61$ kN, $Q_{max} = 610$ kN), was chosen to obtain the same chord nominal stress range as in previously tested series S3 ($\Delta\sigma_{nom,ch} = 35$ MPa).

Crack detection

During the early stages of testing the welded joints were closely inspected in order to detect any initiating fatigue cracks. The inspection was done using a 10× magnifying glass and macro photography. Dye penetrant and magnetic particles tests were also used to detect cracks and measure their surface length. Early cracks detected in joints 3N, 3S and 6 of beam S5-2. These joints being without particular interest, were repaired (needle-peening) so that the fatigue test could continue without affecting the interesting joints nominal stresses. In addition, joint 3S had to be rewelded so that the fatigue test could continue.

Number of cycles

In the present investigation, the failure of a tubular joint is defined as the life corresponding to through-thickness cracking (N_3). However, current $S_{r,hs} - N$ design curves use a different definition of joint failure. According to a study of a large database of fatigue test results carried out by van Wingerde et al. (1997), failure is defined as the number of cycles at which there is a complete loss of strength of the joint (N_4). In the same study the average ratio between N_4 and N_3 was 1.49. Thus, as in Schumacher (2003), in order to compare the present results to previous tests, N_3 values were multiplied by a factor of 1.49.

Alternating Current Potential Drop - ACPD

Electrical Current Potential Drop (Direct Current Potential Drop, DCPD and Alternating Current Potential Drop, ACPD) techniques have been widely used for crack depth monitoring in laboratory experiments on simple specimens for many years.

The basic principle is to introduce an alternating current (AC) to flow between two electrodes (field probes) and measure the local voltage drop over the area adjacent to the weld and over the crack by means of voltage probes (Marsh et al., 1991) (see Figure 3.9).

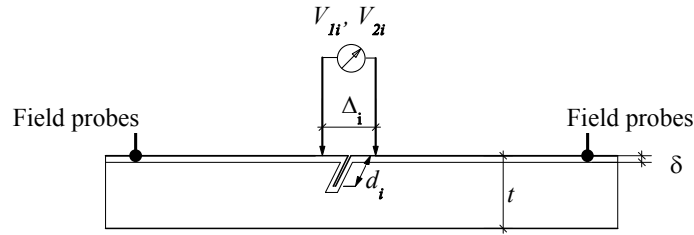


Figure 3.9: Alternating current potential drop theory and notation (adapted from Chiew et al. (2004)).

For an infinitely long crack of constant depth, ACPD estimation of the crack depth is given by:

$$d_i = \frac{\Delta_i}{2} \left(\frac{V_{2i}}{V_{1i}} - 1 \right) \quad (3.1)$$

where,

- d_i : crack depth at probe location i ;
- V_{2i} : potential difference measured with the probe i ;
- V_{1i} : reference potential difference;
- Δ_i : spacing between probe contacts;

The reference measure, V_{1i} , was taken as the average of the first 30 measures on the uncracked joint at location i . Accurate determination of the probe contacts distance is specially hard because of the irregular geometry across the weld toe. This difficulty can be overcome using ACPD systems with independent reference measures for each probe site immediately before the weld toe; however, the complexity of the tubular joint weld toe geometry can lead to other inaccuracies.

This one-dimensional interpretation of the ACPD measurements to give the crack depth is accurate for low crack aspect ratios ($a/2c < 0.1$). As the geometry of the specimen and the weld become more complex, or the crack aspect ratio higher ($a/2c > 0.1$), this estimation is likely to be less accurate, underestimating the crack size. In this case, it is recommended to use a correction factor to calibrate the final result. In the case of tubular joints, the aspect ratio remains low, and it was demonstrated by Michael et al. (1982) that correction factor would be less than 1.05. Therefore Equation (3.2) provides a satisfactory estimation for this type of joints. Another issue with ACPD measurements refers to the impossibility to determine the instant of through thickness penetration of a crack because the depth estimation represents the length along the crack faces and the crack inclination remains unknown until the joint is opened up.

The reported fatigue tests presented two main challenges regarding the use of the ACPD technique: the size and complex geometry (with multiple current paths) of the tubular truss. In order to keep the monitored areas as close to the field probes (primary current introduction) as possible to reduce resistance, only joints j1 and j2 were equipped with voltage probes. The actuator and the supports were electrically insulated.

The ACPD equipment (Electronique, 2007) used is shown in Figure 3.10.

Compared to other ACPD equipments described in literature, the AC frequency (5 to 6 Hz) was found to be about 10000 times lower but compensated by the introduction of higher intensity of 100 to 150A. During preliminary check-up, the acquisition box was damaged and had to be replaced by an earlier existing prototype of acquisition box for S5-1 beam tests. For the S5-2 beam, the repaired system, more precise and with one additional channel, was used. The technical characteristics of both systems can be found in Table 3.2.

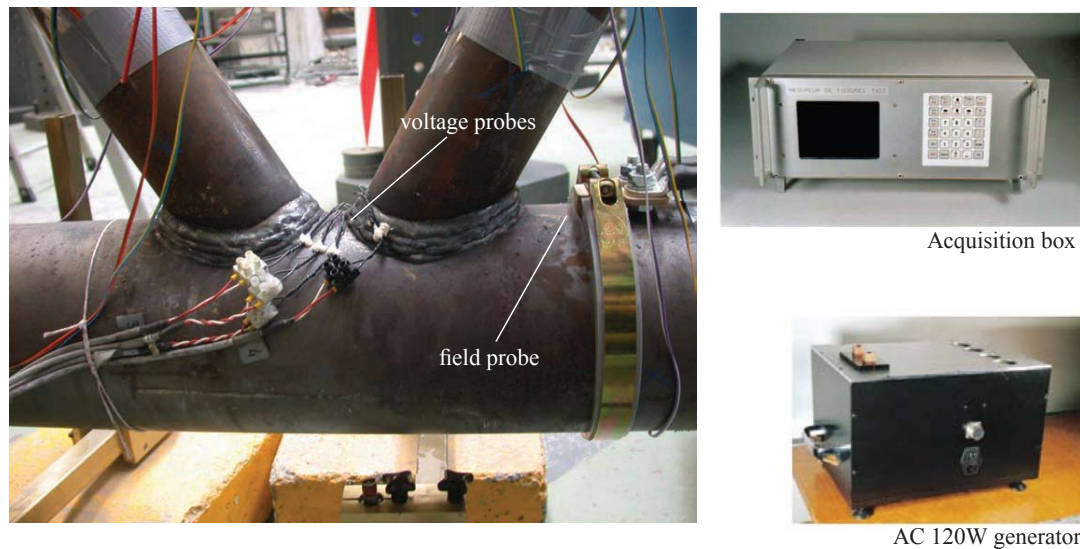


Figure 3.10: Alternating current potential drop system - field probe and crack voltage probes (left) and Acquisition box (up); AC 120W generator (down).

Table 3.2: ACPD systems characteristics.

	Intensity [A]	Frequency [Hz]	no of channels [-]
S5-1*	100	6.25	7
S5-2	150	5	8

*prototype acquisition box

In total, 8 (7 for S5-1) probes were disposed in potential crack sites corresponding to the crack toe, near imperfections found after visual inspection (Figure 3.11).

In the current application, one difficulty is the existence of multiple current paths between the field probes, see figures A.1 and A.1.

Ink marking

In order to obtain more information on crack shape and propagation, for beam S5-2, ink was sprayed into detected cracks and then the test was stopped for one day (drying time). The first ink marking (with alcoholic blue ink) was made after 30000 cycles in joints 1 and 5N, and after 50000 cycles in joints 2 and 5S. A second mark (with water based red ink) was made only in joints 1 and 5N after 145000 cycles.

Beach-marks - Changing stress amplitude marking

Moreover, in order to mark the crack front at other depths, another technique was used, based on the fact that any modification of the fatigue test loading (frequency, amplitude, mean stress) results in another crack surface aspect, thus called "beach-mark". The beach-mark was produced for beam S5-2 after 147000 cycles following the procedure suggested by Husset et al. (1985):

- ◆ Load amplitude is decreased by half, $\Delta Q_{mark} = \Delta Q \div 2$;
- ◆ Maximum load is kept at the same level, $Q_{max,mark} = const.$ This ensures that the plastic zone at crack front is kept approximately constant and thus eliminates possible crack retardation;
- ◆ These loading conditions are applied during 1000 cycles.

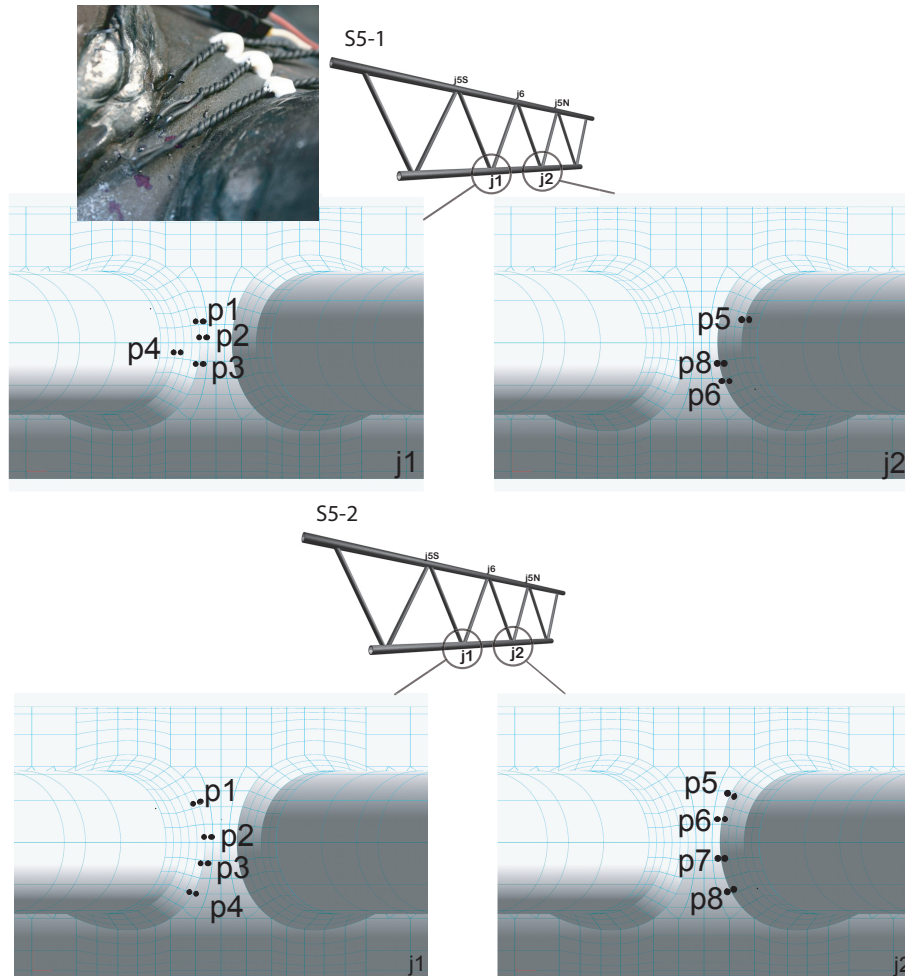


Figure 3.11: Alternating current potential drop probe locations for S5-1 and S5-2.

3.4 Main results and discussion

3.4.1 Static tests

Deflection

Deflections were measured using the actuator internal LVDT at the mid-span of the truss beam. Results are presented in table 3.3. Comparing the rigidity of series S5 with previously tested specimens, which had the same static height and external chord diameters, no major differences in the overall rigidity exist although the previous truss was composed of an I-beam top chord.

The overall stiffness of the truss is not affected by fatigue cracking in any of the test since differences between beginning and end deflections are negligible (except for S1(1,2), 18% attributed to a large crack found in the upper chord, see Schumacher (2003)).

Member and joint strain and stress

The static tests showed linear elastic response of the truss beam (Figure 3.12). Axial member strains at symmetrical positions from the load point have almost equal values, differences being less than 5%. It can thus be assumed that there is symmetrical behaviour of the truss beam.

Joints j1 and j5N of specimen S5-2 (see Figure A.2 in appendix) were instrumented with uniaxial strain gages strips. Figure 3.13 shows the strain range in the different strain gage strips for a corre-

Table 3.3: Load and deflection results.

Specimen	ΔQ [kN]	$\Delta\delta_{begin}$ [mm]	$\Delta\delta_{end}$ [mm]	$\Delta\delta_{begin}/\Delta Q$ [mm/kN] $\times 100$
S1(1,2)*	594	11.5	14.0	1.9
S1(3,4)*	594	11.0	11.0	1.9
S2(1,2)*	594	11.0	11.0	1.9
S2(3,4)*	594	10.5	11.0	1.8
S3(1,2)*	396	—	—	—
S3(3,4)*	396	9.5	9.5	2.4
S4(1,2)*	594	10.5	10.5	1.8
S4(3,4)*	594	10.5	11.0	1.8
S5-1	600	14.8	-	2.5
S5-2	544	12.2	12.3	2.2

$\Delta\delta_{begin}$ - at beginning of test

$\Delta\delta_{end}$ - at end of test

* from Schumacher (2003)

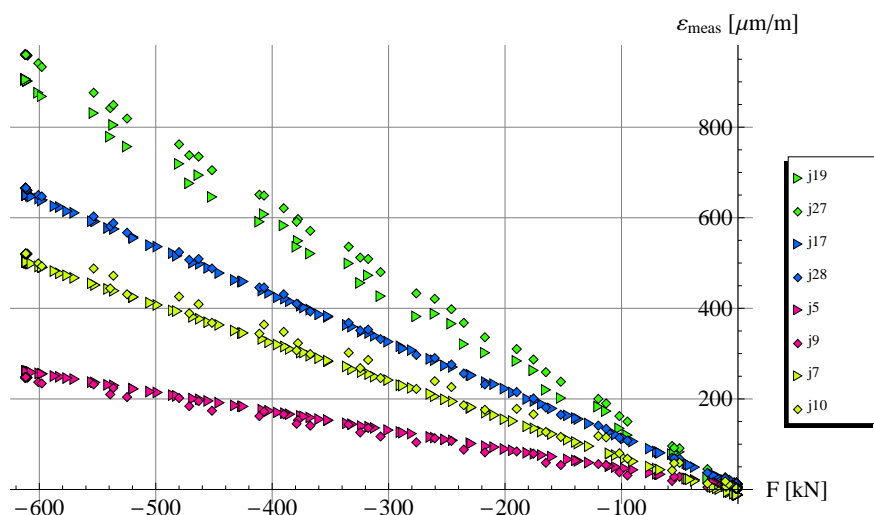


Figure 3.12: Comparison of strain measured by gages (j_i) placed in symmetrical positions in the truss beam, static test of S5-2.

sponding 543 kN force range. The strain at the weld toe was not measured but linearly extrapolated using the measured strain values.

Cracks propagated always at hot-spots 1 (near strip gages ch.1 and ch.2) or $1c$ (near strip gages ch.5 and ch.6). The plot shows higher values of $\Delta\varepsilon$ for the uncracked sites when compared to the cracked sites which is disturbing. This may be due to the following reasons:

- ◆ inappropriate linear extrapolation of surface strains;
- ◆ strip gages for hs 1 and hs 1c make a 30° angle with the tube longitudinal direction due to the lack of space to place them in the gap;
- ◆ the slopes of strains for hs1 and hs1c are steeper and more non-linear than those corresponding to hs11 (strip gages ch.3 and ch.8) or hs3 (strip gages ch.4 and ch.7), possibly due to the

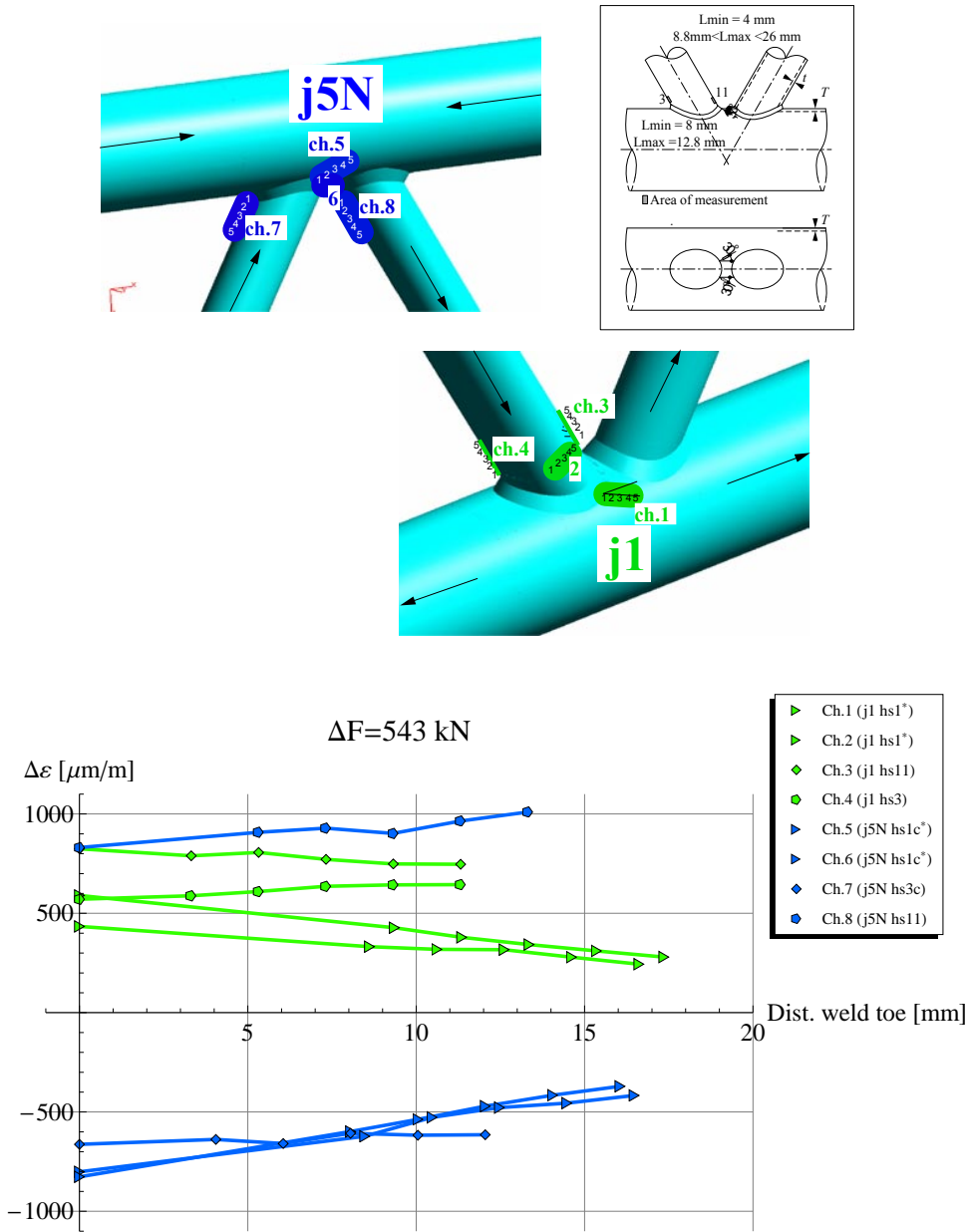


Figure 3.13: Strip gages installed in joint 1 and joint 5N of specimen S5-2. Strain range at surface near the weld toe in joints of specimen S5-2.

different weld transition radius;

- ◆ poor installation - difficult location;
- ◆ local bending of tube wall.

Table 3.4 compares the nominal and hot-spot stresses (obtained as $\sigma = 1.1 \cdot E \cdot \varepsilon$, refer to (Schumacher, 2003)) for experimental series 1 to 5. Brace nominal stress, $\sigma_{nom,br}$, is greater than the chord stress, $\sigma_{nom,ch}$, for all the joints. Different load amplitudes in the different series, make it difficult to compare directly the hot-spot stresses. The total stress concentration factor, SCF_{total} , introduced by Schumacher (2003) provides a basis for comparison between the different test joints. It is defined as:

$$SCF_{total,i} = \frac{\sigma_{hs,i}}{\sigma_{nom,br} + \sigma_{nom,ch}} \tag{3.2}$$

where,

- $SCF_{total,i}$: total stress concentration factor at joint location i ;
- $\sigma_{hs,i}$: hot-spot stress at joint location i ;
- $\sigma_{nom,br}$: scalar value of nominal stress in brace (due to both axial load and bending);
- $\sigma_{nom,ch}$: scalar value of nominal stress in chord (due to both axial load and bending);

Table 3.4: Nominal and hot-spot stresses for test joints.

Joint	β	γ	τ	Brace	Chord	Location 1	
	[–]	[–]	[–]	$\sigma_{nom,br}$ [N/mm ²]	$\sigma_{nom,ch}$ [N/mm ²]	$\sigma_{hs,1}$ [N/mm ²]	$SCF_{total,1}$ [–]
S11 ⁺	0.51	6.83	0.63	77.9	10.9	114*	1.28
S21 ⁺	0.51	6.83	0.63	72.0	15.1	139.6	1.60
S23 ⁺	0.51	6.83	0.63	73.5	12.2	138.8	1.62
S43 ⁺	0.51	6.83	0.63	76.2	15.1	148.4	1.62
S31 ⁺	0.53	6.73	0.64	72.5	35.9	187.0	1.73
S33 ⁺	0.53	6.73	0.64	76.7	39.9	195.7	1.68
S5-2 j1	0.53	4.21	0.40	148.0	32.0	211**	1.17
S5-2 j5N	0.53	4.21	0.40	-149.7	-55.7	-248**	1.21

⁺ from Schumacher (2003)

* Calculated using FEM

** Calculated using validated BEM model

When compared, joints j1 and j5N of beam S5-2 show the lowest values of SCF_{total} . This can be explained by the lower γ and τ parameters as well as low eccentricity ($e/D = 0.13$) - see Table 3.1.

3.4.2 Fatigue tests

$S_{r,hs} - N$ results and comparison with existing data and design lines

Figure 3.14 presents the fatigue results in the form of $S_{r,hs} - N$ logarithmical plot. The $S_{r,hs}$ is the hot-spot stress range and N is the number of cycles to failure.

Fatigue results from series S5 are plotted with series S1, S2 and S3 (Schumacher, 2003) and results from similar fatigue tests carried out at TU Delft. The TU Delft fatigue tests were conducted on multi-planar trusses with welded CHS KK-joints (non-dimensional parameters: $\theta = 45^\circ$, $\beta = 0.40$, $\tau = 0.50$ and $\gamma = 6.0$ and 12.0 (de Koning et al., 1992, Romeijn, 1994).

Series S5 data shows on the graph as only 2 points, but in fact represent 4 fatigue cracks (joints 1 and 2 cracked simultaneously for S5-1 and S5-2). On both test beams, fatigue cracks were obtained in joints j1, j2, j5N and j5S. All the cracks occurred at hot-spots 1 or 1c (compression side in the case of elements in compression). Cracks at hs1c are not represented in the $S - N$ plot.

Moreover, the $S_{r,hs} - N$ design curves (Zhao et al., 2000, Zhao and Packer, 2000) for a reference thickness $T = 16$ mm) is represented on the same figure.

The derivation of the $S_{r,hs} - N$ design curves was carried out based on a different definition of joint failure than the one used in the present investigation. In order to compare the results, the same procedure as in (Schumacher, 2003) is applied: N_3 (through-thickness cracking criterion used in the present investigation) is multiplied by 1.49 to estimate N_4 (number of cycles to complete loss of joint strength). This procedure is based on the average of the N_4/N_3 ratio in the database used to derive the design curves. As the failure of the TU Delft joints was also defined at N_3 , the same adjustment was made to report the results in terms of N_4 .

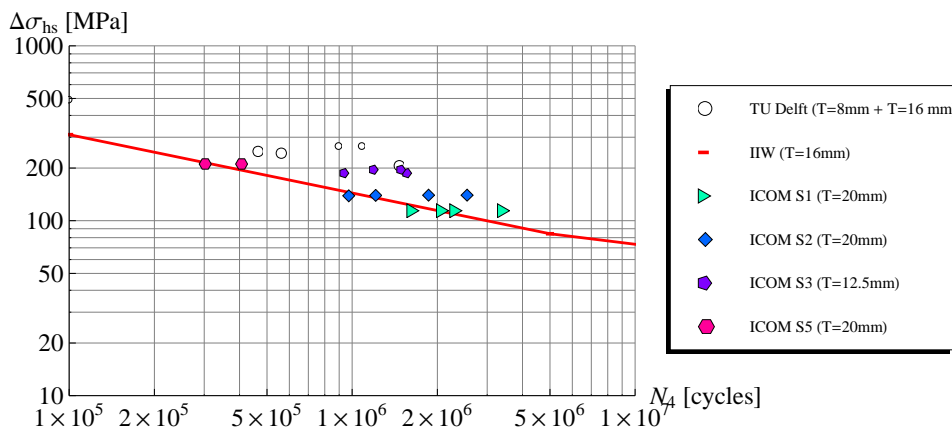


Figure 3.14: Comparison of S5 results to previous similar tests.

Figure (3.15) summarises the S-N results obtained for series S5 comparing them to the complete database on previously tested geometries. As can be noticed, the results from S5 fall below the other test results. The other test results already showed a size effect (thicker joints, corresponding to bigger symbol size, show shorter lives). However, due to the amount of parameters ($\alpha, \beta, \gamma, \tau, \zeta, T$) more tests are needed on truss beams to confirm especial non-proportional scaling effects.

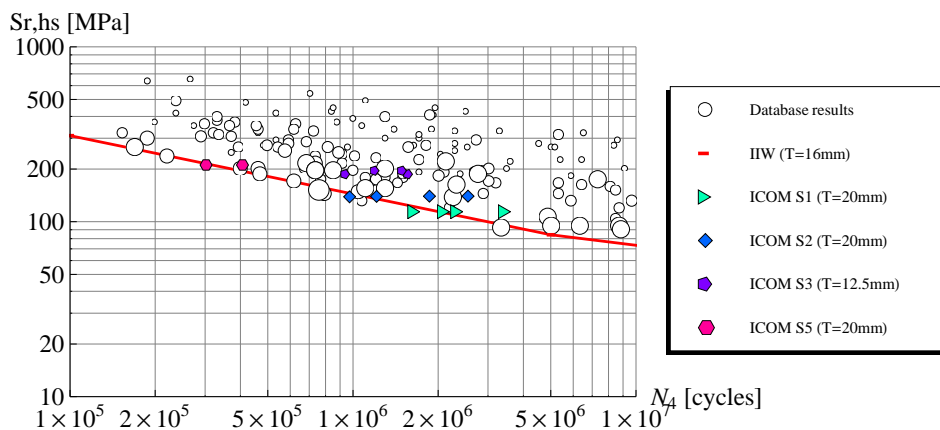


Figure 3.15: Comparison of ICOM test results to CHS joint database.

S5-1

After 169000 cycles, diagonal 4S was ripped-off the chord. This was due to a hidden crack that propagated near the support and this ended the test. The cracks at other joints were thereafter opened and measured. Table 3.5 shows the crack dimensions observed for each joint (following the convention shown in Figure 3.16). A crack depth of $a \approx 10$ mm (joints 1 and 2 of S5-1) was observed.

In order to estimate the number of cycles to through thickness cracking, N_3 , an average value of the crack propagation rate ($da/dN = 5.3 \times 10^{-4}$ mm/cycle for a between 10 mm and 28 mm (through cracking of S5-2), see Figure 3.20) was used. Thus, $N_3 = 169000 + 34000 = 203000$ cycles and $N_4 = 203000 \times 1.49 = 302500$ cycles.

It is interesting to note that joints 5N, 5S and 6 are on the compressed chord and cracked at hs1c, the weld toe between compressed brace-compressed chord, on the chord side.

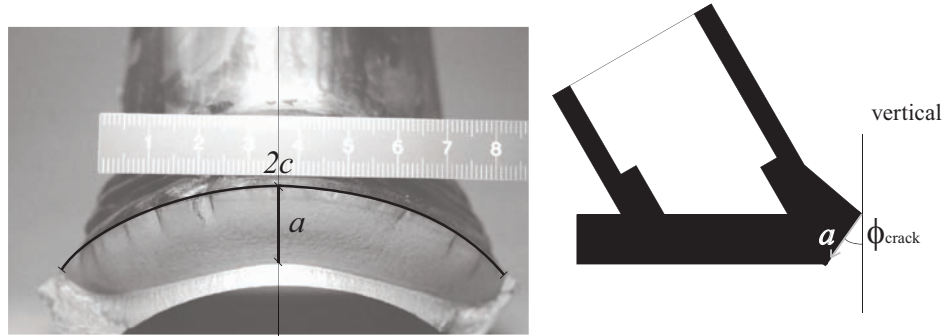


Figure 3.16: 3-D Crack depth (a), length ($2c$) and angle convention.

Table 3.5: Fatigue crack dimensions for beam S5-1 (final crack front after 169000 cycles).

Joint (hs location)	a [mm]	$2c$ [mm]	a/c [-]	Angle [°]
1 (1)	10	85	0.24	44
2 (1)	9	53	0.34	49
5N (1c)	19	120	0.32	41
5S (1c)	12	63	0.38	37
6 (1c)	15	85	0.35	9

S5-2

The fatigue test of beam S5-2 was stopped after 273000 cycles, when a pressure drop indicated a through crack in the bottom chord ($N_3 = 273000$ cycles). Figure 3.17 shows the cracks faces after opening of the respective joints. In this case, $N_4 = 273000 \times 1.49 = 407000$ cycles.

Table 3.6 gives the crack dimensions when the test was stopped (through thickness cracking of joints 1 and 2).

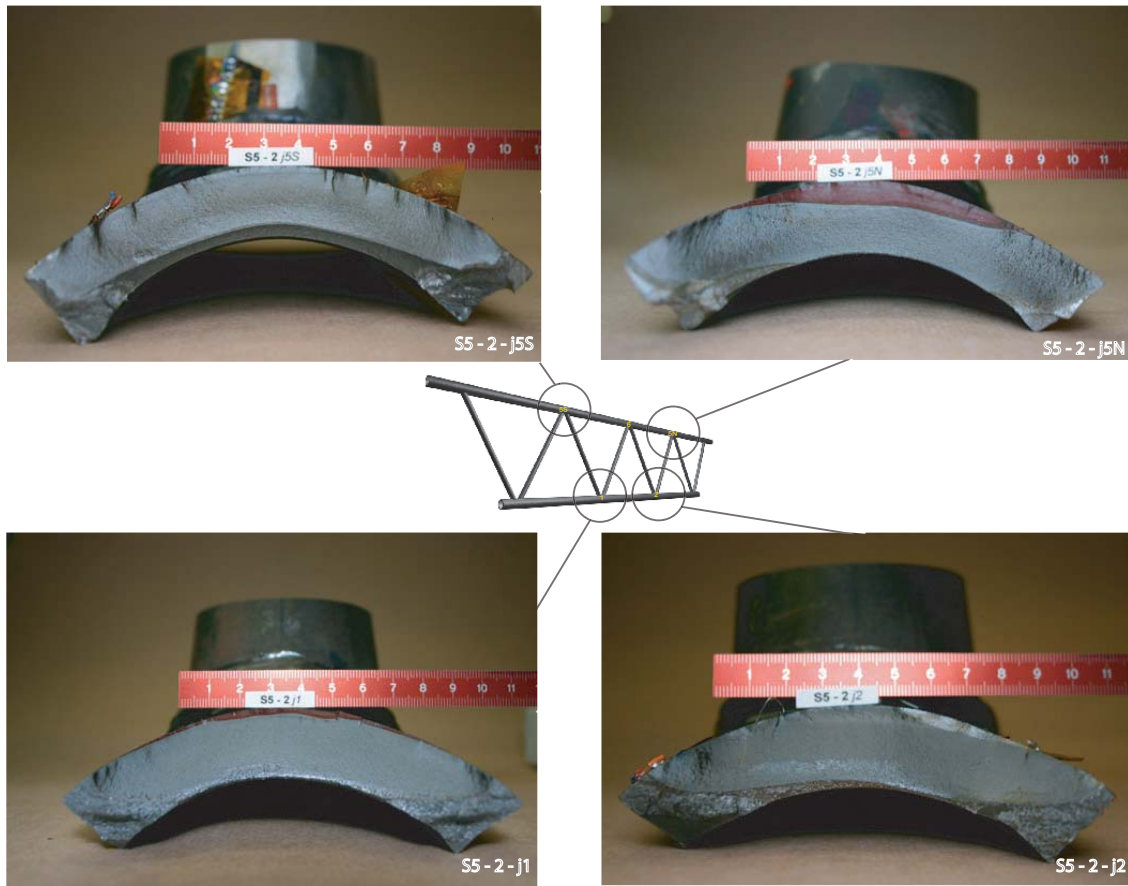


Figure 3.17: Fatigue cracks for beam S5-2, opened after 273000 cycles.

Table 3.6: Fatigue crack dimensions for beam S5-2 (final crack front after 273000 cycles).

Joint (hs location)	a [mm]	$2c$ [mm]	a/c [-]	Angle [°]
1 (1)	28	136	0.41	45
2 (1)	27	138	0.39	48
5N (1c)	25	157	0.32	37
5S (1c)	20	150	0.27	43
6 (1c)	20	124	0.32	7

Alternating Current Potential Drop (ACPD) system

ACPD results were analysed following the procedure given in Figure 3.18. Raw potential results were filtered using Mathematica (Wolfram, 1988) *moving average* algorithm with a sample of 300 points (corresponding to a lapse of approximately 6000 cycles) in order to eliminate any noise effects. This was done at a cost of losing information at the beginning and the end of the test.

Afterwards, using Equation (3.2) the estimated crack depths, d_i , at each of the probe sites were computed. Then, the crack growth rate could be obtained for an interval of $2\Delta N = 750$ cycles using:

$$\frac{dd}{dN} = \frac{d(N + \Delta N) - d(N - \Delta N)}{2\Delta N} \quad (3.3)$$

The experimental stress intensity factors were then obtained using the Paris Equation (3.4) with $C = 2.0 \times 10^{-13} (\text{mm/cycle})(\text{N/mm}^{-3/2})^m$ and $m = 3$ (suggested by Gurney (1979), for ferrite/pearlite steels).

$$\frac{da}{dN} = C\Delta K^m \quad (3.4)$$

Values of ΔK as low as $150 \text{ Nmm}^{3/2}$ could be measured after 5000 cycles, showing the excellent sensitivity of the system.

Crack depth deduced from ACPD

The measurements analysis is carried out for each location according to the method described in Section 3.4.2. The results can be plotted in terms of crack depth at each probe location, d_i , in function of the number of cycles. A typical example of the plot is given in Figure 3.19.

One can observe that the first signs of cracking were detected by probe *P5*, which is on the side of *hs1*.

The first detectable crack happened after less than 10% of the test fatigue life. All measurements made were stable and with the good results and comparisons obtained, we can say that the size and multiple current paths did not disturb the functioning of the ACPD system.

Crack growth rate deduced from ACPD

Using the information on the crack depth, again using the method described in Section 3.4.2, one can find the crack propagation rate and plot the results as in Figure 3.20. For joint S5-1,j1, the results from probe *P4* are not shown as no propagation was measured (probe at *hs11*, see Figure 3.11).

Crack propagation rates from 10^{-7} to 10^{-3} mm/cycle could be measured and correspond to values measured by FORMAT!!! (1982) for fillet welded joints using Direct Current Potential Drop system. For C-Mn steels, the value 10^{-7} mm/cycle corresponds to stress intensity factor ranges near the threshold value (see Figure 3.20).

It was observed that crack growth, at least up to half thickness occurred at about the same rate both in tension or compression joints, with crack shapes (a/c) being also similar.

Stress intensity factor range deduced from ACPD

Experimentally evaluated SIF ranges can be found once a crack propagation law, see Section 3.4.2, has been assumed. A plot of the result is given in Figure 3.21.

It should be noted that the evaluated SIF ranges do not correspond to the deepest point along the crack front but depend on the location of the probe.

Very low ΔK values, between 100 and $200 \text{ N/mm}^{3/2}$ could be evaluated from measurements after only 5000 fatigue cycles, which is remarkable. For comparison, threshold SIF range values, ΔK_{th} , for C-Mn steels, can for example approximately be expressed as follows (Zheng, 1987):

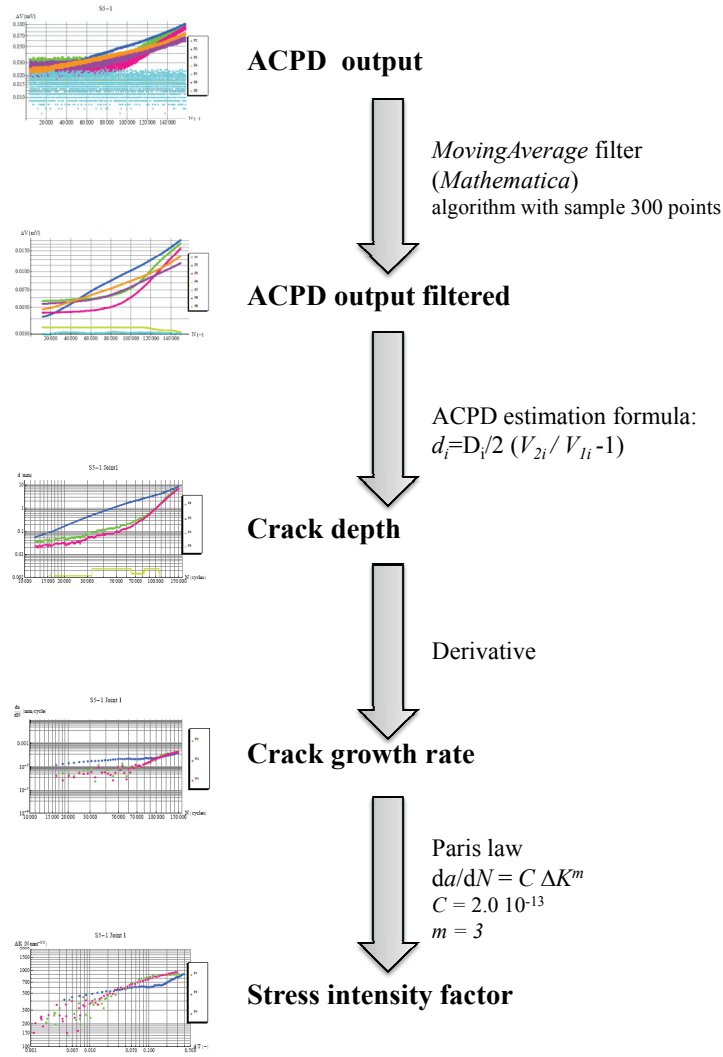


Figure 3.18: Schematic of the procedure to analyse ACPD results to determine SIFs experimentally.

$$\Delta K_{th} = 320 \times (1 - R) \quad (3.5)$$

where,

ΔK_{th} : stress intensity factor range threshold;

R : stress ratio ($\frac{\sigma_{min}}{\sigma_{max}}$);

This means that we are able to measure threshold values ($\Delta K_{th} \approx 288 \text{ N/mm}^{3/2}$ for $R = 0.1$).

3.4.3 Crack initiation

Considering, as suggested by Pook and Frost (1973), that the theoretical threshold for crack propagation corresponds to a growth rate of one lattice spacing per cycle (for metals typically about $4 \times 10^{-7} \text{ mm/cycle}$), and comparing this value to the ACPD measures, it can be concluded that:

- ♦ Welded tubular joints exhibit almost no crack initiation phase, cracks propagating from the very beginning.
- ♦ After 30000 cycles ($\approx 10\%$ of fatigue life) crack growth rates of about $4 \times 10^{-7} \text{ mm/cycle}$ for joints S5-2-j1 and S5-2-j2 were measured;

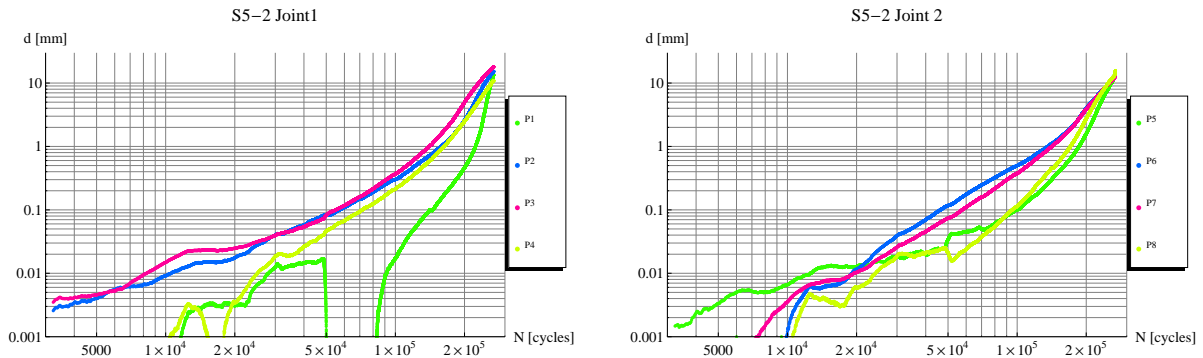


Figure 3.19: Number of cycles vs. crack depth at probe location for series S5-2 joints - using filtered results

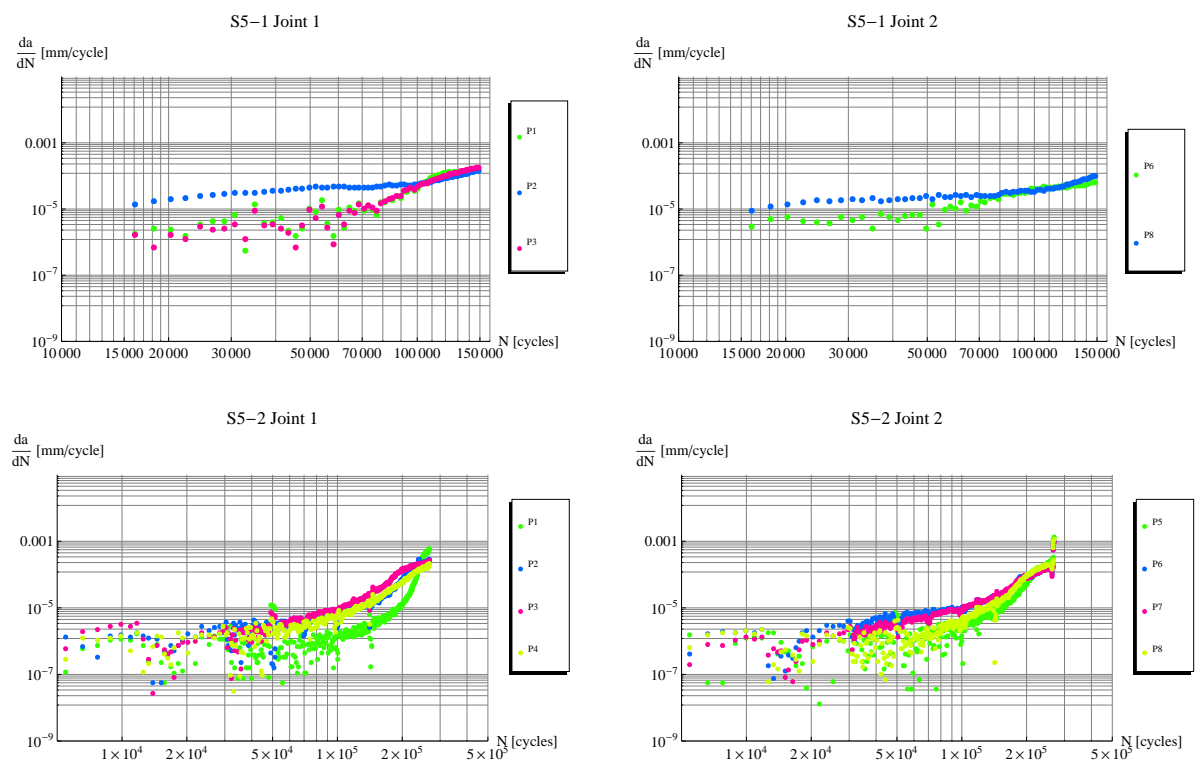


Figure 3.20: Crack growth rate vs. number of cycles - S5-1 and S5-2.

- ◆ Ink marks showing faster propagation at the beginning for joint S5-2-j5N, previous conclusions can be extended to the upper joints (j5) cracking under compressive applied loads;

All the cracks initiated at hot-spots 1 and 1c. No crack growth was observed at hs11, hs2, hs3 or hs4 or from the weld root.

3.4.4 Initial defect size

The cracks were broken-up and cut as illustrated in Figure 3.24. Joint 3N (see Figure 3.25), which was not opened up, was selected to examine the microstructure (the protocol is detailed in Appendix A.3) and identify the Heat Affected Zone (HAZ) and its influence on the crack growth.

The fact that this procedure was only made on a single cross section makes it impossible to conclude regarding the initial defect size and the exact initiation site. From Figure 3.26, it may be inferred

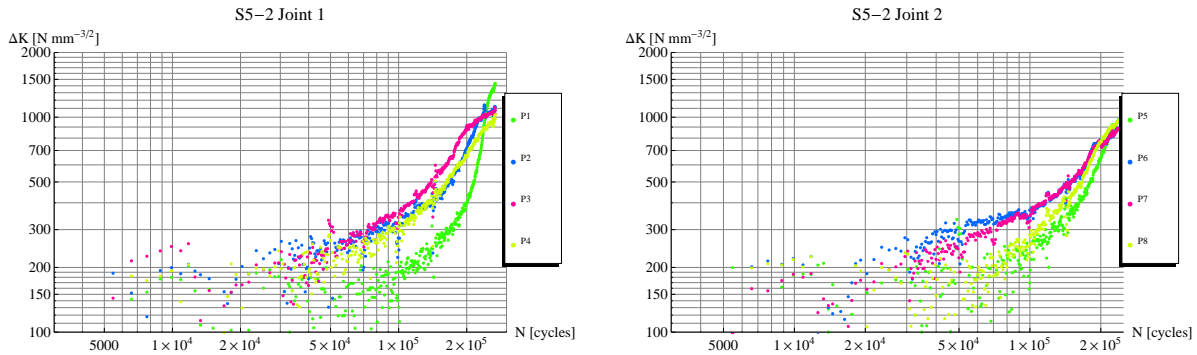


Figure 3.21: Stress intensity factors vs. number of cycles.

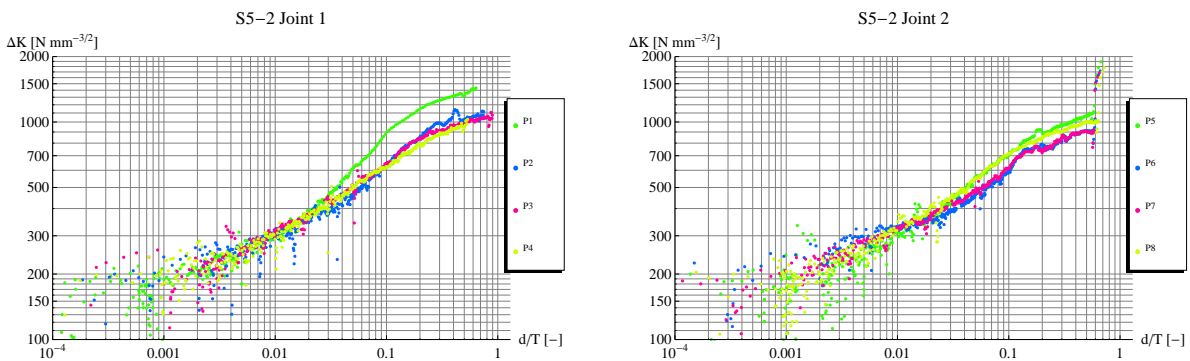


Figure 3.22: Stress intensity factor range ΔK vs. relative crack depth, d/T .

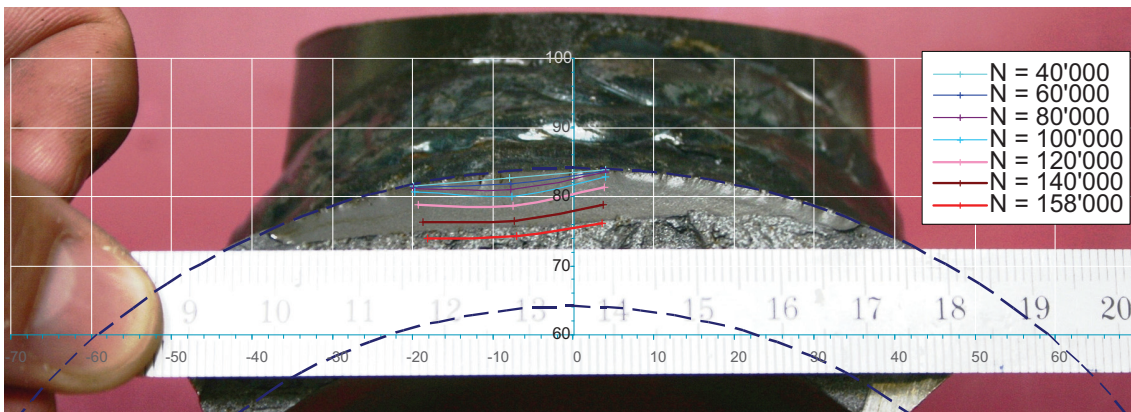


Figure 3.23: Comparison of final crack and crack estimations using ACPD system (S5-1 joint 1) .

that the crack started in the HAZ. This might be false since there is no guarantee that the cut plane corresponds to the initial defect location.

Attempts to measure the initial defect size in uncracked joints by microscopy observation were unsuccessful. As it is impossible to know the exact crack initiation point before cutting the specimen and multiple cuts cannot be done it is thus very difficult and time consuming to measure the initial defect size.

3.4.5 Crack shape

The doubly-curved semielliptical cracks present, after coalescence, a shape ratio a/c in the range from 0.05 to 0.33 for crack depths $a \leq T/2$ with an average of 0.2. For $a > T/2$, the crack shape ratio,

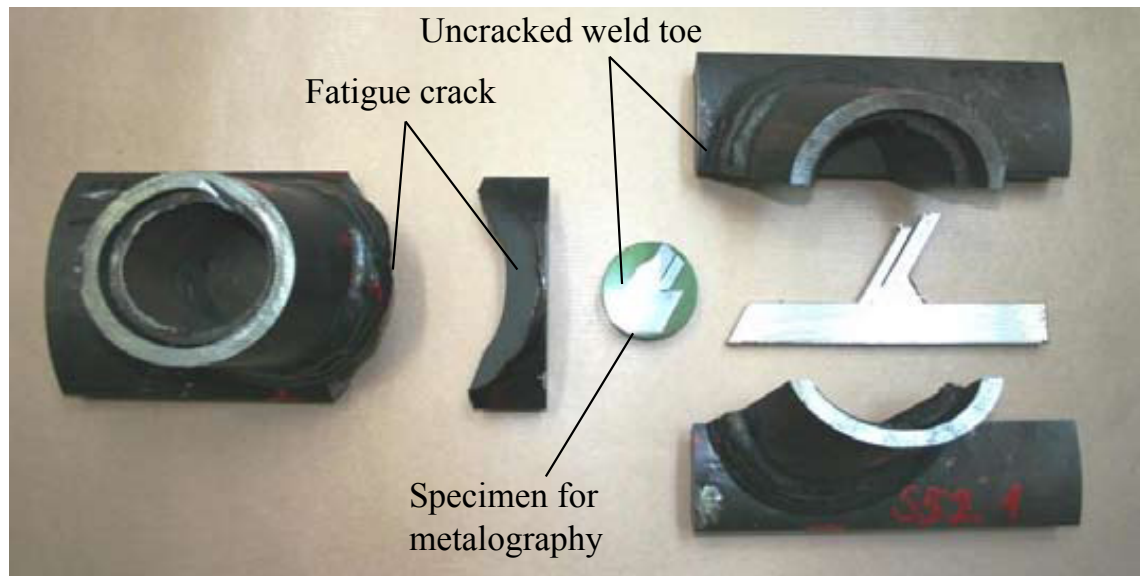


Figure 3.24: Crack opened-up and cutting planes.

a/c , measured was higher: between 0.25 and 0.45 (see Figure 3.27). The crack surface, can be well approximated by a conic surface, as can be seen from Figures 3.17 and 3.16.

3.4.6 Coalescence

In a welded component, cracks usually initiate at different sites and then link up to form a continuous crack (Yamada and Hirt, 1982). Ink marking and macro photos provide evidence of coalescence in the early stage of crack propagation (typically cracks depths ≤ 1 mm).

Macro photos, taken after the crack was opened, allowed to observe coalescence blue ink marks at joint S5-2-j2 after 51000 cycles. Radial lines confirm the coalescence and give an estimation of the size of small cracks at the moment they are joined together (Figure 3.28).

Figure 3.29 shows different crack surface textures, in joint S5-2 j2, and what seem to be beach-marks. At least 4 transitions between different textures are identified (marked as A, B, C and D in the Figure). The "beach-marking" technique was not successful as it is not possible to say which mark corresponds to the different load amplitude applied during 1000 cycles. Comparing these to ACPD results (for 147000 cycles, $d_6 = d_7 = 1.7$ mm, see Figure 3.19), it is admissible that beach-mark A was produced by the single beach-mark made on purpose. However, it is not conclusive, and, as the other marks, it could be caused by residual stress field changes or test interruptions.

3.4.7 Residual stresses, compression cracks

The fact that there was fatigue cracking between compressed elements is due to the residual stresses present in the weld toe region. The measurement of the built-in residual stresses and inclusion in numerical simulations is out of the scope of this thesis. The crack growth, at least until half of the chord thickness, occurred at about the same crack growth rate for hs1c (between compressed members) and hs1 (between tension members). This observation permits to say that high tensile residual stresses from welding are present in these joints and that, for at least most of the cycles amplitude, hs1c is locally in tension. Crack shapes for compression cracks (joints 5N, 5S) are seen to be similar to cracks in joints 1 and 2, see Tables 3.5 and 3.6. Angles ϕ_{crack} seem slightly lower ($\phi_{crack} \leq 43^\circ$) compared to cracks in joints 1 and 2 ($\phi_{crack} \geq 44^\circ$).

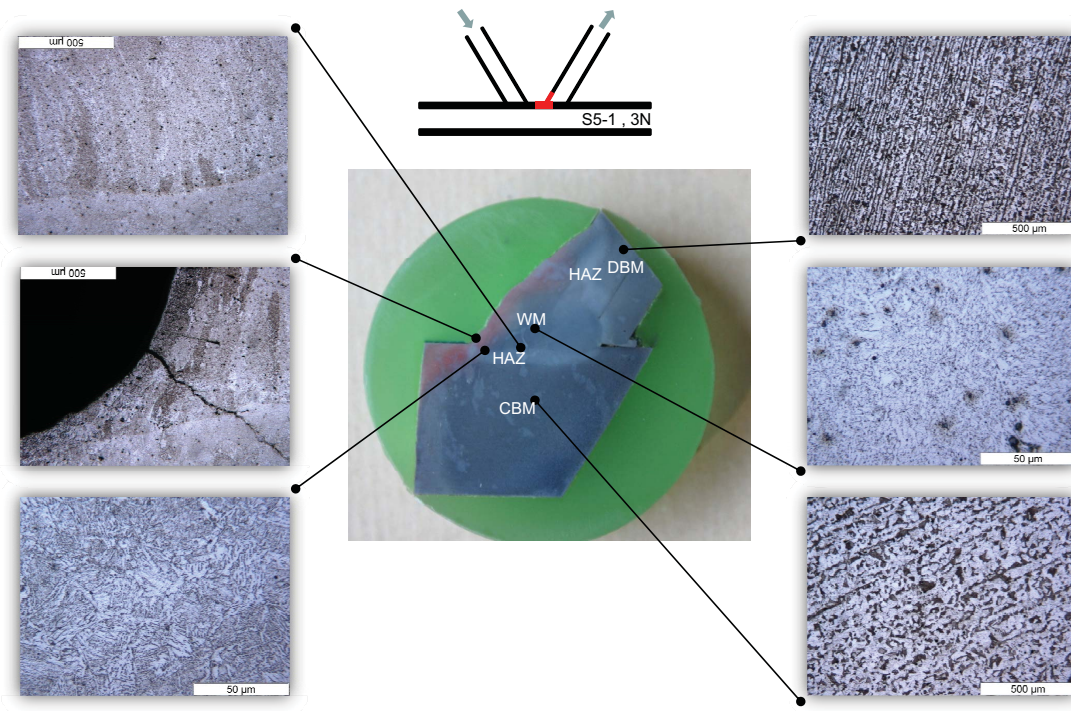


Figure 3.25: Cross-section photos after surface was treated with Nital. (CBM) Chord base metal; (HAZ) Heat affected zone; (WM) Welding material; (DBM) Diagonal base material.

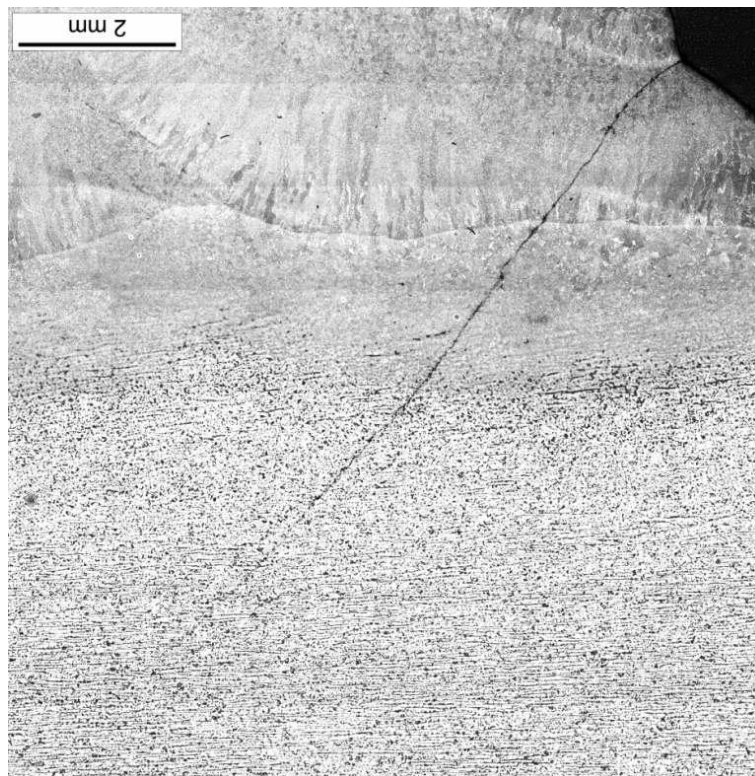


Figure 3.26: Microscopic photo of the crack after Nital etching (S5-2-j5N).

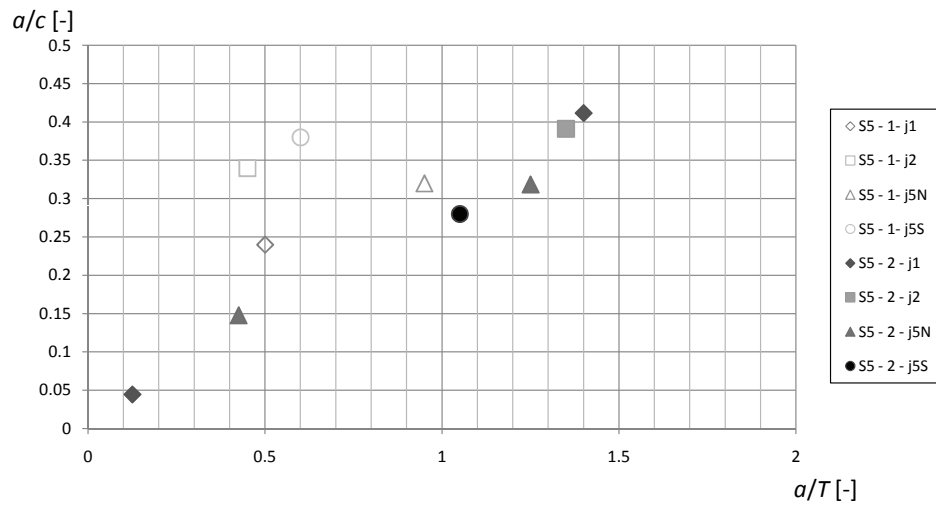


Figure 3.27: Crack shape evolution using final crack and ink marks when available (a is measured in the crack plane).

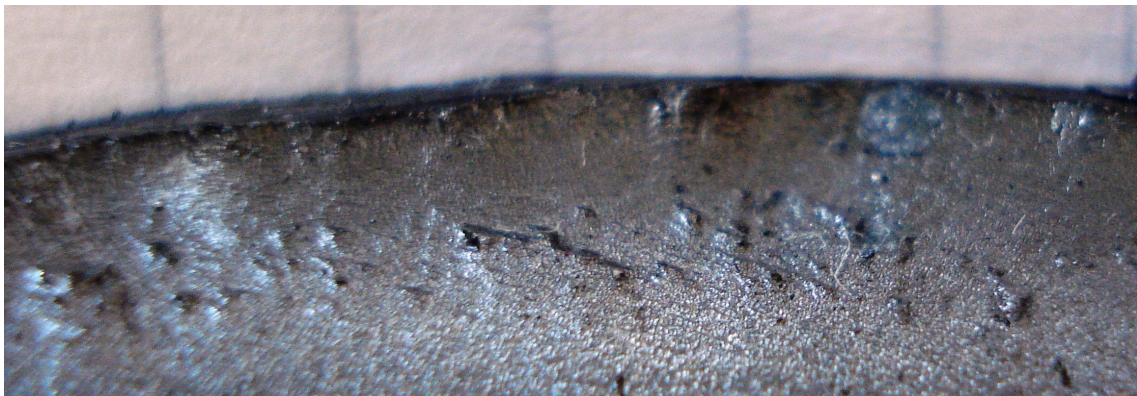


Figure 3.28: Blue ink marks showing independent small cracks and coalescence.

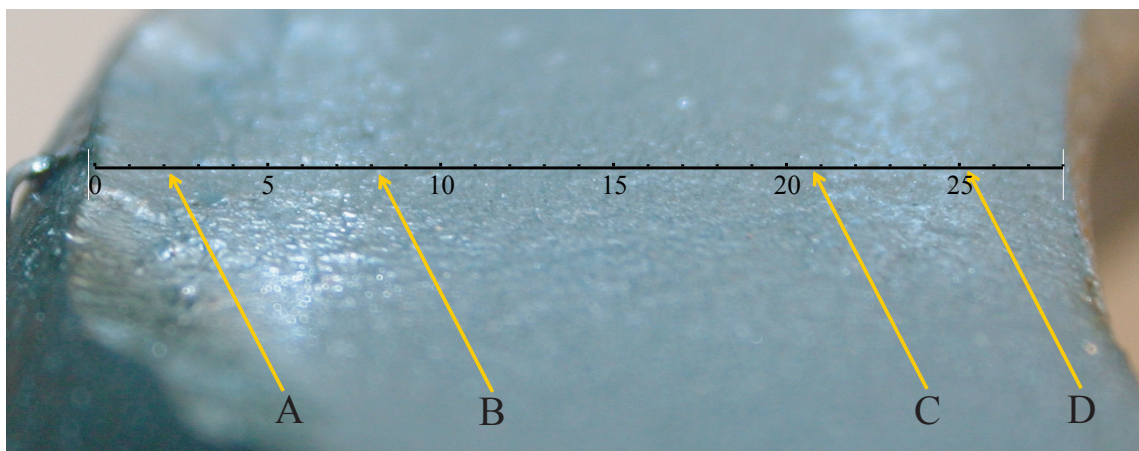


Figure 3.29: Close view of the crack texture - joint S5-2 j2 - with transitions identified as A, B, C and D.

3.5 Summary and conclusions

This chapter presents the laboratory tests of large scale welded CHS K-joints. A description of the procedure and analysis of the results is presented. From the static and fatigue tests the following conclusions can be drawn:

- ◆ The deflection of the truss, and thus its overall rigidity is not affected by cracking of the test joints - including through thickness cracks;
- ◆ All the cracks occurred at locations 1 or 1c (compression side in the case of elements in compression);
- ◆ No crack growth was detected at other hot-spots (11, 2, 3, 4) nor at weld root;
- ◆ Cracks propagate along an approximately conic surface. The crack angles in the beam longitudinal/vertical plane range from 37° to 49° (locations 1 or 1c);
- ◆ Crack shape ratios of the different joints present a considerable scatter. For crack depths $a/T \leq 0.5$, a/c values range from 0.05 to 0.35 with an average of 0.2;
- ◆ Comparing series S5 to previous fatigue tests through $S_{r,hs} - N$ plot (Figure 3.15), size effects seem to be observed; however, due to the amount of parameters involved and the scatter inherent to fatigue test results, more tests are needed to confirm and quantify the non-proportional scale effects and propose improved design rules (compared to Gurney's or CIDECT);
- ◆ During the two tests carried out, we were able to successfully apply an ACPD (Alternative Current Potential Drop) measuring system on a large-scale tubular truss beam with multiple current paths. Previously, ACPD systems had only been used on isolated joints or small specimens;
- ◆ Tests confirm that welded joints in fatigue, also tubular welded joints, show mainly crack propagation because of initial defects. Crack initiation is only approximately 10% of the total fatigue life;
- ◆ With regard to the influence of welding residual stresses, fatigue cracks were observed both in joints with the chord in tension (joints 1 and 2) as well as in joints with the chord in compression (joints 5N, 5S and 6). Crack growth, at least up to half the chord thickness, occurred at about the same rate in both cases (similar crack depths a), with crack shapes (a/c) being also similar.

Numerical Investigation

4.1 Introduction

This chapter describes the development of a versatile numerical model to simulate the propagation of a surface crack in a tubular welded joint under fatigue load. The model includes the calculation of the stress intensity factors (SIF) for different crack depths using a 3-D Boundary Element Method (BEM) model. The crack growth rate is computed using the Paris Law, and then, the number of cycles to failure is obtained by integration.

In Section 4.2 details on the BEM model of the welded joint are given, namely the definitions of the joint geometry, material properties, boundary conditions, crack modelling and model meshing. In section 4.3 the fatigue crack propagation model used to compute the fatigue life of the welded joint, is presented. Section 4.4 details the process of creation of a standard model in order to run a parametric analysis. Model validation, through comparisons to test results is presented in section 4.5. In section 4.6, the superposition of basic load cases to obtain a combined load case is discussed. The main conclusions are summarised in Section 4.7.

The standard model described herein is used in Chapter 5 to carry out a parametric study on the fatigue behaviour of different K-joint sizes, geometries and loadings.

4.2 Boundary element model

In order to create a boundary element model that simulates a cracked uniplanar K-joint, different aspects have to be considered. Firstly, the geometry of the boundaries that define the joint elements and respective intersections have to be parameterised so that different geometries in the framework of the parametric study can be modelled.

The crack path, or, in 3-D, the surface defining crack faces, has also to be defined. A number of zones are created to confine regions of similar mesh density and material properties. The mesh discretising the boundaries is chosen and the external forces and boundary conditions are applied to mesh points.

In the current study, the advantage of symmetry was not taken into account. This choice was made in order to develop a more versatile and valuable model for an extension of the present investigation to study asymmetrical cracks, multiple crack problems and out-of-plane loading.

4.2.1 Geometry definition

In order to define the joint model, its boundaries were parametrically defined. The cylinder parametric equation is first used to define the boundaries of chord and braces (or diagonals). Then the weld and tubes intersections are defined using the intersection cylinder-cylinder system of equations.

Overlapped joints are not considered in this study as they are usually less used in fatigue critical structures (except in mining equipment).

Chord and braces

The chord and braces boundaries consist of concentric cylinders of diameters D and $(D - 2 \times T)$ for the chord respectively d and $(d - 2 \times t)$ for the braces.

The chord outer boundary is given by:

$$x = l \quad (4.1)$$

$$y = \frac{D}{2} \cos(\phi) \quad (4.2)$$

$$z = \frac{D}{2} \sin(\phi) \quad (4.3)$$

where,

l : parameter, length of the element, varies in the interval $[-L_{ch}/2, L_{ch}/2]$;

ϕ : parameter angle centre, varies in the interval $[0, 2\pi]$;

To obtain the inner boundary equations D is replaced by $D - 2 \times T$.

The diagonal outer boundary is defined by the equations:

$$x = \frac{d}{2} \cos(\phi) \sin(\theta_{br}) + l_1 \cos(\theta_{br}) \quad (4.4)$$

$$y = \frac{d}{2} \sin(\phi) \quad (4.5)$$

$$z = l_1 \sin(\theta_{br}) - \frac{d}{2} \cos(\theta_{br}) \cos(\phi) \quad (4.6)$$

where,

θ_{br} : angle between the diagonal axis and the horizontal chord axis;

l_1 : parameter varying in the interval $[0, H/2]$;

ϕ : parameter varying $[0, 2\pi]$;

The inner boundary equation is obtained replacing d by $(d - 2 \times t)$.

Weld geometry

The weld profile has a big influence on the stress concentration at the weld toe and thus on the stress intensity factors (SIF) for surface cracks. Therefore the welds should be modelled as close as possible to the reality. As it is a difficult task to simulate the weld profile realistically, most of previous investigations did not consider it. This results, according to Lee and Wilmshurst (1995), in an underestimation of the fatigue life up to 20%.

In the present study, the weld is defined using three auxiliary curves for each diagonal-chord weld (see Figure 4.1):

- ◆ a. The intersection of the inner boundary of the diagonal with the chord outer boundary;
- ◆ b. The intersection of the outer boundary of the diagonal with the chord, shifted by $(W_1 \cdot \cos(\theta_{br}), 0, W_1 \cdot \sin(\theta_{br}))$;

- ◆ c. The intersection of the chord with an imaginary cylinder with the same angle θ_{br} as the diagonal but diameter equal to $d^* = d + 2W_2$ and translated of $(W_3, 0, 0)$;

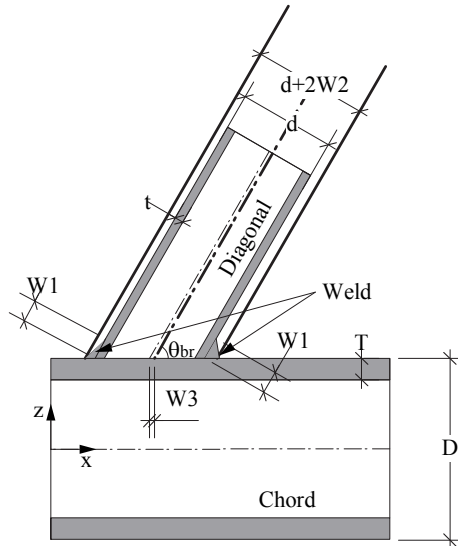
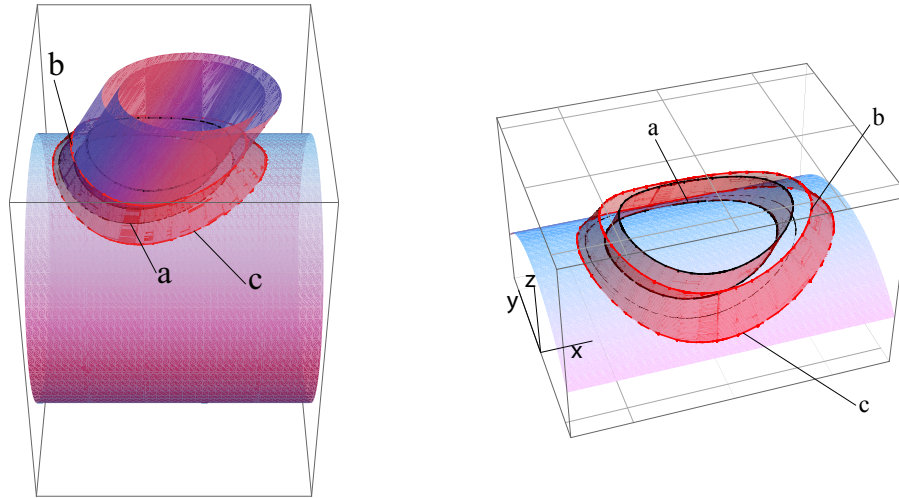


Figure 4.1: Weld geometry.

Figure 4.2 shows the weld dimensions in two sites around the diagonal-chord intersection: the weld crown toe and the weld crown heel. L_w is the weld footprint length, θ_w is the weld toe angle, ψ is the local dihedral angle. Subscripts "br" and "ch" are added to distinguish between brace-side and chord-side parameters.

These dimensions can be calculated using the parameters used to geometrically define the weld: W_1 , W_2 and W_3 as follows:

$$L'_w = \frac{t}{\sin(\pi - \psi)} \tag{4.7}$$

For weld crown toe (hot-spot sites 1 and 11): $\psi = \theta_{br}$

$$L_{w,ch,toe} - L'_w = \frac{W_2}{\sin(\theta_{br})} - W_3 \tag{4.8}$$

For weld crown heel (hot-spot sites 31 and 3): $\psi = \pi - \theta_{br}$

$$L_{w,ch,heel} - L'_w = W_3 + \frac{W_2}{\sin(\theta_{br})} \tag{4.9}$$

$$L_{w,br} = W_1 + \frac{T}{\sin(\theta_{br})} \tag{4.10}$$

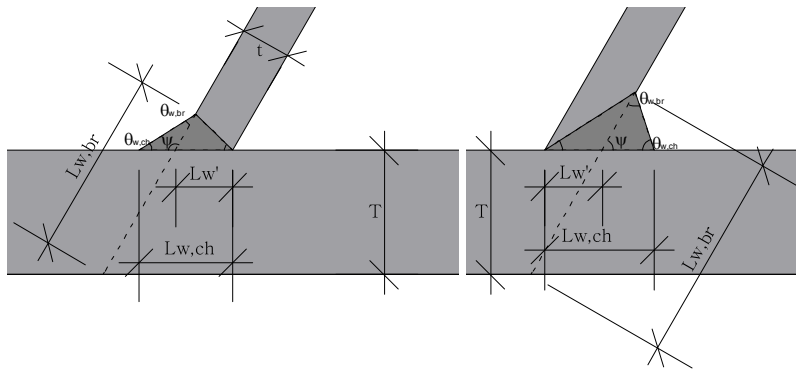


Figure 4.2: Dimensions needed to define weld geometry - left, crown toe and right, weld crown heel.

Figure 4.3 compares the weld toe geometry in the model, obtained following the procedure described, to the weld profile of the fatigue test joint S5-2-j2. The model of the weld profile closely represents the real weld profile. Both weld profiles meet the AWS requirements.

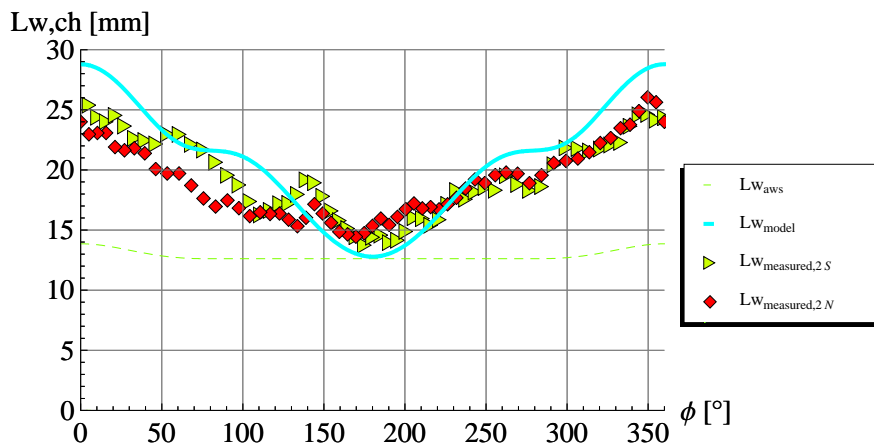


Figure 4.3: Weld footprint length comparison - AWS (AWS, 2000) recommended minimum, S5 BEM model and S5-2 j2 measured.

Tube intersection

The parametric equations describing the intersection between a cylinder whose axis is the coordinate axis xx' and a cylinder whose axis belongs to the plane xoz and has an angle θ_{br} with the xx' axis (see Figure 4.4) are given by:

$$x = \frac{d}{4} \cos(\phi) \sin(\theta_{br}) + \cot(\theta_{br}) \left(\frac{d}{4} \cos(\theta_{br}) \cos(\phi) + \frac{D}{4} \sqrt{1 - \frac{\frac{d^2}{4} \sin(\phi)^2}{\frac{D^2}{4}}} \right) + e \cdot \tan(\theta_{br}) \quad (4.11)$$

$$y = \frac{d}{4} \sin(\phi) \quad (4.12)$$

$$z = \frac{D}{4} \sqrt{1 - \frac{\frac{d^2}{4} \sin(\phi)^2}{\frac{D^2}{4}}} \quad (4.13)$$

$$(4.14)$$

where,

- ϕ : parameter varying in the interval $[0, 2\pi]$;
- e : eccentricity of the brace at axis origin;

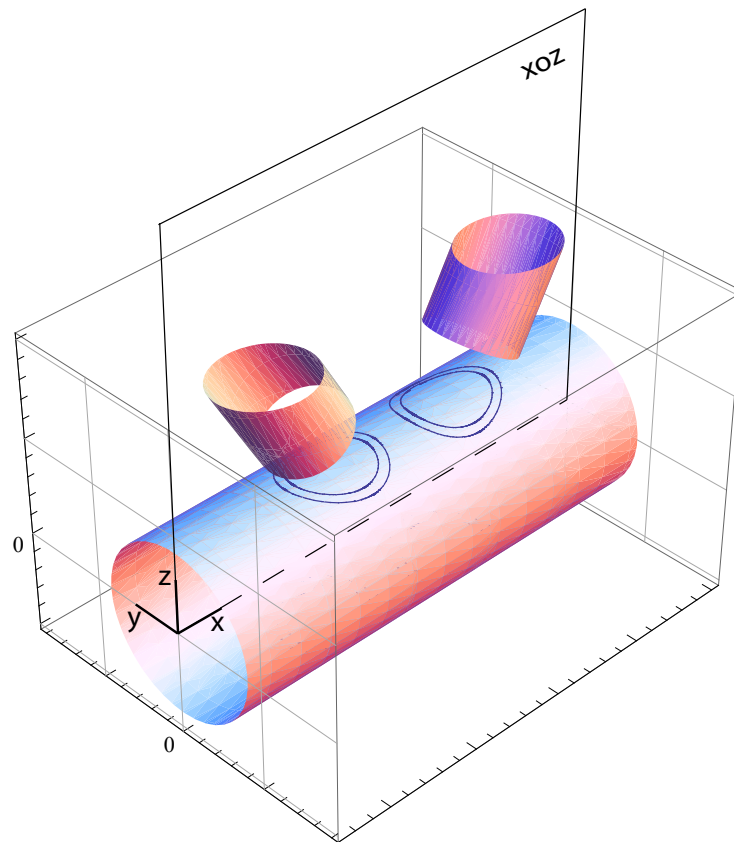


Figure 4.4: Tube intersection.

4.2.2 Material properties

The joint material is elastic linear with Young Modulus $E = 210 \times 10^3 \text{ N/mm}^2$, poisson ratio, $\nu = 0.3$. Rigid rings are 100 times more rigid and have same Poisson ratio.

The Paris law constants $C = 2.0 \times 10^{-13} (\text{mm/cycle})(\text{N/mm}^{-3/2})$ and $m = 3$ were considered for deterministic fracture mechanics calculations and were used to obtain experimental stress intensity factors from ACPD measures (see paragraph 3.4.2).

4.2.3 Boundary conditions

The joint is fixed in the 3 directions at the chord right extremity (see Figure 4.7). External forces are introduced using rigid rings of length $\frac{\pi D^*}{10}$ (D^* diameter of the tube to which the rigid ring is connected) to preserve planar cross-sections.

4.2.4 Crack location and geometry

Stress analysis of the uncracked joint clearly identifies hot-spot site 1 as the point where stress concentration is higher. Therefore, and supported by previous and current experimental evidence (Schumacher, 2003, van Wingerde et al., 1997), hot-spots 1 were primarily considered in the present study. Figure 4.5 shows the different hot-spots and stress concentration at the weld toes.

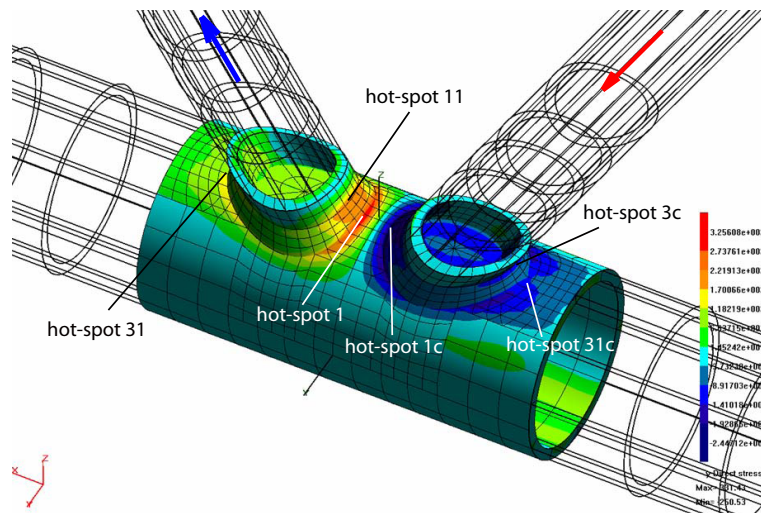


Figure 4.5: Stress concentration in the joint (σ_{xx}) - Series S5 fatigue test loading conditions.

Cracks at hs_{11} were also modelled for a number of geometries to confirm that hs_1 is critical even for cases where the geometry might lead to a switch in the crack location.

Also supported by experimental evidence, (see Section 4.2.4) the crack front corresponding to hot-spot site 1 is obtained by projecting a semi-ellipse over a conic surface. The conic surface directrix is the weld toe and the apex belongs to the xoz plane at a depth of $1.78 \times D$ (this depth was estimated as 300 mm for S5 tested joints, $D = 168.3 \text{ mm}$ - in order to keep it proportional to the absolute size) (see Figure 4.6). The crack angle, ϕ_{crack} , determines the x coordinate of the apex.

4.2.5 Meshing

The mesh is a key aspect when performing parametric studies on the influence of changing the size of the structural elements. In the present study, the proportions of the joint elements may change and it is therefore very important to assure that the results reflect the effect of size changes and not the effect of mesh being somewhat different. The following paragraphs describe the joint and crack

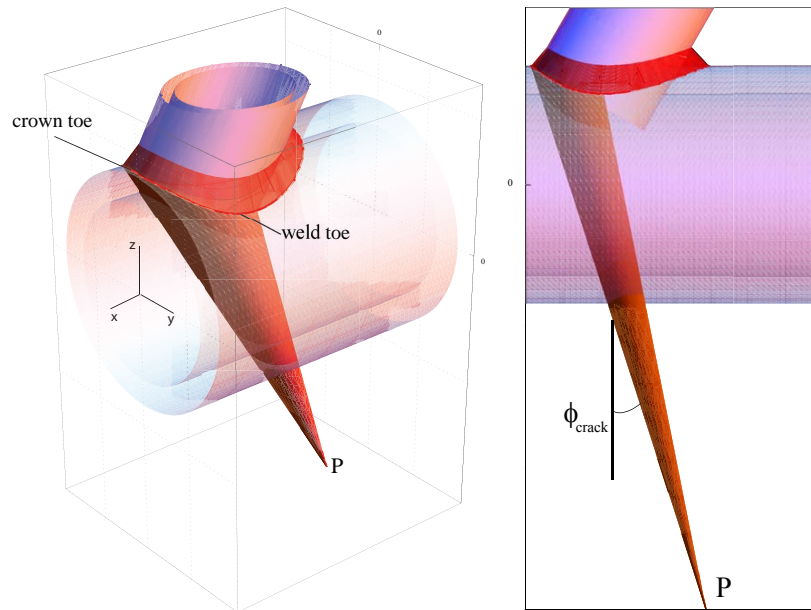


Figure 4.6: Crack surface geometry.

meshing. A mesh size influence test was carried out to ensure the results remain mesh independent in the parametric study range (see paragraph 4.5.3).

For 3-D problems, boundary elements are surfaces. BEASY allows these surfaces to be either quadrilateral or triangular in shape. Each element is used to represent the stress (...) behavior of a small section of the surface area of the component being analysed. Although all 3-D elements are the same in this respect, there are a number of different element types which the user can choose (Figure C.2 in appendix). All 3-D four sided elements have nine mesh points, arranged in a regular 3×3 grid. This defines the position and curvature of the element in a similar way to the 2D and axisymmetric line elements. As there are 9 mesh points, the geometry is quadratic and so may be curved. This is true even for the lower order (e.g. linear) elements. Similarly, triangular elements have six mesh points, with one at each vertex and one on each mid-side. (...) Every element also has a number of nodes. These are the positions where the values of the problem variables are calculated. The order of the element may be constant, linear, reduced quadratic or quadratic. (BEASY, 2003, In)

Joint mesh

The boundary elements model includes about 8100 mesh points and 2300 elements (total of about 30000 degrees of freedom) distributed in 8 zones as shown in Figure 4.7. Zones are groups of elements which can be considered as substructures of the component. Among these 8 zones, Zone 2 (see Figure 4.8), where the crack is located and the stress is highly nonlinear, has a dense mesh; Zones 6, 7 and 8 are rigid rings for the external force introduction.

Even though BEASY has automatic meshing capabilities through its user interface, there is no programming possibility. For this reason, an *Excel Workbook* was prepared to calculate the mesh point coordinates, elements (including the weld profile and crack) and zones definitions. This allowed for the creation of user controlled, validated model files from the joint geometric parameters in a BEASY compatible format.

The entire model is meshed with reduced quadratic four-sided elements Q38 (see Figure C.2 in appendix) wherever possible and exceptionally with triangular quadratic elements. Reduced quadratic elements are the default elements defined in BEASY-IMS (user interface). Tests have shown that these elements provide highly accurate solutions and reduce modeling time and disk requirements (BEASY, 2003).

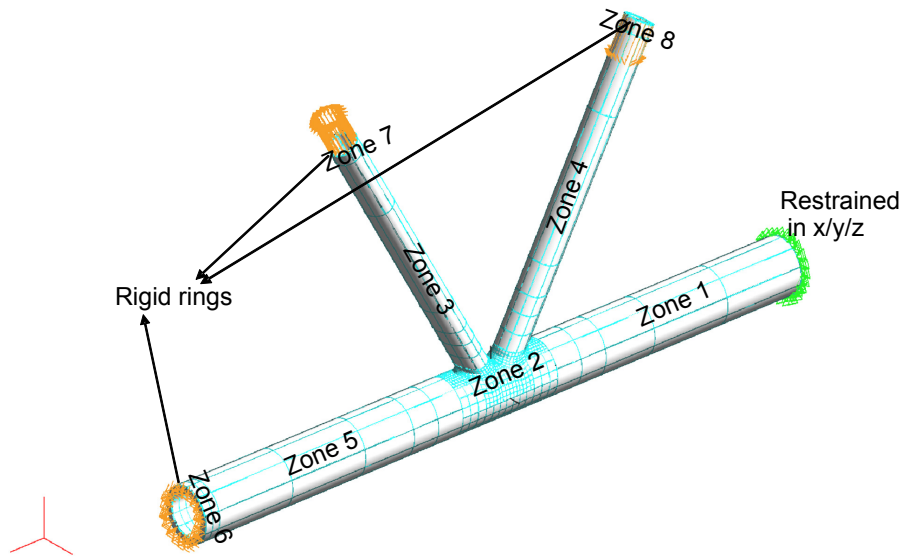


Figure 4.7: Zoning of the boundary element model.

Crack mesh

As described before, the crack faces belong to the conic surface (see Figure 4.6) and the crack front is doubly-curved. This complex geometry makes modelling of the crack and of the propagation of such a crack in a tubular joint a complicated task. The mesh of the crack surface has to be carefully chosen. A good quality mesh depends on the shape of the elements defining the crack surface.

Although Beasy software provides a crack growth tool allowing for automatic crack propagation from an initial crack, a manual, stepwise, crack modelling was preferred. The following reasons justify this option:

- ◆ due to the sharp weld toe geometry, automatic crack growth requires a very small step size so that the crack path remains at the weld toe.
- ◆ the substantial amount of time spent to automatically grow a crack from a_0 to $T/2$ and the model sizes would have made it impossible to carry-out the parametric study in a reasonable amount of time;
- ◆ the need for identical crack path for the different basic load cases to make it possible to isolate/superpose their influence;
- ◆ manual crack growth allows the control of the crack shape, a/c , evolution and thus an indirect inclusion of the coalescence phenomenon;
- ◆ automatic crack growth adds a new row of crack elements to define the new crack front - this leads to crack shapes tending to "semicircular" after a few increments depending on the increments size.

The manual crack growth corresponds to the calculation of a set of models with built-in cracks of different given shapes and depths. The crack follows the conic surface (Figure 4.6). The mesh points are calculated to suit the curved shape. The number of elements and mesh points remains constant for the different crack depths. However, Beasy automatically remeshes the area near the crack in order to optimally adapt the crack mesh within the existing joint mesh (see Figure 4.9).

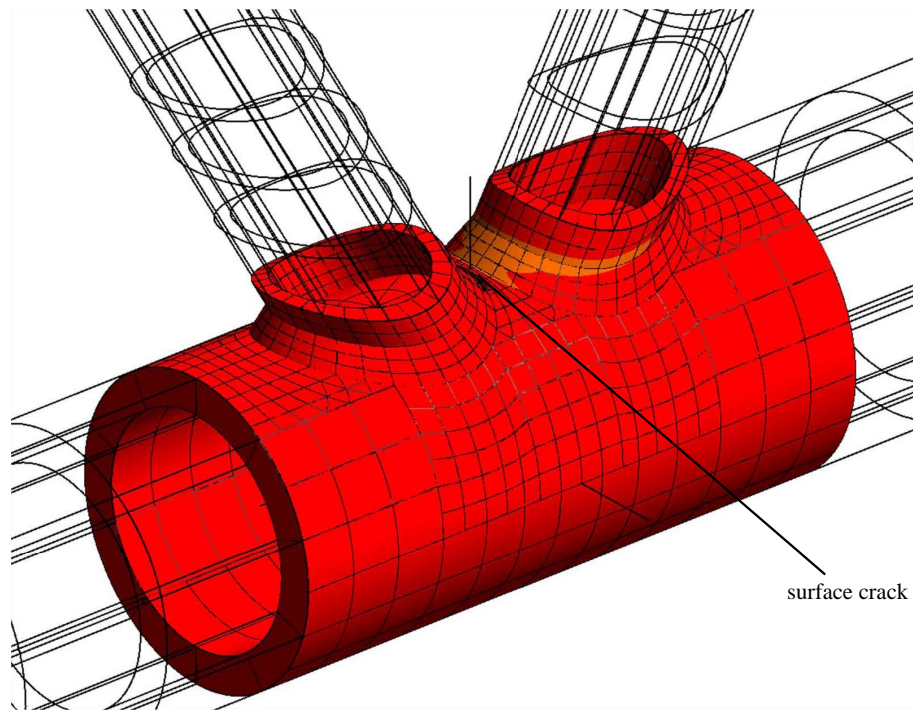


Figure 4.8: Zone 2 - refined mesh in zone where the surface crack is located.

4.2.6 Basic load cases and complex load case

A main objective of the present study is to investigate the effect of the different basic load cases on the fatigue behaviour of tubular K-joints of different sizes. When considering only the in-plane actions, five basic load cases can be defined (see Table 4.1). Several considerations justifying the selected method of decomposing the applied forces can be found in Schumacher (2003).

The developed boundary element model allows for the application of the five basic cases in an independent or combined manner (complex load). A constant nominal stress range, $\Delta\sigma$, is applied as external forces at the rigid rings. Complex load results of the simultaneous application of the selected basic cases, thus giving only in-phase actions in this study. Out of the 5 basic load cases, 3 are considered predominant in this study: LC1, LC4 and LC5.

When applying actions to the model, the stress ratio, is equal to zero, $R = 0$, or $\sigma_{max} = \Delta\sigma$ is used for simplicity. Underlying assumption is that there are no crack closure effects.

4.2.7 Stress intensity factors

For mixed-mode problems, the equivalent stress intensity factor, K_{eq} , is calculated at every mesh-point along the crack front using equation:

$$K_{eq} = \sqrt{(K_I + |K_{III}|)^2 + 2K_{II}} \quad (4.15)$$

where K_I , K_{II} , K_{III} are the stress intensity factors for the three crack opening modes calculated along the crack front (Gerstle, 1986). The same is valid for SIF ranges, ΔK .

For load cases LC1, LC4 and LC5 Figures 4.10 and C.1(in Appendix) show that crack opening mode I is predominant over modes II and III and this is true for all geometries. Indeed, the equivalent stress intensity factor, K_{eq} , is superposing itself with the stress intensity factor for opening mode I, K_I . Schumacher also showed a predominant mode I behaviour even neglecting crack angle. In the present study, crack angle, ϕ_{crack} , is assumed constant and taken as the bisectrix between the weld profile and the chord wall at the crown weld toe.

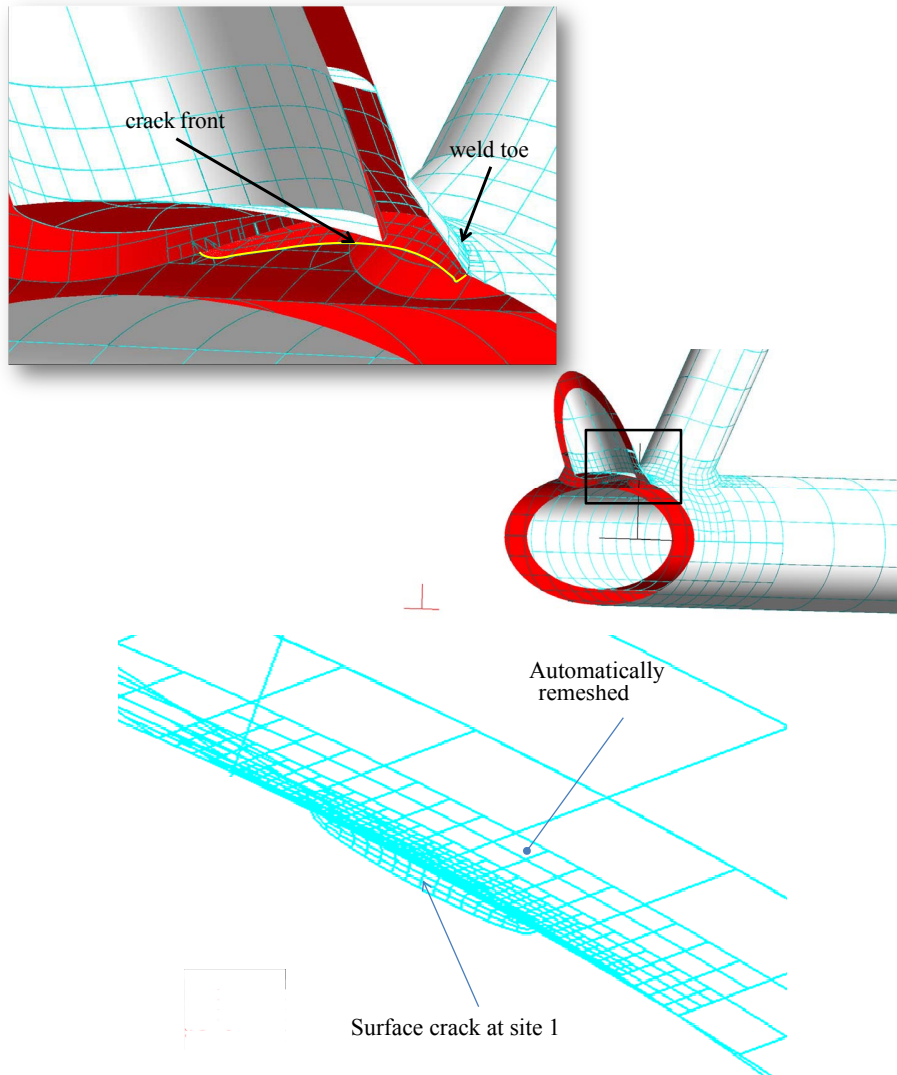


Figure 4.9: Detail of auto-remeshed area near the crack.

4.3 Fatigue crack growth model

The crack growth process is simulated using an incremental crack-extension analysis. For each crack extension, a stress analysis is carried out and the stress intensity factors are computed. SIF values in-between are linearly interpolated.

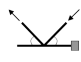
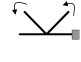
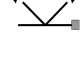
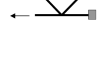
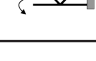
The Paris Law (Paris, 1960) was used to compute the crack growth rate between the different crack sizes:

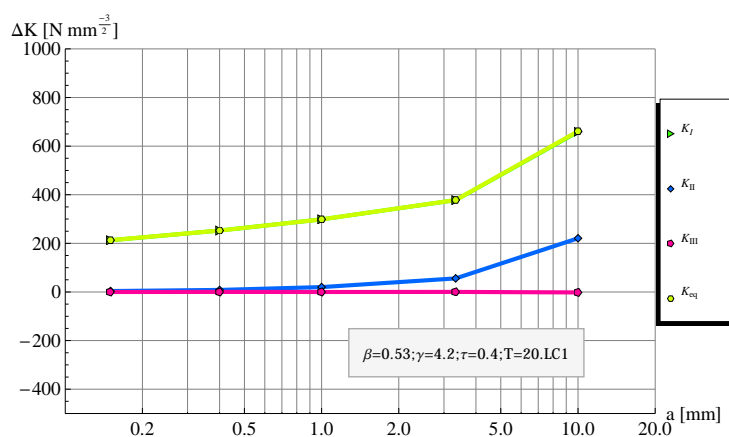
$$\frac{da}{dN} = C \cdot \Delta K_{eq}^m \quad (4.16)$$

where, C and m are the crack growth rate constants for the material and ΔK_{eq} is the equivalent stress intensity factor range.

Crack initiation is not considered in the current crack growth model. This simplification is justified by the fact that for welded joints without treatment the crack initiation phase represents only a small fraction of the fatigue crack through thickness propagation (see Section 2.3). Results of the fatigue tests carried out (see Section 3.1) support this hypothesis as the initiation phase was about 10% of the fatigue life at the end of the test (corresponding to N_3). It is also assumed that the fatigue load is clearly above the fatigue limit (stress intensity factor thresholds not considered), and constant

Table 4.1: Individual basic load cases and boundary conditions (adapted from Schumacher (2003)).

No	External forces		Schematic	Corresponding nominal stress
LC1	Balanced axial brace	$F_{ax,br}$		$\Delta\sigma_1 = \frac{F_{ax,br}}{A_{br}}$
LC2	Un-balanced in-plane bending brace	$M_{ipb1,br}$		$\Delta\sigma_2 = \frac{M_{ipb1,br}}{W_{br}}$
LC3	Balanced in-plane bending brace	$M_{ipb2,br}$		$\Delta\sigma_3 = \frac{M_{ipb2,br}}{W_{br}}$
LC4	Axial chord	$F_{ax,ch}$		$\Delta\sigma_4 = \frac{F_{ax,ch}}{A_{ch}}$
LC5	In-plane bending chord	$M_{ipb,ch}$		$\Delta\sigma_5 = \frac{M_{ipb,ch}}{W_{ch}}$

**Figure 4.10:** Comparison of the ΔK for the three different crack opening modes for load case 1 ($\Delta\sigma_{nom} = 100$ MPa, $\beta = 0.53$; $\gamma = 4.2$; $\tau = 0.4$; $T = 20$ mm).

amplitude cycles are applied.

4.4 Standard model for fatigue life computation

The schematic in Figure 4.11 describes the procedure used to carry out a crack propagation analysis. Information such as the *joint geometry* (namely the members dimensions and weld size), the *crack geometry* (namely the crack site, crack shape, crack angle and crack depths for the different increments) and the *load case* (basic load cases or complex load case combining different basic load cases in a single model) is input. Then, the mesh points coordinates are calculated in Excel for both the joint and the crack geometry corresponding to each crack depth.

The geometry of the joint is exported in Beasy data format. The crack model is also exported in Beasy syntax in a separate file. This is repeated sequentially for all the combinations of basic load cases (or just the complex case) and crack depths. The *Beasy crack adder* routine is then used to add the cracks to the joint models and automatically re-mesh the crack vicinity. Models are then run using *Beasy solver*. For each load case and crack depth increment there is a results file containing the stress intensity factors K_I, K_{II}, K_{III} along the crack front mesh points. These data are imported and treated using *Wolfram Mathematica*® (Wolfram, 1988) software. The equivalent stress intensity factors are then calculated. The crack growth rates are computed using the Paris law and the fatigue

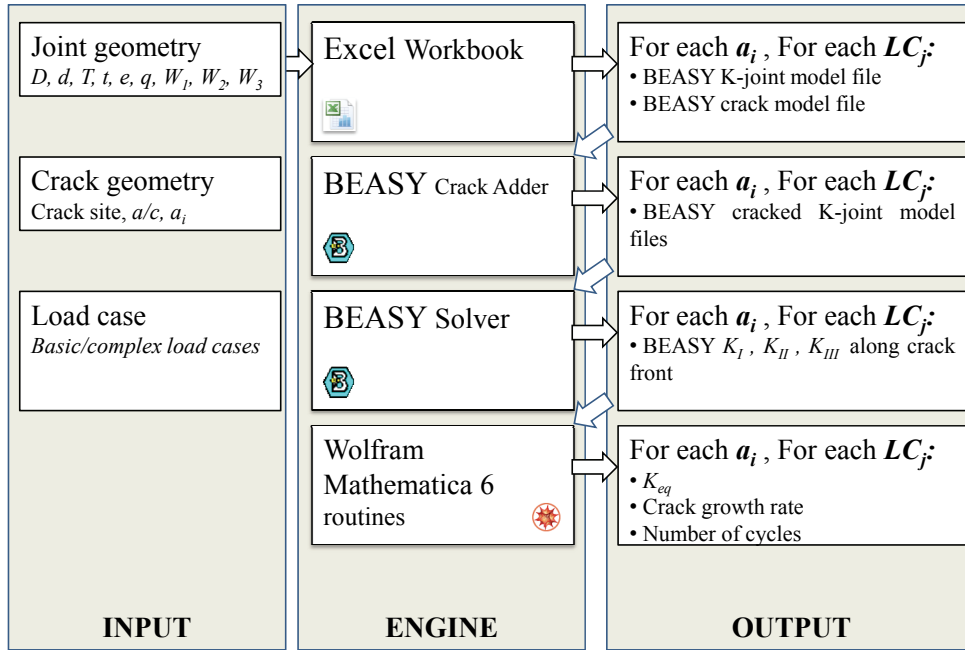


Figure 4.11: Schematic of the procedure used to carry-out a crack propagation analysis.

life calculated using Mathematica discrete linear integration algorithm.

4.4.1 Initial crack size and location, crack increments and failure criterion

As explained in paragraph 4.2.4 the crack is located at hot-spot $hs1$ and grows in a predefined conic surface. The final crack depth, a_f , is taken as equal to half of the wall thickness of the cracked element, $T/2$. Although a final crack depth equal to the wall thickness is more common as failure criterion, it has been set to $a_f = T/2$ by others (Walbridge, 2005). This option is justified by the fact that small variations in the final crack depth have little influence in the final number of cycles as the majority of the crack life is spent at smaller crack depths (Moan and Song, 2000). As the crack front gets close to the "bottom" boundary of the cracked member (the inner boundary of the chord) numerical problems may arise and an extensive crack remeshing would be needed. Furthermore, since through-thickness must consider internal forces redistribution, the problem is no more limited to the joint study but must consider whole structure behaviour.

A constant initial crack size of $a_0 = 0.15$ mm is considered regardless of the geometry of the joint (Walbridge, 2005). Crack growth increments were defined to correspond to crack depths of $a_{inc} = \{0.15 \text{ mm}, T/50, T/20, T/8, T/6, T/2\}$.

4.5 Model validation

The validation of the model was carried out:

- ◆ by comparing the numerical results to the behaviour of the tested specimen. The comparison includes the nominal stresses (in the chord and braces), the stress in the joint and the stress intensity factors for different crack depths;
- ◆ by using the model accuracy evaluation, provided by BEASY;
- ◆ by carrying out a mesh convergence test to investigate the sensitivity of the model with the mesh density.

These different comparisons and tests are presented in the following paragraphs.

4.5.1 Comparison to fatigue test results

In order to compare the numerical results obtained using the standard model described in section 4.4 to the fatigue test results, a model was created with the same nominal dimensions as Series S5 specimens. Tables 4.2 and 4.3 summarise the geometry parameters used to define the model simulating joint S5-2-j1.

Table 4.2: Geometric parameters of model used to compare with S5 fatigue test results.

ID	D [mm]	T [mm]	d [mm]	t [mm]	e [mm]	g [mm]	L_{ch} [mm]	H [mm]	W_1 [mm]	W_2 [mm]	W_3 [mm]
C175	168.3	20.	88.9	8.	22.	19.9	2166.	1800.	15.	10.	5.

Table 4.3: Non-dimensional parameters of model used to compare with S5 fatigue test results.

ID	θ [-]	β [-]	γ [-]	τ [-]	α [-]	ζ [-]	e/D [-]
C175	60.	0.53	4.21	0.4	25.7	0.12	0.13

The nominal stresses introduced at the joint extremities correspond to the values calculated using a simplified bar-model of the truss beam. In this simplified model, the eccentricity is simulated using an extremely rigid bar element as *Model "C"* suggested in (Romeijn, 1994, Walbridge, 2005). The truss model is solved on commercial software RSTAB (RSTAB 2003) - see Figure 4.12.

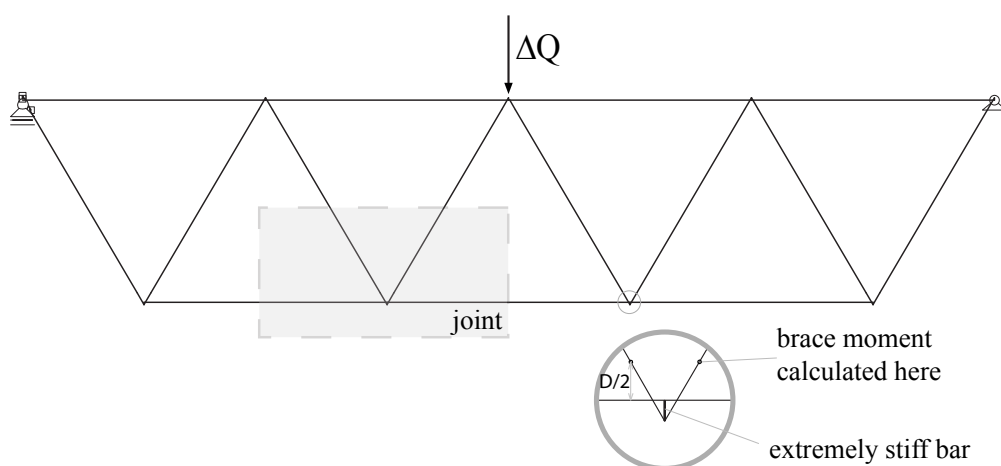


Figure 4.12: Truss model used to calculate forces and bending moment acting in the joint.

Figure 4.13 shows the nominal external forces applied at the extremities of the boundary element joint.

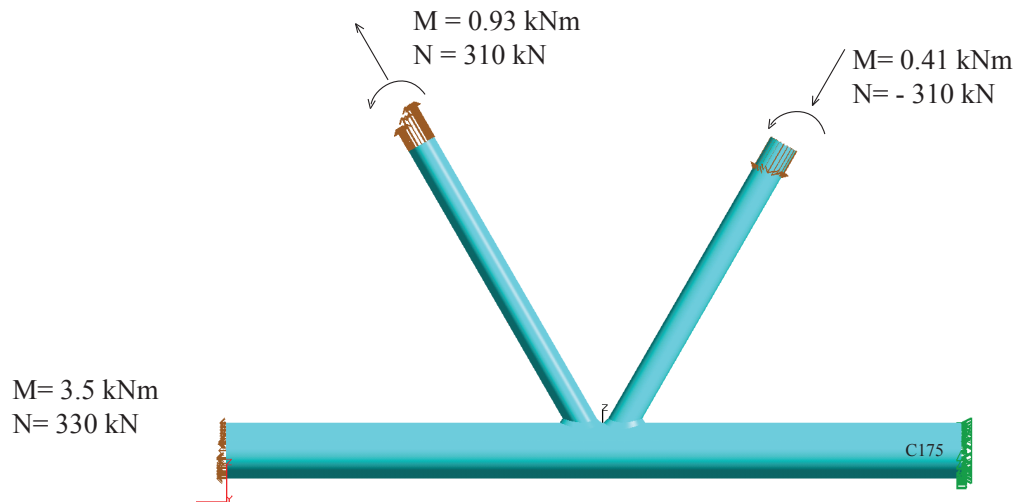


Figure 4.13: Model representing tested joint S5-2 j1 and the external forces applied.

Member and joint stresses

The stresses obtained numerically (parallel to the longitudinal axis of the members) are compared to those obtained from the strains measured at the members and near the welds (at hot-spots 11 and 3 locations). In the truss members, where the stress state is predominantly uniaxial, a simple linear relationship is assumed between stress and strain ($\sigma = E \times \varepsilon$). In the multi-axial stress state regions near the welds, the generalised Hook law can be used to describe the relationship between strains and stresses. Several investigations made on the behaviour of CHS joints (Romeijn, 1994, Schumacher, 2003, van Wingerde, 1992) have found that the stress-strain ratio can vary depending on the load level and the location in the joint but that the average of that value is approximately 1.1 for RHS joints and 1.2 for CHS joints (van Wingerde, 1992, Zhao et al., 2000). The stress-strain ratio of 1.2 is used to derive the stress from measured joint strains. Figures 4.14 and 4.15 show the comparison between stresses obtained numerically and those obtained experimentally from strain gages.

In this comparison, it is included the model with complex load case (LC1+LC2+LC3+LC4+LC5) and the model with only load cases LC1, LC4 and LC5. The calculated stresses appear as a continuous line for clarity despite the fact they were obtained at discrete mesh-points. The three main basic load case combined (LC1+LC4+LC5) is close to the complex case for chord. For the tension brace the difference between these load scenarios is more pronounced.

In the case of the chord (tension brace side), Figure 4.14 shows a good correspondence between experimental and numerical stresses, both for top and bottom chord extreme fibers.

In the case of the brace in tension, Figure 4.15, differences up to 20% can be seen between measured and BEM calculated stresses. These differences are believed to be due to the approximations made in the global truss model, namely the simplified joint rigidity or the eccentricities and the simplified end conditions. It seems that the bending moment in the brace is slightly underestimated by the simplified truss model.

Additionally, a comparison was made using speckle interferometry strain measures and strains from numerical model (Abaqus) for series S21 (Schumacher, 2003). Figure 4.16 shows that Beasy results, for this geometry, superpose with results obtained independently both for location 1 (chord) and location 11 (brace).

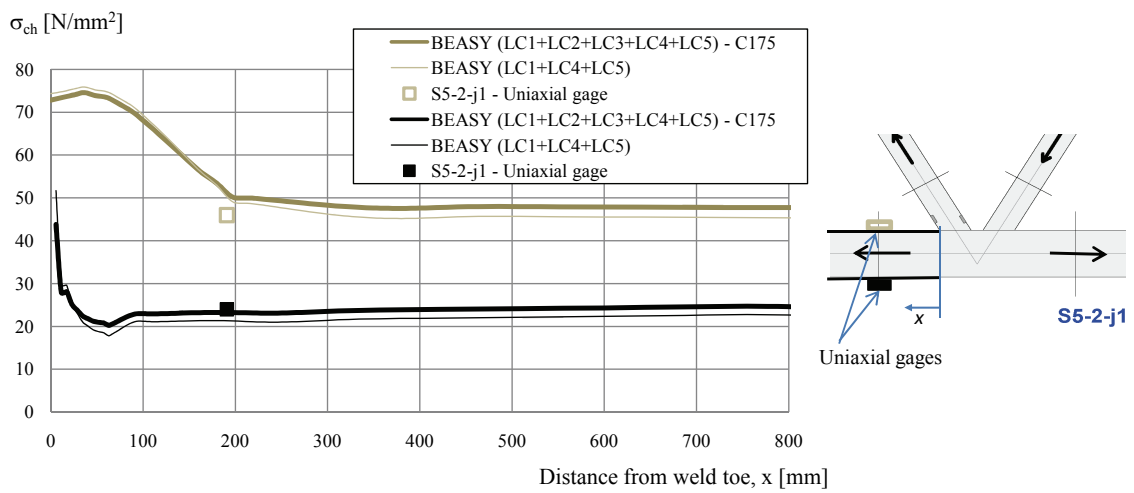


Figure 4.14: Stresses in chord of joint S52-j1, calculated and measured.

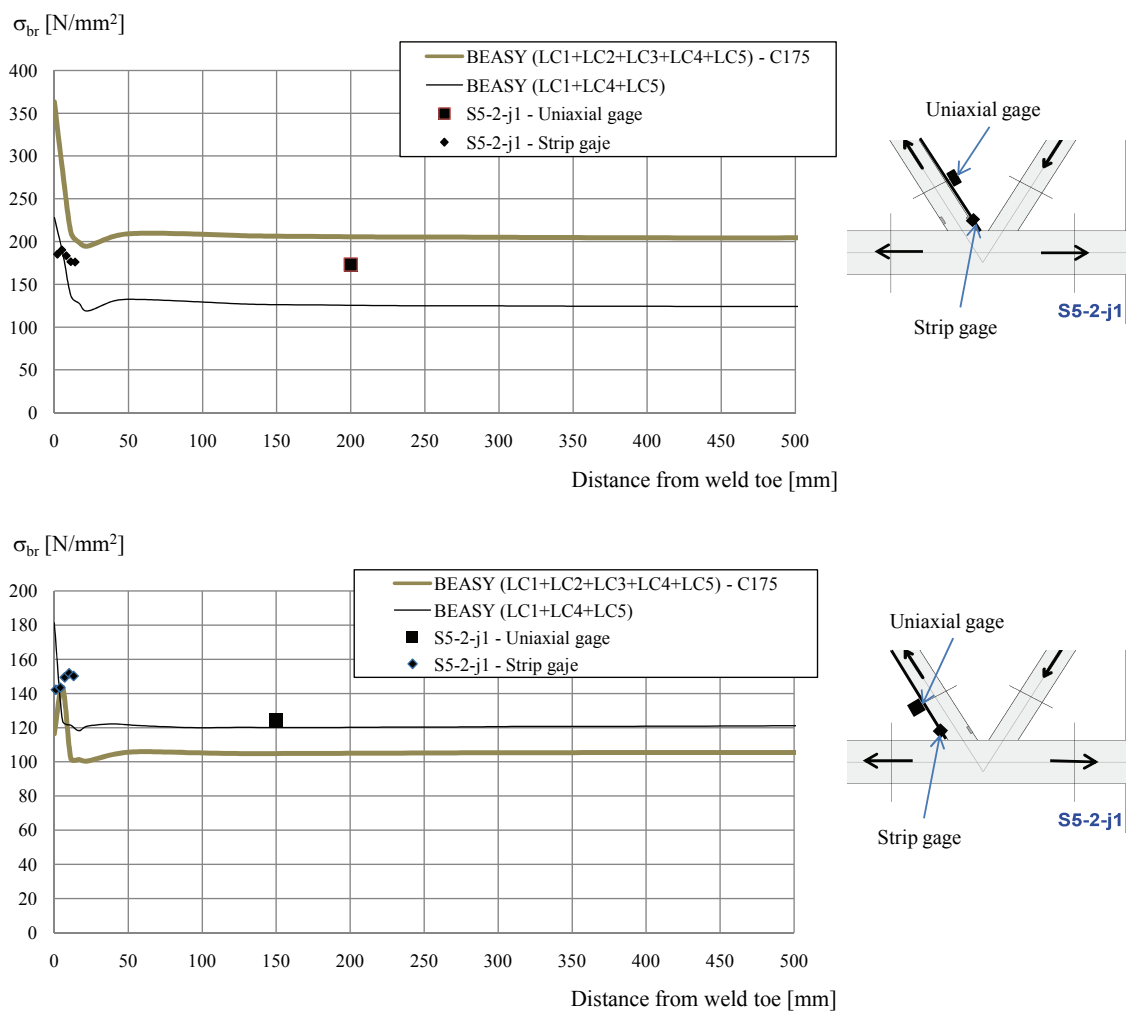


Figure 4.15: Nominal and hot-spot stresses in brace of joint S52-j1, calculated and measured

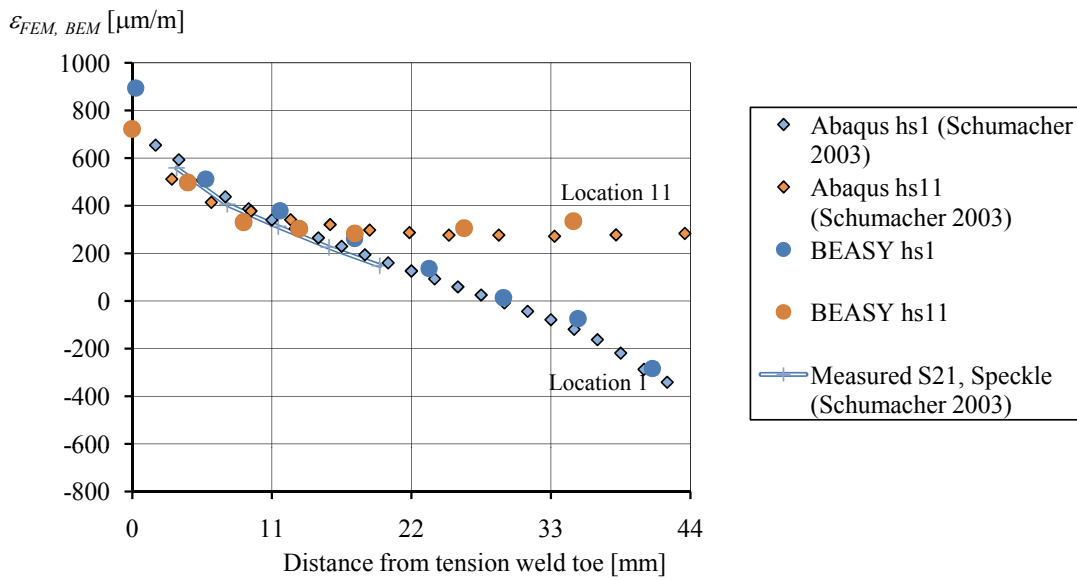


Figure 4.16: Comparison of principal strains at Location 1 and 11 of joint S21, between validated Abaqus model (Schumacher, 2003), BEASY model and measured.

Stress Intensity Factors

Figure 4.17 compares the stress intensity factor range ΔK computed using the model described and the values measured using the Alternating Current Potential Drop system at different locations at the weld toe crown (P1 to P8). It is important to note that in the early stages of crack propagation ($a \approx 1$ mm) the ACPD probes are influenced by multiple cracks that will join together. A good match was found between both results, less good for 2 to 5 mm crack depths.

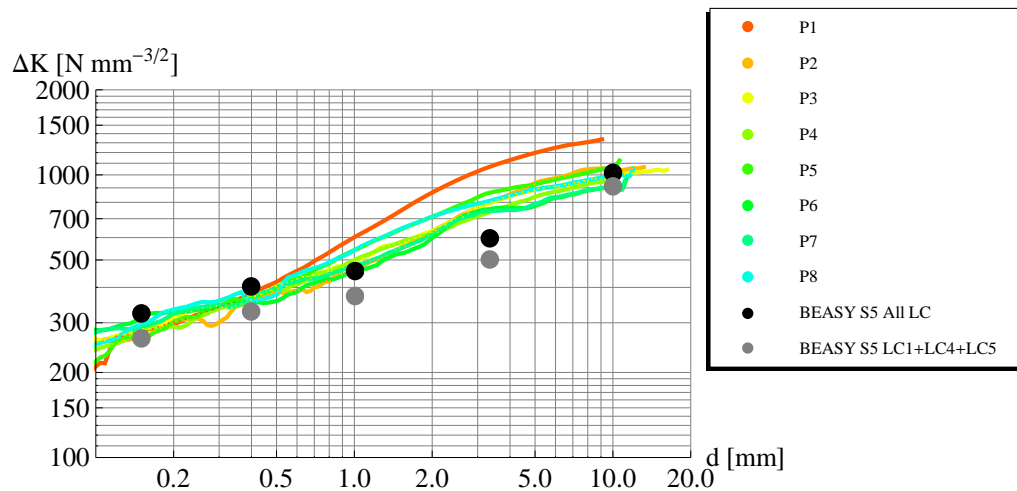


Figure 4.17: Comparison of ΔK values at different crack depths - BEASY and ACPD experimental measures (beam S5-2) (d is the crack depth at the probe location).

4.5.2 BEASY - Accuracy evaluation

BEASY provides post-processing tools to evaluate the model accuracy such as accuracy reports or the stress error norm plot which estimate the accuracy of the results of each element. They provide an estimate of the error in the form of the percentage of the stress. Figure 4.18 shows the *stress error norm* plot for the model simulating the fatigue test. The stress error norm is higher (11.89%) in zone 5, near zone 2, due to the element grading. For zone 2, where the surface crack is located and accurate results are needed, the stress error norm is less than 0.1%.

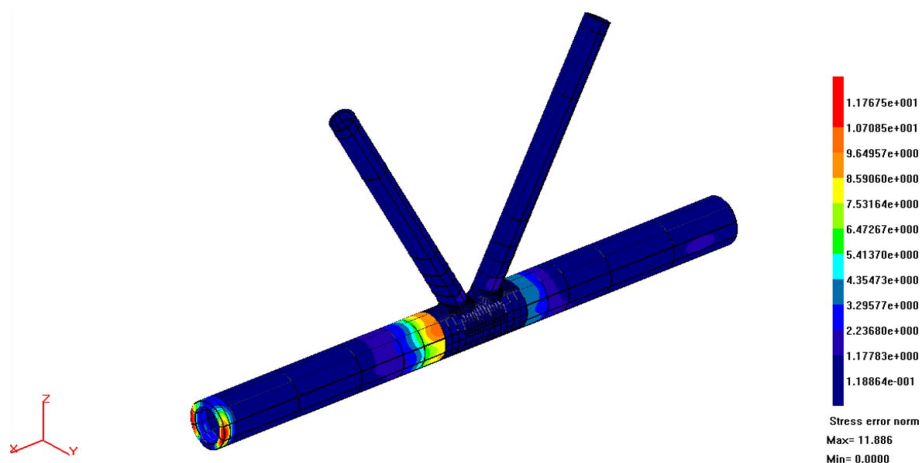


Figure 4.18: Stress error norm.

Table 4.4 shows the result of an accuracy report requested for the same model. This result is obtained by considering the equilibrium convergence in each zone, by summing the surface forces in each direction. The zone stress error norms are as low as 0.01% for zone 2 and as high as 5% for zone 6 (rigid ring in the chord).

Table 4.4: Model accuracy report.

	Zone stress error norm [%]
Zone 1	1.18
Zone 2	0.01
Zone 3	0.33
Zone 4	0.35
Zone 5	2.34
Zone 6	5.07
Zone 7	0.57
Zone 8	0.58

4.5.3 Model mesh convergence

The accuracy of boundary elements model increases with the number and quality of elements used. In order to check the accuracy and stability of the numerical results, five different mesh densities were tested and results compared to the standard model. The geometry taken to perform this mesh sensitivity test is the same as S5, shown in table 4.2.

This test is a thorough task as the model has to be manually defined in BEASYTM interface so that BEASY-IMS Auto-remesh tool can be utilised to generate the different meshes used to compare models.

Figure 4.19 and Table 4.5 show the models and respective mesh qualities near the welds, in the chord and diagonals and crack.

Table 4.5: Models used for mesh convergence testing.

	a. Basic Automesh	b. Improved Automesh	c. Best Automesh	d. B51 <i>BEASY_{mod.99.xls}</i>	e. C154 <i>BEASY_{mod.104.xls}</i>
Welding	1	2	3	3	3
Chord/Diagonals	3	3	3	1	2
Crack	2	2	2	2	2

1 - coarse

2 - fine

3 - extra fine

Model *a.* is a coarse model generated using BEASYTM auto-meshing without special care for the weld and near-crack area. Model *b.* results from model *a.* by improving the mesh quality near the welds and cracked area and model *c.* has the finest mesh in both the weld and the joined elements. Models *d.* and *e.* are generated using EXCEL macros created on purpose. The later results from model *d.* refining the mesh of the chord and diagonals. The cracks imposed at different depths have always the same mesh as described in Section 4.2.5. The mesh of model *e.* is the standard mesh used in the parametric study.

Figure 4.20 shows the values of mode I stress intensity factors, K_I , along the crack front, for a crack depth, $a = 0.15$ mm and load cases LC1, LC4 and LC5. For load case LC1 and LC4, the five sets of results converge convincingly, specially if we compare the deepest point ($y = 0$ mm). For load case LC5, the standard model (C154) and the automatically meshed model differ of about 30% at the deepest point.

Figure 4.21 shows the values of mode I stress intensity factors, K_I , along the crack front, for a crack depth $a = 10$ mm, and load cases LC1, LC4 and LC5. This crack depth ($T/2$) represents the bigger crack modelled. As the number of boundary elements is constant regardless of the crack size, it is the crack size in which the mesh of the crack can most influence the results. Again, for LC1 and LC4 the mesh convergence is achieved convincingly. For LC5, the difference between the most refined automatic mesh and the standard model (C154) is about 30%.

Results put in evidence the influence of the mesh quality on the stress intensity factor values. It is therefore very important to assure the quality of the mesh in the range of parameters studied.

Load case LC5 is the load case that presents bigger influence of the meshing (specially members mesh) on the results. This is because of the predominance of bending in the chord and the relatively thin tube walls. A special caution is thus due when analysing parametric results involving load case LC5, as they may include, an eventual "mesh effect" added to the effect of sizing joint elements.

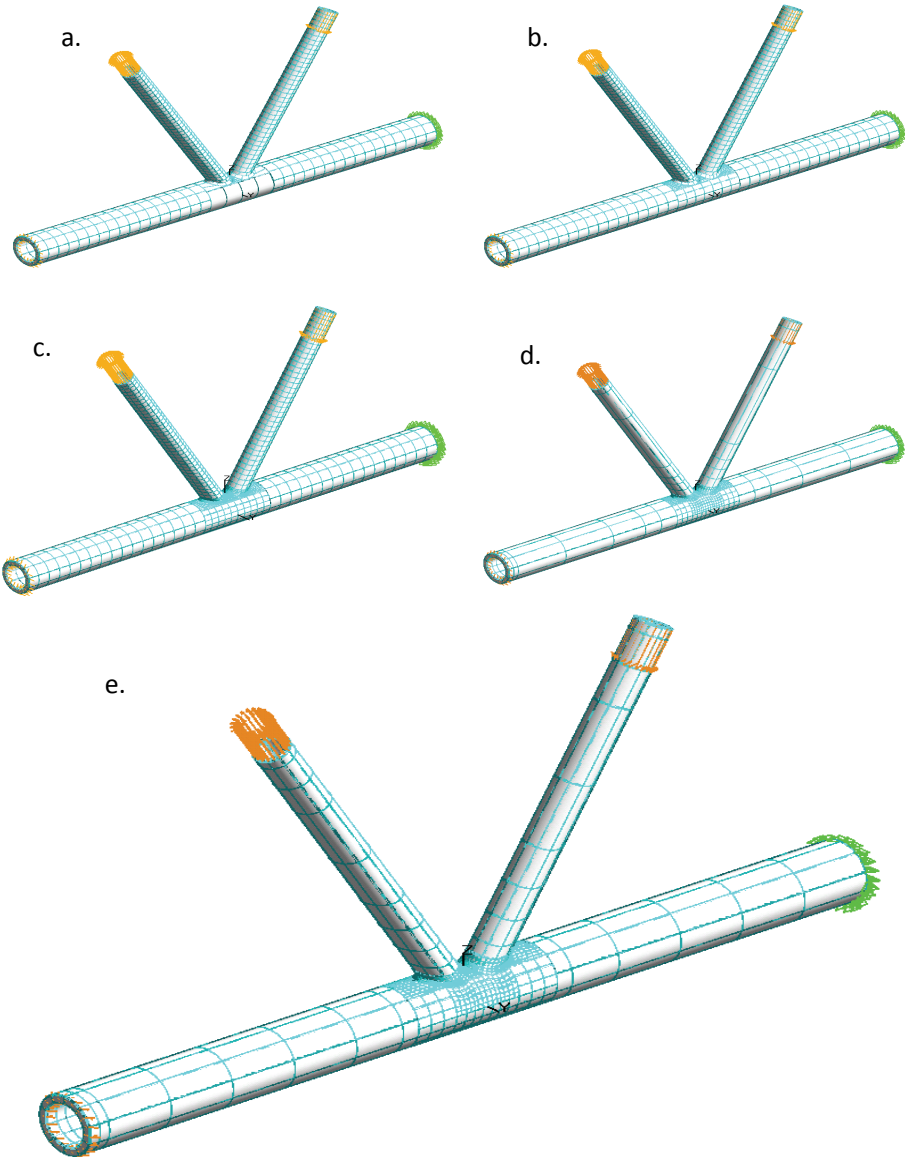


Figure 4.19: Models used for mesh convergence testing.

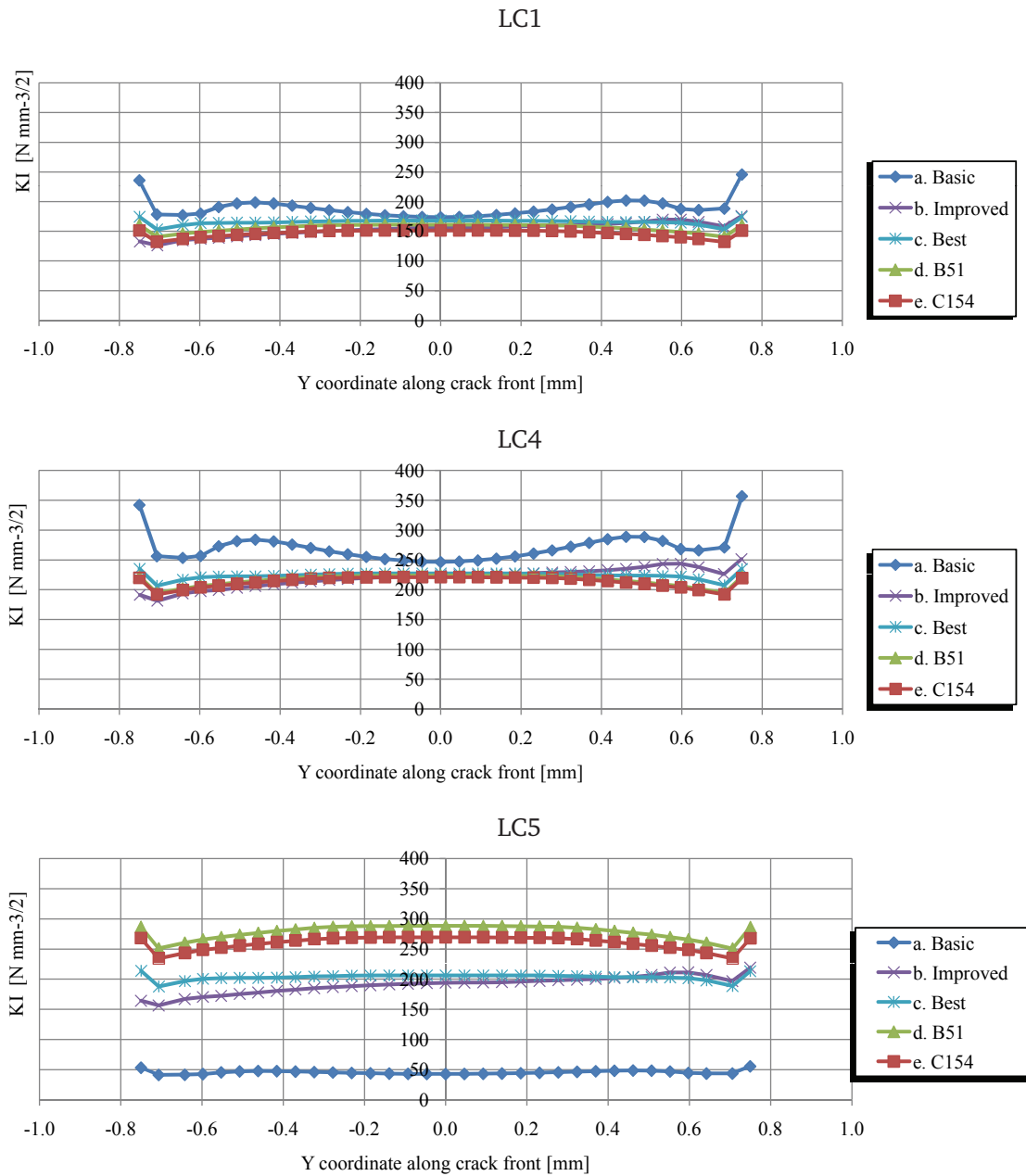


Figure 4.20: Convergence of K_I values along the crack front ($a = 0.15$ mm) for load cases LC1, LC4 and LC5.

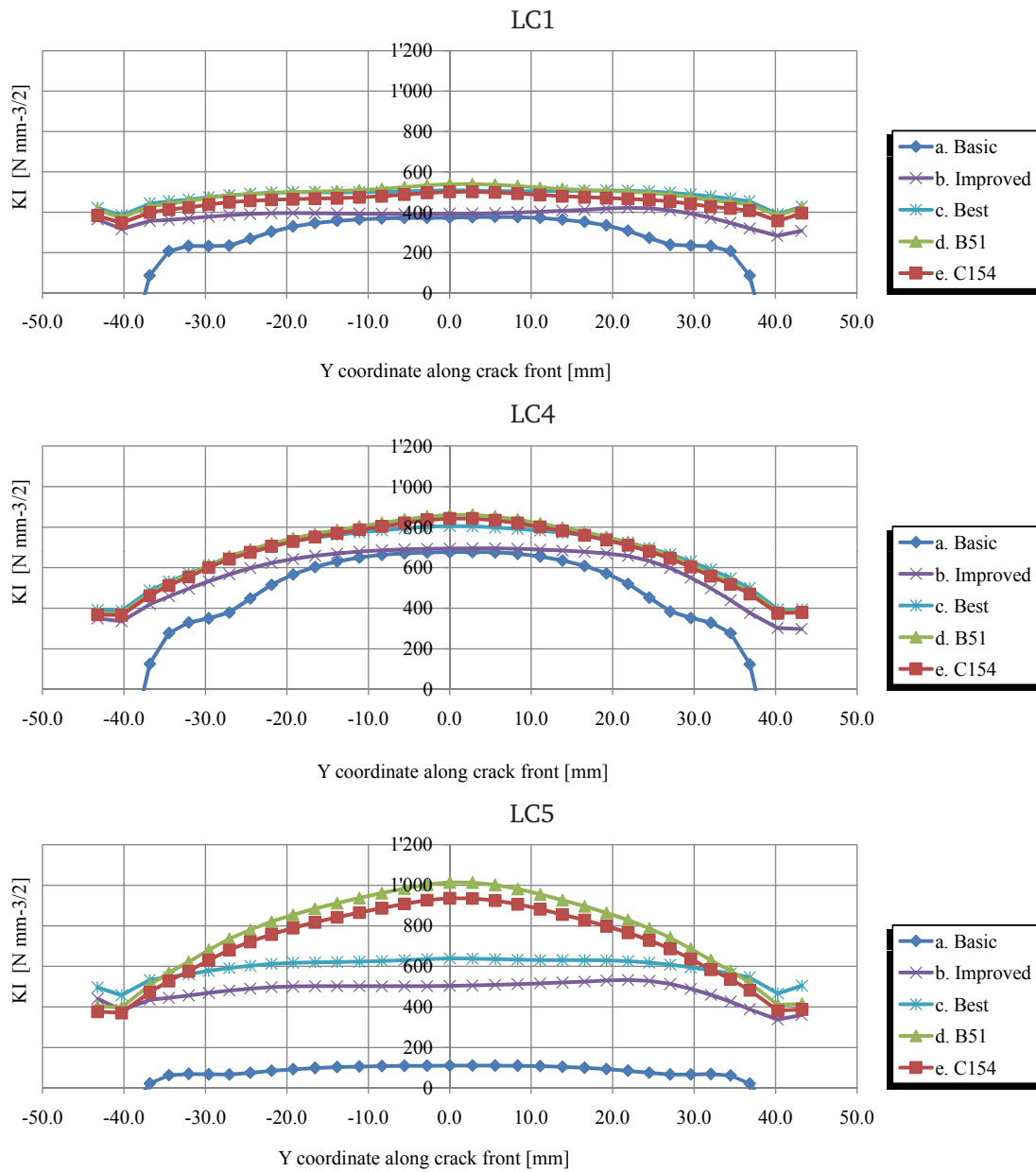


Figure 4.21: Convergence of K_I values along crack front ($a = 10$ mm) for load cases LC1, LC4 and LC5.

4.6 Combining basic load cases

The possibility of combining the results of basic load cases is very useful as it allows the modelling of various real loading conditions without having to rerun crack propagation simulations (to obtain SIF) each time.

Combination is possible, as the superposition principle is valid since:

- ◆ a linear elastic fracture mechanics (LEFM) analysis is carried out on linear elastic material;
- ◆ the crack path is established *a priori* and remains constant for the different basic load cases;
- ◆ crack closure is not considered;
- ◆ proportional basic load cases are considered to be acting in-phase;

The stress intensity factors for the different opening modes are combined, $K_{m,combined}$ and then the combined equivalent stress intensity factor, $K_{eq,combined}$ is calculated according to Equation (4.15). The resulting equations are:

$$K_{m,combined} = \sum_{LCi=1}^{lcn} K_{m,LCi}, \text{ where } m = \{I, II, III\} \quad (4.17)$$

$$K_{eq,combined} = \sqrt{\left(K_{I,combined} + |K_{III,combined}|\right)^2 + 2K_{II,combined}} \quad (4.18)$$

Figure 4.22 shows stress intensity factor range results obtained for the basic load cases acting separately and combined ($K_{eq,LC1}$, $K_{eq,LC4}$, $K_{eq,LC5}$, $K_{eq,combined}$) and the result for the model with complex load case where all the five basic load cases were introduced simultaneously ($K_{eq,complex}$). Resulting SIF ranges compare well, showing that the use of the three main basic load cases (LC1, LC4 and LC5) is a good approximation of the complex load case ($K_{eq,combined}$ and $K_{eq,complex}$ superpose).

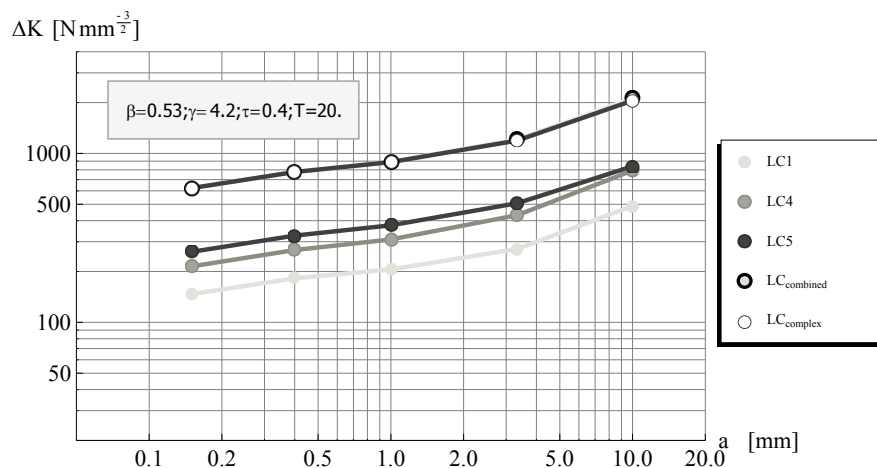


Figure 4.22: Stress intensity factor results obtained for the basic load cases acting isolated and combined and corresponding complex load case

4.7 Summary and conclusions

This chapter presents the description and validation of a CHS K-joint crack propagation model. The 3-Dimensional boundary element model is solved using BEASYTM software. The model was validated through comparisons between calculated stresses with measured stresses (strains) and between calculated stress intensity factors with experimentally measured stress intensity factors. A convergence test on the mesh density was done to validate results obtained for different-sized joints. A standard model for fatigue life computation is defined to be used in the parametric study.

The following conclusions can be drawn:

- ◆ The boundary element method can be used to calculate the stress intensity factors of surface cracks in CHS joints. Within this study specific tools were developed to model this complex crack shape in the double curved weld toe.
- ◆ To date, BEASY automatic crack growth calculation is not effective in the particular case of surface cracks at the weld toe due to the double curved crack geometry. The needed small increments make it too costly in time and computer resources to propagate a crack in the weld toe.
- ◆ Crack opening mode I is predominant for all geometries and for the three load cases considered.
- ◆ Results from the numerical model compare generally well with the measurements made during the tests, or computed from them (nominal stresses, hot-spot strains and stress intensity factors).
- ◆ The convergence of results for different meshes was checked. For load cases LC1 and LC4, the convergence is achieved convincingly. For LC5, results show some mesh effect affecting the results (differences up to 30%); thus, attention must be paid when analysing parametric results for this load case.
- ◆ For truss loading, typical complex load cases, can be well approximated by combining only three of the five main basic load cases, namely:
 - ◇ LC1- Balanced axial brace loading;
 - ◇ LC4- Axial chord loading;
 - ◇ LC5- In-plane bending chord loading.

Parametric study

5.1 Introduction

In this chapter, the numerical model validated and standardised in chapter 4 is used to analyse the fatigue behaviour for a range of welded CHS K-joints. Through comparisons between different joint models, the influences of a set of parameters defining the joint geometry and basic load cases are discussed. Results of the parametric study are compared in the form of stress intensity factors, fatigue life and fatigue strength.

Section 5.2 describes the scope of the parametric study, namely the geometries and load cases considered. The assumptions made, regarding the parameters assumed constant in this parametric analysis, are detailed in Section 5.3. A preliminary study on the influence of parameters assumed constant is presented. Results of the parametric study in terms of stress intensity factors and fatigue strength are presented and discussed in Section 5.4.

5.2 Scope of parametric study

This parametric study is limited to:

- ◆ Non-overlapping, as-welded, K-joints in uniplanar trusses with identical brace dimensions and $\theta = 60^\circ$;
- ◆ Geometry parameters typical to bridge application (detailed in Section 5.2.1);
- ◆ Cracks propagating from hot-spot site 1 (reasons were detailed in 4.2.4);
- ◆ In-phase and in-plane loading;
- ◆ Basic load cases LC1, LC4, LC5 (see Section 5.2.3).

Previous investigations focused on the determination of stress concentration factors at specific locations, correlated these results to the fatigue behaviour and finally made comparisons using either life or strength. Although this procedure is widely accepted and used, it assumes the fatigue behaviour of a joint is fully determined by the surface stress in the uncracked joint, regardless of the stress gradient through the thickness. In order to study in depth the effect of sizes of the connected elements, this hypothesis is not made here and results are shown in the form of stress intensity factors, fatigue life and fatigue strength.

5.2.1 Geometries

The procedure described in Section 4.4 to build and calculate the numerical models is time and resource consuming. Due to the amount of parameters describing the geometry of a CHS K-joint (see figure 2.1), choices had to be made regarding which parameters to consider. Three non-dimensional parameters were selected as main parametric variables: β , γ and τ . These are the parameters that define the relative geometry of the joint elements. For each set of non-dimensional parameters, at least two geometries corresponding to different absolute sizes were studied. This allows for a result checking and provides additional points to proportional sizing and to characterise the geometry correction factor, Y , introduced in the next chapter.

A number of other parameters such as the slenderness α , normalised gap ζ , and normalised eccentricity e/D , are kept constant. Although their effect on fatigue behaviour is recognised, it is believed to be less significant. To confirm this belief, some of these effects are evaluated in a preliminary study (Section 5.3).

Table 5.1 shows the list of geometries covered in the parametric study recalling here the non-dimensional parameters definitions:

$$\beta = \frac{d}{D}; \gamma = \frac{D}{2T}; \tau = \frac{t}{T}; \alpha = \frac{2L_{ch}}{D}; \zeta = \frac{g}{D} \quad (5.1)$$

where,

- d : outside diameter of the brace;
- D : outside diameter of the chord;
- t : thickness of the brace;
- T : thickness of the chord;
- g : gap size;
- L_{ch} : distance between two nodes.

The study of fatigue crack propagation of a single geometry requires the computation of $3 \times 6 = 18$ BEASY models (corresponding to 3 load cases and 6 crack depth increments, defined in 4.4.1).

Table D.2 (in Appendix) lists the details for each of the geometries created for the current investigation. The parametric study covers only cracks at hot-spot site 1. Equivalent Stress Intensity factors (ΔK_{eq} or SIF range similarly to K_{eq} as defined by Equation (4.15)) values for the 6 crack depths and the three basic load cases (LC1, LC4 and LC5) considered are given in Table D.3 (in appendix).

5.2.2 Varying β , γ , τ to resize the CHS joint

Figure 5.1 illustrates the joints resizing by changing each of the non-dimensional parameters β , γ , τ , the assumptions and the resulting constraints are illustrated in Figure 5.1 and can be summarised as follows:

- ◆ Thickness ratio, τ
 - ◇ Eccentricity, e , and gap, g , are kept constant;
 - ◇ Diameters of braces and chord as well as the thickness of chord remain constant;
 - ◇ Thickness of the diagonals and welds are scaled proportionally;
- ◆ Diameters ratio, β
 - ◇ Chord diameter, D , thicknesses of both the chord (T) and the brace (t) are kept constant;
 - ◇ The non-dimensional gap, ζ , remains constant (and so does the gap for constant chord diameters);
 - ◇ The eccentricity, e , increases when β increases;

Table 5.1: Summary of the parametric table ($\beta = 0.53$)

ID	T	β	γ	τ
-	[mm]	[-]	[-]	[-]
180	10	0.53	4.21	0.4
169	20			
181	40			
168	60			
129	20	0.53	4.21	0.5
178	30			
106	60			
107	60	0.53	4.21	0.6
130	20			
108	60	0.53	4.21	0.7
131	20			
109	36	0.53	7.01	0.4
132	12			
110	36	0.53	7.01	0.5
133	12			
111	36	0.53	7.01	0.6
134	12			
112	36	0.53	7.01	0.7
135	12			
113	29.7	0.53	8.5	0.4
136	9.9			
114	29.7	0.53	8.5	0.5
137	9.9			
115	29.7	0.53	8.5	0.6
138	9.9			
116	29.7	0.53	8.5	0.7
139	9.9			

◆ Chord slenderness, γ

- ◇ The thicknesses of both the chord (T) and the brace (t) remain constant;
- ◇ The diameter of the chord (D) is scaled;
- ◇ The ratios e/D and g/D remain constant;

Table 5.2: Summary of the parametric table ($\beta = 0.65$)

ID	T	β	γ	τ
-	[mm]	[-]	[-]	[-]
117	60	0.65	4.21	0.4
140	20			
171	60	0.65	4.21	0.5
172	20			
119	60	0.65	4.21	0.6
142	20			
120	60	0.65	4.21	0.7
170	20			
143	12	0.65	7.01	0.4
183	24			
122	36	0.65	7.01	0.5
144	12			
123	36	0.65	7.01	0.6
145	12			
124	36	0.65	7.01	0.7
146	12			
125	29.7	0.65	8.5	0.4
147	9.9			
126	29.7	0.65	8.5	0.5
148	9.9			
127	29.7	0.65	8.5	0.6
149	9.9			
150	9.9	0.65	8.5	0.71
184	19.8			

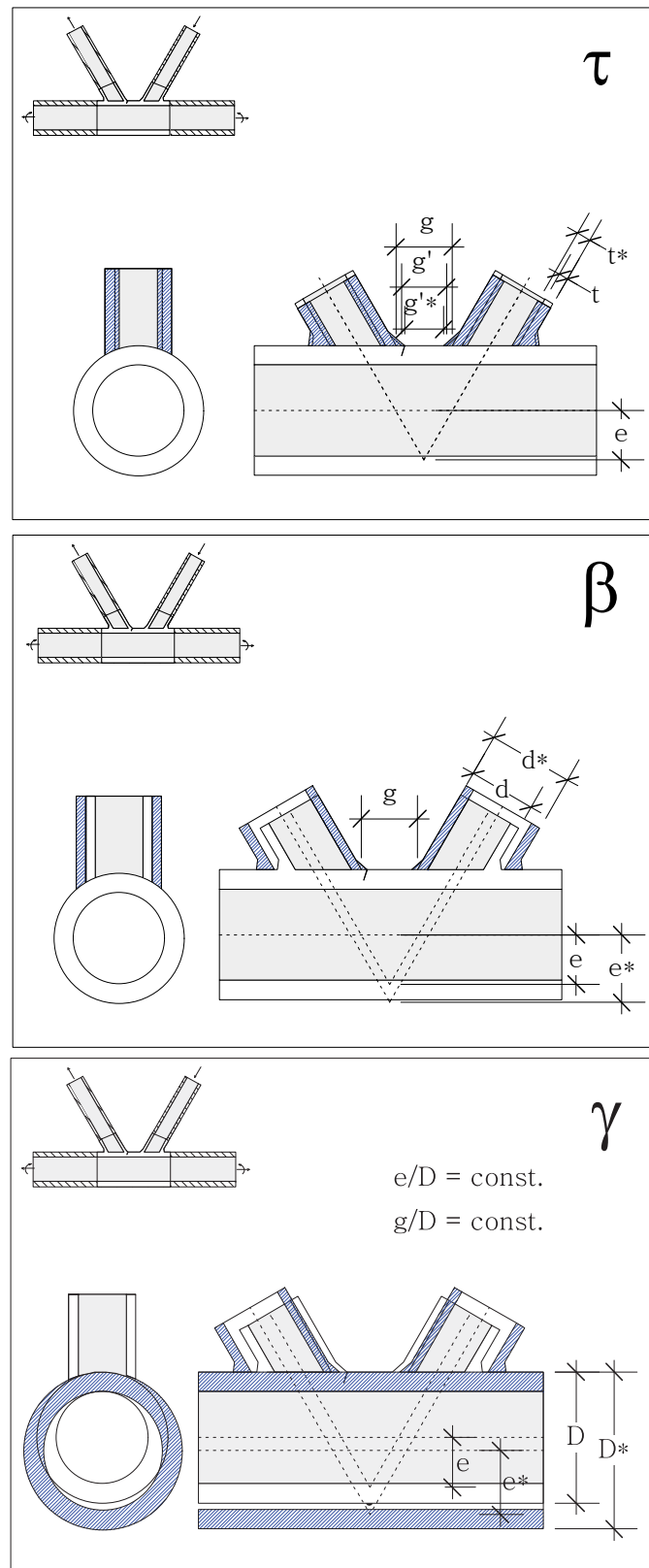
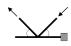
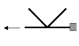



Figure 5.1: Non-dimensional parameters changing: τ , β , γ .

5.2.3 Load cases

The basic load cases acting in the plane of the tubular truss are listed in Table 4.1. Load cases: *Balanced axial brace*, *Axial chord* and *In plane bending chord* (see Table 5.3), were selected as they are predominant (see Section 4.5) for the geometries in bridge application. Calculations were done for nominal stress range, $\Delta\sigma$, equal to 100 MPa (in the case of bending $\sigma_{max} = 100$ MPa corresponds to the absolute values of the stress at extreme fibers of the tube $\frac{\sigma_{max}}{\sigma_{min}} = -1$).

Table 5.3: Basic load cases selected for the parametric study.

Load case	Schematic	Nominal stress range
LC1 Balanced axial brace		$\Delta\sigma_1$
LC4 Axial chord		$\Delta\sigma_4$
LC5 In-plane bending chord		$\Delta\sigma_5$

5.3 Assumptions defining the parameters and estimation of effects

5.3.1 Eccentricity and gap size

The gap (the distance between the outer brace walls at chord crown toe) and the eccentricity are related and influence the stress concentration in the connection.

For practical reasons the gap must ensure enough space. In her investigation, Schumacher (2003) chose the gap as the maximum of two values: $4 \times t$ (minimum space required between the braces for the welding) and $1.6 \times T + 2w_{ch,crown,toe}$ (ensuring sufficient space for the extrapolation of the stresses according to established rules). In the present work, different assumptions are made. As it is the case in many bridge designs, the outer diameters of tubular members remain unchanged while the thicknesses of tubes vary according to the position and stresses along the bridge span. An aesthetic criterion, relating the gap and the eccentricity to the nominal diameter of the chord was preferred. The requirement for space between the braces is generally observed ($g > 4 \times t$) but does not determine the size of the gap in the present parametric study. As the calculation of the hot-spot stresses is not envisaged as a main result, the extrapolation region was not always "preserved" between the braces. The gap size for standard model is considered related to the chord diameter, D . The ratio $\zeta = \frac{g}{D} = 0.23$ is kept constant. This makes the $\frac{g}{D}$ ratio of 0.23 for joints with a $\beta = 0.5$ and 0.36 for joints with $\beta = 0.6$.

One shall emphasise that, in this study, when the τ parameter is being increased while keeping the other non-dimensional parameters constant, the gap, g , remains constant. However, as the brace wall thickness increases the weld size is proportionally increased. The consequence is that the free gap, g' , is decreased for higher τ even if the eccentricity and the gap remain constant (see Figure 5.5).

Figure 5.2 shows the influence of the joint eccentricity and gap size, for the three basic cases considered, on the number of cycles to failure expressed as fatigue strength for geometric parameters $\beta = 0.53$; $\gamma = 4.2$; $\tau = 0.4$. Values are computed using SIF range values determined with BEM, see graphics in Appendix D, and Paris law, Equation (3.4). For load case LC_1 , balanced axial load in diagonals, the higher the gap and eccentricity the higher the stress intensity factors and lower fatigue strength. In other words, longer gaps (and eccentricities) increase the secondary bending at the weld toe, and thus, the eccentricity is unfavourable. This effect is contrary to the one occurring for load

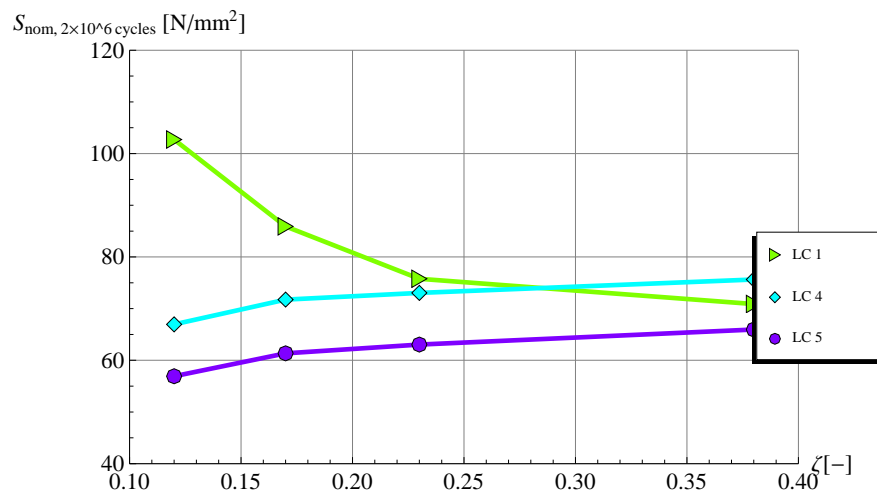


Figure 5.2: Influence of the gap/eccentricity ($\beta = 0.53$; $\gamma = 4.2$; $\tau = 0.4$; for $\zeta = 0.38$, $\zeta = 0.23$, $\zeta = 0.17$ and $\zeta = 0.12$).

cases LC_4 and LC_5 . For the bending and axial load in the chord, the stress concentration decreases as the gap increases, thus the fatigue strength increases.

Eccentricity/gap effect seems to be more pronounced for $\zeta = \frac{e}{D} < 0.23$. More studies covering different joint geometries should be carried out in order to generalise this conclusion.

5.3.2 Chord length between joints, L_{ch} , and truss height, H and diagonal angle, θ

In the parametric matrix, $\alpha = 2L_{ch}/D$ is kept constant, $\alpha = 25.7$. With $\theta = 60^\circ$ also being a constant, the ratio $\frac{L_{ch}}{H} = 1.2$ is also a constant. These ratios, together with $\beta = d/D$, define the *transparency* of the bridge.

Figure 5.3 shows that the chord length, L_{ch} , has little influence over the fatigue strength, for load cases LC1 (balanced axial load in diagonals) and LC4 (axial load in chord). For load case LC5, the fatigue strength decreases as the chord length, L_{ch} , increases and logically the stress intensity factor range values are clearly increasing (see Figure D.1 in Appendix) and

The truss height, H , seems to have no significant influence neither on the fatigue strength nor on the stress intensity factors for the load cases considered (see Figure 5.4 and Figure D.2).

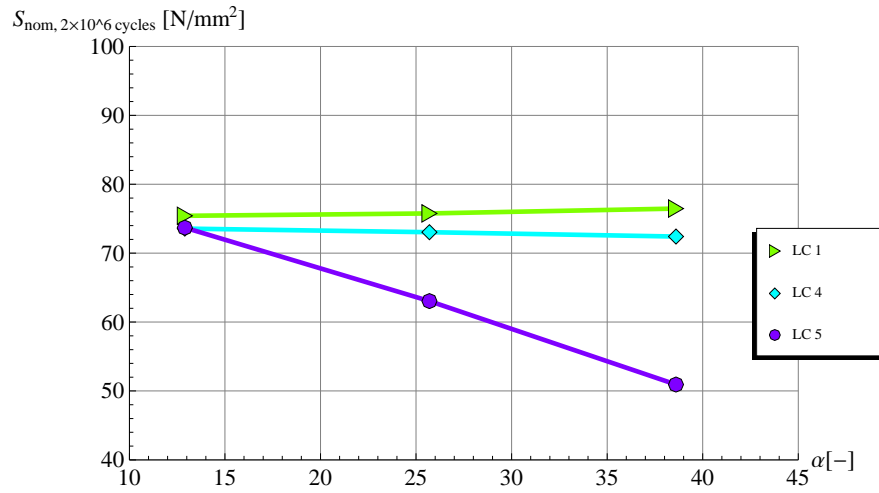


Figure 5.3: Influence of chord length L_{ch} ($\beta = 0.53$; $\gamma = 4.2$; $\tau = 0.4$; for $\alpha = 38.6$, $\alpha = 25.7$, $\alpha = 12.9$).

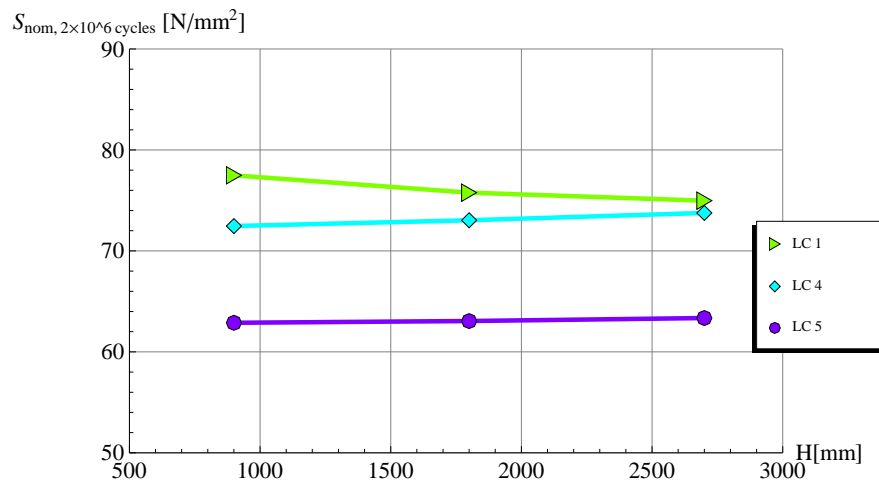


Figure 5.4: Influence of truss height, H ($\beta = 0.53$; $\gamma = 4.2$; $\tau = 0.4$; $T = 20$ mm; for $H = 900$ mm, $H = 1800$ mm, $H = 2700$ mm).

5.3.3 Weld size

The weld profile is defined assuming the following hypotheses. The weld footprint lengths (defined according to Figure 4.2) are calculated with the following relations:

- ◆ $L_{w,ch,heel} = 0.627 \times t + 2.25 \times \frac{t}{\sin(\theta)}$
- ◆ $L_{w,ch,crown} = -0.627 \times t + 2.25 \times \frac{t}{\sin(\theta)}$
- ◆ $L_{w,br} = 1.88 \times t + \frac{T}{\sin(\theta)}$

These relations respect the AWS principles of weld size being proportional to the thickness of the connected elements. When doing a non-proportional sizing of a model, by changing the τ parameter, the weld is resized as shown in Figure 5.5. In this case, although the gap, g , and the eccentricity, e , remain constant, the distance between the weld toes, g' , varies.

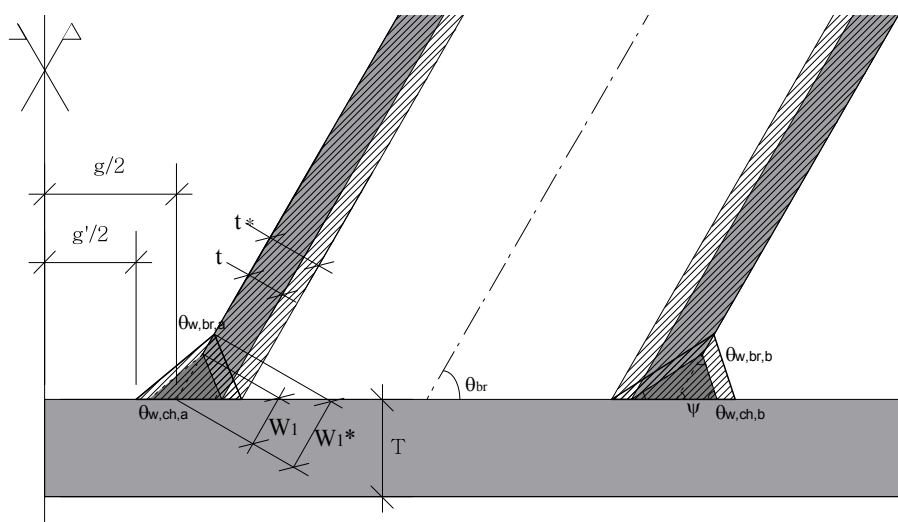


Figure 5.5: Side view of the diagonal to chord wall joint, definition of weld size.

The effect of the weld size depends on the load case analysed. Figure 5.6 shows, for LC1 and LC5, that an increase in the weld size (all the other parameters kept constant, $\beta, \gamma, \tau, e, \alpha, t, T$) leads to a decrease in the calculated stress intensity factors. For LC4, an opposite effect is true. For LC1, an increase in the load carrying weld cross section decreases the stress concentration factor in the weld toe and, as the gap, g , is kept constant (not the distance between weld toes g'), the secondary bending is also reduced for bigger welds. For LC4, an increase in the weld size increases the "stiffener" effect and so do the stress concentration in the weld toe and the stress intensity factor ranges. In terms of fatigue strength, as can be observed in Figure 5.7, an increase in the weld size is favourable, i.e. it increases the fatigue strength, for load case 1 and 5 but unfavourable for load case 4.

5.3.4 Initial crack size, a_i , and final crack depth, a_f

As explained in Section 4.4.1, the initial crack size is considered deterministic and independent of the joint's size: $a_i = 0.15$ mm. The final crack depth, a_f , is considered as half the thickness of the chord, $a_f = \frac{T}{2}$.

Figure 5.8 shows the influence of the initial crack size on the fatigue strength for the different basic load cases. As the initial crack size increases, the fatigue life obviously decreases. In the specific case of K-joints, the load case for which the influence of the initial crack size on fatigue life is higher is LC4: from 74 N/mm^2 when $a_i = 0.05$ mm down to 66 N/mm^2 when $a_0 = 0.5$ mm (Note: Linear

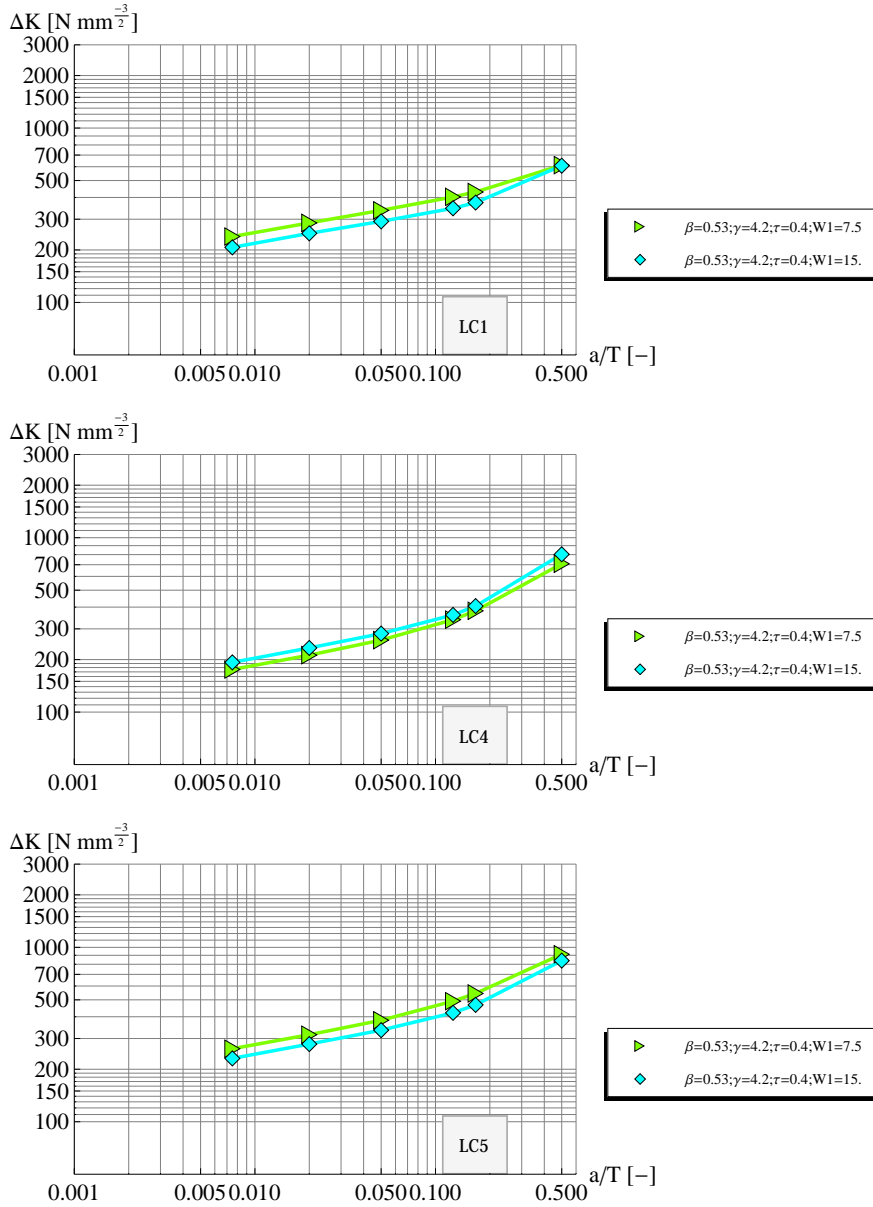


Figure 5.6: Influence of weld size, W_1 ($\beta = 0.53$; $\gamma = 4.2$; $\tau = 0.4$; $T = 20$ mm; for $W_1 = 7.5$ mm and $W_1 = 15$ mm).

interpolation between 0 and SIF for $a = 0.15$ mm, the first crack increment calculated, is done to determine the SIFs for $a_i < 0.15$ mm).

Figure 5.9 shows the fatigue strength, $S_{nom, 2 \times 10^6}$, variation with the relative crack depth. There is little influence of small variations of the final crack size on the number of cycles to failure beyond a crack depth of half of the thickness.

5.3.5 Paris-Erdogan constant, C

The Paris-Erdogan constant has a very high influence on the calculation of the number of cycles to failure due to the inverse proportionality shown in Equation (4.16). Figure 5.10 shows the relation between the C constant and the relative number of cycles to failure and the fatigue strength. It has the same influence on each of the basic cases. The constant, C , is considered as 2.0×10^{-13} (mm/cycle)($\text{N/mm}^{-3/2}$) for all cases run.

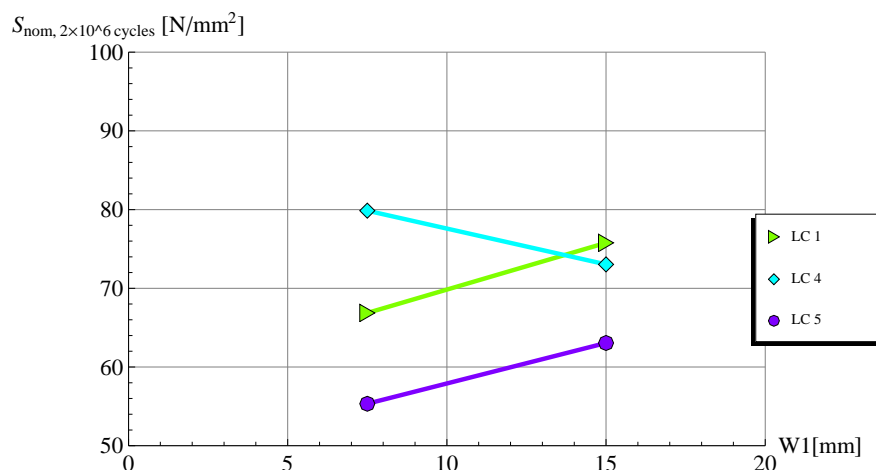


Figure 5.7: Influence of weld size, W_1 . ($\beta = 0.53$; $\gamma = 4.2$; $\tau = 0.4$; $T = 20$ mm; for $W_1 = 7.5$ mm, $W_1 = 15$ mm).

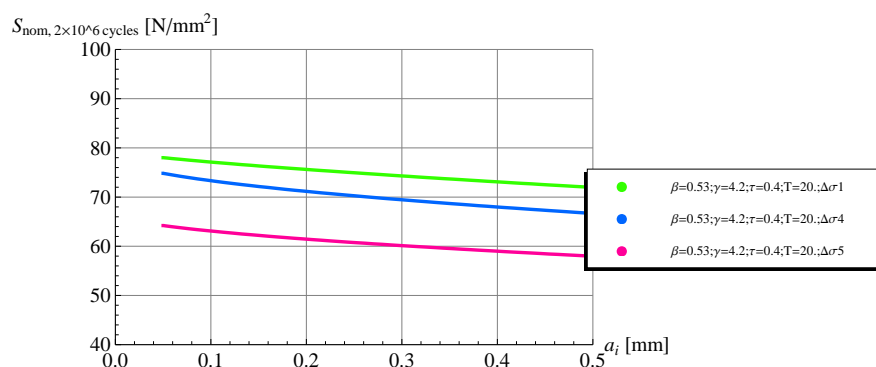


Figure 5.8: Influence of initial defect size, a_0 , on the number of cycles to failure or on the fatigue strength - S5 geometry ($\beta = 0.53$; $\gamma = 4.2$; $\tau = 0.4$; $T = 20$ mm).

5.3.6 Crack shape, a/c

At early crack growth stage, the coalescence phenomenon determines the crack shape. According to experimental evidence (see Section 3.4.5), it seems reasonable to estimate $\frac{a}{c} = 0.20$, in the interval $a = 0.15$ mm to $a = T/2$. This simplification allows for formal superposition of results for different load cases. To investigate the influence of crack shape on the crack propagation process, three different a/c ratios (0.15 and 0.2 and 0.3, in the range of values found experimentally for $a < T/2$) were considered. The ratios are kept constant over the crack propagation and the results then compared.

Figure 5.11 shows the fatigue strength, S_{nom} , for the three crack shapes. A minor influence, of about 15%, is observed when a/c changes from 0.15 to 0.3. This trend is independent from the load case considered. Stress intensity factor ranges, ΔK , corresponding to these geometries, are given in appendix D.2. SIF ranges vary generally less than 10%, with a maximum of 28% for LC1 at $a = T/2$.

5.3.7 Crack angle

The bisectrix between the weld and the chord outer wall (in the vertical longitudinal plane) is used to define the conic shape along which the crack propagates (see Figure 4.6). The crack angle (ϕ_{crack})

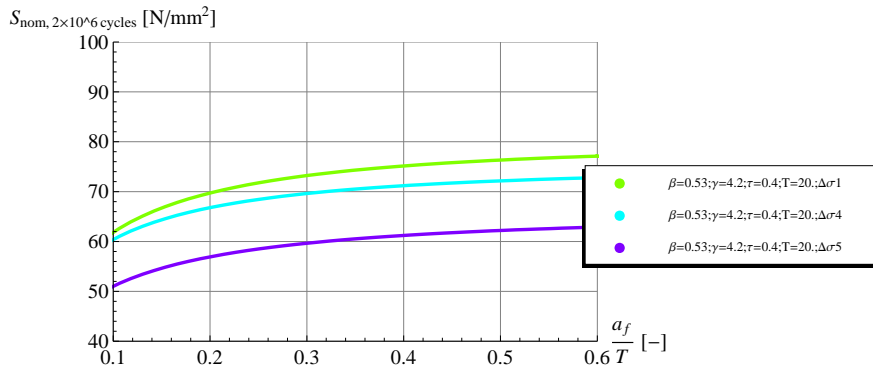


Figure 5.9: Influence of the final crack size, a_f , in the fatigue strength, considering $a_0 = 0.15 \text{ mm}$ - S5 geometry ($\beta = 0.53$; $\gamma = 4.2$; $\tau = 0.4$; $T = 20 \text{ mm}$).

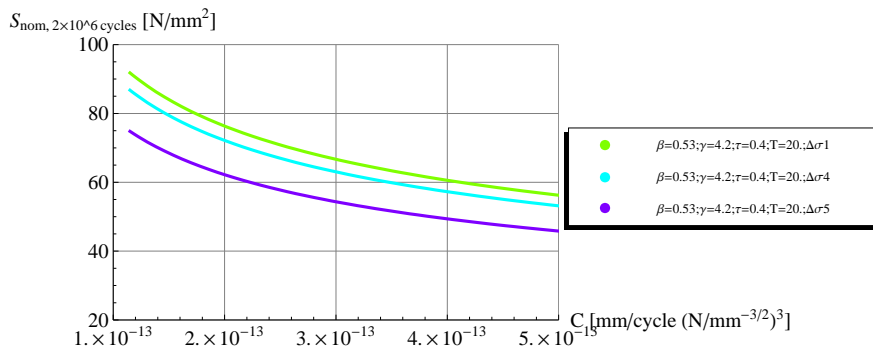


Figure 5.10: Influence of Paris-Erdogan constant C , for $m=3$, on fatigue life or on the fatigue strength - S5 geometry ($\beta = 0.53$; $\gamma = 4.2$; $\tau = 0.4$; $T = 20 \text{ mm}$).

remains constant for the three load cases considered. Figure 5.12 shows the influence of the crack angle (angle measured in the longitudinal mean plane with the vertical) on fatigue strength (the corresponding stress intensity factor ranges, ΔK can be found in Figure D.4). For load case LC1, a crack angle of 40° leads to higher values of stress intensity factors than an angle of 10° . For load cases LC4 and LC5 the effect is the opposite. Magnitudes of this effect can reach up to 30% in the case of SIFs for $a = T/2$ for load case LC1 and 20% in terms of fatigue strength for the three basic load cases.

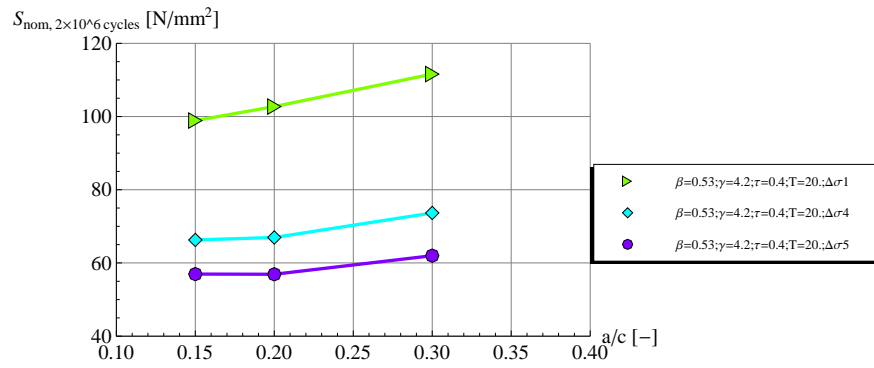


Figure 5.11: Influence of crack shape.

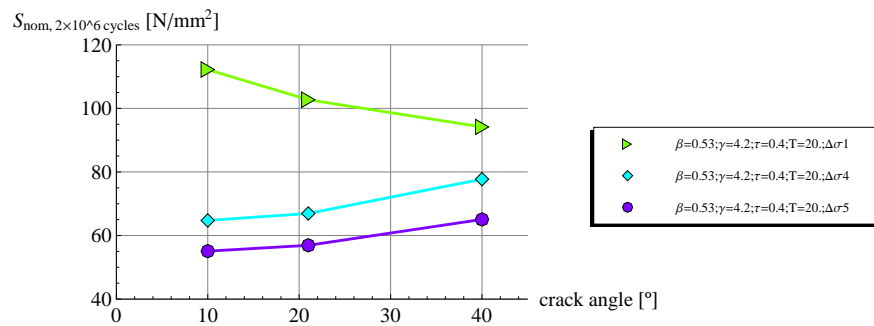


Figure 5.12: Influence of crack angle, ϕ_{crack} .

5.4 Results and discussion of Parametric Study

5.4.1 Introduction

Figure 5.13 shows the fatigue strength (in terms of nominal stress) of 42 joints from the parametric table (D.2) as a function of the parameters τ , γ , β and thickness, T , considering the three basic load cases acting independently. The dispersion shown does not allow for immediate conclusions to be drawn on the influence of parameters as no trend seems to be present.

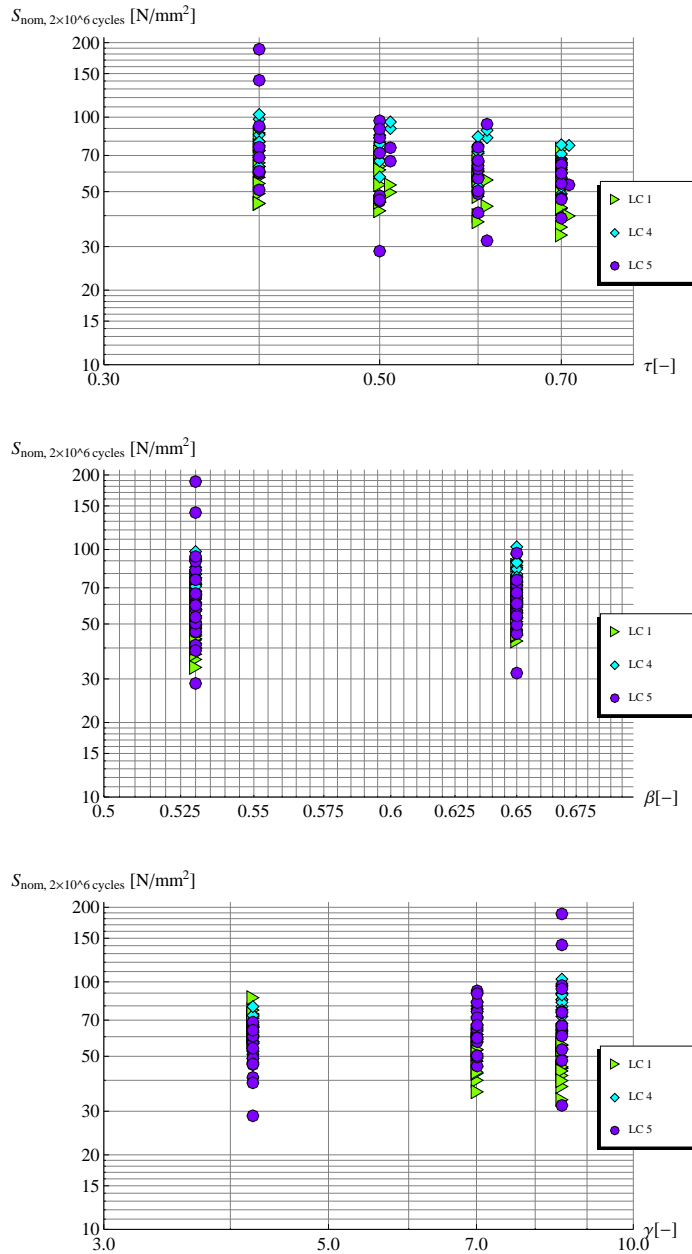


Figure 5.13: Fatigue strength at 2×10^6 cycles function of τ , β , γ .

The fatigue strength in terms of hot-spot stress, S_{hs} , is obtained by multiplying the fatigue strength, S_{nom} , by the stress concentration factors, SCF , corresponding to the load case and joint geometry. The SCF values were taken from tables provided in (Schumacher, 2003), despite the different hypothesis made to define the joint gap, g . Figure 5.14 shows the fatigue strength in terms of hot-spot stress

as a function of the thickness of the chord for the different load cases. It looks like the hot-spot based fatigue strength concept results in a definitive trend for the load case 4. For this load case, the fatigue behaviour seems to be dependent on two parameters: the hot-spot stress range, $\Delta\sigma_{hs}$, and the thickness of the chord, T . The load conditions (axial chord load) are similar to the "plate with non-load-carrying transversal attachment" under axial load. Results for load case 1 and 5 show the influence of the chord thickness in case of proportional scaling of the joints. However, the hot-spot stress and the thickness, T , seem to be not enough to show a trend and to permit to calculate the fatigue strength. More parameters are needed for that.

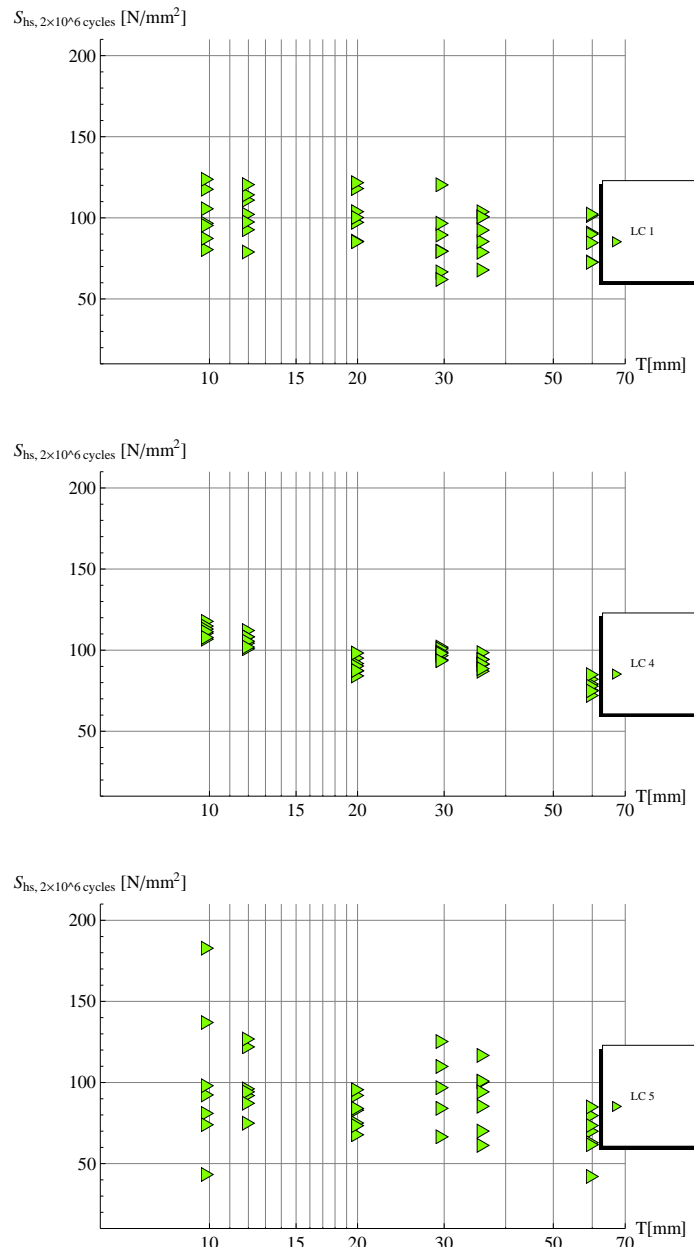


Figure 5.14: Fatigue strength in terms of hot-spot stress function of the chord thickness, T , for the three basic load cases.

In a first attempt to analyse the results, a comparison between the fatigue strength and stress intensity factor range values at different crack depths is carried-out by changing each one of the

parameters (β , γ , τ) at a time, for the three basic load cases studied: balanced axial brace load, LC1, chord axial load, LC4, and chord in-plane bending, LC5. This comparison gives the general trends for the effects of each of these parameters.

By default, the crack depths are the increments considered in the standard model: $a_i = \{ 0.15 \text{ mm}, T/50, T/20, T/8, T/6, T/2 \}$. When the automatic remeshing around the crack produces distorted elements, the model cannot be solved. The solution adopted was to change slightly the crack size so that the elements shape are corrected.

5.4.2 τ - Thicknesses ratio

Balanced axial brace loading

Figure 5.15 presents the stress intensity factor ranges, ΔK , for different relative crack depths, a_i/T , and different τ values under basic load case LC1. Increases in τ , keeping the other parameters constant and the same chord thickness for all the cases, have the effect of increasing the value of the SIF for crack propagating at location 1. At a first glance, this result is not surprising. In fact, as an increase in the brace thickness means an increased force (because the same nominal stress is applied on all geometries), and thus, an increase in the stress acting in the cracked chord. However there are some effects such as the weld being scaled up proportionally to the thickness of the diagonal while keeping constant the gap, g , and the eccentricity, e , that might, for some cases, compensate the effect mentioned before.

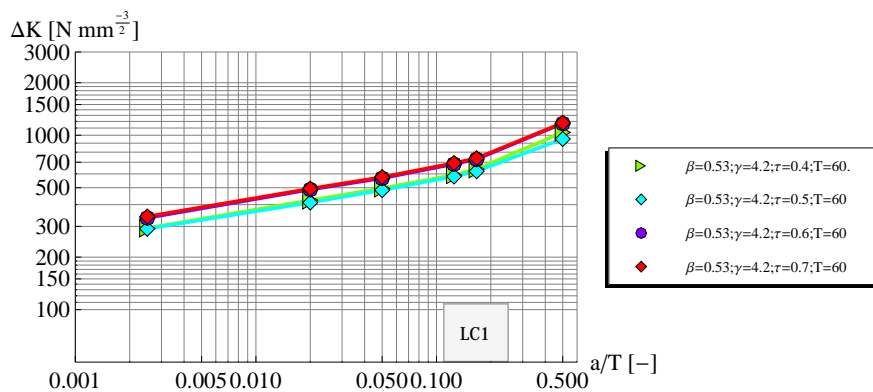


Figure 5.15: Stress intensity factor (SIF) ranges due to balanced axial brace load.

Axial chord loading

Figure 5.16 shows the stress intensity factor ranges at different crack depths for τ values increasing from 0.4 to 0.7. As τ increases, the stress concentration is higher due to a thicker, stiffer brace.

In-plane chord bending

For load case LC5, as shown in Figure 5.17, it is difficult to extract a trend since $\tau = 0.4$ and 0.5 give the extreme curves and $\tau = 0.6$ and 0.7 the average ones.

Fatigue strength

Figure 5.18 shows the fatigue strength as a function of τ , for the three load cases. As can be inferred from the previous graphs (Figures 5.15 to 5.17) the exception is case LC5, $\tau = 0.5$ which seems to be awkward. The fatigue strength decreases when the thickness ratio, τ , increases.

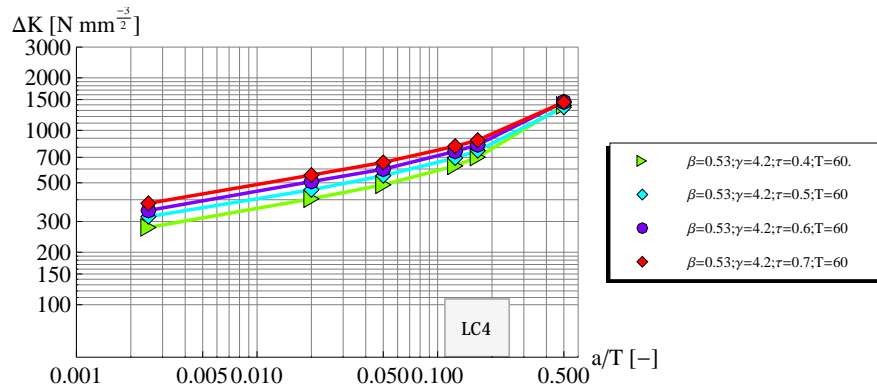


Figure 5.16: Stress intensity factors (SIF) due to balanced axial chord load.

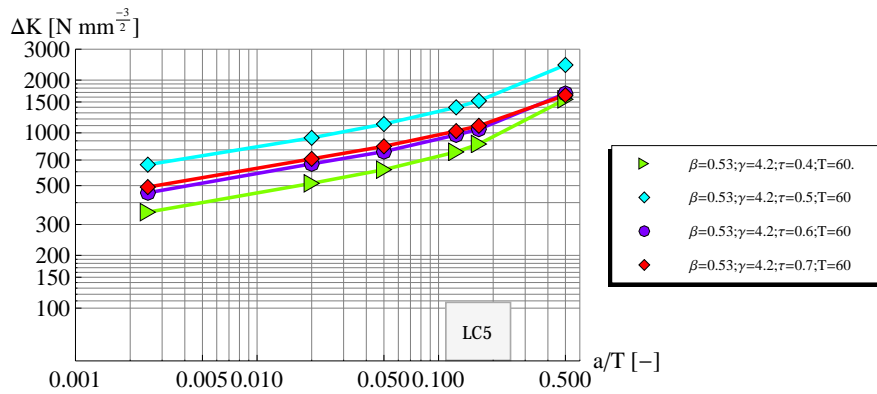


Figure 5.17: Stress intensity factors (SIF) due to in-plane chord bending.

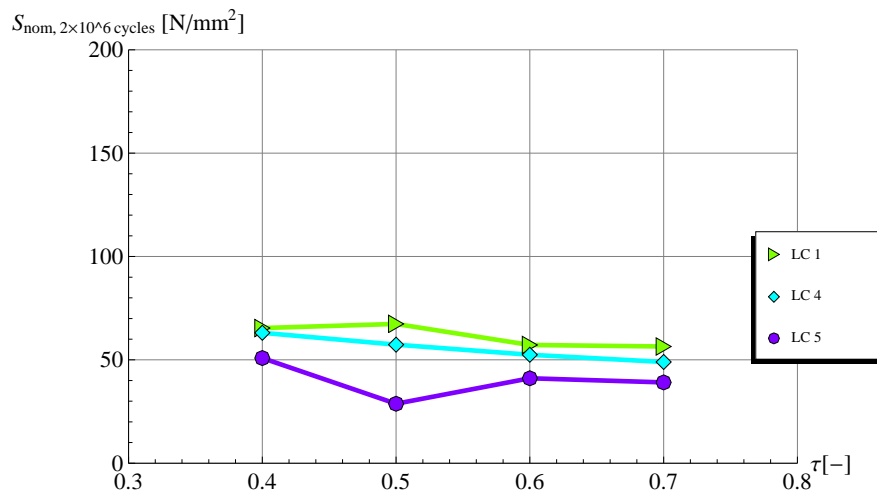


Figure 5.18: Thickness ratio effect in terms of nominal fatigue strength, S_{nom} ($\beta = 0.53$; $\gamma = 4.2$; $T = 60.0$ mm).

5.4.3 γ - Chord slenderness

Balanced axial brace loading

Figure 5.19 shows that when the chord slenderness, γ , increases, keeping the other main parameters (β , τ , T) constant, the stress intensity factor ranges increase for basic load case 1.

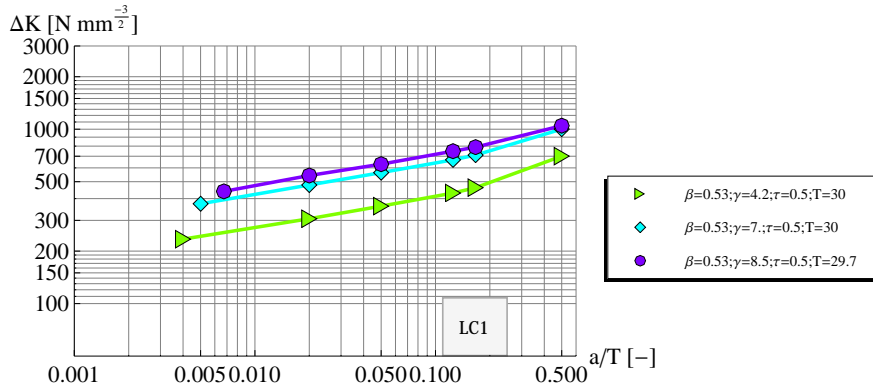


Figure 5.19: Stress intensity factors (SIF) due to balanced axial brace load.

Axial chord loading

Figure 5.20 shows that the stress intensity factor range values decrease as the γ increases. This effect seems to be due to the relative rigidity of the attached brace.

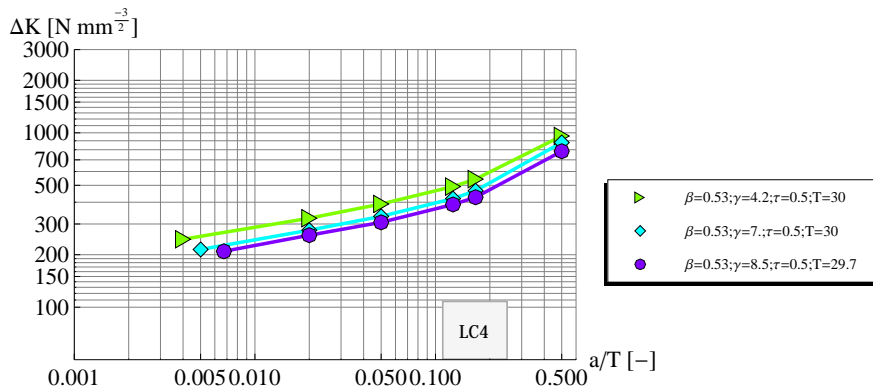


Figure 5.20: Stress intensity factors (SIF) due to balanced axial chord load.

In-plane chord bending

Figure 5.21 shows the stress intensity factor ranges for different γ parameter. No trend is found for this load case.

Fatigue strength

Figure 5.21 shows the fatigue strength as a function of γ . For load case 1, the fatigue strength decreases with γ . For load case 4, the fatigue strength increases slightly with γ . For load case 5 it looks like there is no linear trend between the fatigue strength and the γ parameter.

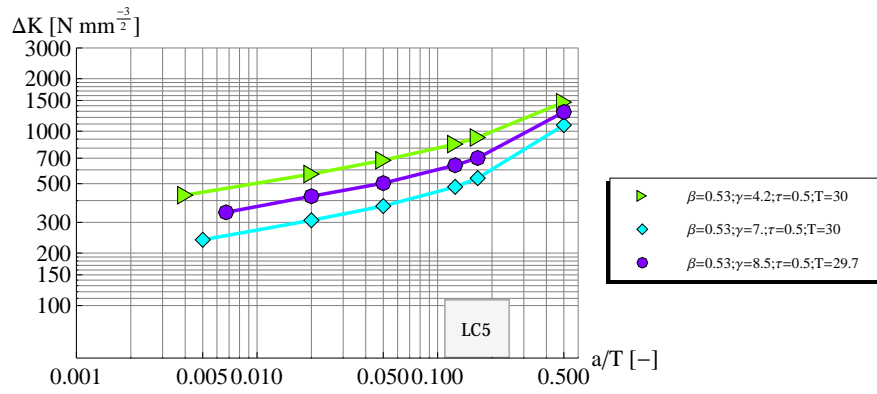


Figure 5.21: Stress intensity factors (SIF) due to in-plane chord bending.

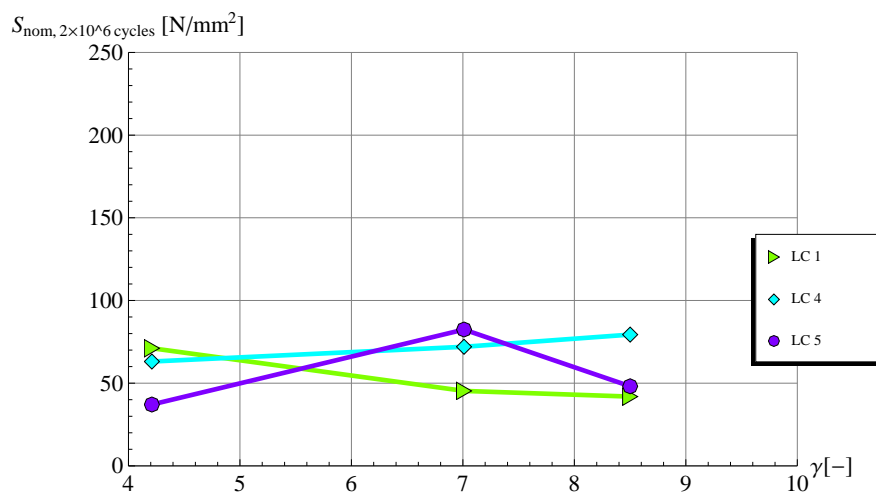


Figure 5.22: Effect of chord slenderness in terms of nominal fatigue strength, S_{nom} , $\beta = 0.53$; $\tau = 0.5$; $T = 30$; $\gamma = 4.2$; $\gamma = 7$; $\gamma = 8.5$.

5.4.4 β - Diameters ratio

Balanced axial brace loading

Figure 5.23 shows that, for load case 1, an increase in β means slightly lower stress intensity factor range values at the considered crack depths. This result appears to contradict the argument used to justify higher SIFs for higher values of τ , since the increase in brace diameter means relative higher force being imposed in the chord. This is, however, balanced by the fact that a higher d/D ratio means also a different flow of stresses in the weld toe region. The higher β means less local bending effect. As the brace diameter gets closer to the chord diameter the transfer vertical component of the brace solicitation is more efficient (see Figure 5.24). Or, in other words, as β increases, the section resisting the brace action passes from a behaviour similar to a supported plate of thickness T to an "effective" circular section.

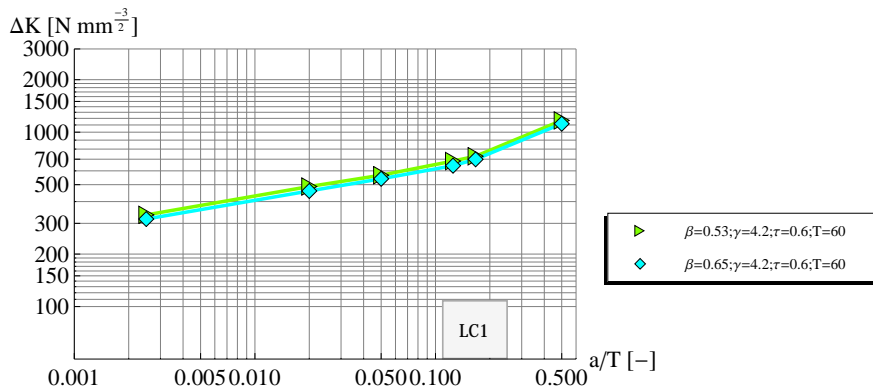


Figure 5.23: Stress intensity factors (SIF) due to balanced axial brace load.

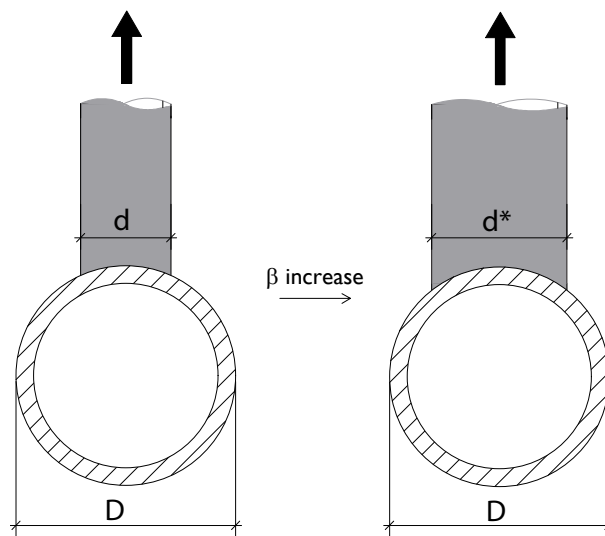


Figure 5.24: Changes in β parameter.

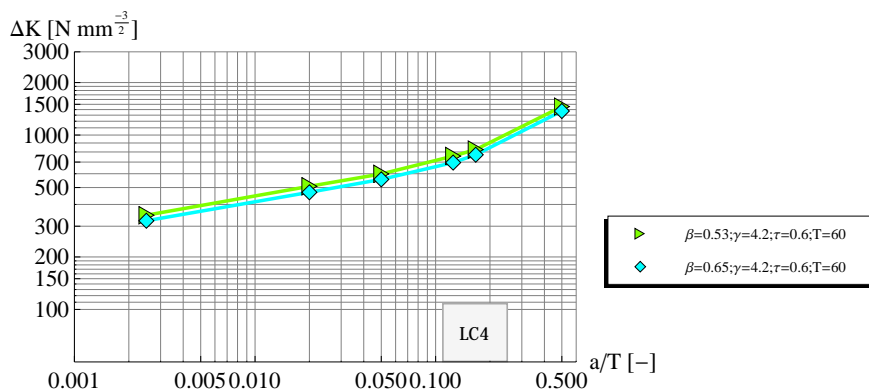


Figure 5.25: Stress intensity factors (SIF) due to balanced axial brace load.

Axial chord loading

For the basic load case LC4, the stress intensity factor ranges show higher SIFs for lower β values. (see Figure 5.25). This effect (comparable to the effect of an attachment) seems to be dependent on the relative rigidity of the brace. When β is lower, the brace (attachment) is more rigid since τ is constant, thus leading to a higher stress concentration at the weld toe.

In-plane chord bending

Apparently, the same arguments as LC4 apply for this basic load case.

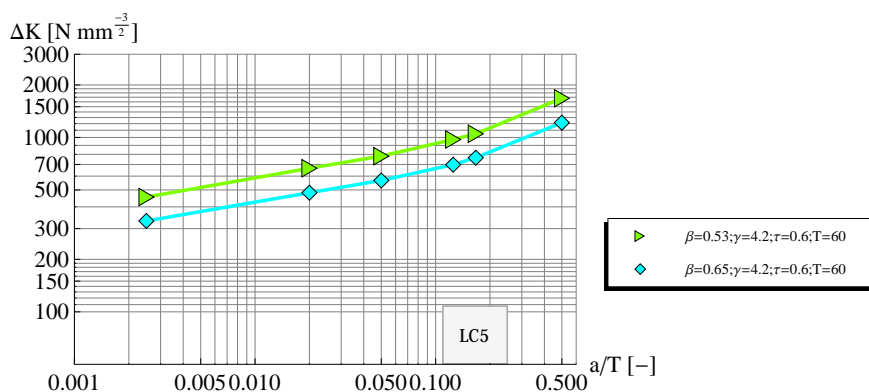


Figure 5.26: Stress intensity factors (SIF) due to in-plane chord bending.

Fatigue strength

An increase in β leads to minor changes in terms of fatigue strength for LC1 and LC4. For LC5, apparently, the fatigue strength increases about 35% when β changes from 0.53 to 0.65.

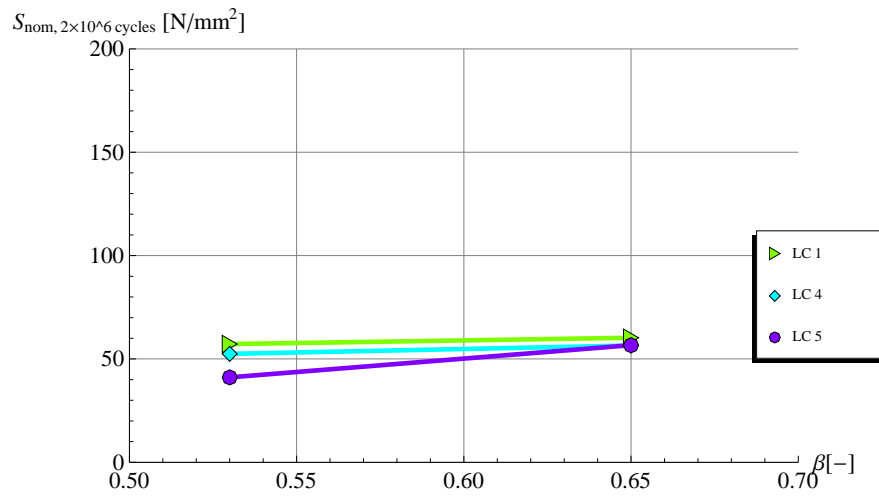


Figure 5.27: Effect of β in terms of nominal fatigue strength, S_{nom} .

5.4.5 *T* - Thickness effect

Balanced axial brace loading

Figure 5.28 shows the stress intensity factor ranges increasing with the thickness of the chord for proportionally scaled joints. This effect has been extensively studied for the case of plates (see sections 1.2 and 2.6): In thicker plates, for a similar crack depth, *a*, the stress at the crack tip is larger than in thinner plates (see Figure 1.2).

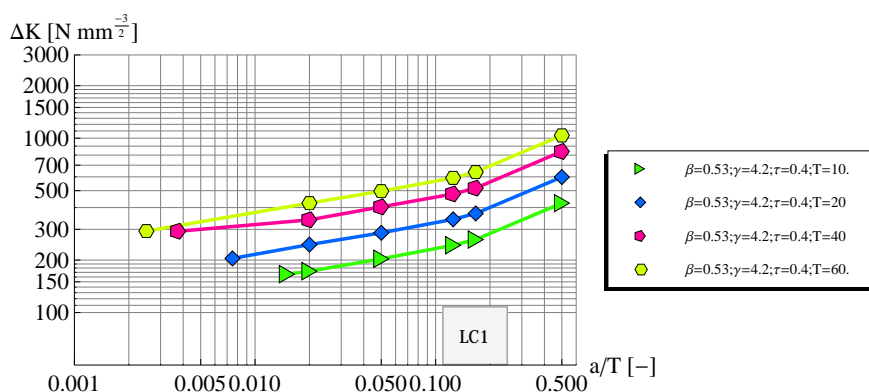


Figure 5.28: Stress intensity factors (SIF) due to balanced axial brace load.

Axial chord loading

A parallel can be established between this case and the thickness effect for plates with transversal attachments. As *T* increases, keeping all the non-dimensional parameters constant, the stress intensity factor ranges are higher for thicker plates at the same relative crack depths (*a*/*T*) (see Figure 5.29).

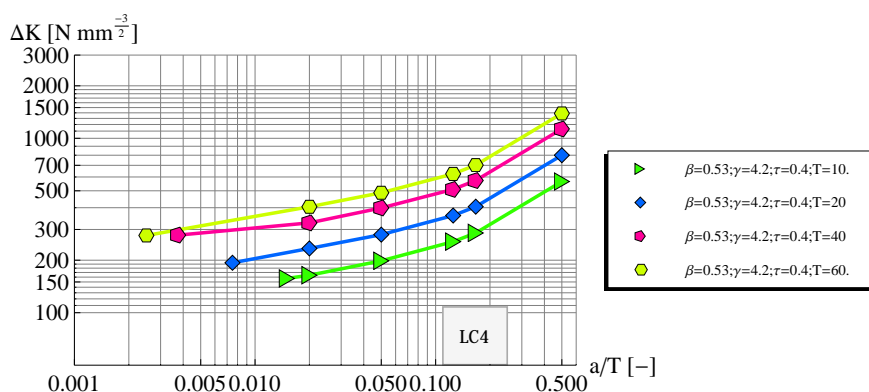


Figure 5.29: Stress intensity factors (SIF) due to balanced axial chord load.

In-plane chord bending

Figure 5.30 shows, for load case 5, the same trend as for load case 1 and 4.

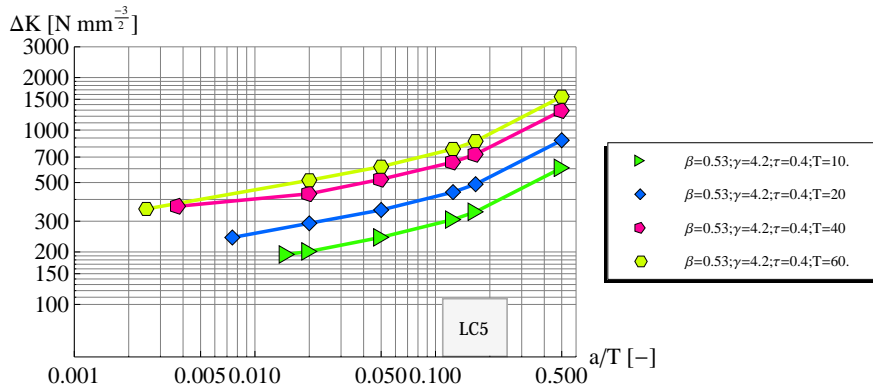


Figure 5.30: Stress intensity factors (SIF) due to in-plane chord bending.

Fatigue strength

Figure 5.31 shows the fatigue strength decreasing as the thickness increases for the three load cases considered. The effect is more pronounced for load case 5, for the selected geometry, but other geometries show, for this load case, that the effect is not always the same (and can be inverted). For LC1 and LC4, the effect seems to be the same for the different geometries studied and constant for both load cases.

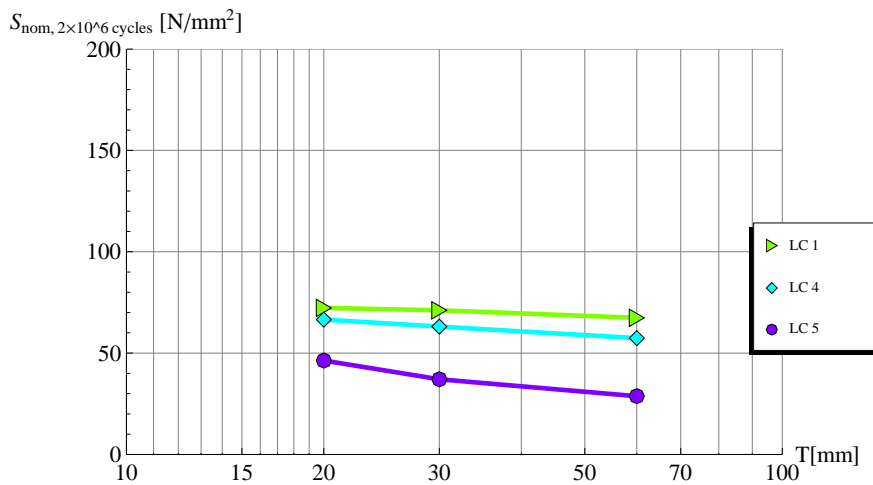


Figure 5.31: Thickness effect in terms of nominal fatigue strength, S_{nom} .

5.5 Summary and comparison with previous studies

Due to the amount of parameters involved in this parametric study, it is not straight forward to analyse the results. By changing the dimensions and geometry parameters of a tubular joint, assuming a constant nominal stress, different effects are seen. On one hand, there is the effect of the load being different for different geometries. On the other hand, there are effects that superpose or balance in some cases.

From the parametric results three categories of geometry related effects were identified:

- ◆ The *load effect* - for the load case braces in balanced axial stress (LC1, LC4). Assuming a constant nominal stress in the braces, varying the β or τ parameters, thus doing a non-proportional scaling, leads to different forces being applied into the same cracked cross-section. Effects for LC5 show some incoherence, the source not being identifiable clearly.
- ◆ The *attachment effect* - as in the previous case, τ and β play an important role as they compare the brace and the chord flexibilities. For the basic load cases 4 and 5, the effect of the unloaded brace attached to the chord can be compared to an attachment on a plate. Both τ and β influence the stress concentration in the connection.
- ◆ *Thickness effect* - When proportional scaling is done, the effect of thickness is present for the three load cases considered. The stress concentration factor, SCF , remains constant, however, the gradient through depth is steeper for thinner joints.

In Table 5.5, the trends observed on stress intensity factor ranges are compared with those observed in previous works. The results are in good agreement with what was observed by Schumacher (2003) for the stress concentration factors, SCF , and by Shao and Tjhen (2005) for the so called "non-dimensional" stress intensity factors, F (in this study, results are available only for *balanced axial brace* load case).

A strong influence of τ (increase of τ leads to an increase of SIF values) for the three load cases is observed. Only a minor influence of the geometric parameter β is observed. Finally, an increase in the geometric parameter γ leads to significantly lower stress intensity factors for *axial in the chord* load case; this is not surprising since an increase in γ means a stronger, thicker chord and consequently less influence on the stress field from the unloaded brace attached onto it. For load case 1, *balanced axial in the brace*, an increase in γ leads to higher stress intensity factors values since, with the braces loaded, the "hard point" effect of the brace attached onto the more stiff chord increases. These results are only general trends. In Chapters 6 and 7, different result analysis focusing respectively in proportional and non-proportional joint scaling are carried out.

5.6 Conclusions

A parametric study of a range of K-joint BEM models has been carried out. All the joints are non-overlapping welded joints and the braces angle is 60° for all the models. The parameters investigated in the study are shown in Table 5.5

The three basic load cases studied are: balanced axial brace load, axial chord load, and in-plane bending in the chord. Trends in SIF are summarised in Table 5.4.

In addition, a preliminary analysis is carried-out to examine the effects of the weld size, crack angle, crack shape eccentricity/gap size and chord length and initial and final crack sizes.

Table 5.7 summarises the results from the sensitivity analysis. The Paris law parameter C has the strongest effect, but always in the same direction (it can be taken out when comparing different joint geometries). Only two cases result in having a major effect on the stress intensity factor and thus fatigue strength: a change in eccentricity under load case 1 and a change in chord length under load case 5. These effects are mitigated by the way the sizing of the joints is made, keeping for example a

Table 5.4: Comparison of *SIF* with Stress Concentration Factors, *SCF* (from Schumacher (2003)), and normalised stress intensity factor, *F* (from Shao and Tjhen (2005)), for the different load cases.

Load case	Increase in	SCF ⁽¹⁾	SIF	F ⁽²⁾
	τ	↗↗	↗↗	↗↗
	β	↔	↘	↘
	γ	↗↗	↗	↗**
	τ	↗↗	↗↗	N/A
	β	↘*	↔	N/A
	γ	↘↘	↘↘	N/A
	τ	↗↗	?	N/A
	β	↘	↔	N/A
	γ	↘*	↘	N/A

⁽¹⁾ from (Schumacher, 2003)

⁽²⁾ from (Shao and Tjhen, 2005)

** variation increases with τ

* minor effect

Table 5.5: Range of parameters β , γ , τ and T used in parametric study.

β [-]	0.53	0.65		
γ [-]	4.2	7	8.5	
τ [-]	0.4	0.5	0.6	0.7
T [mm]	10	20	40	60

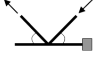
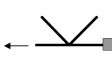
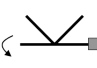
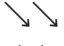



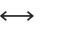
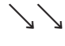
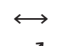
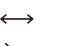
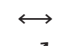






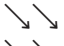


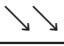
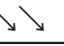
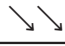
Table 5.6: Effects of changing β , γ and τ on the stress intensity factor.

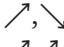
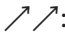
SIF			
τ	↗↗	↗↗	↗
β	↘	↔	↔
γ	↗	↘↘	↘

↗, ↘: minor effects
↗↗: major effects

sufficient gap for welding, and can be viewed as inherent technological effects when doing practical proportional scaling.

Table 5.7: Trends in the fatigue strength obtained from the sensitivity analysis.

Increase in			
eccentricity, e , gap, g			
chord length, L_{ch}			
truss height, H			
weld size, W			
crack shape, a/c			
crack angle, ϕ_{crack}			
Paris law constant C			

: minor effects
: major effects

Proportional scaling

6.1 Introduction

In the previous chapter, three categories of effects related to joint geometry were identified: load effects, attachment effects, thickness effects. The case in which thickness is the only parameter needed to describe the relative fatigue life of two joints is called thickness effect and corresponds to a complete proportional scaling. In practice, complete proportional scaling of a connection is difficult to achieve. This difficulty increases with the joint complexity. In fact the more the number of dimensions intervening in the connection, the harder it is to scale all of them in the same proportions.

For tubular K-joints, complete proportional scaling is hardly achieved in practice, due to the multiplicity of parameters and technological issues. Practical proportional scaling can be achieved if, say as a logical assumption, the non dimensional parameters (β, τ, γ) remain constant. Thickness is, then, one of the parameters needed to describe the differences between two joints.

In order to analyse purely the effect of the thickness, in this chapter, differences between homothetic joints of different absolute sizes will be studied. The parametric results given in chapter 5 are reanalysed focusing on proportional scaling. In Section 6.2, distinction between proportional joint geometry and non-proportional crack size problem is made using LFM concepts. In Section 6.3, the geometry (joint and crack) factor, Y , is introduced. Values of Y , characterising the geometries in the parametric table, are provided for the three basic load cases considered. A procedure to determine the number of cycles to failure of a CHS joint subjected to basic load case is provided in Section 6.4. This assumes a joint geometry being proportionally scaled and the fatigue life comes out as a function of the chord thickness, T . As a result, thickness based correction factors are issued to estimate the effect of thickness on the fatigue life of the CHS joint (Section 6.5). Thickness correction factors, based on nominal fatigue strength, are compared to the classical correction factors derived for plates. The procedure proposed for calculation of fatigue life of joints under basic load cases is extended to the combined load case. A graphical solution, allowing for calculation of the number of cycles for a given geometry and combined load case, is illustrated in Section 6.6. Finally, in Section 6.7, a brief discussion on the efficiency of proportionally scaled K-joints is presented.

6.2 Separation between *Proportional geometry* and *Non-proportional crack size*

Two questions that may arise when scaling proportionally a K-joint submitted to fatigue loading:

What happens to the weld size?

What happens to the crack size?

For the weld size, it is reasonably assumed in the present study that the welds are full-proportionally scaled (see 5.3.3). For the crack size, the hypotheses made in Section 5.3.4, are maintained. That is to say, the final crack size, a_f , defined here as equal to the half thickness, $T/2$, is sized proportionally, while the initial crack size is constant and equal to $a_i = 0.15$ mm, independently of the elements size. The fact that the initial crack size is an absolute value conFigures an exception in the otherwise fully proportional scaled problem. *How does this fact influence the thickness effect?*

In order to quantify this influence, consider, as mentioned before, that the fatigue life of a welded specimen consists wholly of stable crack propagation. The number of cycles to failure can, thus, be calculated using the Equation (2.10), repeated below:

$$N_f = \int_{a_i}^{a_f} \frac{1}{C (\Delta K)^m} da \quad (6.1)$$

where,

- a_i : initial crack size;
- a_f : final crack size ($a_f = T/2$).

In order to isolate a complete proportional problem, this integral can be separated into two parts:

$$N = N_{np} + N_p = \int_{a_i}^{a_1} \frac{1}{C (\Delta K)^m} da + \int_{a_1}^{a_f} \frac{1}{C (\Delta K)^m} da \quad (6.2)$$

the first part contains the "non-proportional" effect of the crack in which the lower limit is considered constant and equal to $a_0 = 0.15$ mm, and the higher limit is taken as $a_1 = T/50$. The second part is limited with $a_1 = T/50$ and $a_f = T/2$, it is the "full proportional integral part".

In order to solve this integral, ΔK , has to be expressed as a function of a . This is done by introducing a geometry factor, function of the relative crack depth, and common to a set of proportionally scaled joints.

6.3 Defining Y , the geometry correction factor

As it is well known, the stress intensity factor, K , is given by the general equation (2.8), that is, $K = Y\sigma\sqrt{\pi a}$ (Broek, 1986, Irwin, 1957), where Y is a geometry correction factor to account for global and local geometry characteristics, loading conditions, crack shape and depth. Newman and Raju (1981) made an important step in determining parametric equations for Y for a semi-elliptical crack in plated joints. Although the geometry correction factor has been object of numerous studies for simple geometries (Murakami, 1987), few solutions exist for tubular joints, and the majority were derived from simplified configurations such as T-butt joints (Bowness and Lee, 1998). This is mainly due to the difficulties in modelling cracks in complex details.

For a given set of homothetic joints (same non-dimensional parameters), the same Y factor should apply. The factor, Y , is function of crack shape, a/c , and relative crack depth, a/T , $Y(a/c, a/T)$. Setting $a/c = 0.2$, Y becomes only function of a/T , $Y(a/T)$. This is an important result as it allows for the calculation of fatigue life of different absolute sized joints based on curves valid for the homothetic joints.

As an example, consider for instance, the geometry of series S5 ($\gamma = 4.2$; $\beta = 0.5$; $\tau = 0.4$; $\alpha = 25.7$; $\zeta = 0.23$; $e/D = 0.23$;) and a set of joints proportionally scaled. Figures 5.28 to 5.30 show the stress intensity factor ranges, ΔK , of proportionally scaled joints as a function of the relative crack depth, a/T , for the three load cases. It can be observed that the stress intensity factor ranges corresponding to thicker joints are higher.

The stress intensity factor range, ΔK , is divided by $\Delta\sigma \cdot \sqrt{\pi a}$, to obtain the geometry correction factor:

$$Y = \frac{\Delta K}{\Delta\sigma \cdot \sqrt{\pi a}} \quad (6.3)$$

It can be seen in Figure 6.1 that the discrete Y values superpose approximately in a single curve.

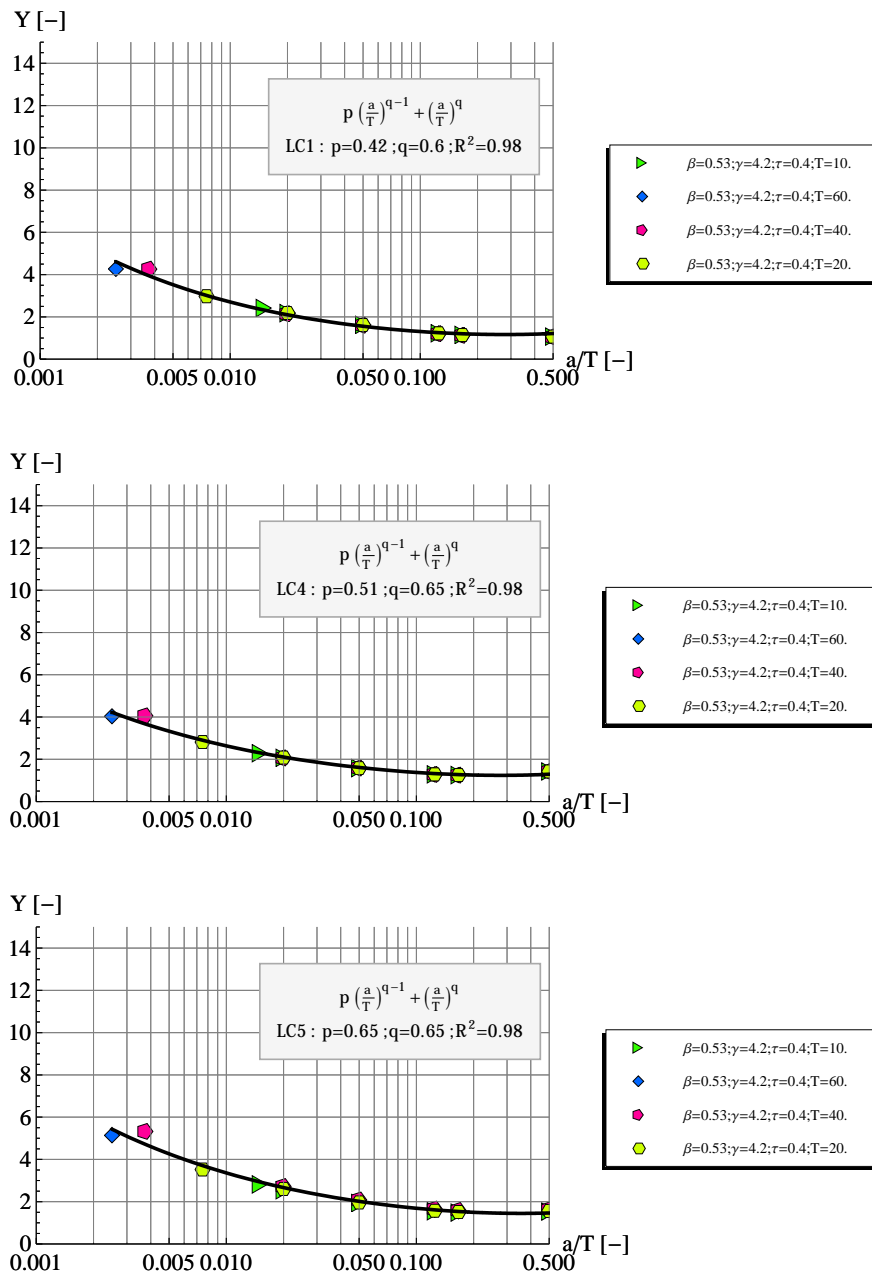


Figure 6.1: Geometry factor Y equation for different crack depths and basic load cases in proportionally sized joints.

The curve representing Y , was found to be well fitted using the following relationship

$$Y \left(\frac{a}{T} \right) = p \cdot \left(\frac{a}{T} \right)^{(q-1)} + \left(\frac{a}{T} \right)^q \quad (6.4)$$

where p and q are parameters that depend on the geometry and basic load case.

Tables 6.3 show p and q values, obtained for the different geometries and load cases. Parameters p and q are obtained from fitting the discrete Y points corresponding to, at least, two different absolute joint dimensions (see Table D.1).

The R^2 parameter is also given, so that the goodness of fit can be checked for every geometry in the parameter range. When $R^2 < 0.85$, it is generally because the results of Y for two homothetic joints do not converge and not because of the inability of the function to fit Y values. If this is the the case, the results are not considered in analysis (results marked with * in Table 6.3). This is an indirect means of testing the results for mesh effects.

A global inspection of R^2 results seems to tell that the poor results (6/72 of the total) concentrate in the most slender chords (higher γ) and for chord bending (LC5) load case. For these cases, a finer mesh (specially at the joined members level) would be needed to guarantee the accuracy of results.

Table 6.1: Y regression parameter p , for different geometries and load cases.

τ	LC	β					
		0.53			0.65		
		γ			γ		
		4.2	7	8.5	4.2	7	8.5
0.4	LC1	0.42	0.73	0.80	0.40	0.65	0.66
	LC4	0.51	0.43	0.38	0.49	0.37	0.36
	LC5	0.65	0.42	0.19*	0.58	0.66*	0.73*
0.5	LC1	0.46	0.79	0.85	0.38	0.66	0.80
	LC4	0.58	0.48	0.41	0.59	0.43	0.38
	LC5	1.01	0.46	0.71	1.15	0.58	0.48*
0.6	LC1	0.55	0.92	1.03	0.50	0.66	0.73
	LC4	0.66	0.54	0.47	0.60	0.44	0.42
	LC5	0.86	0.89	0.38	0.60	0.61	1.47*
0.7	LC1	0.56	0.99	1.17	0.48	0.82	0.77
	LC4	0.70	0.55	0.52	0.64	0.50	0.44
	LC5	0.89	0.67	0.82*	0.74	0.68	0.57

* values corresponding to $R^2 < 0.85$, should not be considered

To illustrate the variability of the geometry factor, Figure 6.2 shows the Y function for $\beta = 0.53$ and the three basic load cases. It can be seen the variability is higher for load cases 1 and 5 than for load case 4.

6.4 Number of cycles to failure to homothetic joints

The number of cycles to failure for a given joint geometry under a basic load case can be calculated by replacing $\Delta K = Y \Delta \sigma \sqrt{\pi a}$ and $Y \left(\frac{a}{T}\right) = p \left(\frac{a}{T}\right)^{(q-1)} + \left(\frac{a}{T}\right)^q$ in Equation (2.10). The parameters p and q are selected from table 6.3 for the respective geometry and load case.

$$N = \int_{a_0}^{T/2} \frac{1}{C \cdot (\Delta \sigma \cdot Y(a/T) \cdot \sqrt{\pi a})^m} da = \int_{0.15}^{T/2} \frac{1}{C \cdot \left(\Delta \sigma \cdot \left(p \cdot \left(\frac{a}{T}\right)^{(q-1)} + \left(\frac{a}{T}\right)^q \right) \sqrt{\pi a} \right)^m} da \quad (6.5)$$

Table 6.2: Y regression parameter q , for different geometries and load cases.

τ	LC	β					
		0.53			0.65		
		4.2	γ 7	8.5	4.2	γ 7	8.5
0.4	LC1	0.60	0.64	0.63	0.63	0.62	0.60
	LC4	0.65	0.65	0.64	0.67	0.64	0.63
	LC5	0.65	0.64	0.64*	0.66	0.71*	0.82*
0.5	LC1	0.62	0.63	0.62	0.64	0.66	0.63
	LC4	0.65	0.65	0.62	0.67	0.64	0.63
	LC5	0.64	0.65	0.65	0.66	0.60	0.70*
0.6	LC1	0.63	0.64	0.64	0.63	0.62	0.64
	LC4	0.66	0.65	0.64	0.66	0.63	0.62
	LC5	0.66	0.70	0.60	0.65	0.62	0.76*
0.7	LC1	0.63	0.62	0.64	0.62	0.63	0.62
	LC4	0.65	0.63	0.64	0.65	0.63	0.62
	LC5	0.65	0.66	0.70*	0.65	0.68	0.62

* values corresponding to $R^2 < 0.85$, should not be considered

Solving the integral analytically, the following expression is obtained:

$$N = f(T, p, q) = \frac{-2.54 \cdot 10^{12} \cdot 8^q \cdot A + 4.64 \cdot 10^{12} \cdot e^{5.69q} \cdot T^{\frac{1}{2}+3q} \cdot B}{(1.0 + 6.0q)\sqrt{T}\Delta\sigma^3} \quad (6.6)$$

where,

$$A = \text{Hypergeometric2F1} \left[3, \frac{1}{2} + 3q, \frac{3}{2} + 3q, -2p \right] \quad (6.7)$$

$$B = \text{Hypergeometric2F1} \left[3, \frac{1}{2} + 3q, \frac{3}{2} + 3q, -6.67pT \right] \quad (6.8)$$

Figure 6.3 illustrates the effect of thickness resulting from Equation (6.6) in terms of number of cycles to failure. The relatively small contribution of the non-proportional initial defect size is also put in evidence and compared to the complete proportional problem (Equation (6.2)).

6.5 Thickness correction factor

The effect of the chord thickness on the number of cycles to failure can be described using a correction factor. To this end, the fatigue life for given joint geometry (corresponding to chord thickness T) and basic load case (see Equation (6.6)), N_T , is divided by $N_{T_{\text{ref}}}$, the number of cycles to failure for an homothetic joint of different absolute dimensions and chord thickness T_{ref} under the same basic load case. For simplification, this is done in a first step by considering any of the basic load cases, acting independently.

Table 6.3: Y regression goodness of fit R^2 , for different geometries and load cases.

τ	LC	β					
		0.53			0.65		
		4.2	γ 7	8.5	4.2	γ 7	8.5
0.4	LC1	0.98	0.98	0.99	0.98	0.99	0.96
	LC4	0.98	0.99	0.99	1.00	1.00	0.99
	LC5	0.98	0.99	0.38*	1.00	0.67*	0.03*
0.5	LC1	0.97	0.99	0.99	0.88	0.93	0.99
	LC4	1.00	1.00	0.99	0.97	0.99	1.00
	LC5	0.93	0.90	0.93	0.98	0.93	0.74*
0.6	LC1	0.99	0.99	0.99	0.99	0.98	0.93
	LC4	1.00	1.00	1.00	1.00	1.00	0.99
	LC5	1.00	0.87	0.99	0.99	0.98	0.33*
0.7	LC1	0.99	1.00	1.00	0.99	0.99	0.98
	LC4	1.00	1.00	0.99	1.00	1.00	1.00
	LC5	1.00	0.90	0.79*	0.99	0.92	0.99

* values corresponding to $R^2 < 0.85$, should not be considered

$$f_N = \left(\frac{N_T}{N_{T_{ref}}} \right) = \frac{\sqrt{T_{ref}}}{\sqrt{T}} \times \frac{\left(-2.54 \times 10^{12} 8^q A + 4.64 \times 10^{12} e^{5.69q} T^{\frac{1}{2}+3q} B \right)}{\left(-2.54 \times 10^{12} 8^q A + 4.64 \times 10^{12} e^{5.69q} T_{ref}^{\frac{1}{2}+3q} B \right)} \quad (6.9)$$

In this expression, $\sqrt{\frac{T_{ref}}{T}}$ reflects the effect of complete proportional sizing (including crack size bounds, second part of integral (6.2)). This value is an upper bound of the correction factor for the full problem (see Figure 6.3). The rest of the expression accounts for the absolute initial crack size and depends on the (non-dimensional) geometry and load case.

The thickness correction factor can be expressed in terms of fatigue strength:

$$N_T = C_T \cdot \Delta\sigma_{nom,T}^{-m} \Rightarrow f_S = \frac{S_{r,nom,T}}{S_{r,nom,T_{ref}}} = \left(\frac{N_T}{N_{T_{ref}}} \right)^{1/m} = f_N^{1/m} \quad (6.10)$$

where,

- N_T : number of cycles for a joint of chord thickness T ;
- $N_{T_{ref}}$: number of cycles for a joint of chord thickness, T_{ref} ;
- C_T : constant for the detail with chord thickness T ;
- m : Paris law constant ($m = 3$);
- $\Delta\sigma_{nom,T}$: nominal stress range for a joint of chord thickness T
- $S_{r,nom,T}$: fatigue strength for a joint of chord thickness T (based on the nominal stress range) at 2×10^6 cycles
- $S_{r,nom,T_{ref}}$: fatigue strength for a joint of chord thickness T_{ref} (based on the nominal stress range) at 2×10^6 cycles;
- f_S : thickness correction factor in terms of strength;
- f_N : thickness correction factor in terms of fatigue life.

6.5.1 Analogy with plates thickness effect

The correction factors obtained for proportionally scaled joints, can be compared to the classical correction factor used in welded plated joints (Gurney, 1979). The complicated expression (6.9) can be approximated using a function similar to Gurney (1979):

$$f_S = \frac{S_{r,nom,T} \times SCF}{S_{r,nom,T_{ref}} \times SCF} = \frac{S_{r,hs,T}}{S_{r,hs,T_{ref}}} \approx \left(\frac{T_{ref}}{T} \right)^{n_S} \quad (6.11)$$

where, n_S is the thickness correction factor exponent (for plates, Gurney used $T_{ref} = 25$ mm and $n_S = 0.25$). As can be seen, the connection factor for proportionally scaled joints remains the same regardless of being based on nominal or hot-spot stress.

The thickness correction factor can also be expressed in function of N . In this case it comes as

$$f_N \approx \left(\frac{T_{ref}}{T} \right)^{n_N} \quad (6.12)$$

$$n_N = n_S \cdot m$$

where,

- n_N : thickness correction factor exponent, dependent on the (non-dimensional) geometry and load case;
- m : $S - N$ curve slope ($m = 3$).

Tables 6.4 and 6.5 show the exponents found for the different geometries and basic load cases, when considering the correction factors in terms of number of cycles to failure, f_N , or the correction factors in terms of the fatigue resistance (nominal) for a specific number of cycles to failure (here taken as 2×10^6 cycles), f_S .

Regarding tables, the following remarks can be made:

- ◆ Size effect exponents for proportional scaling range from 0.37 to 0.43, in terms of fatigue life.
- ◆ Size effect exponents for proportional scaling range from 0.12 to 0.14, in terms of fatigue strength.
- ◆ Size effect is generally slightly more pronounced for load cases LC1 and LC5 than for LC4.

In order to investigate proportional scaling in tubular joints, Schumacher (2003) evaluated, using the approximate approach proposed by Albrecht and Yamada (1977), the fatigue strength of three joint geometries ($\beta = 0.51$; $\gamma = 6.9$; ($\tau = 0.3, \tau = 0.5, \tau = 0.7$)) and increased the thickness from 20 mm to 40 mm. The values obtained compare well for LC1 but for LC4 the values found in our study are about the double (see Table 6.6). For LC1 and LC4, this study confirms that:

- ◆ for proportional scaled joints CIDECT thickness correction is too conservative, as was shown by Schumacher (2003);
- ◆ even Gurney correction factor for plated joints (exponent $n = 0.25$) is too conservative;

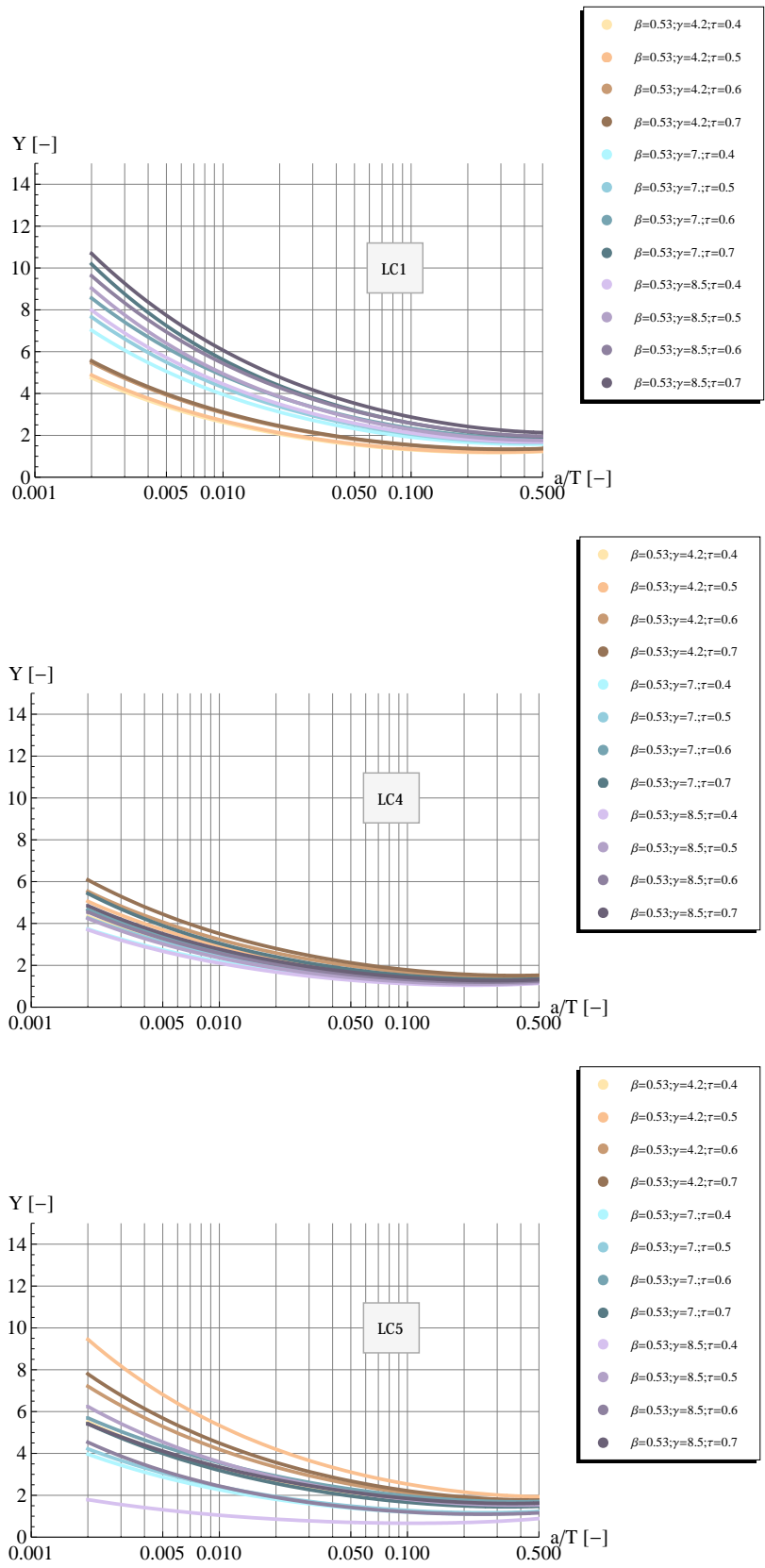


Figure 6.2: Geometry factor, Y , function of crack depth, for $\beta = 0.53$ and basic load cases LC1, LC4 and LC5.

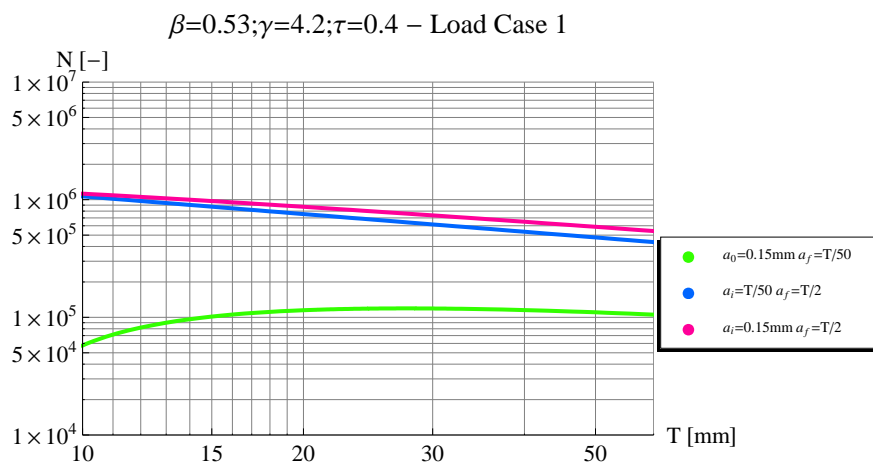


Figure 6.3: Number of cycles to failure function of the thickness of the chord in proportionally scaled joints for load case 1 (and specific geometry $\beta = 0.53; \gamma = 4.2; \tau = 0.4$).

Table 6.4: Thickness correction factor exponents n_N , for CHS joint geometries proportionally sized and different basic load cases, in terms of number of fatigue life (f_N) ($T_{ref} = 16$ mm)

τ	LC	β					
		0.53			0.65		
		4.2	γ 7	8.5	4.2	γ 7	8.5
0.4	LC1	0.41	0.42	0.42	0.39	0.42	0.43
	LC4	0.39	0.38	0.39	0.37	0.38	0.38
	LC5	0.40	0.39	0.33*	0.39	0.35*	0.21*
0.5	LC1	0.41	0.42	0.43	0.38	0.40	0.42
	LC4	0.39	0.39	0.40	0.38	0.39	0.39
	LC5	0.42	0.39	0.40	0.41	0.43	0.35*
0.6	LC1	0.41	0.42	0.42	0.41	0.42	0.41
	LC4	0.40	0.39	0.40	0.39	0.40	0.40
	LC5	0.41	0.37	0.41	0.40	0.42	0.33*
0.7	LC1	0.41	0.43	0.42	0.41	0.42	0.42
	LC4	0.40	0.41	0.40	0.40	0.40	0.40
	LC5	0.41	0.39	0.37*	0.41	0.38	0.42


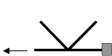
* values corresponding to $R^2 < 0.85$, should not be considered

Table 6.5: Thickness correction factor exponents n_S , for CHS joint geometries proportionally sized and different basic load cases, in terms of number of fatigue resistance (f_S) ($T_{ref} = 16\text{ mm}$)

τ	LC	β					
		0.53			0.65		
		4.2	γ 7	8.5	4.2	γ 7	8.5
0.4	LC1	0.14	0.14	0.14	0.13	0.14	0.14
	LC4	0.13	0.13	0.13	0.12	0.13	0.13
	LC5	0.13	0.13	0.11*	0.13	0.12*	0.07*
0.5	LC1	0.14	0.14	0.14	0.13	0.13	0.14
	LC4	0.13	0.13	0.13	0.13	0.13	0.13
	LC5	0.14	0.13	0.13	0.14	0.14	0.12*
0.6	LC1	0.14	0.14	0.14	0.14	0.14	0.14
	LC4	0.13	0.13	0.13	0.13	0.13	0.13
	LC5	0.14	0.12	0.14	0.13	0.14	0.11*
0.7	LC1	0.14	0.14	0.14	0.14	0.14	0.14
	LC4	0.13	0.14	0.13	0.13	0.13	0.13
	LC5	0.14	0.13	0.12*	0.14	0.13	0.14

* values corresponding to $R^2 < 0.85$, should not be considered

Table 6.6: Comparison of thickness correction factor exponents for proportional scaling, using σ_{nom} .

Geometry				
	n_S	n_S (Schumacher, 2003)	n_S	n_S (Schumacher, 2003)
$\beta = 0.5; \gamma = 7; \tau = 0.5;$	0.14	0.143	0.13	0.059
$\beta = 0.5; \gamma = 7; \tau = 0.7;$	0.14	0.124	0.13	0.061

6.6 Generalisation for combined load case / Load case interaction

In Section 6.4, a procedure to estimate the number of cycles to failure for a joint under single basic load cases is detailed. The situation, in which a single basic case acts isolated in a joint, is, however, not common in practice. Therefore, it is important to extend this result to combined load cases. As presented in paragraph 4.6, the stress intensity factors for a combined load case can be obtained from the basic load cases.

As the crack opening mode I is predominant for the load cases considered (see Figure 4.10), the equivalent stress intensity factor, K_{eq} , is replaced by K_I in order to simplify the superposition of effects of the three basic load cases.

$$\begin{aligned}\Delta K_{I,combined} &= \Delta K_{I,LC1} + \Delta K_{I,LC4} + \Delta K_{I,LC5} \\ &= \Delta\sigma_{LC1} \cdot Y_{LC1}(a/T) \cdot \sqrt{\pi a} + \Delta\sigma_{LC4} \cdot Y_{LC4}(a/T) \cdot \sqrt{\pi a} + \Delta\sigma_{LC5} \cdot Y_{LC5}(a/T) \cdot \sqrt{\pi a}\end{aligned}\quad (6.13)$$

Replacing $\Delta K = \Delta K_{I,combined}$ in expression (2.10)

$$\begin{aligned}N_f &= \int_{a_i}^{a_f} \frac{1}{C (\Delta K_{I,combined})^m} da = \\ &= \int_{a_i}^{a_f} \frac{1}{C (\Delta K_{I,LC1} + \Delta K_{I,LC4} + \Delta K_{I,LC5})^m} da\end{aligned}\quad (6.14)$$

6.6.1 Graphical solution

Some hypothesis have to be made so that the integral can be solved. Regarding the stress ranges from the load cases, LC_4 and LC_5 are considered as fractions of LC_1 .

$$\begin{aligned}\Delta\sigma_{LC1} &= k_1 \cdot \Delta\sigma \\ \Delta\sigma_{LC4} &= \%_{LC4} \times \Delta\sigma_{LC1} \\ \Delta\sigma_{LC5} &= \%_{LC5} \times \Delta\sigma_{LC1}\end{aligned}\quad (6.15)$$

Replacing in Equation (6.16) it comes:

$$\begin{aligned}N_f &= \int_{a_i}^{a_f} \frac{1}{C (\Delta\sigma_{LC1} Y_{LC1}(a/T) \sqrt{\pi a} + \Delta\sigma_{LC4} Y_{LC4}(a/T) \sqrt{\pi a} + \Delta\sigma_{LC5} Y_{LC5}(a/T) \sqrt{\pi a})^m} da = \\ &= (k_1 \cdot \Delta\sigma)^{-m} \int_{a_i}^{a_f} \frac{1}{C (Y_{LC1}(a/T) \sqrt{\pi a} + \%_{LC4} Y_{LC4}(a/T) \sqrt{\pi a} + \%_{LC5} Y_{LC5}(a/T) \sqrt{\pi a})^m} da\end{aligned}\quad (6.16)$$

The integral (6.16) is numerically solved for a mesh of $\%_{LC4}$ and $\%_{LC5}$ values assuming $\Delta\sigma = 100$ MPa. Figure 6.4 illustrates the result for joint geometry: $\beta = 0.53$; $\gamma = 4.2$; $\tau = 0.4$; $T = 20$. The number of cycles to failure is obtained entering $\%_{LC4}$ (horizontal axis) and $\%_{LC5}$ (vertical axis) and then multiplying the value found by k_1^{-m} to take in account the magnitude of the stress ranges.

6.6.2 Comparison with fatigue test results

As an example, the procedure to estimate the number of cycles to failure is applied to fatigue test joint (series S5 joint 1).

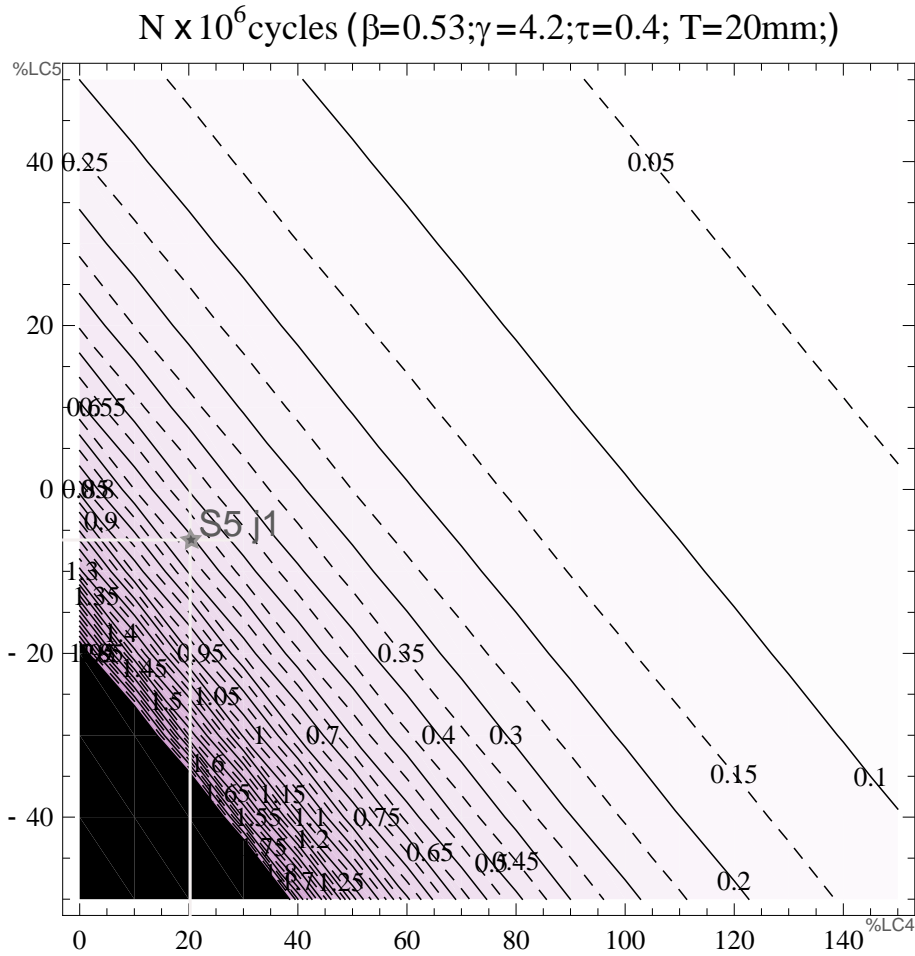


Figure 6.4: Reference number of cycles to half thickness crack depth, $N_{T/2}$, function of the combination of the three basic load cases, for $\Delta\sigma = 100 \text{ N/mm}^2$.

$$\begin{aligned}
 \Delta\sigma_{LC1} &= 152 \text{ MPa} \rightarrow (k_1 = 1.52) \\
 \Delta\sigma_{LC4} &= 33 \text{ MPa} \rightarrow (\%LC4 = 33/1.52 = 21.7\%) \\
 \Delta\sigma_{LC5} &= -11 \text{ MPa} \rightarrow (\%LC5 = -11/1.52 = -7.2\%)
 \end{aligned}
 \tag{6.17}$$

The reference number of cycles to half thickness crack depth is obtained from the Figure with $\%LC_4$ and $\%LC_5$ and leads to 0.63×10^6 cycles. The predicted number of cycles is then obtained by multiplying 0.63×10^6 by $k_1^{-m} = 1.52^{-3} = 0.285$ ($\Delta\sigma_1 = 152 \text{ MPa}$). The result is, $N_{S5j1} = 179000$ cycles, which is very close to the test result ($N = 169000$ cycles for crack depth $a = T/2 = 10 \text{ mm}$).

This procedure is repeated for S1, S2 and S3 (Schumacher (2003) proportionally scaled series) and results compare well (see Figure 6.5).

6.7 Efficiency of proportionally scaled joints

For the designer, the presentation of the size effects in terms of fatigue strength, $S_{r,nom}$, as a function of the chord thickness, T , does not give an indication on the admissible force range, ΔF . In fact, an increase in the chord thickness is associated with a decrease in fatigue strength of the joint. However, the cross-section increases, and thus, the force range, ΔF , it can resist. It is interesting to analyse these results in terms of cross-sectional area and force range, ΔF . This is made in Figure 6.6 for a given joint geometry ($\beta = 0.53; \gamma = 4.2; \tau = 0.4$), whose scale is represented by the chord thickness, T , under

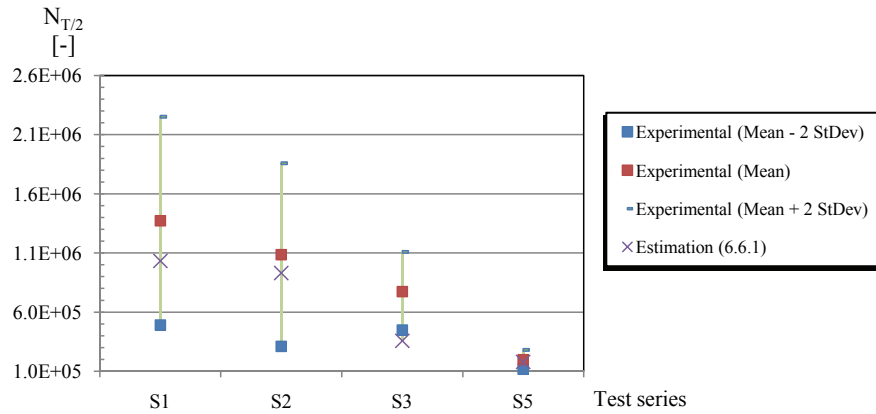


Figure 6.5: Comparison between experimental results and estimations obtained using procedure described in 6.6.1.

LC1 with:

- ◆ $F_{LC1} = A_{br} \times f_y$ - the admissible force in the brace, when considering the cross-section static resistance;
- ◆ $\Delta F_{fatigue}$ - the admissible force range in the braces, for a fatigue life of 2×10^6 cycles;
- ◆ $\Delta F_{fatigue T16 \times A}$ - the admissible force range in the braces, obtained by multiplying the fatigue strength at 2×10^6 cycles, for a 16 mm thick chord, by the surface of the joint's brace without any thickness correction factor;
- ◆ $\Delta F_{fatigue CIDECT correction}$ - the admissible force range in the braces, obtained by multiplying the fatigue strength at 2×10^6 cycles, for a 16 mm thick chord, by the corresponding brace surface and CIDECT thickness correction factor $(16/T_{chord})^{0.378}$;

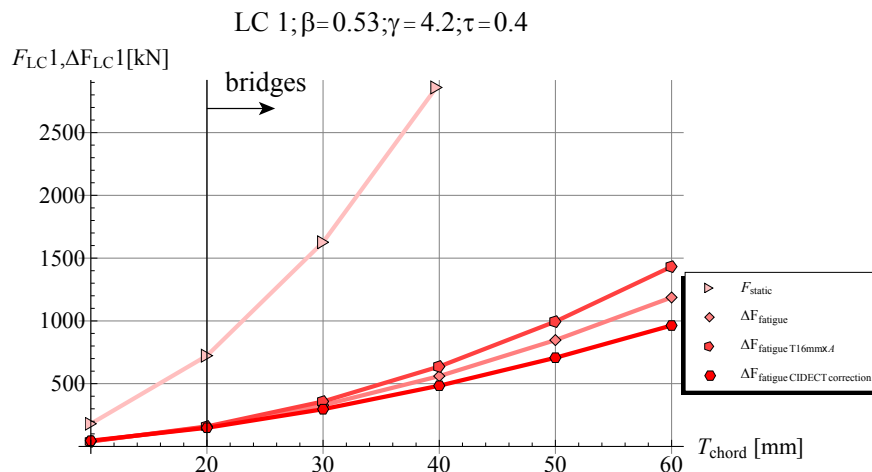


Figure 6.6: Comparison of static admissible force to admissible fatigue force range, calculated according to different hypotheses for proportionally scaled geometries.

Figure 6.6 highlights the fact that simple extrapolation of CIDECT recommendations for geometries typical of bridge design ($\gamma < 12$ and $T > 20$ mm) can be too conservative. Note that conservatism increases with increasing thickness of chord.

6.8 Summary and conclusions

In this chapter, the effect of chord thickness on fatigue of welded tubular joints was isolated by proportionally scaling the joints. This procedure was repeated for the relevant geometries from the parametric study presented in the previous chapter.

The geometry correction factor, Y , accounts for the stress concentration through the thickness along the crack path. This geometry factor is calculated at a set of discrete points for the non-dimensional joint geometries in the parametric matrix, including, at least, two absolute joint sizes and was made for the three main basic load cases. The geometry correction factor is best approximated as a function of the relative crack depth (a/T) namely, $Y \left(\frac{a}{T} \right) = p \cdot \left(\frac{a}{T} \right)^{(q-1)} + \left(\frac{a}{T} \right)^q$ and remains constant for homothetic joints.

Curve fitting is then used to determine a function representing the Y for each joint geometry. By introducing the Y factor, a methodology is suggested to calculate the fatigue life for a specific geometry and basic load case. Correction factors to account for reduction of fatigue life/strength are deduced for proportional scaling. Then, this procedure is generalised for the combined load case.

Based on the work presented in this chapter, the following conclusions can be drawn:

- ◆ The Y factor coefficients p and q depend on the load case and geometry of the joint. The thickness correction factor exponents (n_S and n_N) are not dependent on the geometry and only slightly dependent on the load case.
- ◆ Geometry factor, Y , scatter band is more pronounced for load cases 1 and 5 than for load case 4.
- ◆ Thickness effect is slightly more pronounced for load cases LC1 and LC5 than for LC4.
- ◆ When proportional scaling is done, the thickness correction factor remains the same regardless of being based on nominal or hot-spot stress range (as the SCF remains the same for homothetic joints).
- ◆ The thickness correction factor exponent (accounting for proportional scaling), can be expressed as the classical form for plates $\left(\frac{T_{\text{ref}}}{T} \right)^n$. The exponents vary from 0.12 to 0.14, when referring to fatigue strength, and 0.37 to 0.43 when referring to fatigue life. The lowest values correspond to LC1 and the highest to LC4. These values confirm that it is not justified to use exponent as high as CIDECT, and even exponents lower than Gurney can be used safely.
- ◆ The use of thickness correction factors is recommended for proportional scaling, when based on nominal stress (same as hot-spot in the case of proportional scaling, Equation (6.11)). However, the fatigue behaviour for a reference homothetic joint is needed.

Non-proportional scaling

7.1 Introduction

Proportional scaling is a reasonable scenario in applications where the entire size of the detail or joint will increase relatively with an increase in the applied load. In tubular bridges, however, it is common to see that along the length of a span, the outside diameters of the tubular truss members are much more likely to remain constant, while the thicknesses of the brace and chord members will be adjusted to account for the changes in load at different span locations. This is an example of non-proportional scaling, a scenario where not only the changing wall thickness of the fatigue-critical member, but also the size of the attachment (brace) may affect the relative fatigue behaviour between joints (from Schumacher (2003)).

In the previous chapter, the effect of chord thickness was isolated from the effects of the non-dimensional parameters considered (β, γ, τ). This was done through comparisons of fatigue behaviour of proportionally scaled joints. In this chapter, the discussion is focused on load and attachment effects.

Basic load case LC5, bending of the chord, is not considered in this chapter because the independence of results on the mesh could not be assured. Moreover, for a loaded truss, load case 5 is normally less important, negative and tending to close the weld toe crack at position 1.

In Section 7.2, the effects of the non-dimensional parameters on the geometry correction factor, Y , are shown qualitatively. An alternative approach to assess the fatigue behaviour of CHS-joints is proposed in section 7.3. This method, based on the geometry correction factor, Y , relies on a scalar to represent the local stress state, and thus to estimate the fatigue behaviour as in the case of the hot-spot stress method. However, in this case, the scalar contains information on the through depth stress gradient and not only on the structural stress at a surface single point, as it is the case for the hot-spot method. The Y_{α_r} method is applied to the series tested at ICOM and results are compared. A comparison between the values obtained for Y_{α_r} and SCF values is presented and discussed in Section 7.4. Finally, in Section 7.5, considerations are issued on geometries efficiency towards fatigue resistance.

7.2 Effect on the geometry correction factor, Y

In Section 6.3, the geometry correction factor was introduced as a property for homothetic joints independently of their absolute dimension. For this reason, it is an interesting function to use when comparing the influence of the relative dimensions on the fatigue behaviour.

Furthermore, results in terms of Y for different basic load cases can be superposed. That is an advantage when compared to representing the results in terms of fatigue strength, $S_{r,nom}$, or the number of cycles to failure, N . For this cases the results remain dependent on the basic load case and

are not possible to combine.

7.2.1 Influence of thickness ratio, τ

Varying the thickness ratio, τ , has a double effect: attachment when unloaded, or, when the brace is loaded, loading effect. The attachment effect, for load case 4, is influenced by τ as this parameter relates the rigidity of the brace (attachment) to the chord cross-section. When load case 1 is considered, comparing joints with the same nominal stress in the braces but different brace thicknesses, a load effect exists, the thicker brace transmits a higher force to the same chord cross-section. The crack is, thus, subjected to a higher stress amplitude.

Figure 7.1 shows that when the thickness ratio increases, the geometry correction factor, Y , also increases. For load case 1, the load effect, as defined in Section 5.5, is the main responsible for the increase of Y as the τ increases. For load case 4, the "attachment" size determines the stress concentration and, thus, the geometry correction factor. Attachment size and load effects vary in the same way and are "added" if load cases 1 and 4 are combined.

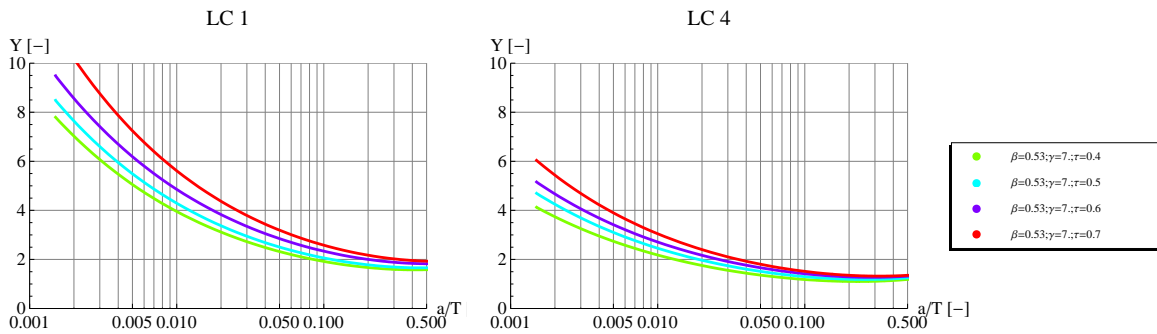


Figure 7.1: Geometry correction factor, influence of the thickness ratio, τ .

7.2.2 Influence of chord slenderness, γ

Figure 7.2 shows the influence of the chord slenderness, γ , over the geometry correction factor. For load case 1, as γ increases the correction factor Y increases. For load case 4, the effect is the opposite, Y decreases as the γ increases. The variation is less pronounced for load case 4 than for load case 1.

For a combination of load cases 1 and 4, the effects may cancel depending on the relative importance of each load case.

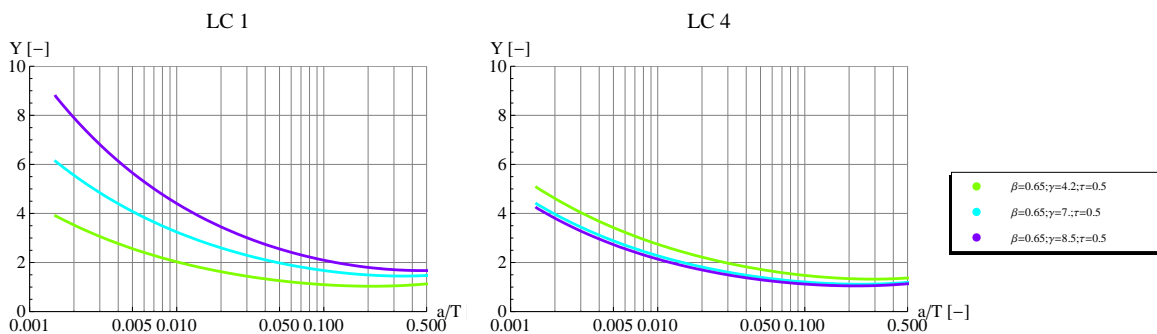


Figure 7.2: Geometry correction factor, influence of the chord slenderness, γ .

7.2.3 Influence of diameters ratio β

The effect of β on the geometry correction factor Y is shown in Figure 7.3. As the β increases, the Y decreases for both load case 1 and load case 4. When β increases, the brace is more flexible and leads to lower stress concentration in the weld toe. As already discussed in Section 5.4.4, the stress flow is more efficient when β increases, thus leading to lower Y values.

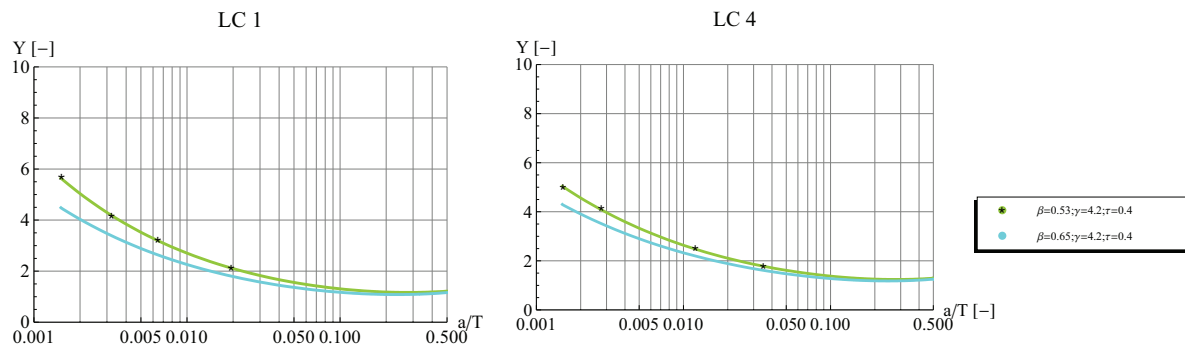


Figure 7.3: Geometry correction factor, influence of the diameters ratio β .

Although qualitative comparisons can be made using the Y function concerning the fatigue behaviour, it is not straight forward to use the function in practice. In fact, the p and q values defining the Y function (see Equation (6.4)) influence both the mean and the gradient of the Y function and it is complicated to conclude on the fatigue behaviour just based on each of these values. An alternative approach is proposed and detailed in the next section.

7.3 Alternative approach for fatigue assessment of CHS joints

7.3.1 Principle

As already discussed in chapters 1 and 2 of this thesis, recently, the most widely used design methods for fatigue of tubular joints is based on the hot-spot structural stress at the weld toe. This method relies on a scalar to estimate the fatigue strength of the joint. It assumes the surface stresses on a structural member provide an indication of the stress state at a potential fatigue crack location. However, as the hot-spot stress is extrapolated from measures or calculations at the surface, it does not account for cases with the same surface stress but different stress gradients through the thickness. These may occur for different load cases (with different degree of bending) or different geometries. For the latter, a correction factor is prescribed to account for the effect of the thickness of the cracked plate.

One of the advantages that can be associated with the hot-spot stress method, besides the amount of existing formulas for SCF calculation and the experience in applying this method, is the fact that all the problem complexity (load cases, eccentricity and stress gradient) is reduced to a single scalar value. This is common to other local stress approaches (e.g. 1-mm stress (Xiao and Yamada, 2004)). In addition, the fact that the structural stress is considered (excluding local stress raisers such as the weld profile) keeps it less dependent on the random (as dependent on the weld shape and angle), highly non-linear and mesh-dependent stress in the weld toe.

Although the advantages are evident, the methods relying on surface stress arouse many questions when the stress gradient along the potential crack path has a different shape, for instance, due to a predominance of bending.

Xiao and Yamada (2004) proposed the 1 – mm stress method to assess the fatigue behaviour of welded joints. This method possesses the ability of predicting size effect including thickness effect "to a certain extent" at least. They explored the fact that correlation of crack propagation life can be established between an object detail and the reference detail with an equivalent geometric stress at a

certain point in the crack path. For in-plane gusset, it was found that the equivalent geometric stress can be located at a point close to 1 – mm in the expected crack path (see Section 2.4.1). Although it proposes a new approach to assess the fatigue behaviour and highlights advantages of considering the stress over the crack depth, it is not completely satisfactory, namely for details with a high degree of bending (Xiao and Yamada, 2004).

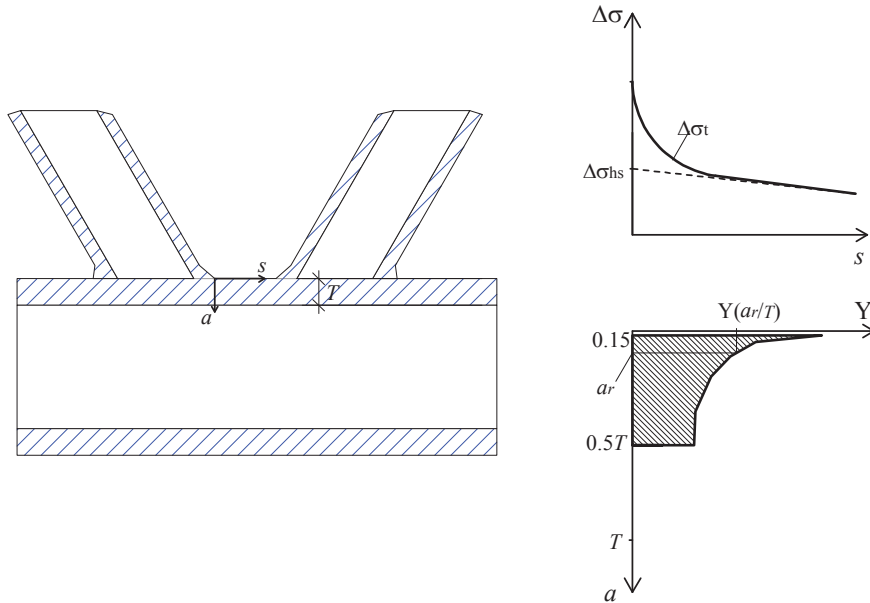


Figure 7.4: Schematic comparing 1-D hot-spot approach to 2-D Y approach.

In order to find a parameter that could solely estimate the fatigue behaviour of tubular joints, consider the geometry correction factor, Y , as defined in section 6.3. Recalling the integral that allows for the calculation of the number of cycles for crack propagation from an initial crack depth, $a_i = 0.15$ mm, to a final crack depth, $a_f = T/2$:

$$N = \int_{a_i}^{a_f} \frac{1}{C (\Delta\sigma_{nom} \cdot Y(a/T) \cdot \sqrt{\pi a})^m} da \quad (7.1)$$

Inspired by the developments made by Xiao and Yamada (2004), the Second Mean Value Theorem for integrals is applied. There is a crack depth, a_r , in the interval $[a_i, a_f]$, for which the following relation is valid:

$$N = \frac{1}{C (\Delta\sigma_{nom} Y(a_r/T))^m} \int_{a_i}^{T/2} \frac{1}{(\sqrt{\pi a})^m} da \quad (7.2)$$

$$= \frac{1}{C (\Delta\sigma_{nom} Y(a_r/T))^m} \left(0.927075 - \frac{0.507949}{\sqrt{T}} \right) \quad (7.3)$$

The representative crack depth, a_r , allows for a reduction of the geometry correction factor function to an equivalent single value over the crack depth $Y(a_r/T)$ or Y_{a_r} for simplicity. Figure 7.4 compares schematically the hot-spot approach with the Y_{a_r} approach. If the hot-spot method relies on the extrapolated structural stress at a single weld toe location. The Y_{a_r} method takes a value that is equivalent to the stress gradient through depth (between a_i and a_f), adding one dimension to the information provided. From reporting on a single point structural stress (1-D), as the hot-spot approach, to reporting the effect equivalent to the stress gradient through depth.

Another difference between hot-spot approach and Y_{a_r} approach is the use of the total stress instead of structural stress. Although the local stress concentrations due to weld geometry and irregularities at the weld toe have influence on fatigue strength, the use of the structural stress can be justified when the comparison stress is measured or calculated at the weld toe. In fact, as it is well known, the stress raising due to the weld profile is highly dependent, on physical models, on the local weld profile and in numerical analysis on the mesh refinement. By taking the structural stress, these sources of uncertainty and imprecisions are mitigated. The structural stress is then directly correlated to fatigue life of details.

The Y_{a_r} approach proposed herein takes the value of the geometry correction factor at some distance from the weld-toe, in the through thickness direction. As defined in Section 6.3, the geometry correction factor includes the stress raising due to the weld profile (defined according to the hypotheses stated in Section 5.3.3). Although the stress raising due to the weld profile is highly dependent, in numerical analysis, on the mesh refinement, Xiao and Yamada (2004) found a convergence of the stress gradients due to different weld toe geometries (radius and angle) and using different mesh grades, at less than 1 mm away from the weld toe, in the thickness direction. It is therefore not likely that the inclusion of the nonlinear gradient due to the weld profile introduces a significant change in the Y function mean value nor in the representative distance a_r due to different weld toe geometries or mesh grading. This assumption should be confirmed in future investigations.

An advantage of the Y_{a_r} approach is the use of a single $S_{a_r} - N$ resistance line. The $S_{a_r} - N$ line results of plotting the Equation (7.2) as a function of $\Delta\sigma_{nom} \cdot Y(a_r/T)$. As can be seen in Figure 7.5, $S_{a_r} - N$ resistance lines for thicknesses $T = 16$ mm and $T = 60$ mm almost superpose. Line corresponding to thickness 16 can thus be used as representative for thicknesses up to 60 mm.

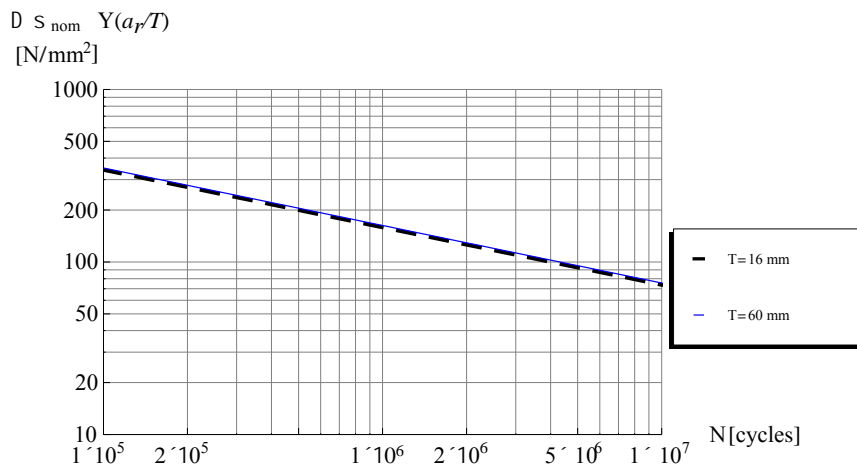


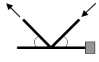
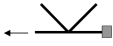
Figure 7.5: $S_{a_r} - N$ lines resulting from plotting the Equation (7.2) as a function of $\Delta\sigma \cdot Y(a_r/T)$ for chord thicknesses $T = 16$ mm and $T = 60$ mm.

7.3.2 Single basic load cases

Representative depth, a_r

In order to find the representative crack depth values, a_r , the expressions (7.1) and (7.2) are equaled and the resultant Equation is solved for the different geometries (from the parametric table) and the chord thicknesses: 16 mm, 20 mm, 30 mm, 50 mm. The results are presented in Table 7.1. The representative crack depth, a_r , i.e. at which the geometry correction factor assumes its equivalent value, ranges from 0.64 mm to 1.5 mm, depending, as would be expected, on the geometry of the joint and the load case. This dependency is mainly on the load case and the chord thickness, and only then, on the non-dimensional parameters (see Figure 7.7 for $T = 16$ mm).

Table 7.1: Representative coordinate a_r [mm] for load cases LC1 and LC4, considering joints of three different absolute sizes.

a_r [mm] Joint geometry								
	$T = 16$	$T = 20$	$T = 30$	$T = 50$	$T = 16$	$T = 20$	$T = 30$	$T = 50$
$\beta = 0.53; \gamma = 4.2; \tau = 0.4$	0.71	0.80	0.98	1.30	0.69	0.77	0.93	1.20
$\beta = 0.53; \gamma = 4.2; \tau = 0.5$	0.71	0.79	0.96	1.20	0.72	0.80	0.96	1.20
$\beta = 0.53; \gamma = 4.2; \tau = 0.6$	0.74	0.82	1.00	1.30	0.74	0.82	0.99	1.30
$\beta = 0.53; \gamma = 4.2; \tau = 0.7$	0.74	0.82	1.00	1.30	0.76	0.84	1.00	1.30
$\beta = 0.53; \gamma = 7.; \tau = 0.4$	0.80	0.89	1.10	1.40	0.64	0.71	0.86	1.10
$\beta = 0.53; \gamma = 7.; \tau = 0.5$	0.82	0.91	1.10	1.40	0.68	0.75	0.91	1.20
$\beta = 0.53; \gamma = 7.; \tau = 0.6$	0.84	0.93	1.10	1.50	0.70	0.77	0.94	1.20
$\beta = 0.53; \gamma = 7.; \tau = 0.7$	0.88	0.99	1.20	1.60	0.74	0.82	1.00	1.30
$\beta = 0.53; \gamma = 8.5; \tau = 0.4$	0.83	0.92	1.10	1.50	0.64	0.71	0.86	1.10
$\beta = 0.53; \gamma = 8.5; \tau = 0.5$	0.86	0.96	1.20	1.50	0.67	0.75	0.91	1.20
$\beta = 0.53; \gamma = 8.5; \tau = 0.6$	0.86	0.96	1.20	1.50	0.69	0.77	0.93	1.20
$\beta = 0.53; \gamma = 8.5; \tau = 0.7$	0.88	0.98	1.20	1.50	0.71	0.79	0.95	1.20
$\beta = 0.65; \gamma = 4.2; \tau = 0.4$	0.66	0.73	0.89	1.10	0.66	0.73	0.88	1.10
$\beta = 0.65; \gamma = 4.2; \tau = 0.5$	0.63	0.70	0.85	1.10	0.69	0.77	0.93	1.20
$\beta = 0.65; \gamma = 4.2; \tau = 0.6$	0.72	0.80	0.98	1.30	0.72	0.80	0.97	1.20
$\beta = 0.65; \gamma = 4.2; \tau = 0.7$	0.71	0.79	0.97	1.20	0.74	0.83	1.00	1.30
$\beta = 0.65; \gamma = 7.; \tau = 0.4$	0.80	0.89	1.10	1.40	0.63	0.70	0.85	1.10
$\beta = 0.65; \gamma = 7.; \tau = 0.5$	0.74	0.82	0.99	1.30	0.66	0.73	0.89	1.10
$\beta = 0.65; \gamma = 7.; \tau = 0.6$	0.79	0.88	1.10	1.40	0.69	0.77	0.93	1.20
$\beta = 0.65; \gamma = 7.; \tau = 0.7$	0.84	0.93	1.10	1.50	0.71	0.78	0.95	1.20
$\beta = 0.65; \gamma = 8.5; \tau = 0.4$	0.83	0.93	1.10	1.50	0.63	0.69	0.84	1.10
$\beta = 0.65; \gamma = 8.5; \tau = 0.5$	0.82	0.92	1.10	1.50	0.65	0.72	0.87	1.10
$\beta = 0.65; \gamma = 8.5; \tau = 0.6$	0.79	0.88	1.10	1.40	0.68	0.76	0.92	1.20
$\beta = 0.65; \gamma = 8.5; \tau = 0.7$	0.83	0.92	1.10	1.50	0.70	0.78	0.95	1.20
$a_{r_{\text{mean}, T_i}}$	0.78	0.87	1.06	1.38	0.69	0.77	0.93	1.19
Standard Deviation	0.070	0.079	0.096	0.137	0.037	0.042	0.049	0.068
$a_{r_{\text{mean}}} \cdot \sqrt{\frac{T_0}{T_i}}$	0.78	0.78	0.78	0.78	0.69	0.68	0.68	0.67

The reference geometry is considered as:

$$T_0 = 16 \text{ mm}; \beta_0 = 0.53; \gamma_0 = 4.2; \tau_0 = 0.4$$

and is used in the next sections.

Analysing Table 7.1, it was found that the mean representative depth can be expressed as

$$a_{r_{\text{mean,corrected, LC1}}} = 0.78 \sqrt{\frac{T}{T_0}} \quad (7.4)$$

for load case 1 and

$$a_{r_{\text{mean,corrected, LC4}}} = 0.69 \sqrt{\frac{T}{T_0}} \quad (7.5)$$

for load case 4. At these depths, the Y function is considerably steep, it is therefore important to investigate the error introduced when considering the mean value $a_{r_{\text{mean}}}$ (for the chord thickness considered) instead of the value obtained for each specific geometry.

The relative error for the fatigue life, obtained using expression (7.2), when the mean value for the respective thickness, $a_{r_{\text{mean}}}$, is used instead of the determined a_{r_i} , is calculated for each geometry in the parametric table, as follows:

$$\begin{aligned} \text{rel. error}(\%) &= \frac{\frac{1}{C(\Delta\sigma Y(a_{r_i}/T))^m} \int_{a_0}^{T/2} \frac{1}{(\sqrt{\pi a})^m} da - \frac{1}{C(\Delta\sigma Y(a_{r_{\text{mean}}}/T))^m} \int_{a_0}^{T/2} \frac{1}{(\sqrt{\pi a})^m} da}{\frac{1}{C(\Delta\sigma Y(a_{r_i}/T))^m} \int_{a_0}^{T/2} \frac{1}{(\sqrt{\pi a})^m} da} \\ &= \frac{\frac{1}{(Y(a_{r_i}/T))^m} - \frac{1}{(Y(a_{r_{\text{mean}}}/T))^m}}{\frac{1}{(Y(a_{r_i}/T))^m}} \end{aligned} \quad (7.6)$$

where,

- Y : geometry correction factor;
- T : chord thickness;
- m : constant for Paris law ($m = 3$);
- a_{r_i} : value calculated for the considered joint geometry;
- $a_{r_{\text{mean}}}$: mean value of the a_r values for the same thickness;

Figure 7.6 shows the relative errors for load cases 1 and 4.

The error values, disposed in the same order as table 7.1, indicate that the a_r value should be further corrected (major influences of γ for LC1 and τ for LC4).

The *FindFit* function in Mathematica6 (least squares fitting) (Wolfram, 1988) was used to find an expression of a_r as a function of the non-dimensional parameters and the joint absolute size represented by the chord thickness, T . Table 7.1 was used as input data and the model was chosen in the form

$$a \cdot (\beta/\beta_0)^b \cdot (\gamma/\gamma_0)^c \cdot (\tau/\tau_0)^d \cdot (T/T_0)^e \quad (7.7)$$

The following enhancements on the formulas improve the results:

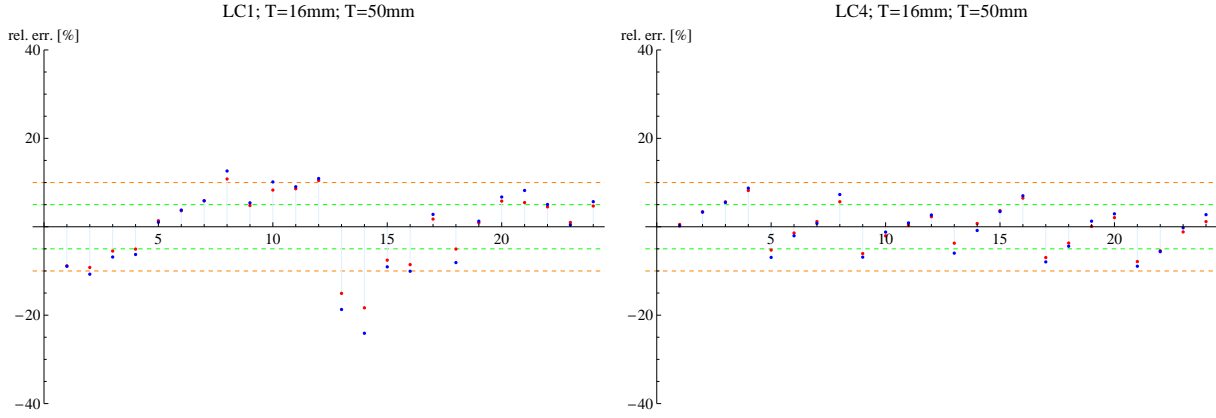


Figure 7.6: Relative error on the fatigue life when using the $a_{r_{\text{mean},T_i}}$ (obtained using expressions (7.4) and (7.5)) for the geometries in the parametric table, considering two absolute dimensions for each case: $T = 16$ mm (red dots) and $T = 50$ mm (blue dots) as defined by Equation (7.12).

$$a_{r_{LC1}} = 0.70 \left(\frac{T}{T_0} \right)^{0.49} \cdot \left(\frac{\beta}{\beta_0} \right)^{-0.26} \cdot \left(\frac{\gamma}{\gamma_0} \right)^{0.26} \cdot \left(\frac{\tau}{\tau_0} \right)^{0.098} \quad (7.8)$$

for load case 1 and

$$a_{r_{LC4}} = 0.67 \left(\frac{T}{T_0} \right)^{0.48} \cdot \left(\frac{\beta}{\beta_0} \right)^{-0.13} \cdot \left(\frac{\gamma}{\gamma_0} \right)^{-0.083} \cdot \left(\frac{\tau}{\tau_0} \right)^{0.21} \quad (7.9)$$

for load case 4. They are valid within the parametric matrix limits defined in Section 5.2. The relative error drops under 9% and 5%, for load cases 1 and 4 respectively (see Figure 7.8). Figure 7.7 shows the representative crack depth as a function of the non-dimensional parameters γ and τ for the basic load cases 1 and 4.

Generally the representative crack depth $a_r < 1$ mm and it is found to be deeper for load case 1 than for load case 4. For load case 1, β and γ are the most influencing non-dimensional parameters. The a_r increases with γ and decreases with β . For load case 4, τ is the parameter influencing the representative crack depth the most.

Equivalent geometry correction value $Y(a_r/T)$

The fatigue behaviour of a CHS joint under basic load cases 1 or 4 can be estimated by determining the value of Y at the respective representative crack depths. The equivalent correction factor values, $Y(a_r/T)$, were computed for the geometries in the parametric matrix and the absolute sizes corresponding to thicknesses: 16 mm, 20 mm, 30 mm, 50 mm. The results are shown in table 7.1 for load cases 1 and 4.

Once again, the *FindFit* function (Wolfram, 1988) was used to find an expression of $Y(a_r/T)$ as a function of the non-dimensional parameters and the absolute size represented by the chord thickness, T . Table 7.2 was used as input data and the model was chosen as Equation (7.7)

Expressions (7.10) and (7.11) were obtained for load cases 1 and 4 respectively.

$$Y^{LC1}_{a_r}(\beta, \gamma, \tau, T) = 1.62 \left(\frac{T}{T_0} \right)^{0.16} \cdot \left(\frac{\beta}{\beta_0} \right)^{-0.86} \cdot \left(\frac{\gamma}{\gamma_0} \right)^{0.70} \cdot \left(\frac{\tau}{\tau_0} \right)^{0.39} \quad (7.10)$$

$$Y^{LC4}_{a_r}(\beta, \gamma, \tau, T) = 1.68 \left(\frac{T}{T_0} \right)^{0.15} \cdot \left(\frac{\beta}{\beta_0} \right)^{-0.34} \cdot \left(\frac{\gamma}{\gamma_0} \right)^{-0.32} \cdot \left(\frac{\tau}{\tau_0} \right)^{0.44} \quad (7.11)$$

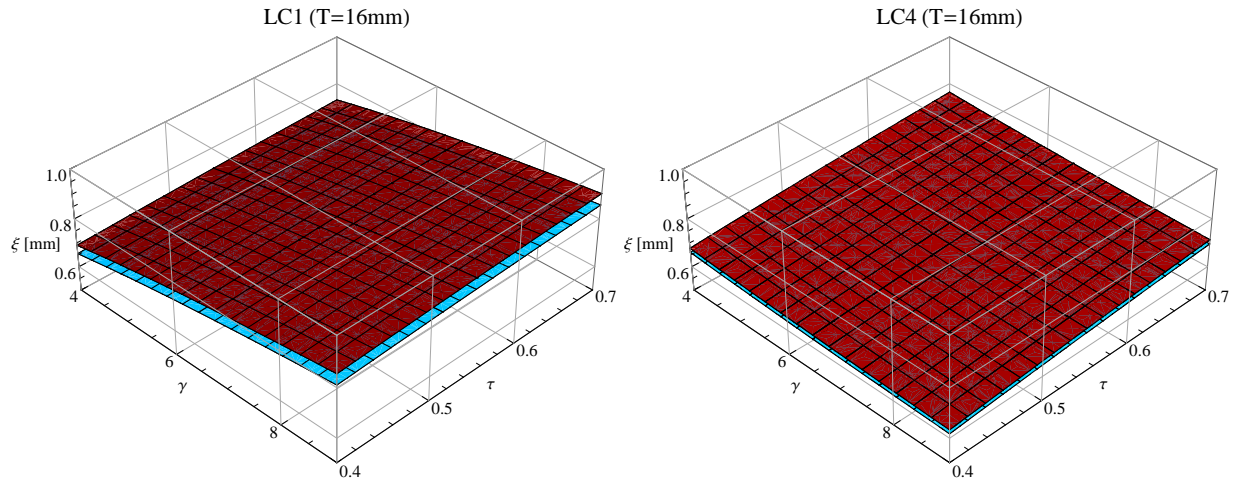


Figure 7.7: Representative crack depth, a_r , for basic load cases 1 and 4, as a function of non-dimensional parameters γ and τ (Dark red surface: $\beta = 0.53$; Blue surface: $\beta = 0.63$). The absolute size corresponds to a chord thickness of $T = 16$ mm.

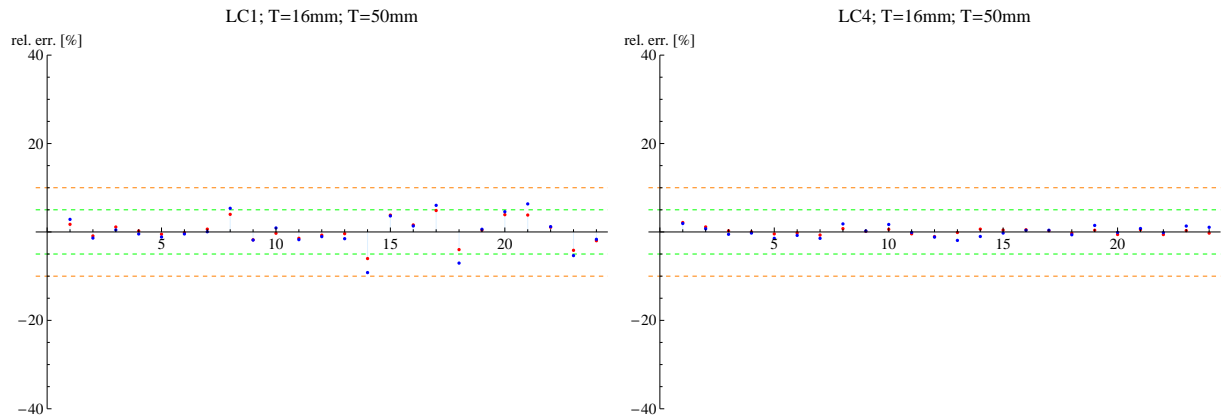


Figure 7.8: Relative error on the fatigue life when using the representative depth $a_{r_{\beta,\gamma,\tau,Ti}}$ (obtained using expressions (7.8) and (7.9)) for the geometries in the parametric table, considering two absolute dimensions for each case: $T = 16$ mm (red dots) and $T = 50$ mm (blue dots).

Figure 7.9 plots expressions (7.10) and (7.11) as a function of γ and τ . It can be noticed, for the load case 1, the Y_{a_r} increases with γ and τ . For load case 4, the Y_{a_r} decreases with the chord slenderness, γ , and increases with the thickness ratio, τ . The influence of the non-dimensional parameters over Y_{a_r} parameter is more pronounced for load case 1 than for load case 4. For both load cases the Y_{a_r} decreases as the β parameter increases.

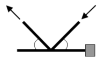
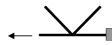
The relative error introduced using these expressions was calculated using Equation (7.12). Figure 7.10 shows the relative errors calculated for load cases 1 and 4 and the chord thicknesses $T = 16$ mm and $T = 50$ mm. It can be noticed that the relative error remains negligible, below 10% for load case 1 and below 5% for load case 4.

$$\text{rel. error}(\%) = \frac{Y(a_r/T) - Y_{(a_r/T)}(\beta, \gamma, \tau, T)}{Y(a_r/T)} \quad (7.12)$$

where,

- $Y_{(a_r/T)}(\beta, \gamma, \tau, T)$: equivalent geometry correction factor value calculated using Equations (7.10) and (7.11);
- $Y(a_r/T)$: equivalent geometry correction factor value from Table 7.2;

Table 7.2: Equivalent geometry correction value $Y(a_r/T)$ for load cases LC1 and LC4, considering joints of three different absolute sizes.

$Y(a_r/T)[-]$ Joint geometry								
	$T = 16$	$T = 20$	$T = 30$	$T = 50$	$T = 16$	$T = 20$	$T = 30$	$T = 50$
$\beta = 0.53; \gamma = 4.2; \tau = 0.4$	1.60	1.70	1.80	1.90	1.70	1.70	1.80	2.00
$\beta = 0.53; \gamma = 4.2; \tau = 0.5$	1.60	1.70	1.80	2.00	1.80	1.90	2.00	2.20
$\beta = 0.53; \gamma = 4.2; \tau = 0.6$	1.90	1.90	2.10	2.20	2.00	2.10	2.20	2.40
$\beta = 0.53; \gamma = 4.2; \tau = 0.7$	1.90	1.90	2.10	2.30	2.20	2.20	2.40	2.60
$\beta = 0.53; \gamma = 7.; \tau = 0.4$	2.30	2.40	2.60	2.80	1.40	1.50	1.60	1.70
$\beta = 0.53; \gamma = 7.; \tau = 0.5$	2.50	2.60	2.80	3.00	1.60	1.60	1.70	1.90
$\beta = 0.53; \gamma = 7.; \tau = 0.6$	2.80	2.90	3.10	3.40	1.70	1.80	1.90	2.00
$\beta = 0.53; \gamma = 7.; \tau = 0.7$	3.10	3.20	3.40	3.70	1.80	1.90	2.00	2.20
$\beta = 0.53; \gamma = 8.5; \tau = 0.4$	2.60	2.60	2.80	3.10	1.40	1.40	1.50	1.60
$\beta = 0.53; \gamma = 8.5; \tau = 0.5$	2.70	2.80	3.00	3.30	1.50	1.50	1.60	1.80
$\beta = 0.53; \gamma = 8.5; \tau = 0.6$	3.10	3.20	3.40	3.70	1.60	1.70	1.80	1.90
$\beta = 0.53; \gamma = 8.5; \tau = 0.7$	3.40	3.60	3.80	4.10	1.70	1.80	1.90	2.10
$\beta = 0.65; \gamma = 4.2; \tau = 0.4$	1.40	1.50	1.60	1.70	1.50	1.60	1.70	1.80
$\beta = 0.65; \gamma = 4.2; \tau = 0.5$	1.30	1.40	1.50	1.60	1.80	1.80	2.00	2.10
$\beta = 0.65; \gamma = 4.2; \tau = 0.6$	1.70	1.80	1.90	2.10	1.90	1.90	2.10	2.20
$\beta = 0.65; \gamma = 4.2; \tau = 0.7$	1.70	1.70	1.90	2.00	2.00	2.10	2.20	2.40
$\beta = 0.65; \gamma = 7.; \tau = 0.4$	2.20	2.30	2.40	2.60	1.30	1.40	1.50	1.60
$\beta = 0.65; \gamma = 7.; \tau = 0.5$	2.00	2.10	2.20	2.40	1.50	1.50	1.60	1.70
$\beta = 0.65; \gamma = 7.; \tau = 0.6$	2.20	2.30	2.40	2.60	1.60	1.60	1.70	1.90
$\beta = 0.65; \gamma = 7.; \tau = 0.7$	2.60	2.70	2.90	3.10	1.70	1.70	1.90	2.00
$\beta = 0.65; \gamma = 8.5; \tau = 0.4$	2.30	2.40	2.60	2.80	1.30	1.30	1.40	1.50
$\beta = 0.65; \gamma = 8.5; \tau = 0.5$	2.50	2.60	2.80	3.00	1.40	1.40	1.50	1.60
$\beta = 0.65; \gamma = 8.5; \tau = 0.6$	2.30	2.40	2.60	2.80	1.50	1.60	1.70	1.80
$\beta = 0.65; \gamma = 8.5; \tau = 0.7$	2.50	2.60	2.70	3.00	1.60	1.70	1.80	1.90
Mean	2.26	2.35	2.51	2.72	1.65	1.70	1.81	1.95
Standard Deviation	0.556	0.573	0.603	0.664	0.230	0.239	0.256	0.283

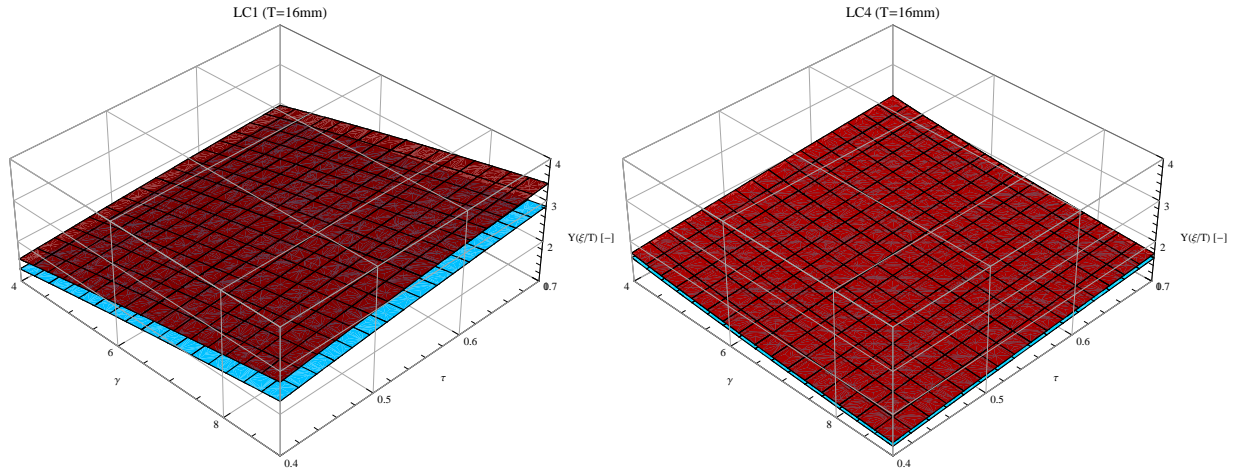


Figure 7.9: Equivalent correction factor, Y_{a_r} , for basic load cases 1 and 4, as a function of non-dimensional parameters γ and τ (Dark red surface: $\beta = 0.53$; Blue surface: $\beta = 0.63$). The absolute size corresponds to a chord thickness of $T = 16$ mm.

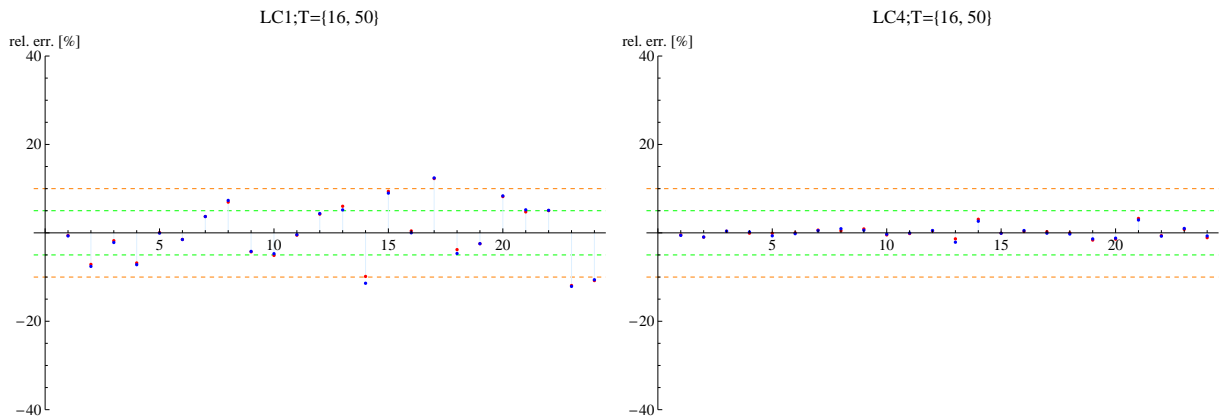


Figure 7.10: Relative error of expressions obtained from regression.

The fatigue strength size correction can be represented, expressing the results in Equations (7.10) and (7.11), as a function of the chord thickness, the non-dimensional parameters and basic load cases as follows:

$$\frac{S_{nom,LC1}(\beta, \gamma, \tau, T)}{S_{nom,LC1}(\beta_0, \gamma_0, \tau_0, T_0)} = \left(\frac{T_0}{T}\right)^{0.16} \cdot \left(\frac{\beta_0}{\beta}\right)^{-0.86} \cdot \left(\frac{\gamma_0}{\gamma}\right)^{0.70} \cdot \left(\frac{\tau_0}{\tau}\right)^{0.39} \quad (7.13)$$

$$\frac{S_{nom,LC4}(\beta, \gamma, \tau, T)}{S_{nom,LC4}(\beta_0, \gamma_0, \tau_0, T_0)} = \left(\frac{T_0}{T}\right)^{0.15} \cdot \left(\frac{\beta_0}{\beta}\right)^{-0.34} \cdot \left(\frac{\gamma_0}{\gamma}\right)^{-0.32} \cdot \left(\frac{\tau_0}{\tau}\right)^{0.44} \quad (7.14)$$

where,

- $S_{nom,LCi}(\beta, \gamma, \tau, T)$: nominal fatigue strength of the joint with geometric parameters β, γ, τ and chord thickness T for load case LCi;
- $S_{nom,LCi}(\beta_0, \gamma_0, \tau_0, T_0)$: reference fatigue strength (or reference $S_{a_r} - N$ curve) for a joint with reference geometric parameters for load case LCi;

Figure 7.11 illustrates the variation of the correction factors as a function of $\frac{T_0}{T}$, $\frac{\beta_0}{\beta}$, $\frac{\gamma_0}{\gamma}$, $\frac{\tau_0}{\tau}$ for the basic load cases LC1 and LC4.

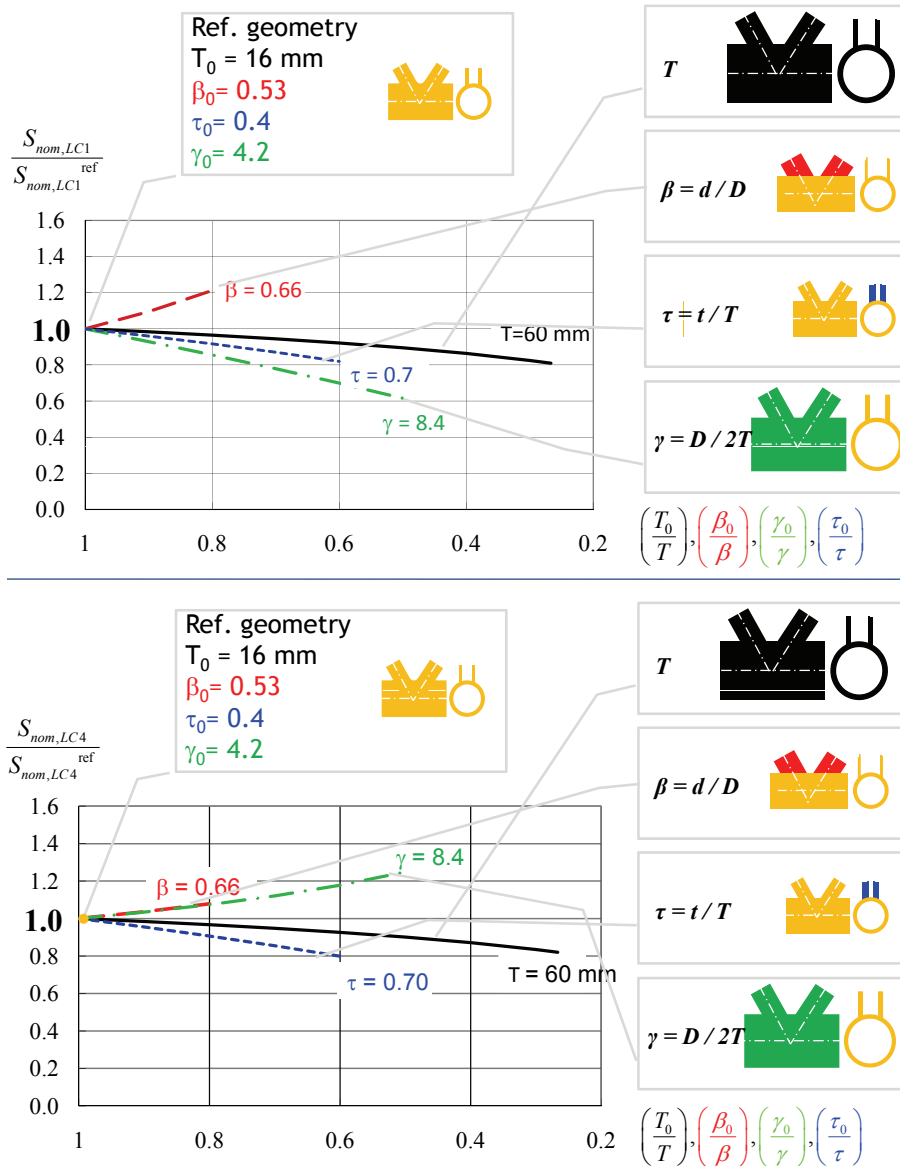


Figure 7.11: Fatigue strength size correction factor as a function of the chord thickness and the non-dimensional parameters for LC1 and LC4.

It can be observed that the thickness correction has an exponent close to the values found in 6.5.1 (0.13 and 0.14) for proportionally scaled joints. Since proportional scaling is a particular case of non-proportional scaling, Equations (7.13) can be used with $\beta = \beta_0, \gamma = \gamma_0$ and $\tau = \tau_0$.

7.3.3 Combined load case

For a load case resulting of combining the basic load cases, LC1 and LC4, the fatigue life can be calculated using Equation (6.13). Considering only superposition of basic load cases 1 and 4, it comes:

$$N = \int_{a_i}^{T/2} \frac{1}{C ((\Delta\sigma_{LC1} \cdot Y_{LC1}(a/T) + \Delta\sigma_{LC4} \cdot Y_{LC4}(a/T))\sqrt{\pi a})^m} da \quad (7.15)$$

In order to simplify the integral in Equation (7.15), it is formally not possible to apply the Second Mean Value Theorem as above and combine both basic load cases conserving the values a_r for the respective basic load cases as if they were acting alone. A different a_r would result for each combination of the basic load cases. This is not practical to use. In an attempt to use the same $S_{a_r} - N$ curve, as for the isolated basic load case, the following equation was solved for the various geometries in the parametric matrix and load cases corresponding to different $\Delta\sigma_1/\Delta\sigma_4$ ratios. The error introduced by adding $\Delta\sigma_1 \cdot Y_1(a_{r_1}/T) + \Delta\sigma_4 \cdot Y_4(a_{r_4}/T)$ (the representative depths found for individual basic load cases) was found, for each case, solving the following equation:

$$\int_{a_i}^{T/2} \frac{1}{C \left(\Delta\sigma_{LC1} \cdot Y_1(a_{r_1}/T) + \Delta\sigma_{LC4} \cdot Y_4(a_{r_4}/T) \sqrt{\pi a} \right)^m} da = (1 + Error) \times \frac{1}{C \left(\Delta\sigma_{LC1} \cdot Y_1(a_{r_1}/T) + \Delta\sigma_{LC4} \cdot Y_4(a_{r_4}/T) \right)^m} \int_{a_0}^{T/2} \frac{1}{(\sqrt{\pi a})^m} da \quad (7.16)$$

For the geometries and stress range ratios mentioned above, Figure 7.12 shows the envelope of the errors as defined in Equation (7.16). Negative values for the error are found which means that the simplified formulation gives unconservative fatigue lives. However, the simplified superposition in the form $\Delta\sigma_1 \cdot Y_1(a_{r_1}/T) + \Delta\sigma_4 \cdot Y_4(a_{r_4}/T)$ is admissible as the error, for the combined case considered as a simple superposition, remains low (less than 2%) and can be neglected.

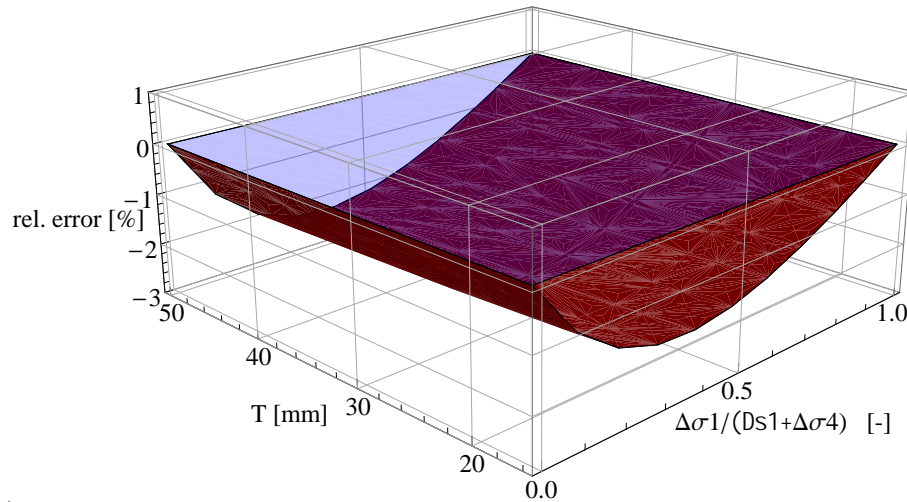


Figure 7.12: Envelope of the relative error over the parametric matrix geometries for the combined case, considering different absolute sizes (represented by the chord thickness, T) and different combination ratios $\frac{\Delta\sigma_1}{\Delta\sigma_4}$.

Since strength using nominal stress cannot be represented by a single parameter anymore, for combined load case 1 and 4, it is represented by a size correction factor given with respect to the fatigue life, N :

$$\frac{N(LC, \beta, \gamma, \tau, T)}{N(LC, \beta_0, \gamma_0, \tau_0, T_0)} = \left(\frac{1.62 \cdot \Delta\sigma_{LC1} + 1.68 \cdot \Delta\sigma_{LC4}}{1.62 \left(\frac{T_0}{T} \right)^{0.16} \left(\frac{\beta_0}{\beta} \right)^{-0.86} \left(\frac{\gamma_0}{\gamma} \right)^{0.70} \left(\frac{\tau_0}{\tau} \right)^{0.39} \Delta\sigma_{LC1} + 1.68 \left(\frac{T_0}{T} \right)^{0.15} \left(\frac{\beta_0}{\beta} \right)^{-0.34} \left(\frac{\gamma_0}{\gamma} \right)^{-0.32} \left(\frac{\tau_0}{\tau} \right)^{0.44} \Delta\sigma_{LC4}} \right)^3 \quad (7.17)$$

where,

- $N(LC, \beta, \gamma, \tau, T)$: fatigue life of the joint with geometric parameters β, γ, τ and chord thickness T for combined load case ($\Delta\sigma_{LC1} + \Delta\sigma_{LC4}$);
- $N(LC, \beta_0, \gamma_0, \tau_0, T_0)$: reference fatigue life for a joint with reference geometric parameters for combined load case ($\Delta\sigma_{LC1} + \Delta\sigma_{LC4}$);

As it can be observed, the correction factor for non-proportional sizing depends upon the different geometric parameters γ, β, τ and T but the parameters have different influences, in good agreement with the trends given in Table 5.6.

7.3.4 Validation/Example

The procedure described in the previous paragraphs was applied to the tested series S1, S2, S3 and S5. Table 7.3 shows the calculation steps needed to compute the $\Delta\sigma_{nom} \cdot Y(a_r/T)$ value and the ratios between predicted fatigue life and experimental number of cycles ($a = T/2$ in both cases). A good prediction (when speaking about fatigue lives) was found, ratios being between 0.5 and 1.53.

Figure 7.13 shows the $S_{a_r} - N$ plot of the fatigue tests carried out at ICOM and the results obtained for the geometries in the parametric matrix considering two absolute sizes (represented by chord thicknesses $T = 16$ mm and $T = 50$ mm) and three load cases (100% LC1, 50%LC1 + 50% LC4, 100% LC5).

Results for the geometries in the parametric matrix superpose with the $S_{a_r} - N$ resistance line both for isolated and combined load cases. For the experimental tests, some scatter is still present, although the points are narrower than in the $S_{r,hs} - N$ plot (see Figure 3.14). This is due to the number of random processes that may influence fatigue crack propagation but are not accounted for in the numerical models.

Table 7.4 details the parameters used to model the tested series S1, S2, S3 and S5 and case C100 from the parametric study. The effect of the eccentricity can be shown by analysing the results obtained for the tested series, with e/D ratios different from parametric geometries ($e/D = 0.23$) for instance between S5 test and C100 case. For these cases, although the main non-dimensional parameters ($\beta, \gamma,$

Table 7.3: Example of application of the procedure to the fatigue tested joints.

Series	T_i [mm]	a_{r_1} [mm]	$Y_1 \left(\frac{a_{r_1}}{T_i} \right)$ [-]	a_{r_4} [mm]	$Y_4 \left(\frac{a_{r_4}}{T_i} \right)$ [-]	$\Delta\sigma_1$ [N/mm ²]	$\Delta\sigma_4$ [N/mm ²]	$\Sigma\Delta\sigma Y \left(\frac{a_r}{T_i} \right)$ [N/mm ²]	$\frac{N_{pred.}}{N_{test}^{(a=T/2)}}$ [-]
S11	20	0.86	2.41	0.77	1.67	47.7	22.9	153.2	0.82
S12	20	0.86	2.41	0.77	1.67	48.1	22.9	154.2	0.54
S13	20	0.86	2.41	0.77	1.67	42.6	21.8	139.3	1.21
S14	20	0.86	2.41	0.77	1.67	50.6	22.5	159.6	1.03
S21	20	0.97	3.32	0.77	1.38	43.3	25.6	179.2	0.64
S22	20	0.97	3.32	0.77	1.38	42.2	25.4	175.4	0.50
S23	20	0.97	3.32	0.77	1.38	42.4	21.2	170.3	1.14
S31	12.5	0.77	3.08	0.61	1.29	50.2	37.8	203.2	0.84
S32	12.5	0.77	3.08	0.61	1.29	48.5	38.2	198.6	0.54
S33	12.5	0.77	3.08	0.61	1.29	49.6	38.9	202.6	0.59
S34	12.5	0.77	3.08	0.61	1.29	51.0	39.1	207.4	0.50
S5	20	0.70	1.23	0.79	1.89	152.0	33.3	250.5	1.53

$$\Delta\sigma \cdot Y \left(\frac{a_r}{T_i} \right) = \Delta\sigma_1 Y_1 \left(\frac{a_{r_1}}{T_i} \right) + \Delta\sigma_4 Y_4 \left(\frac{a_{r_4}}{T_i} \right)$$

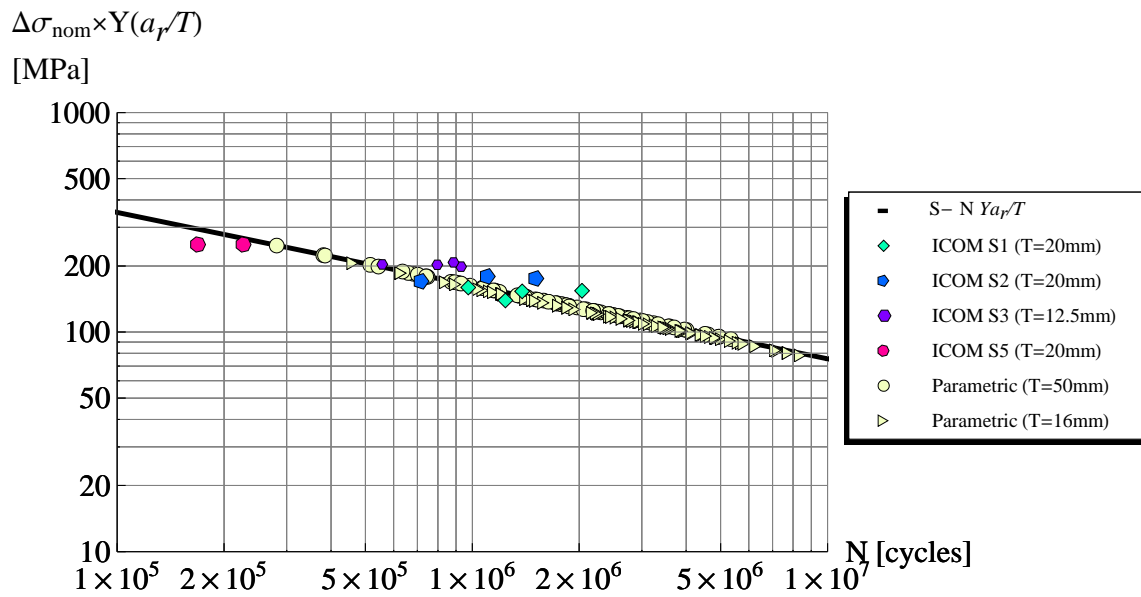


Figure 7.13: Application of the procedure described in Section 7.3.3 to fatigue tested series and geometries in parametric matrix. For the parametric table geometries two chord thicknesses ($T = 16$ mm and $T = 50$ mm) and three load cases are considered (100% LC1, 50%LC1 + 50% LC4, 100% LC5).

τ) are the same, by changing the e/D ratio, differences of about 35% for load case 1 and 10% for load case 4 are found. This highlights the importance of the eccentricity, e . Attention should be paid when using the expressions deduced in this thesis for K-joints exhibiting a different e/D ratio, as the results may vary significantly.

The Y_{a_r} approach proposed herein covers geometrical size effects due to thickness and relative tube sizes. However, uncertainties and inevitable variables influencing the fatigue behaviour include:

- ◆ Specimen preparation and fabrication;
- ◆ Location and conditions of tests (labs, set-ups, machines, procedures...);
- ◆ Type of loading: axial in the chord, braces or both, in-plane and out-of-plane bending;
- ◆ Technological size effects (welding procedure, residual stresses, etc.);

Table 7.4: Influence of the eccentricity/gap in the determination of representative crack depth $Y(a_r/T)$.

Id	geometry	e/D	W_1/t	a_{r_1}	$Y(a_{r_1}/T)$	a_{r_4}	$Y(a_{r_4}/T)$
S1	$\beta = 0.51; \gamma = 6.8; \tau = 0.63; T = 20$ mm	0.08*	1.20	0.86	2.41	0.84	1.63
S2	$\beta = 0.51; \gamma = 6.8; \tau = 0.63; T = 20$ mm	0.20*	1.20	0.97	3.32	0.79	1.48
S3	$\beta = 0.51; \gamma = 6.8; \tau = 0.63; T = 12.5$ mm	0.20*	1.20	0.77	3.08	0.62	1.37
S5	$\beta = 0.53; \gamma = 4.2; \tau = 0.40; T = 20$ mm	0.13*	1.88	0.70	1.23	0.79	1.89
C100	$\beta = 0.53; \gamma = 4.2; \tau = 0.40; T = 20$ mm	0.23	1.88	0.80	1.65	0.75	1.73

* mean values

7.4 Comparison $Y(a_r/T)$ and SCF

Figure 7.14 shows the comparison between the SCF values and $Y(a_r/T)$ values for the geometries in the parametric matrix for basic load cases 1 and 4. The SCF were obtained from interpolation of SCF tables provided by Schumacher (2003). The hypotheses made regarding the eccentricity in the current study and Schumacher's were not exactly the same (see Section 5.3.1). It can be seen that the $Y(a_r/T)$ values are generally higher than the SCF values. This may be explained by the fact that they include the stress raising due to the weld profile. Values for load case 4 seem to present some correlation while for load case 1 the scatter seems to indicate no relation between SCF and Y_{a_r} . The reason for this fact may be searched analysing Figures 7.7. For load case 4 the representative depth plot is flatter than for load case 1. It means the representative depth is more sensitive to non-dimensional parameters and might explain why for load case 4, the correlation between surface structural stress and total stress at an "almost" constant through thickness depth is more pronounced.

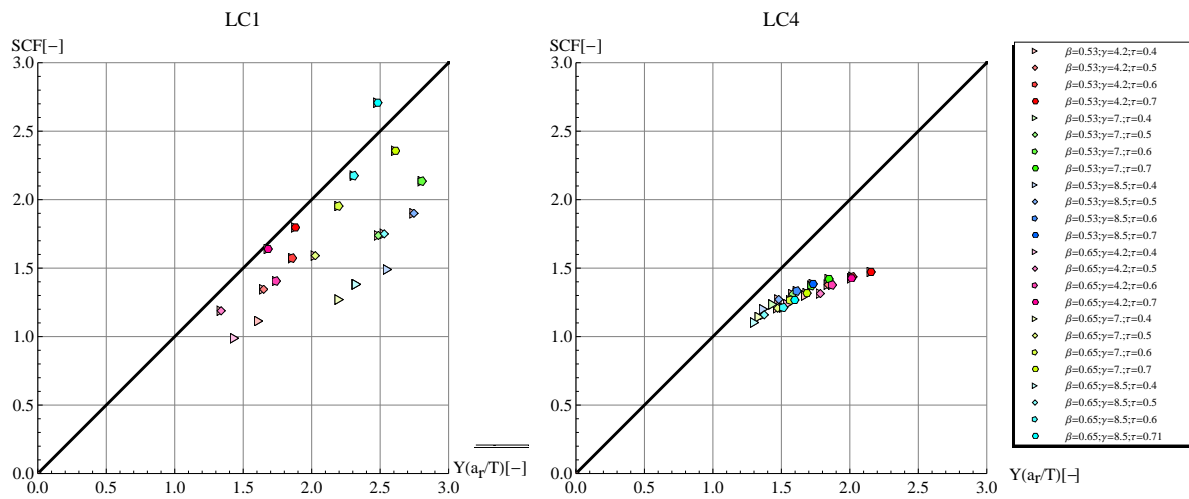


Figure 7.14: Comparison of SCF values and Y ($T = 16$ mm).

7.5 Efficiency of joint geometries

For the designer, the presentation of the size effects in terms of fatigue strength, $S_{r,nom}$, as a function of β , γ , τ does not provide immediate help regarding the choice of tubes dimensions. In fact, an increase in the chord thickness is associated with a decrease in fatigue strength of the joint. However the cross-section increases as well, and thus, the force range it can resist. It is therefore interesting to analyse these results in terms of cross-sectional area of joined elements and force range the joint would resist, ΔF (see Figure 7.15).

The joint efficiency to resist fatigue loading (force range per area of joined elements cross sectional area) depends on the load case and geometric parameters. It is higher for lower γ and τ values when the joint is under load case 1. Joint efficiency is higher for higher γ and lower τ values for load case 4. Figure 7.15 may be used to help on choosing the tubes sizes, when fatigue basic load case 1 or 4 is predominant, comparing the fatigue efficiency of different sections.

Figure 7.16 shows the force range admissible in the brace (ΔF_{LC1}) or in the chord (ΔF_{LC4}), but, this time, assuming a distribution of stresses typical to bridge truss loading ($30\% \Delta \sigma_4 + 70\% \Delta \sigma_1$). The same trends as for isolated basic load cases except for the effect of γ in the ΔF_{LC4} : for combined load case an increase of γ reduces the admissible axial force range in the chord.

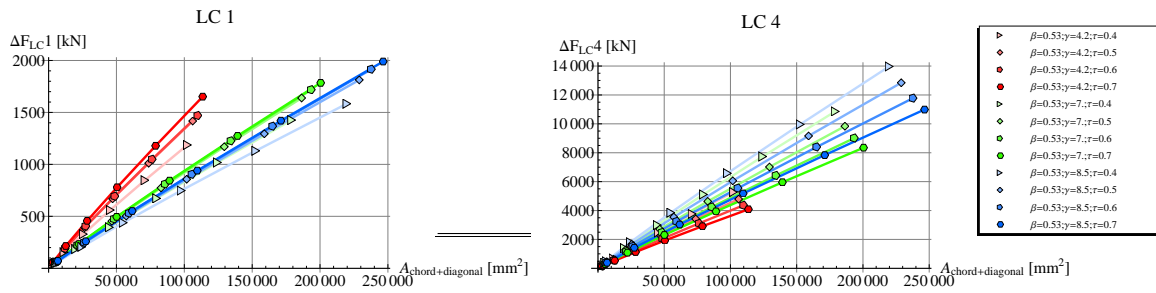


Figure 7.15: Force range the joint would resist, ΔF , against cross-sectional area of joined elements, $A_{\text{chord+diagonal}}$, considering basic load cases acting alone.

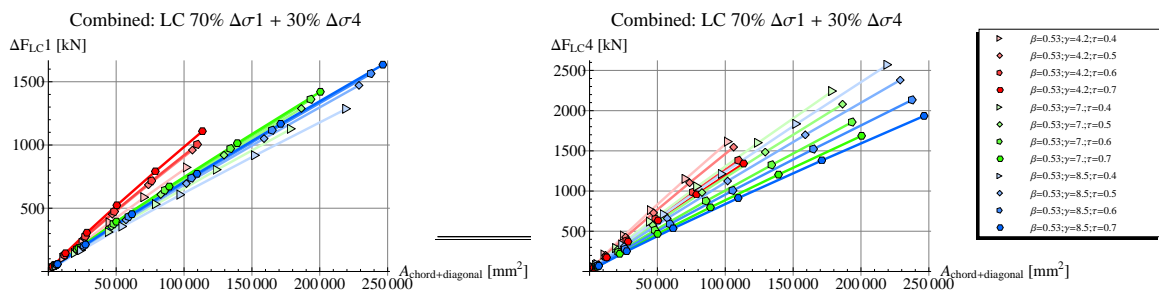


Figure 7.16: Force range the joint would resist, ΔF , against cross-sectional area of joined elements, $A_{\text{chord+diagonal}}$, considering a combined load case typical to bridge truss.

7.6 Conclusions

In this chapter, in order to uncover the non-proportional scaling effect, the parametric results were analysed focusing on the geometry correction factor, Y . Based on LFM, a representative crack depth, a_r , at which the geometry correction factor takes an equivalent through depth value Y_{a_r} was determined for each geometry in the parametric matrix. The stress range is calculated at a depth depending on the joint geometry, and load case considered. Thickness effects as well as other geometric size effects (attachment and load effects) are encapsulated in both the geometry correction factor and the representative distance at which the stress should be calculated. As a disadvantage to this method it can be pointed that the stress values can be numerically calculated but not experimentally measured through depth. An alternative approach for fatigue assessment of CHS joints is suggested based on the equivalent geometry correction factor value, Y_{a_r} . This method proposes, basically, one $S_{a_r} - N$ resistance line valid for all geometries and joint thicknesses in the parametric range. Based on the work presented in this chapter, the following conclusions are made on the following topics:

- ◆ Representative crack depth a_r :
 - ◇ Depends on the thickness, the non-dimensional parameters and load case;
 - ◇ Generally $a_r < 1$ mm and it is deeper for load case 1 than for load case 4;
 - ◇ Varies approximately with \sqrt{T} .
 - ◇ For load case 1, β and γ are the most influencing non-dimensional parameters. For load case 4, τ and β are the parameters influencing the representative crack depth the most.
 - ◇ Expressions are proposed to estimate the representative crack depth as a function of β , γ , τ , T . They are valid within the parametric matrix limits defined in section 5.2;
- ◆ Equivalent geometry correction factor values, Y_{a_r}

- ◇ Depends on T at a great extent (exponent of about 0.15 similar for both load cases 1 and 4);
 - ◇ Depends also on β, γ, τ parameters;
 - ◇ Formulas to compute the equivalent geometry correction factor are proposed - valid within the parametric limits;
 - ◇ Attention should be paid to the importance of the eccentricity. The blind use of formulas for the same tube dimensions but different joint eccentricities can lead to bad estimations, this being dependent on the acting load case;
 - ◇ Compared to SCF values, $Y(a_r/T)$ values are generally higher for the same geometry. This would be expected since the $Y(a_r/T)$ includes not only the structural stress but also the stress peak due to the weld profile. It seems to exist a correlation between SCF and Y_{a_r} values, at least for basic load case 4;
 - ◇ Two expressions, describing the equivalent correction factor values, for the geometries in the parametric range as a function of the non-dimensional parameters and chord thickness are proposed for load case 1 and 4. More parametric studies are needed, specially to include the effect of joint eccentricity and thus provide a more general expression.
- ◆ Equivalent geometry correction factor method:
 - ◇ Approach accounts for the thickness, attachment and load effects;
 - ◇ Applicable for basic and combined load cases;
 - ◇ Single $S_{a_r} - N$ is needed;
 - ◇ Provided a good estimation of fatigue life for the fatigue tests on CHS K-joints carried out at ICOM.
 - ◇ Extensive validation using fatigue tests is needed before it can be safely used in design practice and establish design factors.
 - ◇ The use of the proposed method is extensible to other welded details. Its application requires the knowledge of the equivalent geometry correction factor, $Y(a_r/T)$, or the geometry correction factor function, Y ;
 - ◇ Size correction factors, function of β, γ, τ, T , were determined for basic load cases (in terms of fatigue strength, see Equations (7.13) and (7.14)) and for combined load case (in terms of fatigue life, see Equation (7.17));
 - ◆ Efficiency of the joint geometry
 - ◇ Joint geometry efficiency is higher for lower γ and τ values for load case 1.
 - ◇ Joint geometry efficiency is higher for higher γ and lower τ values for load case 4.

Summary, conclusions and future work

This chapter summarises the work outlined in the previous chapters and presents the main conclusions as a synthesis of the conclusions found at the end of each chapter. In the course of this research work, scientific issues were raised that could not be resolved. The most important ones are presented here as recommendations for future work.

8.1 Summary

At the experimental level, two large-scale S355 steel trusses made of welded CHS were tested. These fatigue tests were aimed at augmenting the existing database and follow the investigation previously carried out at ICOM on proportionally scaled joints. As a novelty, an Alternating Current Potential Drop (ACPD) system was used to monitor the fatigue crack growth in a large scale truss specimen and thus to allow for more thorough numerical model validation.

At the analytical level, a numerical model was developed to simulate fatigue crack propagation. The isolated K-joint geometry was modelled using BEM Beasy software. Weld profiles were realistically modelled and the possibility to introduce an initial surface crack at hot-spot locations 1 and 11 was implemented. The crack propagation was simulated in a step wise way by incrementally increasing the crack size.

Non-dimensional geometrical parameters and different absolute sizes, typical to bridge designs but currently not covered by static and fatigue design specifications, were studied in a parametric study. The main parameters of interest in this investigation were: the brace-to-chord diameter ratio (β), the chord slenderness (γ), thickness ratio (τ) and chord thickness (T). A number of assumptions regarding other parameters and dimensions were made in order to define a standard geometry and to ensure uniformity in the models created for the parametric study. A preliminary study was carried out to qualitatively investigate the effect of eccentricity (e), chord length (L_{ch}), truss height (H), weld size (W), crack shape (a/c) and crack angle (ϕ_{crack}). Results of the parametric study were discussed in terms of stress intensity factor at different crack depths and in terms of fatigue strength.

Parametric study results were then used to determine the geometry correction factor, Y , as a function of the relative crack depth, a/T , for the different geometries and main basic load cases under investigation. This geometry correction factor is common to a set of homothetic joints and was used to investigate how proportional scaling of a joint can affect its fatigue behaviour - that is to evaluate what is commonly known as the thickness effect. As the result of this analysis, thickness correction factors were determined for the geometries in the parametric matrix.

Non-proportional scaling is often the dominant scenario for tubular bridge applications. This occurs when the members' relative dimensions change with respect to one another. A new approach to assess

fatigue behaviour of non-proportionally scaled tubular joints was proposed. It is based on Linear Elastic Fracture Mechanics (LEFM) and makes use of the geometry correction factor, Y , that accounts for geometric size effects. According to this approach, there is, for each geometry and load case, a representative crack depth, a_r , at which the geometry correction factor function equals a through thickness equivalent value. This equivalent value can be correlated to fatigue life using a specific $S_{a_r} - N$ resistance line, valid for thicknesses in the range of 16 mm to 60 mm. The chord thickness as well as other geometric and loading parameters effects are encapsulated in the geometry correction factor, Y , calculated at the representative crack depth, $Y(a_r/T)$. Based on this approach, it is shown that size correction factors, for main basic load cases (balanced axial load in the braces: LC1, or axial load in the chord: LC4), can be expressed as a function of the chord thickness, and the non-dimensional parameters defining the joint geometry.

8.2 Conclusions

The main goals of this thesis work were to understand the fatigue behaviour of as-welded CHS K-joints and clarify the geometrical size effects involved. Other principal objectives are listed in Section 1.4. The most significant conclusion of this investigation regarding the understanding of size effects is that the fatigue behaviour of welded tubular joints is highly influenced by the members dimensions, not only by the failing member wall thickness, and the applied load cases. It is shown that a size correction factor describing these influences can be found for the principal basic load cases, and for a load case resultant of combining these. Simultaneously, a new local stress approach, deduced using LEFM, is proposed in order to predict the fatigue life of welded tubular K-joints made out of CHS, taking into account both the joint geometry and the loading scenario. The other main conclusions include:

- ◆ Terms and parameters associated with size effects have been clearly defined (see Section 2.6.1);
- ◆ The range of applicability of current fatigue specifications is limited and does not cover geometries typical to tubular bridge design. There is a lack of data for joint thicknesses common to bridge applications and scatter in the data related to the inclusion of many different parameters;
- ◆ ACPD (Alternative Current Potential Drop) measuring system can be applied on a large-scale tubular truss beam with multiple current paths;
- ◆ Fatigue tests confirm that welded tubular joints show crack propagation mainly because of initial weld toe defects. Crack initiation accounted for only approximately 10% of the fatigue life;
- ◆ High tensile welding residual stresses are present within the tubular joints. With regard to the influence of welding residual stresses, fatigue cracks were observed both at hot-spot 1 of joints with the chord in tension as well as at hot-spot 1c of joints with the chord in compression;
- ◆ Results from the numerical model compare well with the experimental measurements (nominal strains, hot-spot strains and stress intensity factors), thus giving a good estimation of the fatigue life of the joints;
- ◆ When proportional scaling is done, the thickness correction factor remains the same regardless of whether it is based on nominal or hot-spot stress (as the SCF remains the same for homothetic joints);
- ◆ The thickness correction factor exponent (accounting for proportional scaling), can be expressed using the classical form for plates $\left(\frac{T_{ref}}{T}\right)^n$. The exponent values (n) found from the parametric study vary from 0.12 to 0.14, when referring to fatigue strength, and 0.37 to 0.43 when referring to fatigue life, for the basic load cases LC1 and LC4 respectively;
- ◆ Advantages of the LEFM equivalent geometry correction factor value method include:

- ◊ Accounts for the thickness, the non-dimensional parameters and the load effects.
 - ◊ Applicable for basic and combined load cases.
 - ◊ Single $S_{a_r} - N$ line is able to account for thickness, attached tubes and load effects.
 - ◊ Provides a good estimation of fatigue life for the fatigue tests on CHS K-joints carried out at ICOM.
 - ◊ Can be generalised to other welded details. However, its application requires the knowledge of the geometry correction factor in the form of a function.
- ◆ Two functions describing the size effect correction factors are proposed for load cases LC1 and LC4. These are valid for the geometries within the parametric range and are expressed as functions of the non-dimensional parameters and chord thickness. The effect of joint eccentricity is not included and thus the expressions do not have a general applicability.
 - ◆ The size effect (non-proportional scaling) correction factors:
 - ◊ Depend on chord thickness, T , at a great extent (exponent of about 0.15 similar for both load cases LC1 and LC4).
 - ◊ Were shown to also depend on β, γ, τ parameters.
 - ◆ Attention should be paid to the importance of the eccentricity. The blind use of formulas for the same tube dimensions but different joint eccentricities can lead to bad estimations, this being dependent on the acting load case.
 - ◆ The efficiency of the joint geometry:
 - ◊ Is higher for lower γ and τ values under load case LC1.
 - ◊ Is higher for higher γ and lower τ values under load case LC4.
 - ◊ For a load scenario typical to bridge truss loading ($30\%\Delta\sigma_4 + 70\%\Delta\sigma_1$), the same trends as for isolated basic load cases exist, except that an increase in γ reduces the admissible axial force range in the chord.

8.3 Future work

The current investigation scope is limited to non-overlapping welded K-joints made out of CHS. A natural and valuable follow-up of this thesis would be to extend the domain of validity of these results to different joint types and geometries. In particular, it would be of interest to study the behaviour of multi-planar KK-joints. Another specific aspect that was briefly discussed and requires further work, is the effect of joint eccentricity. The joint eccentricity should be included in future parametric studies in order to find expressions of general applicability.

In Section 7, the basis for a new method to assess fatigue life of tubular joints are presented. More validation work and broad discussions are needed in order to include it in recommendations for the fatigue design of tubular joints.

A future step related to the work presented here is the study of post-weld improvement techniques and how these affect the size effect findings for as-welded joints. This requires the inclusion of residual stresses (tension resulting from welding and compression from post-weld treatment) in the numerical modelling. This step is necessary to better simulate crack growth under different stress ratios and under variable amplitude loading.

The inclusion of post-weld improvement implies, simultaneously, that the model becomes much more complex. In fact, as the crack initiation period becomes non-negligible and cracks are more likely to initiate at other joint locations along the weld toe/root (whose resistances were not improved).

A probabilistic study that includes multiple crack sites, which simulates both crack initiation and crack propagation, as well as the uncertainties involved in residual stresses and technological size effects, is desirable. It would allow to establish the reliability of welded K-joints of different sizes under different loadings. This effort will be a major step towards efficient design of tubular bridges and make them truly economically competitive.

Appendices

Appendix

A

Fatigue tests instrumentation

A.1 Map of gages - S5-1

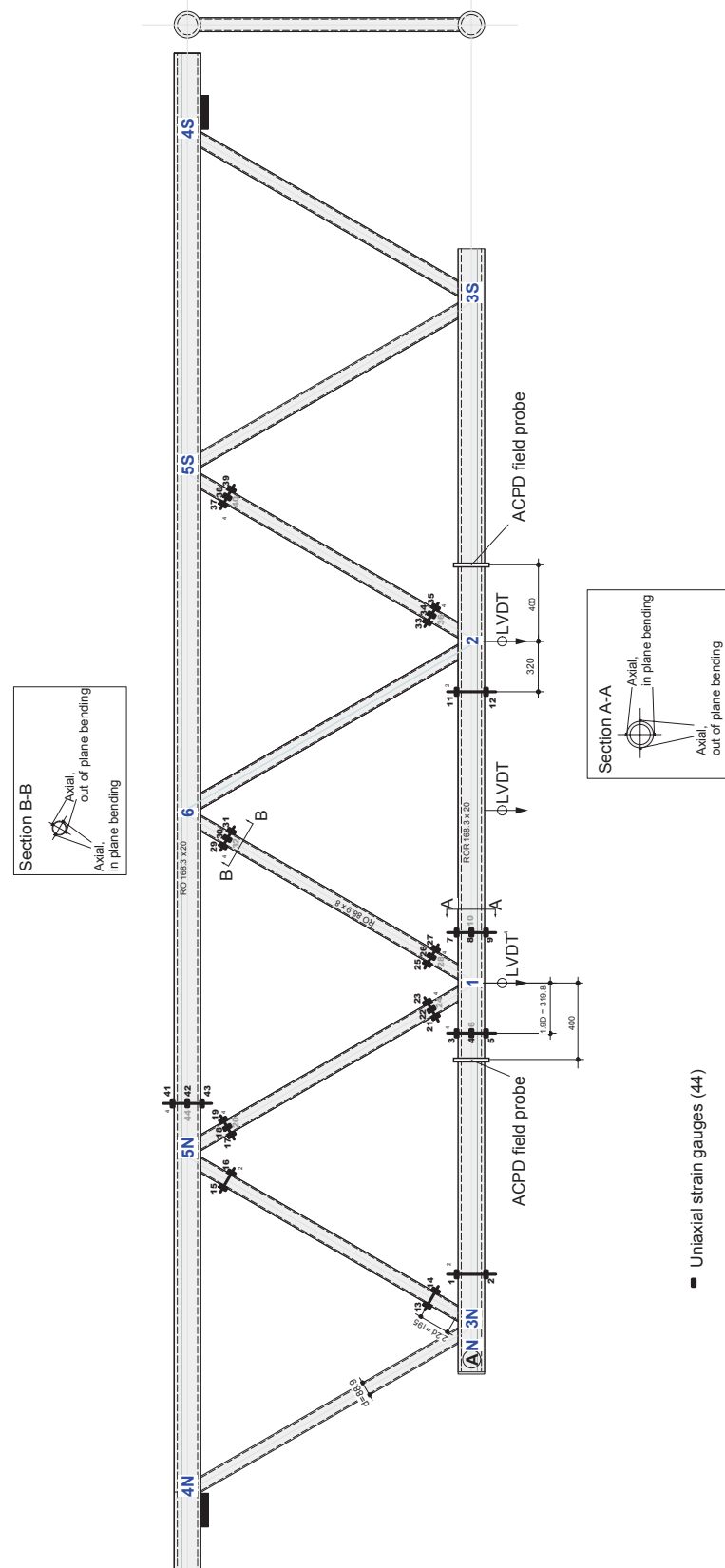
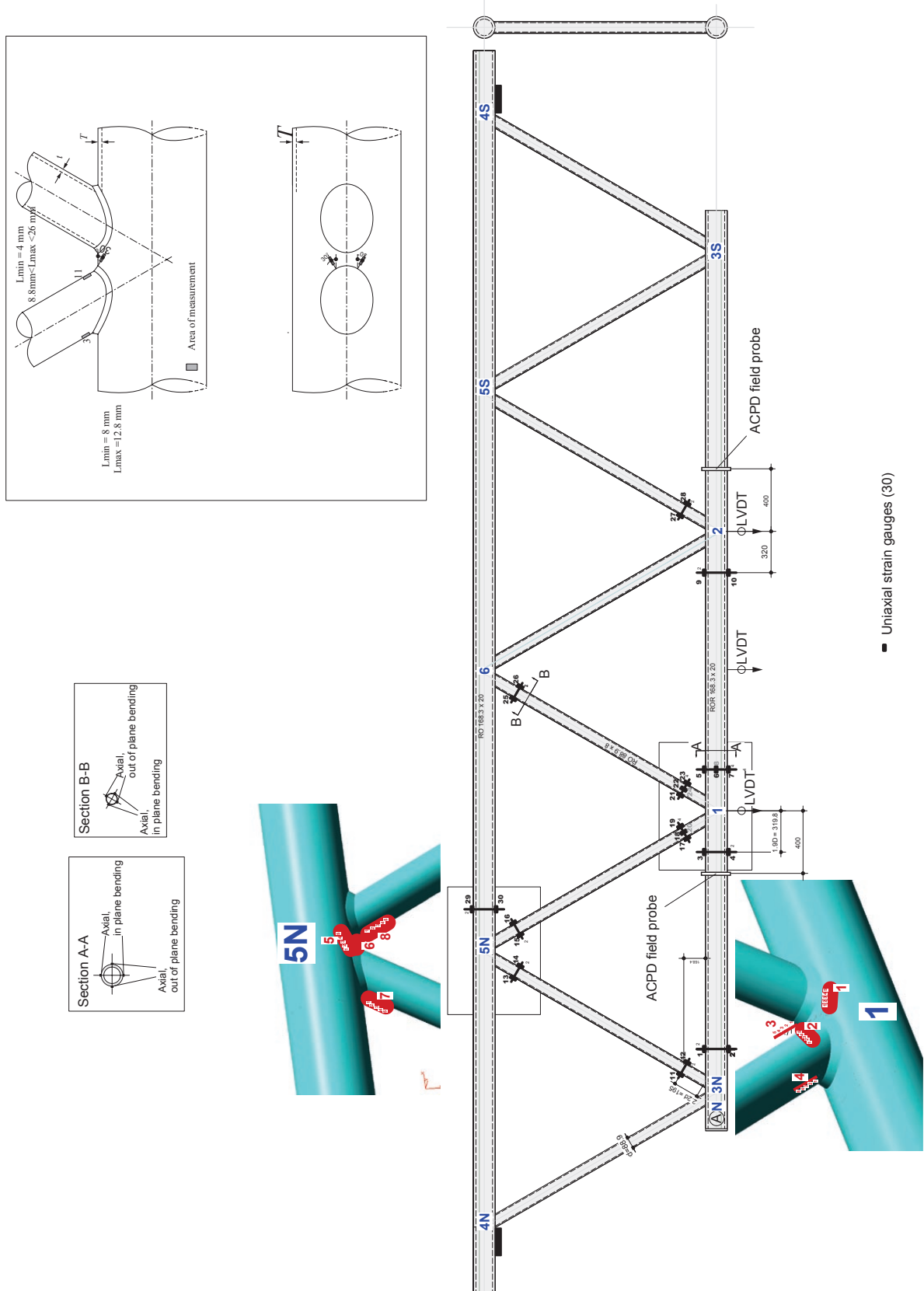


Figure A.1: Tubular truss strain gages and displacement transducers map (S5-1).

A.2 Map of gages - S5-2



■ Uniaxial strain gauges (30)

Figure A.2: Tubular truss strain gages and displacement transducers map (S5-2).

A.3 Metallography procedure

The following protocol was used (Labat, 2007):

- ◆ Cutting of the specimen: area near the weld toe;
- ◆ Section to look in detail: longitudinal symmetry plan;
- ◆ Specimen polishing (mirror polishing): using sand paper with decreasing granulometry (250-500-1000-2400 grains per *inch*²) and then with diamond powder (6 μm -1 μm)
- ◆ Nital etching (acid nitric 2% - ethanol): attack for 10 sec and then neutralization by washing with ethanol;
- ◆ Naked eye and microscopic observation up to 50 \times (see Figure 3.25);

Appendix

B

Fatigue tests results

B.1 Simplified bar model

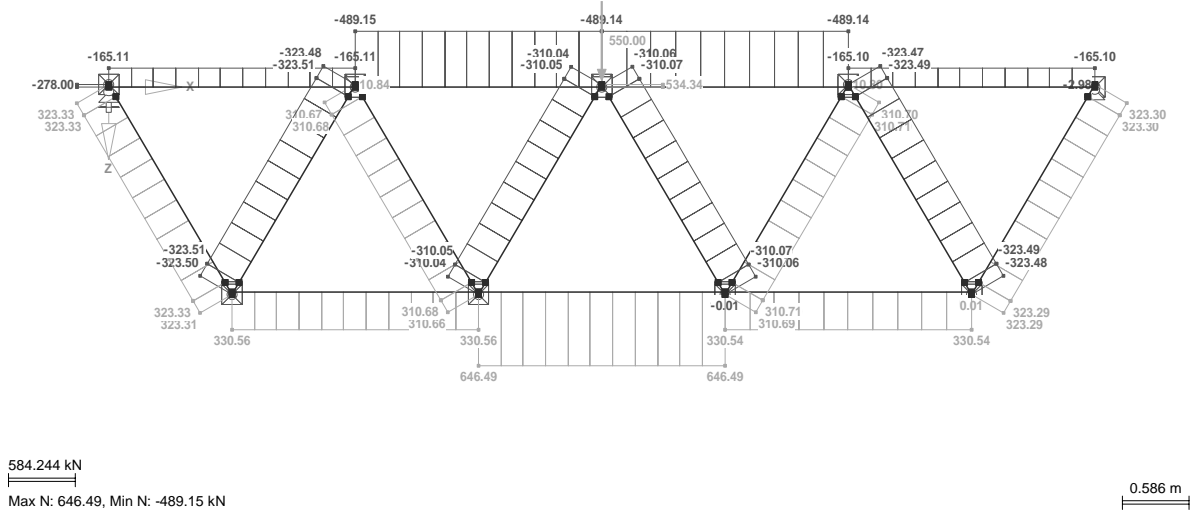


Figure B.1: Simplified bar model - Axial force.

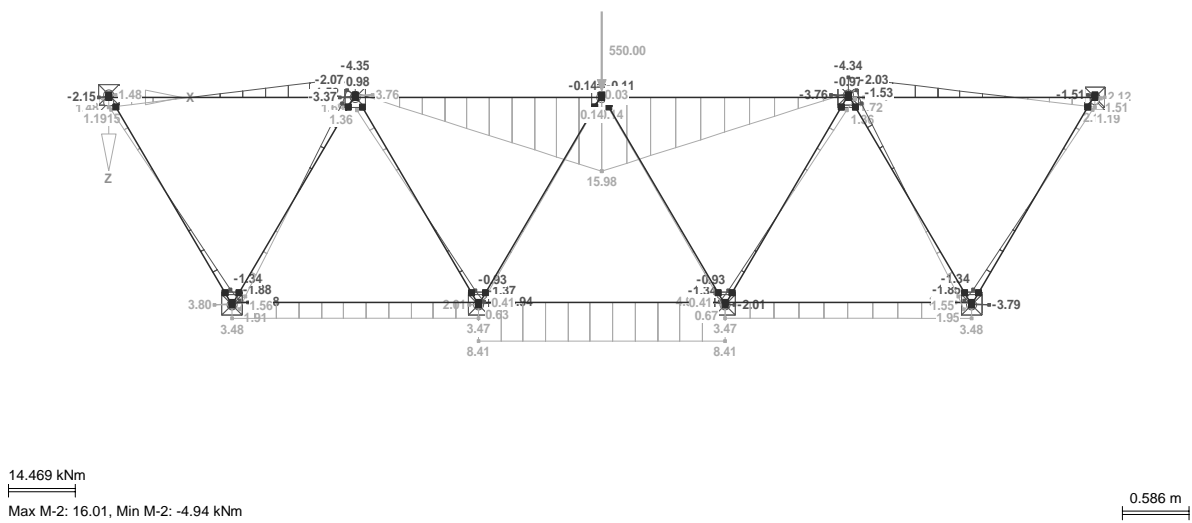
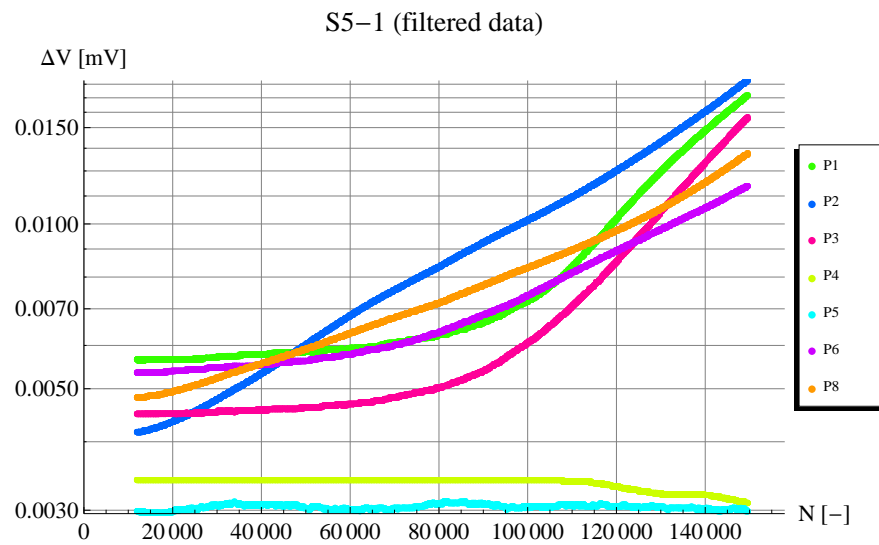
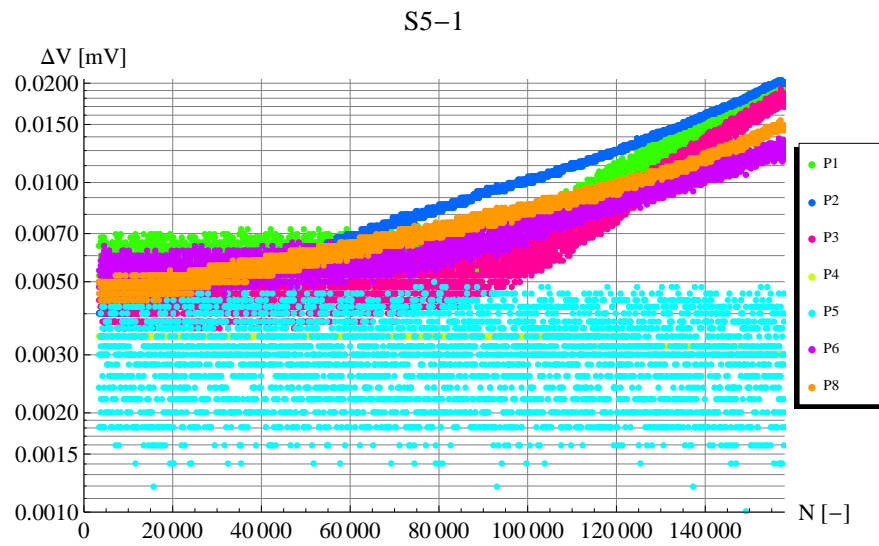


Figure B.2: Simplified bar model - Bending moment.

B.2 ACPD results

B.2.1 ACPD results



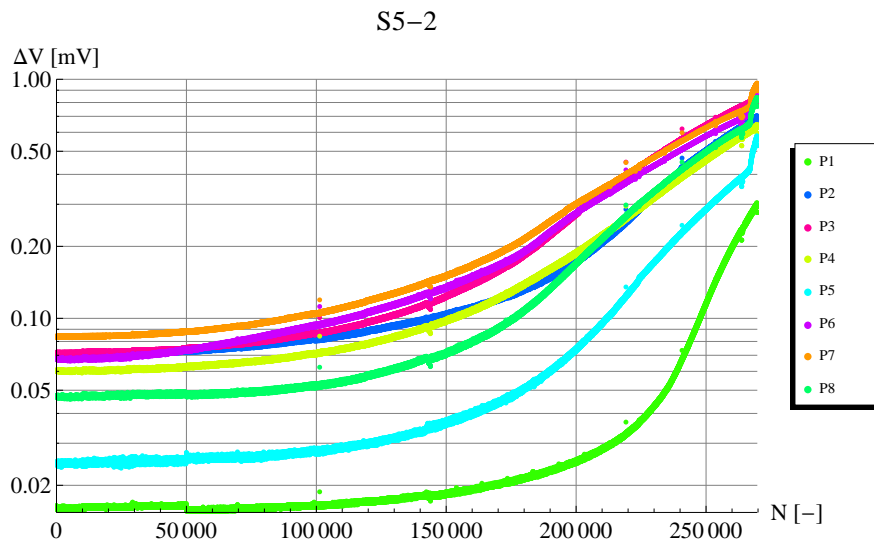


Figure B.5: ACPD results, S5-2, unfiltered.

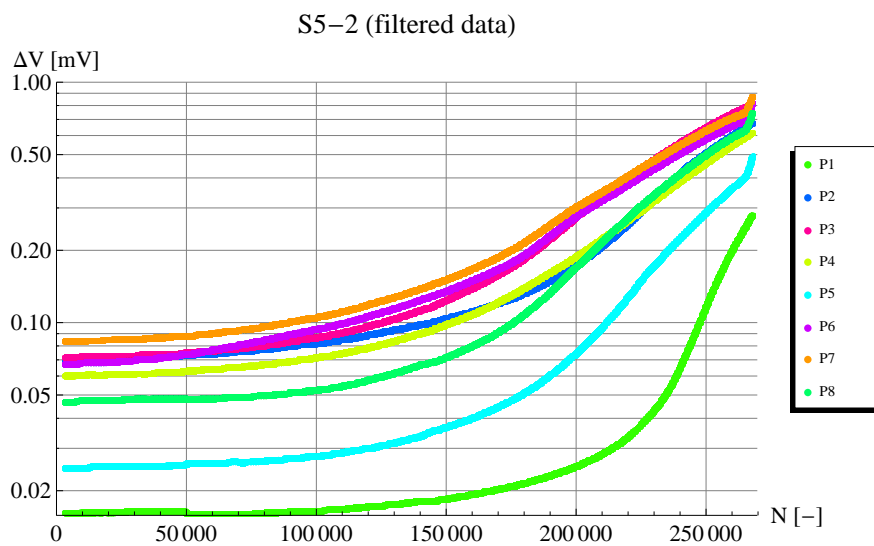


Figure B.6: ACPD results, S5-2, filtered.

B.2.2 ACPD results - Crack depth against number of cycles

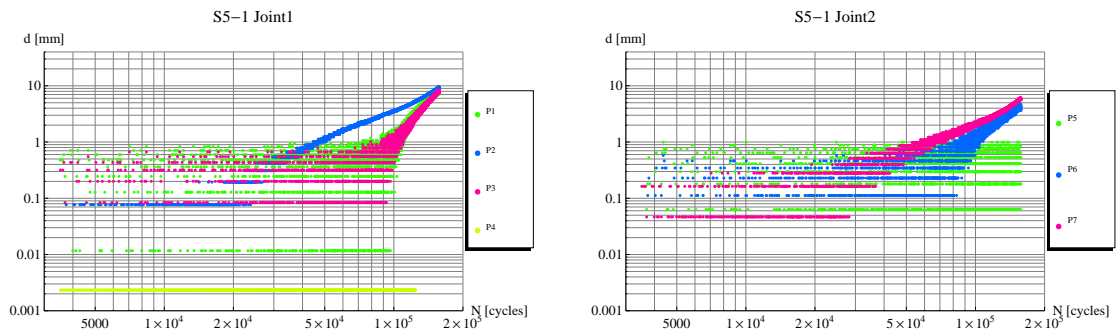


Figure B.7: Number of cycles vs. crack depth at probe location for series S5-1 joints.

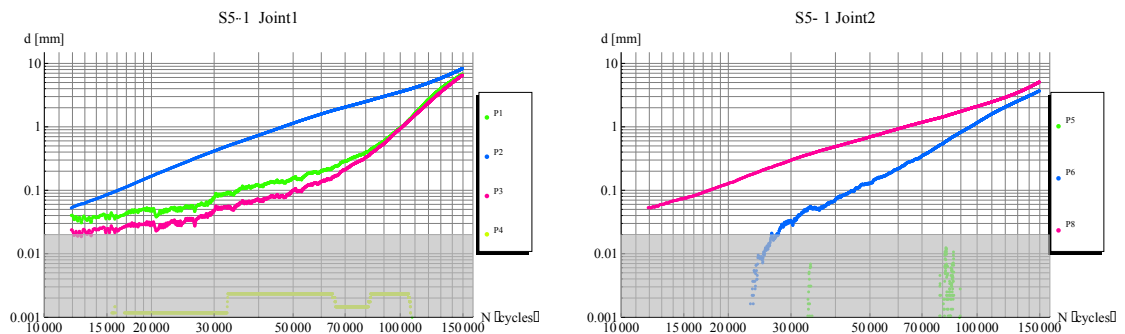


Figure B.8: Number of cycles vs. crack depth at probe location for series S5-1 joints - using filtered results.

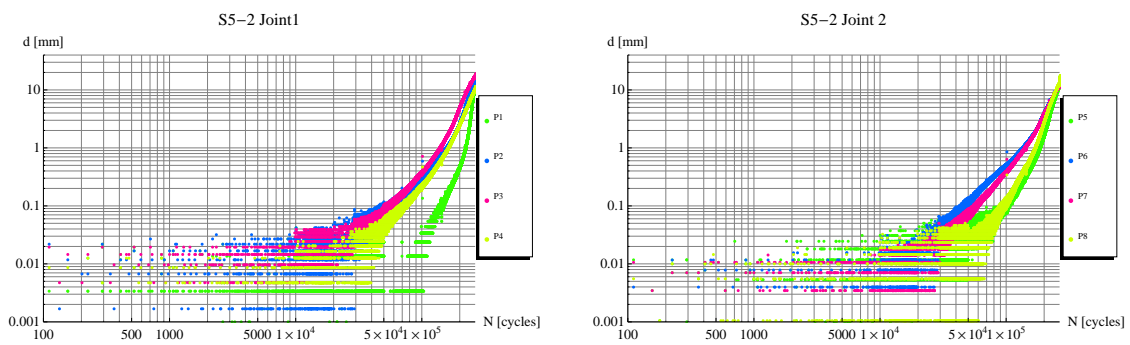


Figure B.9: Number of cycles vs. crack depth at probe location for series S5-2 joints.

B.2.3 ACPD results - Crack growth against number of cycles

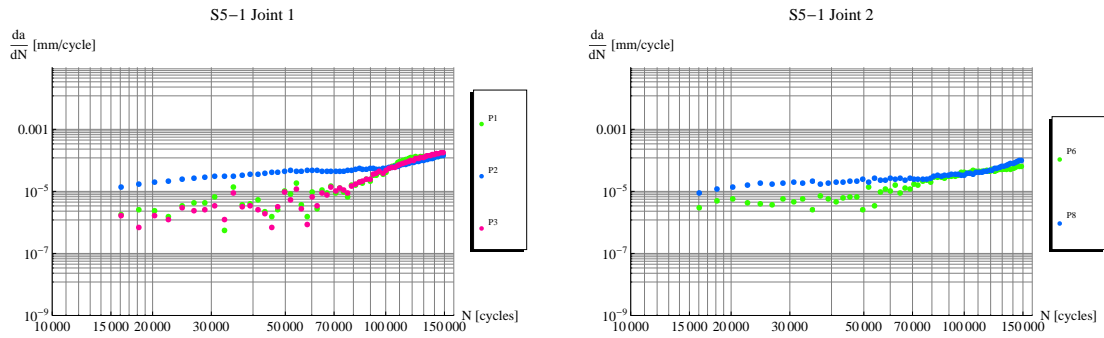


Figure B.10: Crack growth rate vs. number of cycles - S5-1.

B.2.4 ACPD results - SIF against number of cycles

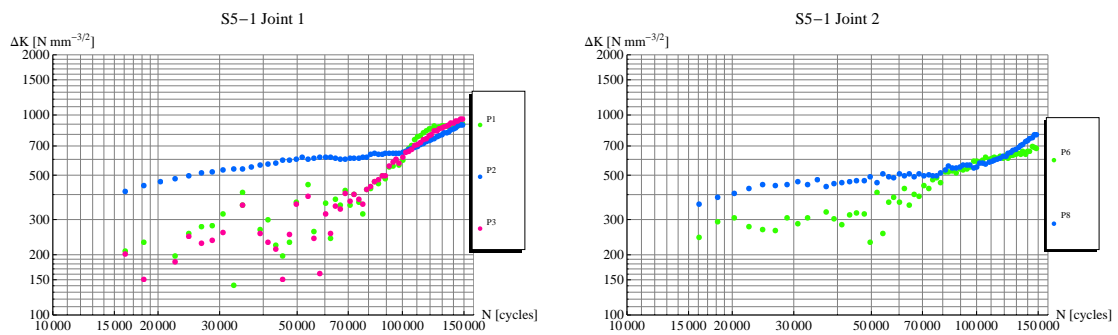


Figure B.11: Stress intensity factors vs. number of cycles.

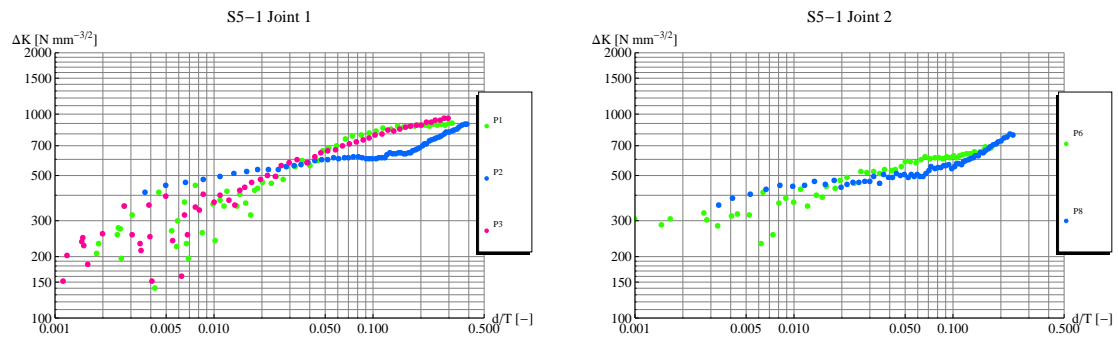
B.2.5 ACPD results - Crack growth against number of cycles

Figure B.12: Stress intensity factor range ΔK vs. relative thickness (d/T).

Numerical model

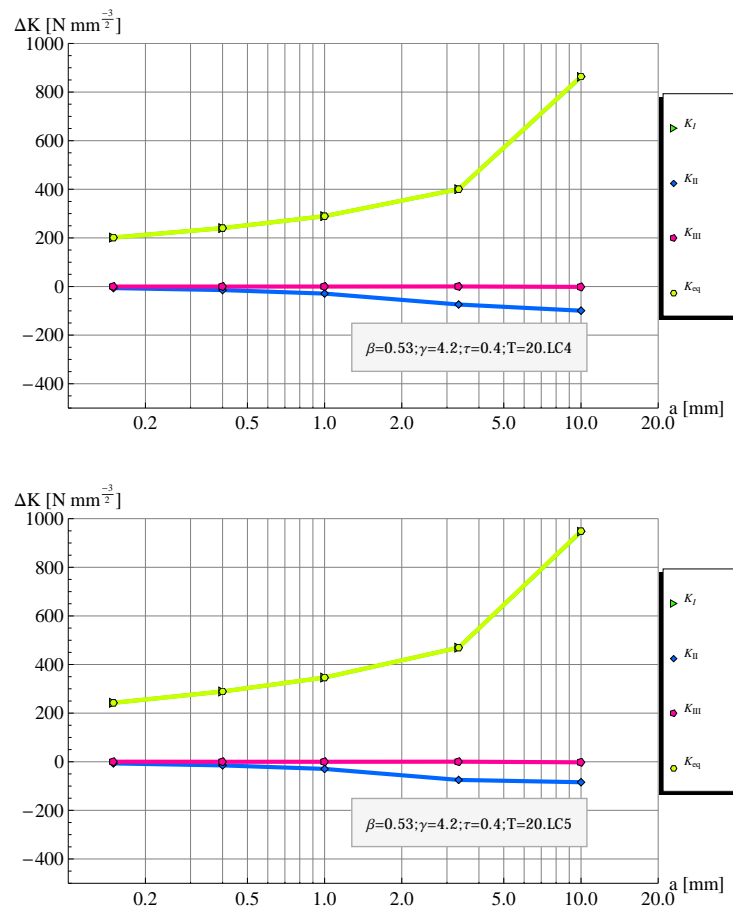


Figure C.1: Comparison of the ΔK for the three different crack opening modes for load cases 4 and 5 ($\Delta\sigma_{nom} = 100$ MPa, $\beta = 0.53$; $\gamma = 4.2$; $\tau = 0.4$; $T = 20$ mm).

Looking at the amplified deformation of the joint (Load case 1), one can identify the different potential crack sites.

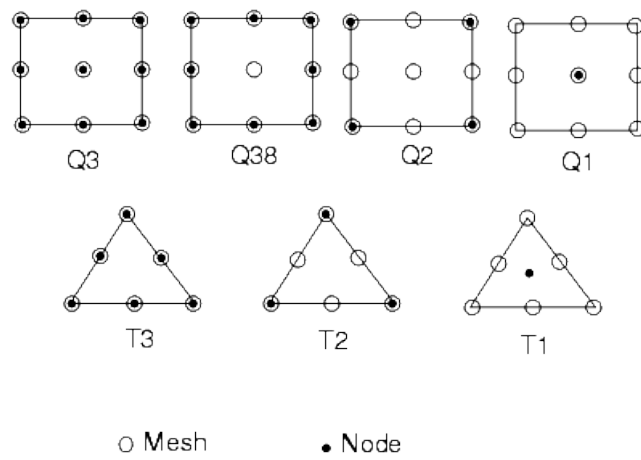


Figure C.2: Available boundary elements in BEASY (from BEASY (2003)).

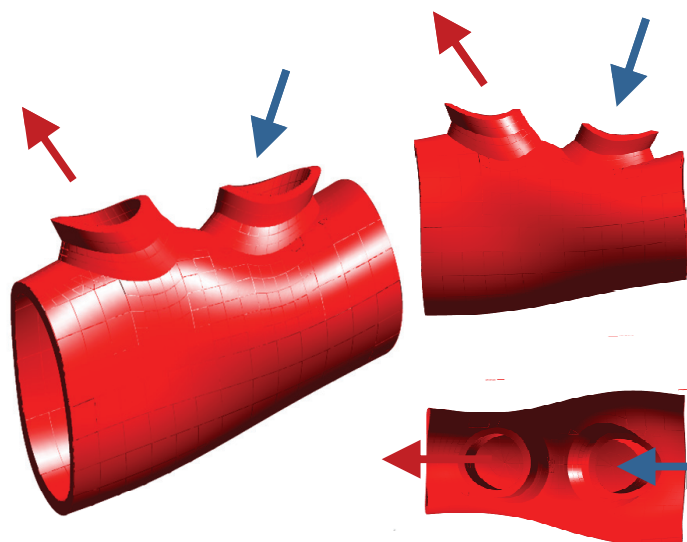


Figure C.3: Joint deformation mode (Load case 1).

D**Parametric study****D.1 Parametric table****Table D.1:** Parametric cases ID.

τ	β					
	0.53			0.65		
	4.2	γ 7	8.5	4.2	γ 7	8.5
0.4	180, 169, 181, 168	109, 132	113, 136	117, 140	143, 183	125, 147
0.5	129, 178, 106	110, 133, 179	114, 137	171, 172	122, 144	126, 148
0.6	107, 130	111, 134	115, 138	119, 142	123, 145	127, 149
0.7	108, 131	112, 135	116, 139	120, 170	124, 146	150, 184

Table D.2: Parametric table.

Parametric table																		
ID	D	T	d	t	e	θ	β	γ	τ	α	ζ	g	e/D	L_{ch}	H	W1	W2	W3
	[mm]	[mm]	[mm]	[mm]	[mm]	-	-	-	-	-	-	[mm]	-	[mm]	[mm]	[mm]	[mm]	[mm]
C87	168.3	10.0	88.9	7.0	22.0	60	0.53	8.42	0.70	25.80	12	19.9	0.13	2167.0	1800.0	9.5	6.3	3.2
C88	168.3	20.0	88.9	8.0	22.0	60	0.53	4.21	0.40	25.70	12	19.9	0.13	2166.0	1800.0	15.0	10.0	5.0
C89	168.3	20.0	88.9	8.0	38.0	60	0.53	4.21	0.40	25.70	23	38.4	0.23	2166.0	1800.0	15.0	10.0	5.0
C90	84.2	10.0	44.5	4.0	19.0	60	0.53	4.21	0.40	25.70	23	19.2	0.23	1083.0	900.0	7.5	5.0	2.5
C91	336.6	40.0	177.8	16.0	76.0	60	0.53	4.21	0.40	25.70	23	76.8	0.23	4332.0	3600.0	30.0	20.0	10.0
C92	504.9	60.0	266.7	24.0	114.0	60	0.53	4.21	0.40	25.70	23	115.2	0.23	6498.0	5400.0	45.0	30.0	15.0
C93	252.5	30.0	133.4	12.0	57.0	60	0.53	4.21	0.40	25.70	23	57.6	0.23	3249.0	2700.0	22.5	15.0	7.5
C94	168.3	10.0	88.9	4.0	38.0	60	0.53	8.42	0.40	25.70	23	38.4	0.23	2166.0	1800.0	9.5	6.3	3.2
C95	168.3	10.0	88.9	5.0	38.0	60	0.53	8.42	0.50	25.70	23	38.4	0.23	2166.0	1800.0	9.5	6.3	3.2
C96	168.3	10.0	88.9	7.0	38.0	60	0.53	8.42	0.70	25.70	23	38.4	0.23	2166.0	1800.0	9.5	6.3	3.2
C97	169.3	10.0	88.9	8.0	38.0	60	0.53	8.47	0.80	25.60	23	39.	0.22	2166.0	1801.0	9.5	6.3	3.2
C98	84.2	10.0	44.5	4.0	19.0	60	0.53	4.21	0.40	25.70	23	19.2	0.23	1083.0	900.0	7.5	5.0	2.5
C99	168.3	20.0	88.9	8.0	38.0	60	0.53	4.21	0.40	25.70	23	38.4	0.23	2166.0	1800.0	15.0	10.0	5.0
C100	168.3	20.0	88.9	8.0	38.0	60	0.53	4.21	0.40	25.70	23	38.4	0.23	2166.0	1800.0	15.0	10.0	5.0
C101	168.3	20.0	88.9	8.0	22.0	60	0.53	4.21	0.40	25.70	12	19.9	0.13	2166.0	1800.0	15.0	10.0	5.0
C102	336.6	40.0	215.0	28.0	120.0	60	0.64	4.21	0.70	25.70	25	84.6	0.36	4332.0	3600.0	52.5	35.0	17.5
C103	508.0	60.0	325.0	42.0	180.0	60	0.64	4.23	0.70	25.20	25	125.9	0.35	6400.0	5000.0	78.8	52.5	26.3
C104	168.3	20.0	108.0	14.0	60.0	60	0.64	4.21	0.70	25.70	25	41.7	0.36	2166.0	1800.0	26.3	17.5	8.8
C105	273.0	32.0	175.0	22.5	98.0	60	0.64	4.27	0.70	25.60	25	68.7	0.36	3500.0	2900.0	42.3	28.2	14.1
C106	504.9	60.0	266.7	30.0	116.1	60	0.53	4.21	0.50	25.70	23	117.6	0.23	6488.0	5406.6	56.4	37.6	18.8
C107	504.9	60.0	266.7	36.0	116.1	60	0.53	4.21	0.60	25.70	23	117.6	0.23	6488.0	5406.6	67.7	45.1	22.6
C108	504.9	60.0	266.7	42.0	116.1	60	0.53	4.21	0.70	25.70	23	117.6	0.23	6488.0	5406.6	79.0	52.6	26.3
C109	504.9	36.0	266.7	14.5	116.1	60	0.53	7.01	0.40	25.70	23	117.6	0.23	6488.0	5406.6	27.3	18.2	9.1
C110	504.9	36.0	266.7	18.0	116.1	60	0.53	7.01	0.50	25.70	23	117.6	0.23	6488.0	5406.6	33.8	22.6	11.3

... continued

ID	D	T	d	t	e	θ	β	γ	τ	α	ζ	g	e/D	L_{ch}	H	W1	W2	W3
C111	504.9	36.0	266.7	21.5	116.1	60	0.53	7.01	0.60	25.70	23117.6		0.23	6488.0	5406.6	40.4	26.9	13.5
C112	504.9	36.0	266.7	25.3	116.1	60	0.53	7.01	0.70	25.70	23117.6		0.23	6488.0	5406.6	47.6	31.7	15.9
C113	504.9	29.7	266.7	12.0	116.1	60	0.53	8.50	0.40	25.70	23117.6		0.23	6488.0	5406.6	22.6	15.0	7.5
C114	504.9	29.7	266.7	14.8	116.1	60	0.53	8.50	0.50	25.70	23117.6		0.23	6488.0	5406.6	27.8	18.5	9.3
C115	504.9	29.7	266.7	17.9	116.1	60	0.53	8.50	0.60	25.70	23117.6		0.23	6488.0	5406.6	33.7	22.4	11.2
C116	504.9	29.7	266.7	20.7	116.1	60	0.53	8.50	0.70	25.70	23117.6		0.23	6488.0	5406.6	38.9	25.9	13.0
C117	504.9	60.0	330.0	24.0	180.0	60	0.65	4.21	0.40	25.70	23118.3		0.36	6488.0	5406.6	45.1	30.1	15.0
C118	504.9	60.0	330.0	30.0	180.0	60	0.65	4.21	0.50	25.70	23118.3		0.36	6488.0	5406.6	56.4	37.6	18.8
C119	504.9	60.0	330.0	36.0	180.0	60	0.65	4.21	0.60	25.70	23118.3		0.36	6488.0	5406.6	67.7	45.1	22.6
C120	504.9	60.0	330.0	42.0	180.0	60	0.65	4.21	0.70	25.70	23118.3		0.36	6488.0	5406.6	79.0	52.6	26.3
C121	504.9	36.0	330.0	14.5	180.0	60	0.65	7.01	0.40	25.70	23118.3		0.36	6488.0	5406.6	27.3	18.2	9.1
C122	504.9	36.0	330.0	18.0	180.0	60	0.65	7.01	0.50	25.70	23118.3		0.36	6488.0	5406.6	33.8	22.6	11.3
C123	504.9	36.0	330.0	21.5	180.0	60	0.65	7.01	0.60	25.70	23118.3		0.36	6488.0	5406.6	40.4	26.9	13.5
C124	504.9	36.0	330.0	25.3	180.0	60	0.65	7.01	0.70	25.70	23118.3		0.36	6488.0	5406.6	47.6	31.7	15.9
C125	504.9	29.7	330.0	12.0	180.0	60	0.65	8.50	0.40	25.70	23118.3		0.36	6488.0	5406.6	22.6	15.0	7.5
C126	504.9	29.7	330.0	14.8	180.0	60	0.65	8.50	0.50	25.70	23118.3		0.36	6488.0	5406.6	27.8	18.5	9.3
C127	504.9	29.7	330.0	17.9	180.0	60	0.65	8.50	0.60	25.70	23118.3		0.36	6488.0	5406.6	33.7	22.4	11.2
C128	504.9	29.7	330.0	20.7	180.0	60	0.65	8.50	0.70	25.70	23118.3		0.36	6488.0	5406.6	38.9	25.9	13.0
C129	168.3	20.0	88.9	10.0	39.0	60	0.53	4.21	0.50	25.70	23 39.5		0.23	2162.7	1802.2	18.8	12.5	6.3
C130	168.3	20.0	88.9	12.0	39.0	60	0.53	4.21	0.60	25.70	23 39.5		0.23	2162.7	1802.2	22.6	15.0	7.5
C131	168.3	20.0	88.9	14.0	39.0	60	0.53	4.21	0.70	25.70	23 39.5		0.23	2162.7	1802.2	26.3	17.5	8.8
C132	168.3	12.0	88.9	4.8	39.0	60	0.53	7.01	0.40	25.70	23 39.5		0.23	2162.7	1802.2	9.0	6.0	3.0
C133	168.3	12.0	88.9	6.0	39.0	60	0.53	7.01	0.50	25.70	23 39.5		0.23	2162.7	1802.2	11.3	7.5	3.8
C134	168.3	12.0	88.9	7.2	39.0	60	0.53	7.01	0.60	25.70	23 39.5		0.23	2162.7	1802.2	13.5	9.0	4.5
C135	168.3	12.0	88.9	8.4	39.0	60	0.53	7.01	0.70	25.70	23 39.5		0.23	2162.7	1802.2	15.8	10.5	5.3
C136	168.3	9.9	88.9	4.0	39.0	60	0.53	8.50	0.40	25.70	23 39.5		0.23	2162.7	1802.2	7.5	5.0	2.5

... continued

ID	D	T	d	t	e	θ	β	γ	τ	α	ζ	g	e/D	L_{ch}	H	W1	W2	W3
C137	168.3	9.9	88.9	5.0	39.0	60	0.53	8.500	.51	25.70	.23	39.5	0.23	2162.7	1802.2	9.4	6.3	3.1
C138	168.3	9.9	88.9	6.0	39.0	60	0.53	8.500	.61	25.70	.23	39.5	0.23	2162.7	1802.2	11.3	7.5	3.8
C139	168.3	9.9	88.9	7.0	39.0	60	0.53	8.500	.71	25.70	.23	39.5	0.23	2162.7	1802.2	13.2	8.8	4.4
C140	168.3	20.0	110.0	8.0	60.0	60	0.65	4.210	.40	25.70	.23	39.4	0.36	2162.7	1802.2	15.0	10.0	5.0
C141	168.3	20.0	110.0	10.0	60.0	60	0.65	4.210	.50	25.70	.23	39.4	0.36	2162.7	1802.2	18.8	12.5	6.3
C142	168.3	20.0	110.0	12.0	60.0	60	0.65	4.210	.60	25.70	.23	39.4	0.36	2162.7	1802.2	22.6	15.0	7.5
C143	168.3	12.0	110.0	4.8	60.0	60	0.65	7.010	.40	25.70	.23	39.4	0.36	2162.7	1802.2	9.0	6.0	3.0
C144	168.3	12.0	110.0	6.0	60.0	60	0.65	7.010	.50	25.70	.23	39.4	0.36	2162.7	1802.2	11.3	7.5	3.8
C145	168.3	12.0	110.0	7.2	60.0	60	0.65	7.010	.60	25.70	.23	39.4	0.36	2162.7	1802.2	13.5	9.0	4.5
C146	168.3	12.0	110.0	8.4	60.0	60	0.65	7.010	.70	25.70	.23	39.4	0.36	2162.7	1802.2	15.8	10.5	5.3
C147	168.3	9.9	110.0	4.0	60.0	60	0.65	8.500	.40	25.70	.23	39.4	0.36	2162.7	1802.2	7.5	5.0	2.5
C148	168.3	9.9	110.0	5.0	60.0	60	0.65	8.500	.51	25.70	.23	39.4	0.36	2162.7	1802.2	9.4	6.3	3.1
C149	168.3	9.9	110.0	6.0	60.0	60	0.65	8.500	.61	25.70	.23	39.4	0.36	2162.7	1802.2	11.3	7.5	3.8
C150	168.3	9.9	110.0	7.0	60.0	60	0.65	8.500	.71	25.70	.23	39.4	0.36	2162.7	1802.2	13.2	8.8	4.4
C151	168.3	20.0	88.9	8.0	60.0	60	0.53	4.210	.40	25.70	.38	63.8	0.36	2166.0	1800.0	15.0	10.0	5.0
C152	168.3	20.0	88.9	8.0	39.0	60	0.53	4.210	.40	25.70	.23	39.5	0.23	2166.0	1800.0	15.0	10.0	5.0
C153	168.3	20.0	88.9	8.0	30.0	60	0.53	4.210	.40	25.70	.17	29.2	0.18	2166.0	1800.0	15.0	10.0	5.0
C154	168.3	20.0	88.9	8.0	22.0	60	0.53	4.210	.40	25.70	.12	19.9	0.13	2166.0	1800.0	15.0	10.0	5.0
C155	168.3	20.0	88.9	8.0	22.0	60	0.53	4.210	.40	25.70	.12	19.9	0.13	2166.0	1800.0	15.0	10.0	5.0
C156	168.3	20.0	88.9	8.0	22.0	60	0.53	4.210	.40	25.70	.12	19.9	0.13	2166.0	1800.0	15.0	10.0	5.0
C157	168.3	20.0	88.9	8.0	22.0	60	0.53	4.210	.40	25.70	.12	19.9	0.13	2166.0	1800.0	15.0	10.0	5.0
C158	168.3	20.0	88.9	8.0	22.0	60	0.53	4.210	.40	25.70	.12	19.9	0.13	2166.0	1800.0	15.0	10.0	5.0
C159	168.3	20.0	88.9	8.0	22.0	60	0.53	4.210	.40	25.70	.12	19.9	0.13	2166.0	1800.0	15.0	10.0	5.0
C160	168.3	20.0	88.9	8.0	39.0	60	0.53	4.210	.40	38.60	.23	39.5	0.23	3249.0	1800.0	15.0	10.0	5.0
C161	168.3	20.0	88.9	8.0	39.0	60	0.53	4.210	.40	12.90	.23	39.5	0.23	1083.0	1800.0	15.0	10.0	5.0
C162	168.3	20.0	88.9	8.0	39.0	60	0.53	4.210	.40	25.70	.23	39.5	0.23	2166.0	2700.0	15.0	10.0	5.0

... continued

ID	D	T	d	t	e	θ	β	γ	τ	α	ζ	g	e/D	L_{ch}	H	W1	W2	W3
C163	168.3	20.0	88.9	8.0	39.0	60	0.53	4.21	0.40	25.70	0.23	39.5	0.23	2166.0	900.0	15.0	10.0	5.0
C164	168.3	20.0	88.9	8.0	39.0	60	0.53	4.21	0.40	25.70	0.23	39.5	0.23	2166.0	1800.0	22.5	15.0	7.5
C165	168.3	20.0	88.9	8.0	39.0	60	0.53	4.21	0.40	25.70	0.23	39.5	0.23	2166.0	1800.0	7.5	5.0	2.5
C166	168.3	20.0	88.9	8.0	22.0	60	0.53	4.21	0.40	25.70	0.13	19.9	0.13	2166.0	1800.0	15.0	10.0	5.0
C167	168.3	20.0	88.9	8.0	22.0	60	0.53	4.21	0.40	25.80	0.13	19.9	0.13	2167.0	1801.0	15.0	10.0	5.0
C168	504.9	60.0	266.7	24.0	116.1	60	0.53	4.21	0.40	25.70	0.23	117.6	0.23	6488.0	5406.6	45.1	30.1	15.0
C169	168.3	20.0	88.9	8.0	38.7	60	0.53	4.21	0.40	25.70	0.23	39.2	0.23	2162.7	1802.2	15.0	10.0	5.0
C170	168.3	20.0	110.0	14.0	60.0	60	0.65	4.21	0.70	25.70	0.36	39.4	0.36	2162.7	1802.2	26.3	17.5	8.8
C171	504.9	60.0	330.0	30.0	180.0	60	0.65	4.21	0.50	25.70	0.36	118.3	0.36	6488.0	5406.6	56.4	37.6	18.8
C172	168.3	20.0	110.0	10.0	60.0	60	0.65	4.21	0.50	25.70	0.36	39.4	0.36	2162.7	1802.2	18.8	12.5	6.3
C173	168.3	20.0	88.9	8.0	22.0	60	0.53	4.21	0.40	25.70	0.13	19.9	0.13	2166.0	1800.0	15.0	10.0	5.0
C174	168.3	20.0	88.9	8.0	38.0	60	0.53	4.21	0.40	25.70	0.23	38.4	0.23	2166.0	1800.0	15.0	10.0	5.0
C175	168.3	20.0	88.9	8.0	22.0	60	0.53	4.21	0.40	25.70	0.13	19.9	0.13	2166.0	1800.0	15.0	10.0	5.0
C176	273.0	20.0	139.7	12.5	54.0	60	0.51	6.83	0.63	15.40	0.2	58.7	0.2	2100.0	1781.0	15.0	12.0	8.0
C177	504.9	36.0	330.0	14.5	180.0	60	0.65	7.01	0.40	25.70	0.36	118.3	0.36	6488.0	5406.6	27.3	18.2	9.1

D.2 Parametric results

Table D.3: Parametric results.

Parametric results														
ID	T	e	β	γ	τ	α	ζ	e/D	a_0	$T/50$	$T/20$	$T/8$	$T/6$	$T/2$
[-]	[mm]	[mm]	[-]	[-]	[-]	[-]	[-]	[-]	SIF (a_i)	$LC_{(1,4,5)}$	$Nmm^{-3/2}$			
C106	60	116.1	0.53	4.2	0.50	25.7	0.23	0.23	0.15	1.20	3.00	7.50	10.00	30.00
									291	411	485	580	622	952
									320	456	549	694	765	1356
									658	937	1123	1397	1522	2439
C107	60	116.1	0.53	4.2	0.60	25.7	0.23	0.23	0.15	1.20	3.00	7.50	10.00	30.00
									335	488	566	683	728	1168
									347	509	599	758	825	1456
									455	666	781	973	1049	1677
C108	60	116.1	0.53	4.2	0.70	25.7	0.23	0.23	0.15	1.20	3.00	7.50	10.00	30.00
									342	494	575	692	738	1177
									381	554	654	811	877	1451
									490	711	837	1023	1096	1639
C109	36	116.1	0.53	7.0	0.40	25.7	0.23	0.23	0.15	0.72	1.80	4.50	6.00	18.00
									356	484	565	680	720	1007
									196	268	321	417	464	908
									209	284	341	440	488	925
C110	36	116.1	0.53	7.0	0.50	25.7	0.23	0.23	0.15	0.72	1.80	4.50	6.00	18.00
									393	522	616	733	780	1101
									224	300	361	459	508	955
									200	267	319	402	442	791
C111	36	116.1	0.53	7.0	0.60	25.7	0.23	0.23	0.12	0.72	1.80	4.50	6.00	18.00
									429	599	703	818	883	1224
									236	332	397	490	548	979
									279	391	466	569	632	1067
C112	36	116.1	0.53	7.0	0.70	25.7	0.23	0.23	0.15	0.72	1.80	4.50	6.00	20.00

... continued

ID	T	e	β	γ	τ	α	ζ	e/D	a_0	$T/50$	$T/20$	$T/8$	$T/6$	$T/2$
[-]	[mm]	[mm]	[-]	[-]	[-]	[-]	[-]	[-]	SIF (a_i)	$LC_{(1,4,5)}$	[Nmm ^{-3/2}]			
									527	663	782	931	983	1451
									284	359	430	538	588	1117
									271	343	410	508	551	980
C113	29.7	116.1	0.53	8.5	0.40	25.7	0.23	0.23	0.15	0.59	1.49	3.71	4.95	14.85
									381	499	588	701	730	1011
									180	236	285	365	398	784
									75	99	122	165	186	439
C114	29.7	116.1	0.53	8.5	0.50	25.7	0.23	0.23	0.20	0.59	1.49	3.71	4.95	14.85
									440	543	630	748	789	1048
									209	259	307	388	427	784
									343	423	504	638	702	1288
C115	29.7	116.1	0.53	8.5	0.60	25.7	0.23	0.23	0.15	0.59	1.49	3.71	4.95	14.85
									464	594	697	826	872	1203
									220	284	339	423	463	842
									214	276	328	407	444	774
C116	29.7	116.1	0.53	8.5	0.70	25.7	0.23	0.23	0.15	0.59	1.49	3.71	4.95	13.50
									521	671	790	931	970	1351
									236	305	364	451	485	843
									254	328	391	480	512	856
C117	60	180.0	0.65	4.2	0.40	25.7	0.23	0.36	0.10	1.20	3.00	7.50	10.00	30.00
									238	373	447	529	576	914
									233	369	452	573	646	1309
									278	440	534	663	738	1334
C119	60	180.0	0.65	4.2	0.60	25.7	0.23	0.36	0.15	1.20	3.00	7.50	10.00	30.00
									317	460	541	642	698	1118
									323	470	557	695	771	1373

... continued

ID	T	e	β	γ	τ	α	ζ	e/D	a_0	$T/50$	$T/20$	$T/8$	$T/6$	$T/2$
[-]	[mm]	[mm]	[-]	[-]	[-]	[-]	[-]	[-]	SIF (a_i)	$LC_{(1,4,5)}$	[Nmm ^{-3/2}]			
									332	482	566	698	764	1214
C120	60	180.0	0.65	4.2	0.70	25.7	0.23	0.36	0.15	1.20	3.00	7.50	10.00	30.00
									307	442	521	620	666	1109
									354	514	613	748	809	1388
									406	589	698	838	895	1373
C122	36	180.0	0.65	7.0	0.50	25.7	0.23	0.36	0.10	0.72	1.80	4.50	6.00	18.00
									263	379	433	518	537	794
									195	282	329	420	453	903
									348	501	581	721	764	1327
C123	36	180.0	0.65	7.0	0.60	25.7	0.23	0.36	0.15	0.72	1.80	4.50	6.00	18.00
									348	450	530	626	643	921
									235	305	366	456	485	907
									351	454	542	666	703	1227
C124	36	180.0	0.65	7.0	0.70	25.7	0.23	0.36	0.15	0.72	1.80	4.50	6.00	18.00
									427	561	657	776	819	1160
									251	331	393	489	532	942
									269	354	419	514	555	920
C125	29.7	180.0	0.65	8.5	0.40	25.7	0.23	0.36	0.15	0.59	1.49	3.71	4.95	14.85
									380	494	580	688	739	1050
									170	223	266	339	381	783
									57	75	95	145	179	575
C126	29.7	180.0	0.65	8.5	0.50	25.7	0.23	0.36	0.15	0.59	1.49	3.71	4.95	14.85
									381	488	576	685	734	1023
									185	239	287	362	403	768
									165	213	255	317	351	628
C127	29.7	180.0	0.65	8.5	0.60	25.7	0.23	0.36	0.15	0.59	1.49	3.71	4.95	14.85

... continued

ID	T	e	β	γ	τ	α	ζ	e/D	a_0	$T/50$	$T/20$	$T/8$	$T/6$	$T/2$
[-]	[mm]	[mm]	[-]	[-]	[-]	[-]	[-]	[-]	SIF (a_i)	$LC_{(1,4,5)}$	[Nmm ^{-3/2}]			
									316	409	474	556	585	803
									207	269	317	394	430	805
									265	342	402	493	533	929
C129	20	39.0	0.53	4.2	0.50	25.7	0.23	0.23	0.15	0.40	1.00	2.50	3.33	10.00
									222	265	308	368	394	589
									223	267	318	402	443	776
									330	396	467	582	634	1006
C130	20	39.0	0.53	4.2	0.60	25.7	0.23	0.23	0.11	0.40	1.00	2.50	3.33	10.00
									233	288	335	398	427	680
									238	296	351	437	477	841
									304	378	446	546	589	943
C131	20	39.0	0.53	4.2	0.70	25.7	0.23	0.23	0.15	0.40	1.00	2.50	3.33	10.00
									247	292	336	403	430	676
									272	323	378	468	506	832
									343	409	476	580	622	924
C132	12	39.0	0.53	7.0	0.40	25.7	0.23	0.23	0.15	0.24	0.60	1.50	2.00	6.00
									263	284	333	393	417	585
									144	156	188	240	267	524
									144	156	187	238	264	504
C133	12	39.0	0.53	7.0	0.50	25.7	0.23	0.23	0.15	0.24	0.60	1.50	2.00	6.00
									276	303	359	421	446	630
									159	174	211	264	291	549
									150	165	198	246	269	480
C134	12	39.0	0.53	7.0	0.60	25.7	0.23	0.23	0.15	0.24	0.60	1.50	2.00	6.00
									317	343	403	464	498	696
									179	195	232	284	316	570

... continued

ID	T	e	β	γ	τ	α	ζ	e/D	a_0	$T/50$	$T/20$	$T/8$	$T/6$	$T/2$
[-]	[mm]	[mm]	[-]	[-]	[-]	[-]	[-]	[-]	SIF (a_i)	$LC_{(1,4,5)}$	[Nmm ^{-3/2}]			
									275	299	355	430	475	809
C135	12	39.0	0.53	7.0	0.70	25.7	0.23	0.23	0.15	0.24	0.60	1.50	2.00	6.00
									359	380	445	523	548	776
									198	210	250	309	334	593
									241	256	304	371	399	666
C136	9.9	39.0	0.53	8.5	0.40	25.7	0.23	0.23	0.15	0.20	0.50	1.24	1.65	4.95
									266	280	331	394	411	566
									128	134	163	208	227	446
									87	92	112	145	159	326
C137	9.9	39.0	0.53	8.5	0.51	25.7	0.23	0.23	0.15	0.20	0.49	1.24	1.65	4.95
									294	311	360	426	451	601
									144	152	180	227	250	455
									194	205	243	305	336	605
C138	9.9	39.0	0.53	8.5	0.61	25.7	0.23	0.23	0.15	0.20	0.50	1.24	1.65	4.95
									329	348	411	482	509	701
									156	166	199	246	269	486
									141	149	179	219	238	409
C139	9.9	39.0	0.53	8.5	0.71	25.7	0.23	0.23	0.15	0.20	0.50	1.24	1.65	5.20
									362	382	452	530	551	785
									170	179	215	265	285	530
									249	262	314	384	409	725
C140	20	60.0	0.65	4.2	0.40	25.7	0.23	0.36	-	0.40	1.00	2.50	3.33	10.00
									-	218	256	306	333	528
									-	214	259	330	373	756
									-	256	308	384	428	774
C142	20	60.0	0.65	4.2	0.60	25.7	0.23	0.36	0.15	0.40	1.00	2.50	3.33	10.00

... continued

ID	T	e	β	γ	τ	α	ζ	e/D	a_0	$T/50$	$T/20$	$T/8$	$T/6$	$T/2$
[-]	[mm]	[mm]	[-]	[-]	[-]	[-]	[-]	[-]	SIF (a_i)	$LC_{(1,4,5)}$	[Nmm ^{-3/2}]			
									221	266	312	367	399	636
									227	274	326	402	445	787
									242	292	344	418	457	721
C144	12	60.0	0.65	7.0	0.50	25.7	0.23	0.36	0.15	0.24	0.60	1.50	2.00	-
									240	262	303	358	373	-
									151	165	194	245	266	-
									193	211	248	308	332	-
C145	12	60.0	0.65	7.0	0.60	25.7	0.23	0.36	-	0.24	0.60	1.50	2.00	6.00
									-	281	325	389	402	577
									-	178	209	265	283	526
									-	227	266	332	353	609
C146	12	60.0	0.65	7.0	0.70	25.7	0.23	0.36	-	0.24	0.60	1.50	2.00	6.00
									-	318	377	440	461	658
									-	192	231	283	306	548
									-	256	307	371	399	666
C147	9.9	60.0	0.65	8.5	0.40	25.7	0.23	0.36	0.15	0.20	0.50	1.24	1.65	4.95
									227	239	277	332	352	507
									122	128	152	196	218	452
									213	223	263	332	365	684
C148	9.9	60.0	0.65	8.5	0.51	25.7	0.23	0.36	-	-	0.50	1.24	1.65	4.95
									-	-	331	390	417	588
									-	-	168	210	233	448
									-	-	218	269	296	533
C149	9.9	60.0	0.65	8.5	0.61	25.7	0.23	0.36	0.15	0.20	0.50	1.24	1.65	4.95
									262	278	322	376	395	550
									148	157	184	228	248	462

... continued

ID	T	e	β	γ	τ	α	ζ	e/D	a_0	$T/50$	$T/20$	$T/8$	$T/6$	$T/2$
[-]	[mm]	[mm]	[-]	[-]	[-]	[-]	[-]	[-]	SIF (a_i)	$LC_{(1,4,5)}$	[Nmm ^{-3/2}]			
									420	446	521	635	686	1193
C168	60	116.1	0.53	4.2	0.40	25.7	0.23	0.23	0.15	1.20	3.00	7.50	10.00	30.00
									293	424	496	592	639	1037
									277	405	487	625	702	1389
									353	515	616	779	864	1553
C169	20	38.7	0.53	4.2	0.40	25.7	0.23	0.23	0.15	0.40	1.00	2.50	3.33	10.00
									204	245	287	342	370	598
									193	233	280	360	406	799
									242	292	348	441	489	874
C170	20	60.0	0.65	4.2	0.70	25.7	0.23	0.36	0.15	0.40	1.00	2.50	3.33	10.00
									217	254	296	352	380	633
									255	299	353	432	468	801
									300	351	413	497	532	814
C171	60	180.0	0.65	4.2	0.50	25.7	0.23	0.36	0.12	1.00	3.00	7.50	10.00	30.00
									199	314	356	432	465	763
									272	430	502	640	706	1322
									581	913	1064	1328	1450	2416
C172	20	60.0	0.65	4.2	0.50	25.7	0.23	0.36	0.20	0.33	1.00	2.50	3.33	10.00
									207	208	236	284	304	490
									250	251	291	371	408	764
									441	445	516	642	699	1163

D.3 Other effects

D.3.1 Chord length between joints, L_{ch} , and truss height, H and crack angle, θ

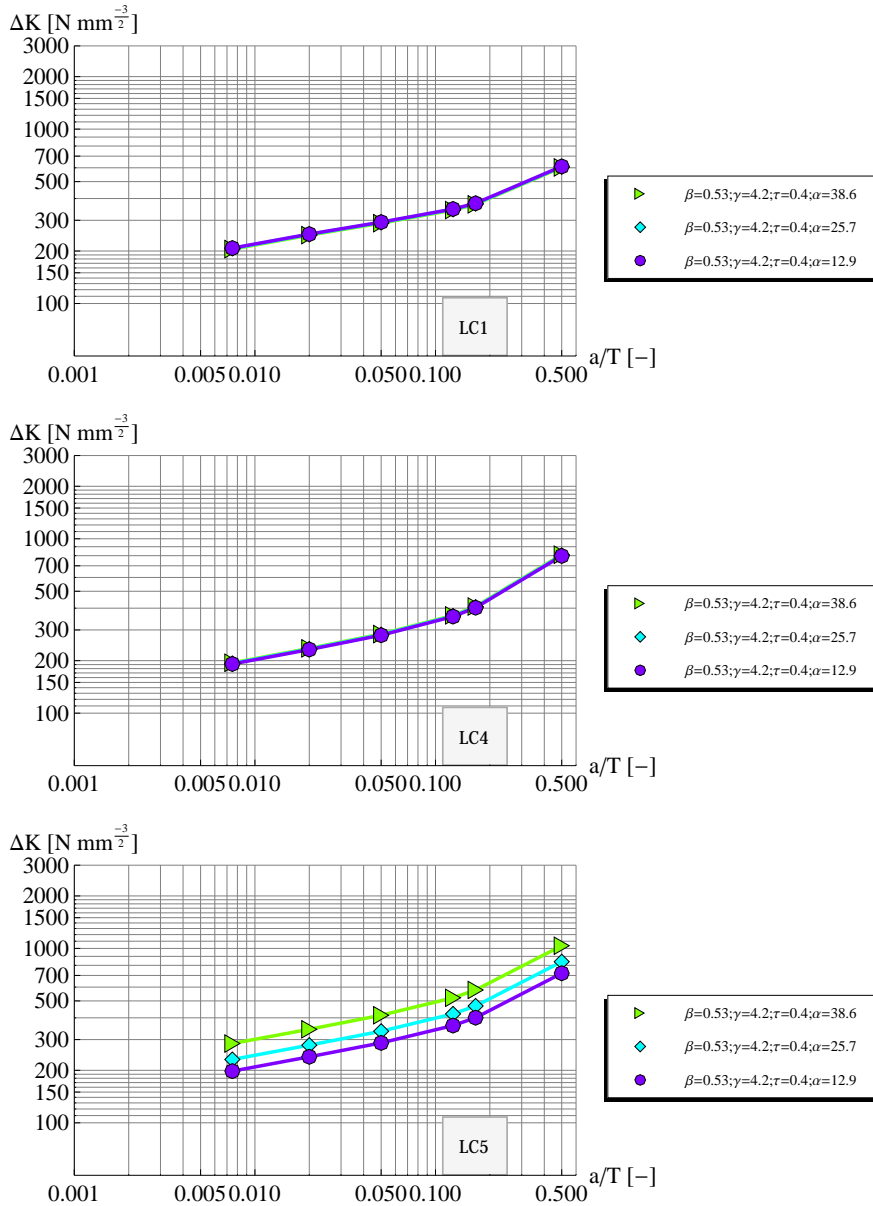


Figure D.1: Influence of chord length L_{ch} ($\beta = 0.53$; $\gamma = 4.2$; $\tau = 0.4$; $\alpha = 38.6^\circ$); ($\beta = 0.53$; $\gamma = 4.2$; $\tau = 0.4$; $\alpha = 25.7^\circ$); ($\beta = 0.53$; $\gamma = 4.2$; $\tau = 0.4$; $\alpha = 12.9^\circ$).

D.3.2 Truss height, H

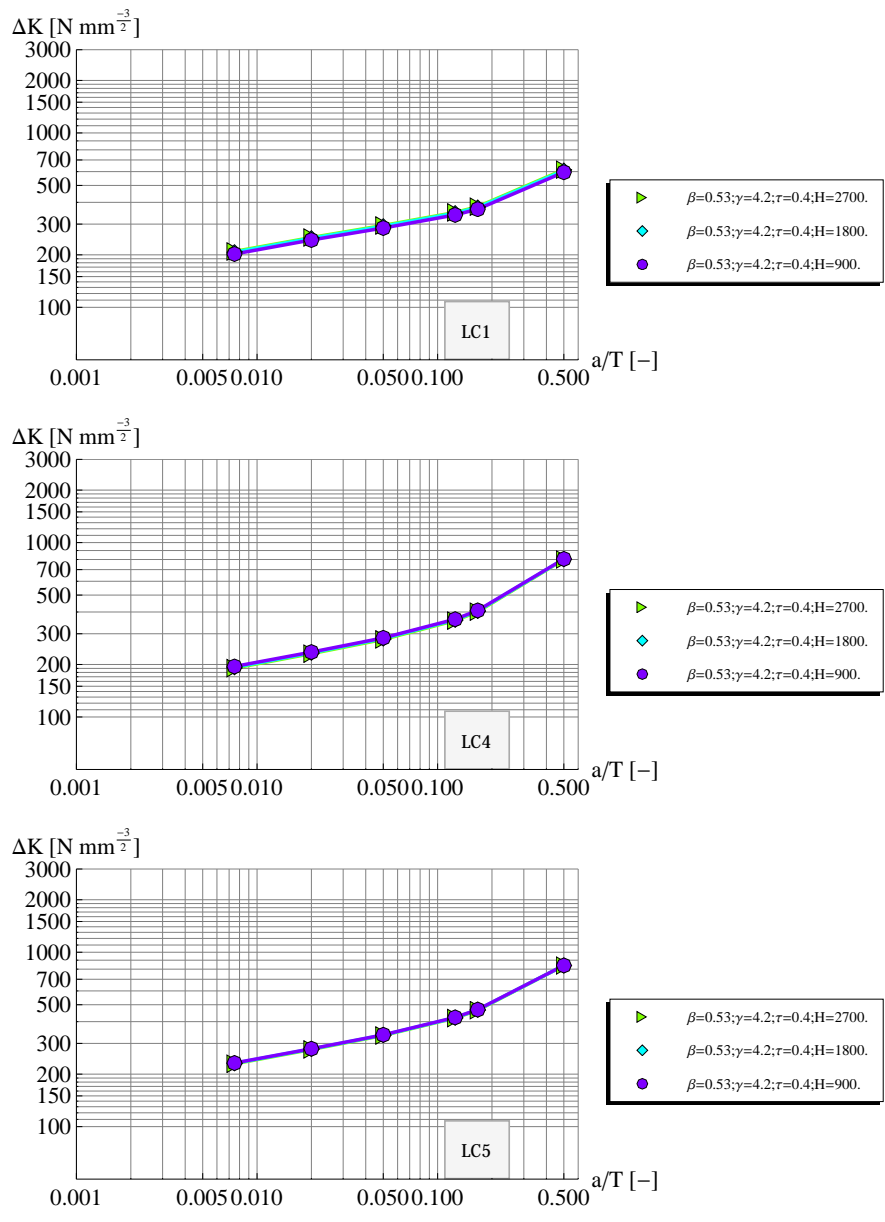


Figure D.2: Influence of truss height, H .

D.3.3 Crack shape, a/c

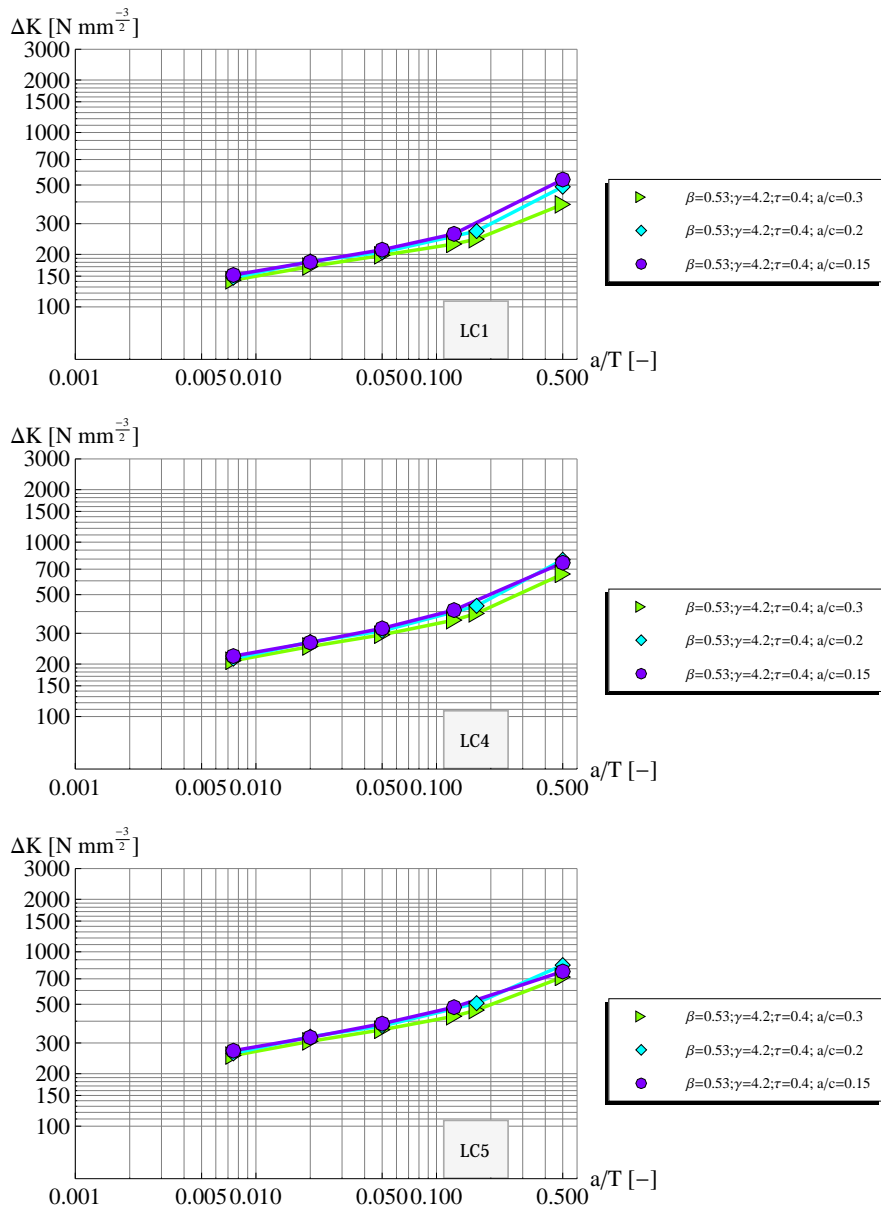


Figure D.3: Influence of crack shape.

D.3.4 Crack angle, ϕ_{crack}

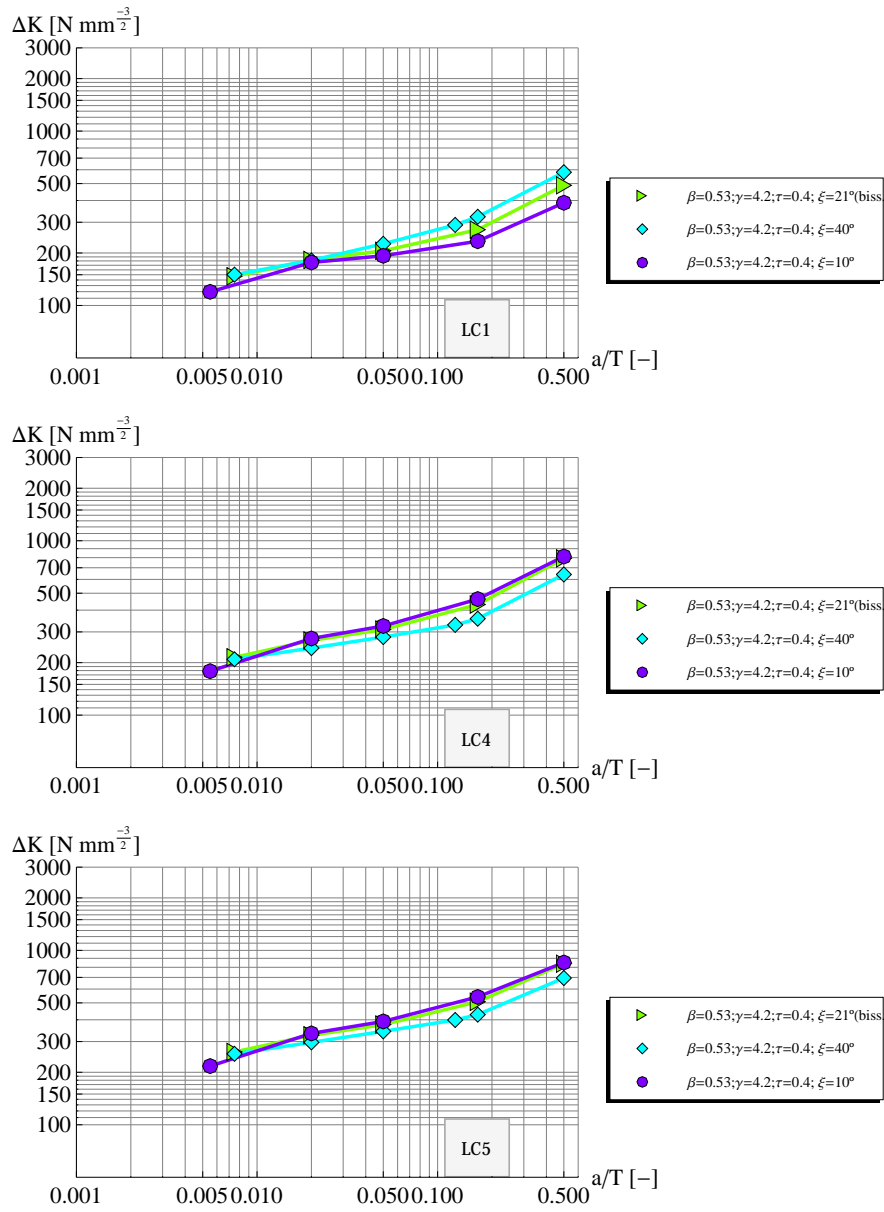


Figure D.4: Influence of crack angle, ϕ_{crack} .

E

Proportional scaling

E.1 Behaviour of function $p \left(\frac{a}{T}\right)^{q-1} + \left(\frac{a}{T}\right)^q$

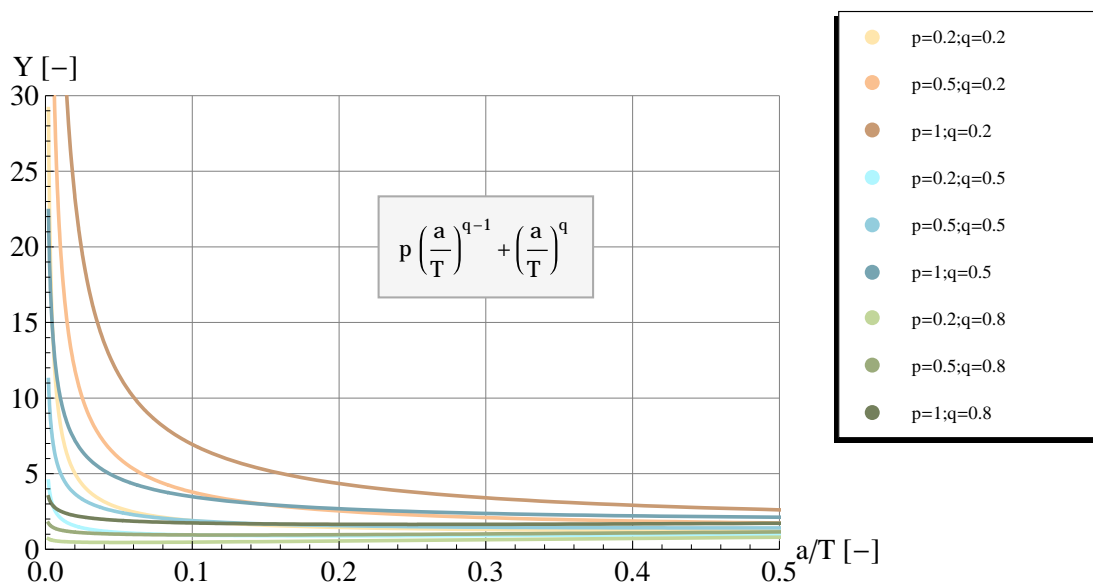


Figure E.1: Behaviour of function $p \left(\frac{a}{T}\right)^{q-1} + \left(\frac{a}{T}\right)^q$.

E.2 Fatigue life function of load case

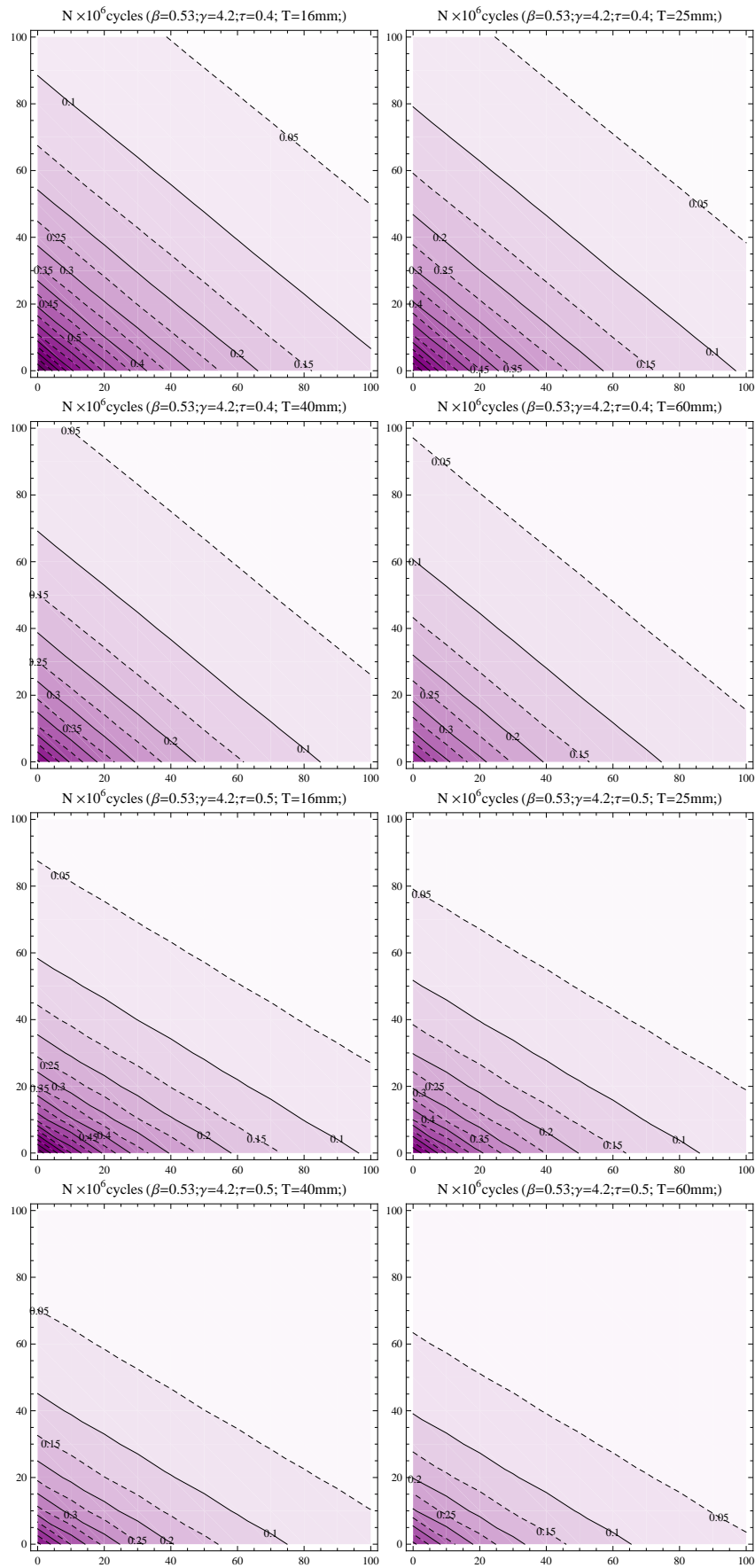


Figure E.2: Fatigue life function of load case and geometry.

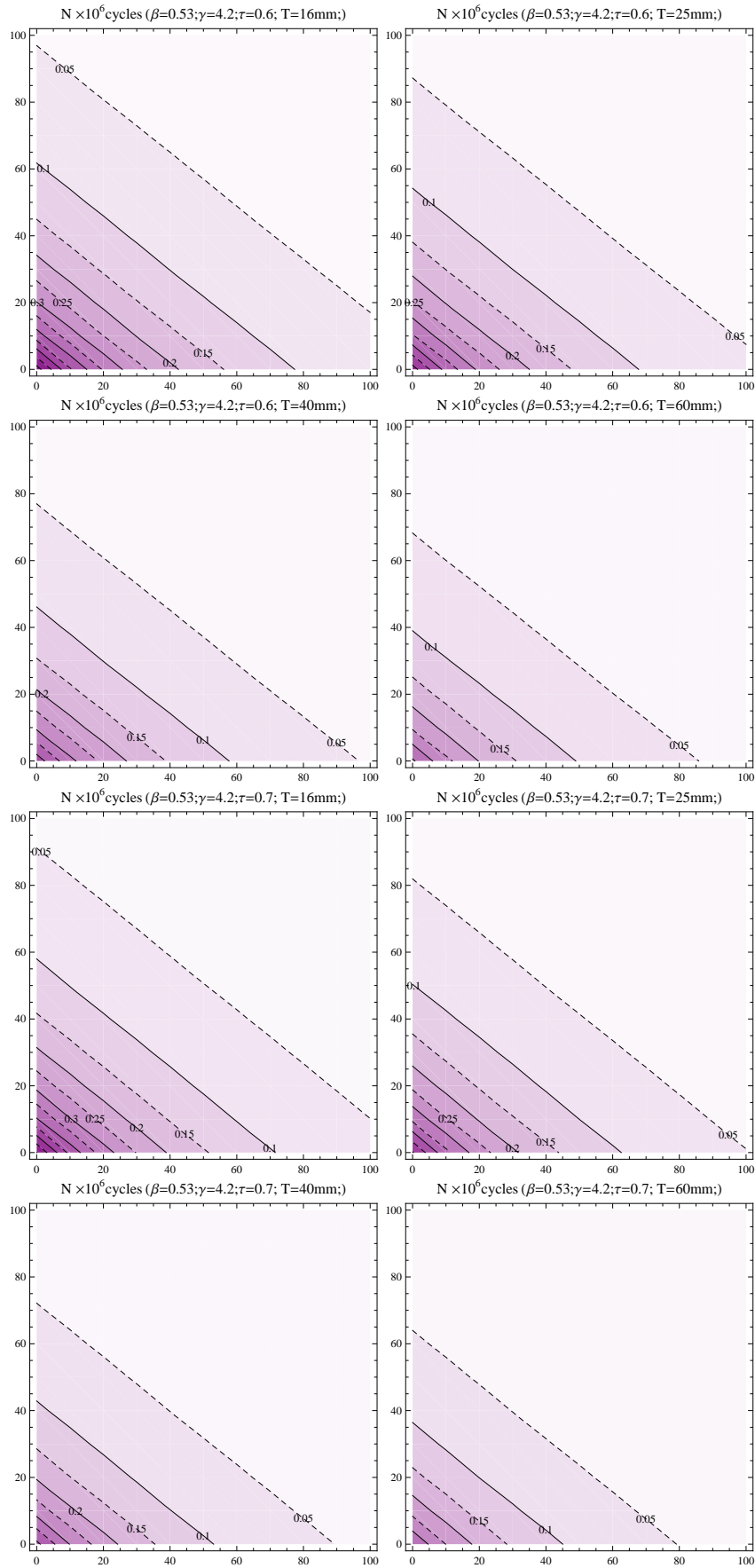


Figure E.3: Fatigue life function of load case and geometry.

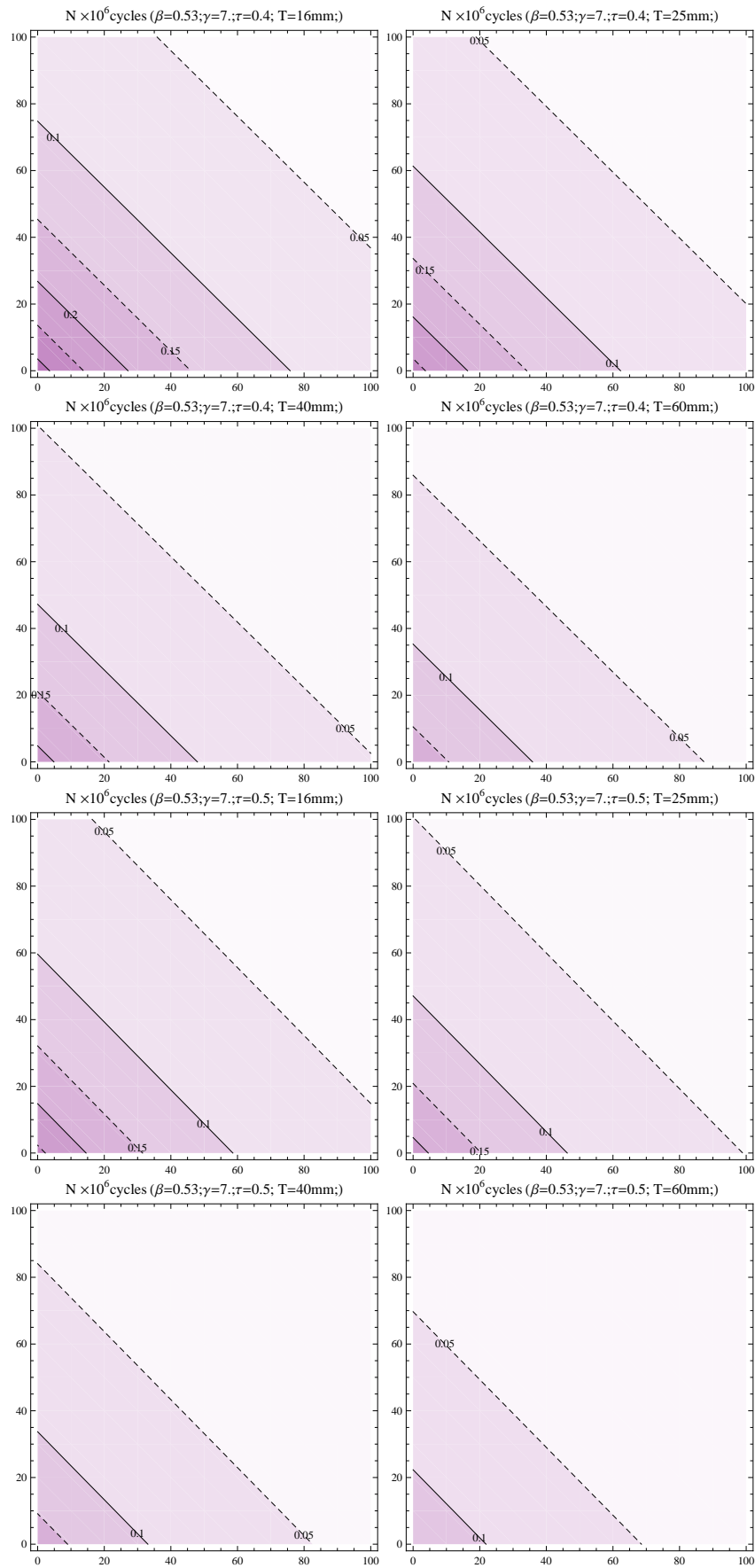


Figure E.4: Fatigue life function of load case and geometry.

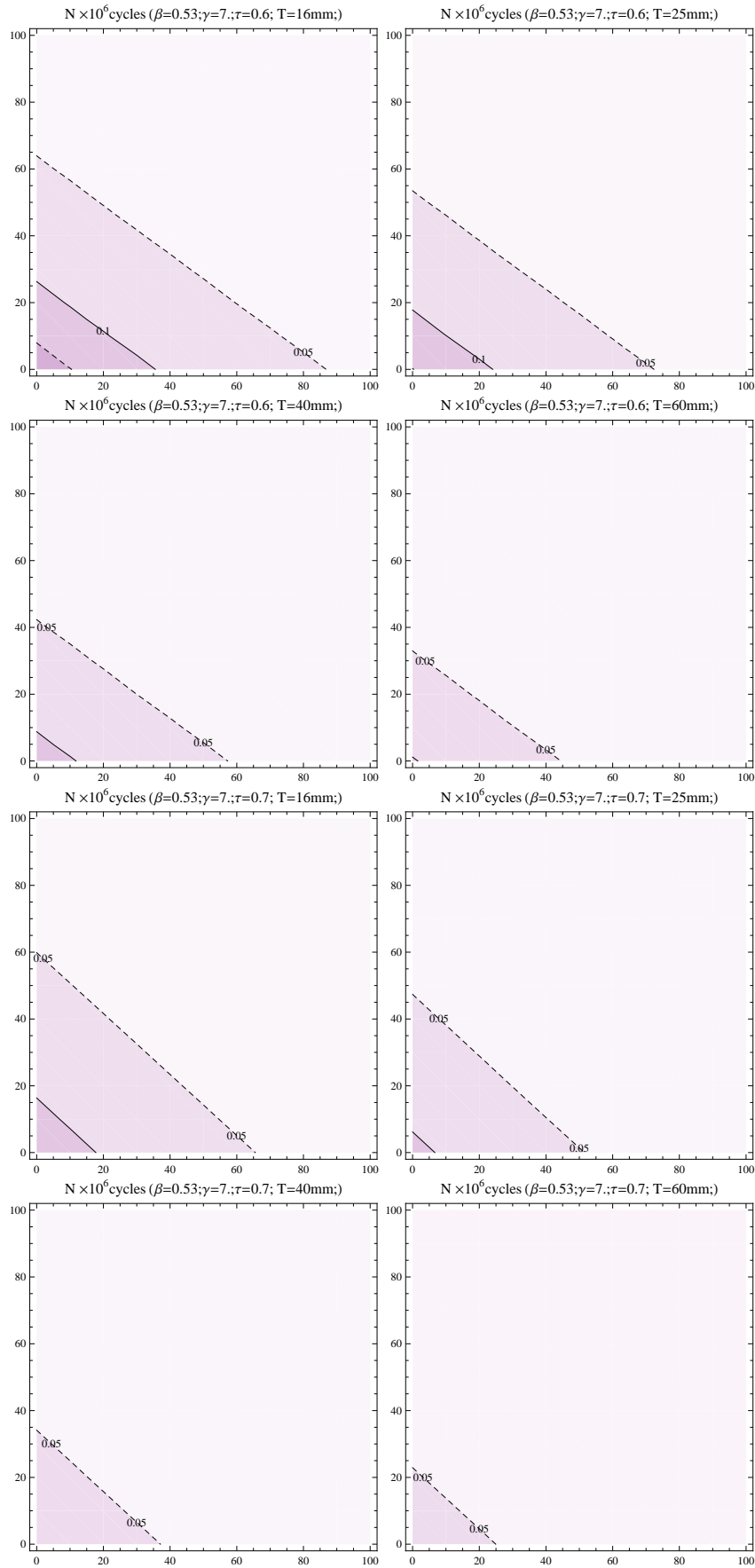


Figure E.5: Fatigue life function of load case and geometry.

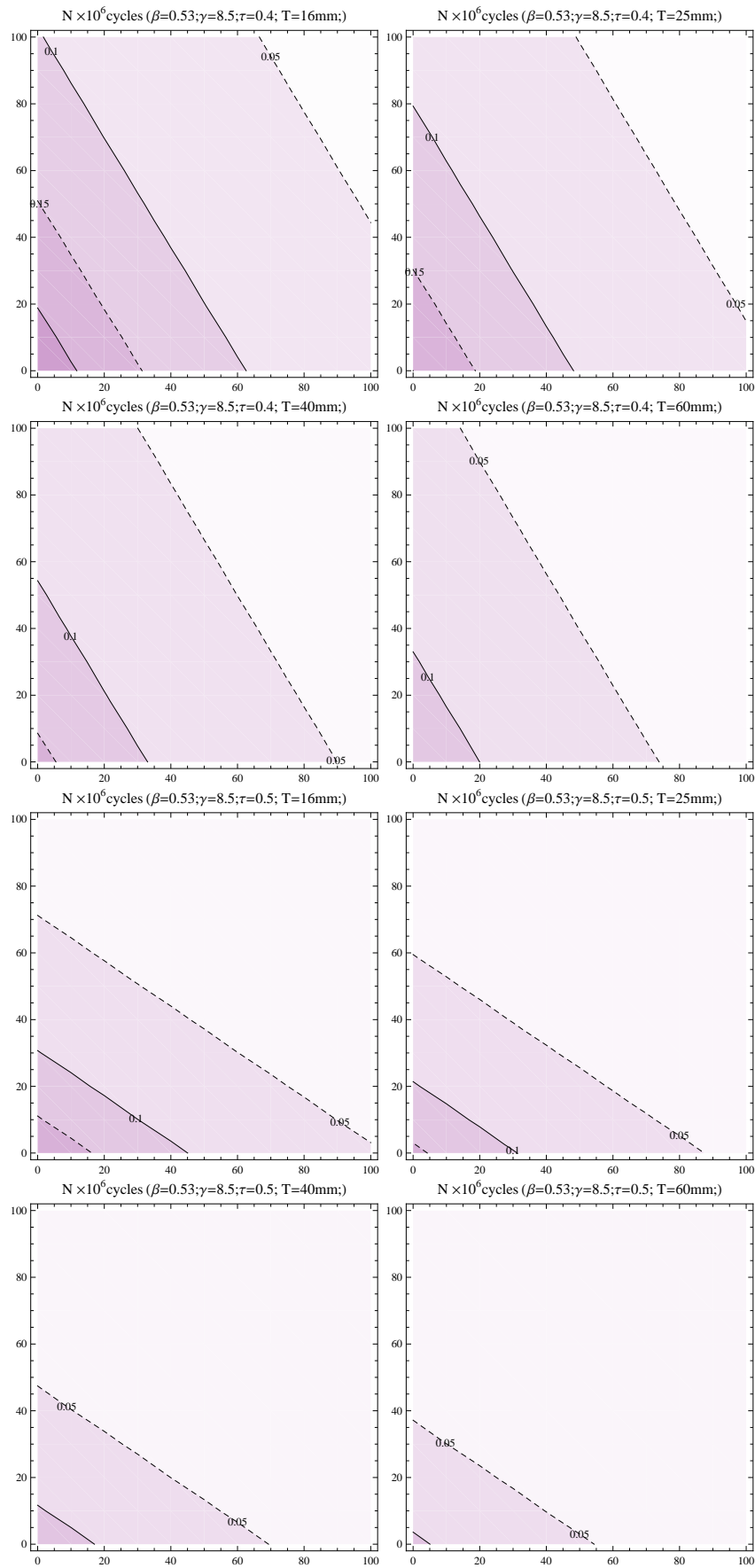


Figure E.6: Fatigue life function of load case and geometry.

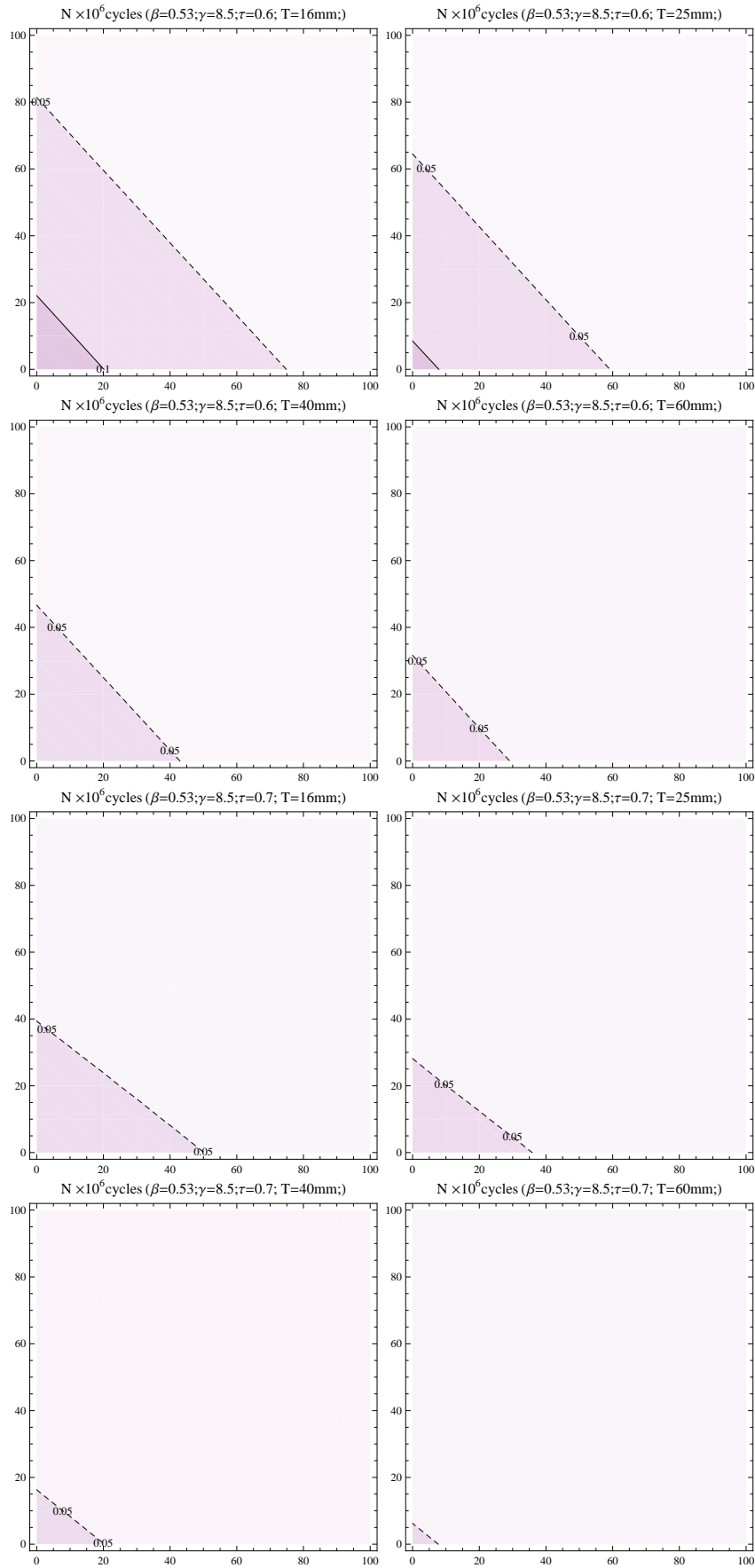


Figure E.7: Fatigue life function of load case and geometry.

F

Non-proportional scaling

F.1 Effect over fatigue strength, S

F.1.1 Influence of thickness ratio, τ

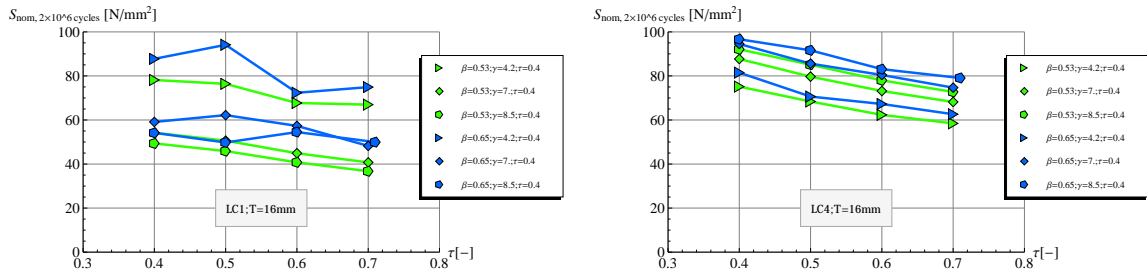


Figure E.1: Fatigue strength, influence of the thicknesses ratio, τ .

F.1.2 Influence of diameters ratio, β

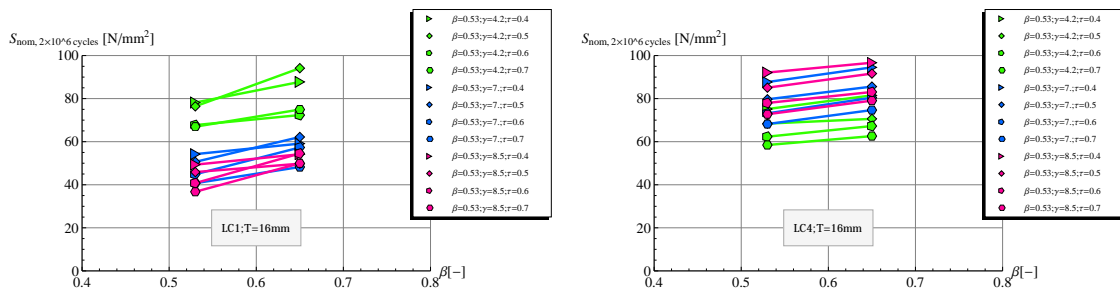


Figure E.2: Fatigue strength, influence of the diameters ratio, β .

F.1.3 Influence of chord slenderness, γ

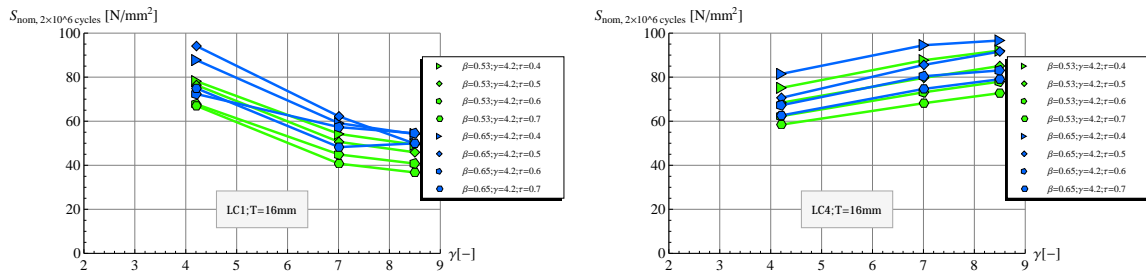


Figure F.3: Fatigue strength, influence of the chord slenderness, γ .

References

- Albrecht, P. and Yamada, K. Rapid Calculation of Stress Intensity Factors. *Journal of the Structural Division, ASCE*, 103(ST2):377 – 389, February 1977.
- API. *Recommended practice for planning, designing and constructing fixed offshore platforms*. API Recommended Practice 2A (RP2A), 21st Edition, Washington, USA, 2000.
- ASTM, S. . *Mechanics of fatigue crack closure*. Edited by J.C. Newmann, Jr and W. Elber. American society for testing and materials, 1988.
- AWS. *Structural Welding Code*. American Welding Society, D 1.1-2000, 2000.
- Basquin, O. H. The exponential law of endurance tests. *Proc*, 10:625–630, 1910.
- Bazant, Z. P. Size effect in blunt fracture: concrete, rock, metal. *Jnl Engrg Mech*, 110:518–535, 1984.
- Bazant, Z. P. Size effect on structural strength: a review. *Archive of applied mechanics*, 69:703, 1999.
- Beale, L. and Toprac, A. Analysis of in-plane T, Y and K welded tubular connections. *Welding Research Council Bulletin*, 125, October 1967.
- BEASY. *BEASY User Guide*. Computational mechanics BEASY Ltd, Ashurst, Southampton, UK, 2003.
- Berge, S. and Webster, S. E. The size effect on the fatigue behaviour of welded joints. In *Steel in Marine Structures*, pp. 179–203. Elsevier, 1987.
- Bowness, D. and Lee, M. Guidance on the selection of stress intensity factor solutions for fracture mechanics assessment of cracked offshore tubular joints. In *Tubular Structures VIII*, pp. 361–370. Balkema, 1998. ISBN 90-5809-001-9.
- Bremen, U. Amélioration du comportement à la fatigue d'assemblages soudés : étude et modélisation de l'effet des contraintes résiduelles, Thèse N° 787. *Thèse N° 787*, 1989.
- Broek, D. *Elementary Engineering Fracture Mechanics*. 1986.
- Cao, J. J., Yang, G. J., Packer, J. A. and Burdekin, F. M. Crack modeling in FE analysis of circular tubular joints. *Engineering Fracture Mechanics*, 61:537–553, November 1998.
- Carpinteri, A. Scaling laws and renormalization groups for strength and toughness of disordered materials. *Int Jnl Solids Struct*, pp. 291–302, 1994.
- Carpinteri, A., Landini, A. and Spagnoli, A. Theoretical Interpretation Of Size Effect In Fatigue. *Mechanika z.67, Pokrzywna, Poland*, 2001.
- Chiew, S.-P., Lie, S.-T., Lee, C.-K. and Huang, Z.-W. Fatigue performance of cracked tubular T joints under combined loads. I: Experimental. *Journal of Structural Engineering*, pp. 562–571, April 2004.
- Chimie, R. *Rhodorsil – SIL 01 021 1*. Fiche technique, Rhodia Chimie - Silicones Europe, 55 Av. des frères Perret, BP 60, 69192, St-Fons-Cedex, France, 2002.
- Coffin, L. Low cycle fatigue – A thirty year perspective. In *Second International Conference on Fatigue and Fatigue Thresholds 'Fatigue 84*, pp. 1213–1234. Univ. of Birmingham, U.K., 1984.
- de Koning, C. H. M., Wardenier, J. and Dutta, D. *Fatigue behaviour of multiplanar welded hollow section joints and reinforcement measures for repair*. TNO-Bouw Report No. BI-92-0005/21.4.6394, TNO, 1992.

- Dijkstra, O. and van Straalen, I. Fracture mechanics and fatigue of welded structures. In *WRC Proceedings IIW*, pp. 225–239. IIW, 1997.
- Dong, P. A structural stress definition and numerical implementation for fatigue analysis of welded joints. *Int. journal of fatigue*, 23:865–876, 2001.
- Dong, P. A Robust Structural Stress Method for Fatigue Analysis of Offshore/Marine Structures. *Journal of Offshore Mechanics and Arctic Engineering*, 127(1):68–74, February 2005.
- Dowling, N. E., Brose, W. R. and Wilson, W. K. Notched member fatigue life predictions by the local strain approach in fatigue under complex loading. *Advanced Engineering*, Vol. 6, 1977.
- Dubois, V. Fatigue de détails soudés traités sous sollicitations d'amplitude variable. *Thèse N° 1260*, 1994.
- Dutta, D., Wardenier, J., Yeomans, N., Sakae, K., Bucak, O. and Packer, J. A. *Design guide for fabrication, assembly and erection of hollow section structures*. CIDECT, Comité International pour le développement et l'étude de la construction tubulaire, TÜV-Verlag Rheinland, Köln, 1998.
- Eekhout, M. Tubular and Glass Structures. In *Tubular structures: The 4th International Symposium Delft*, pp. 148–173. Delft University Press, 1991.
- Eekhout, M. *Tubular structures in architecture*. TU Delft - CIDECT, 1996.
- Electronique, L. *Mesureur de fissure – 7422*. Technical Report, Av. de la Rochelle 12, CH-1008 Prilly, Switzerland, 2007.
- EN 1993-1-1:2005. *Eurocode 3: Design of steel structures – Part 1-1: General rules and rules for buildings*. CEN, 2005.
- Fisher, J. W., Frank, K. H., Hirt, M. A. and McNamee, B. M. Effect of Weldments on the Fatigue Strength of Steel Beams. *National Cooperative Highway Research Program, Report No.102*, 1970.
- FORMAT!!!, I. N. Measuring Fatigue Cracks In Fillet Welded Joints. *International Journal of Fatigue*, (4):41–45, 1982.
- Forth, S. and Staroselsky, A. A hybrid FEM/BEM approach for designing an aircraft engine structural health monitoring. *CMES - Computer Modeling in Engineering and Sciences*, 9(3):287–298, October 2005.
- Fricke, W. Fatigue Analysis of welded joints: state of development. In *Marine Structures 16*, pp. 185–200. Elsevier, TU Hamburg-Harburg, 2003.
- Fricke, W. Effects of residual stresses on the fatigue behavior of welded steel structures. *Proceedings of the first symposium on structural durability*, pp. 111–124, 2005.
- Gerstle, W. H. *Finite and boundary element modelling of crack propagation in two- and three-dimensions using interactive computer graphics*. Ph.D. thesis, Cornell University, Ithaca, NY, 1986.
- Gurney, T. Theoretical Analysis of the Influence of Toe Defects on the Fatigue Strength of Fillet Welded Joints. *Report No.E/32/1977*, March 1977.
- Gurney, T. *Fatigue of Welded Structures*. 1979.
- Gurney, T. *Cumulative damage of welded joints*. CRC, October 2006. ISBN 978-0849334757.
- Gurney, T. R. The influence of thickness on fatigue of welded joints – 10 years on (a review of british work). In *Proc. 8th Intn. Conference, Offshore Mechanics & Arctic Engng.*, volume 3. 1989.
- Haagensen, P. Fatigue of tubular joints and fatigue improvement methods. *Progress in Structural Engineering and Materials*, pp. 96–106, 1997.
- Haldimann-Sturm, S. C. *Ermüdungsverhalten von Stahlgussknoten in Brücken aus Stahlhohlprofilen*. PhD thesis EPFL n°3274, Ecole polytechnique fédérale de Lausanne (EPFL), December 2005.
- Hartmann, F. *Introduction to boundary elements*. Springer-Verlag, 1989. ISBN 3-540-50430-3.
- Hobbacher, A. *Recommendations for fatigue design of welded joints and components, IIW document XIII-1965-03 / XV-1127-03*. International Institute of welding, July 2003.
- HSE. *Comparison of fatigue provisions in codes and standards*. OFFSHORE TECHNOLOGY REPORT. Health and Safety Executive, United Kingdom, 2001. ISBN 0 7176 2281 9.
- Husset, J., Lieurade, H., Maltrud, F. and Truchon, M. Fatigue crack growth monitoring using a crack front marking technique. *Welding in the World*, pp. 276–282, 1985.
- Irwin, G. Analysis of Stresses and Strains near the End of a Crack Traversing a Plate. *Journal of Applied Mechanics*, 24:361–364, 1957.
- James, M., Hughes, D., Chen, Z., Lombard, H., Hattingh, D., Asquith, D., Yates, J. and Webster, P. Residual

- stresses and fatigue performance. *Engineering Failure Analysis*, 14:384–395, 2007.
- JCSS. *JCSS Probabilistic Model Code*. Joint Committee on Structural Safety, 2001.
- Labat, O. *Etudes de matériaux et de structures pour le génie civil*. Stage de fin d année, ICOM / IMAT, 2007.
- Lampman, S. R., Davidson, G. M., Reidenbach, F., Boring, R. L., Hammel, A., Henry, S. D. and Scott, W. W. *ASM Handbook: Fatigue and fracture*, ASM International, volume 19. 1996.
- Lawrence, F. V., Dimitrakis, S. D. and Munse, W. H. *Factors influencing weldment fatigue*, volume 19, chapter Section 3 - Fatigue strength prediction and analysis, pp. 274–286. ASM International, 1996.
- Lee, M. M. K. and Wilmshurst, S. R. Numerical modelling of CHS joints with multiplanar double-K configuration. *Journal of Constructional Steel Research*, 32(3):281–301, 1995.
- Lie, S., Lee, C., Chiew, S. and Shao, Y. Mesh modelling and analysis of cracked uni-planar tubular K-joints. *Journal of Constructional Steel Research*, 61:235–264, 2005a.
- Lie, S., Lee, C., Chiew, S. and Shao, Y. Validation of surface crack stress intensity factors of a tubular K-joint. *International Journal of Pressure Vessels and Piping*, 826:610–6172, 2005b.
- Lie, S.-T., Chiew, S.-P., Lee, C.-K. and Huang, Z.-W. Fatigue Performance of Cracked Tubular T Joints under Combined Loads. II: Numerical. *Journal of Structural Engineering*, 130(4):572–581, April 2004.
- Livieri, P. and Lazzarin, P. Fatigue strength of steel and aluminium welded joints based on generalised stress intensity factors and local strain energy values. *International Journal of Fracture*, 133(3):247–276, 2005. URL <http://dx.doi.org/10.1007/s10704-005-4043-3>.
- Lotsberg, I. and Larsen, P. K. Developments in Fatigue Design Standards for Offshore Structures. In *Proceedings of the Eleventh International Offshore and Polar Engineering Conference*, pp. 23–29. The International Society of Offshore and Polar Engineers, June 2001. ISBN 1-880653-51-6.
- Maddox, S. The Effect of Plate Thickness on The Fatigue Strength of Fillet Welded Joints. *The Welding Institute*, 1987.
- Maddox, S. *Hot-Spot Fatigue Data for Welded Steel and Aluminium as a Basis for Design*. International Institute of Welding (IIW), Doc. XIII-1900a-01, IIW, 2001.
- Maddox, S. Review of fatigue assessment procedures for welded aluminium structures. *International Journal of Fatigue*, 25(12):1359–1378, December 2003.
- Maddox, S. J. Scale effect in fatigue of fillet welded aluminium alloys. In *Proceedings 6th International Conference on Aluminium Weldments*, pp. 77–94. American Welding Society, Miami, FL, 1995.
- Manson, S. S. Behavior of Materials under Conditions of Thermal Stress. *Heat Transfer Symposium*, 1953.
- Marsh, K. J., Smith, R. A. and Ritchie, R. O. *Fatigue Crack Measurement: Techniques and applications*. EMAS Engineering Materials Advisory Service LTD, 1991. ISBN 0947817468.
- Marshall, P. *Design of welded tubular connections, Basis and use of AWS provisions*. Elsevier Science Publishers, Amsterdam, 1992a.
- Marshall, V. G. Improvement in tubular jacket closure weld fatigue performance through fabrication techniques. *OTC 6906*, pp. 295–300, 1992b.
- Mashiri, F. R., Zhao, X. L. and Dong, P. Approaches for fatigue design of tubular joints. In *12th International Symposium on Tubular Structures (ISTS 12)*, Shanghai, ISTS 12, 2008. 2008.
- Mashiri, F. R., Zhao, X.-L., Hirt, M. A. and Nussbaumer, A. Size effect of welded thin-walled tubular joints. *International Journal of Structural Stability and Dynamics*, 7(1):101–127, 2007.
- Mellings, S., Baynham, J., Adey, R. A. and Curtin, T. Durability prediction using automatic crack growth simulation in stiffened panel structures. *Structures and Materials*, 12:193–202, 2003.
- Mi, Y. and Aliabadi, M. H. Three-dimensional crack growth simulation using BEM. *Computers & Structures*, 52:871–878, 1994.
- Michael, D. H., Waechter, R. T. and Collins, R. The measurement of surface cracks in metals by using a.c. electric fields. *Proceedings of the Royal Society of London. Series A, Mathematical and Physical Sciences (1934-1990)*, 381(1780):139–157, May 1982.
- Moan, T. and Song, R. Implications of Inspection and Repair on System Fatigue Reliability of Offshore Structures. *Journal of Offshore Mechanics and Arctic Engineering, Transactions of the ASME*, 122:173–180, August 2000.
- Morrow, J. Cyclic Plastic Strain Energy and Fatigue of Metals. *International Friction, Damping, and Cyclic Plasticity ASTM STP 378*, 1965.
- Murakami, Y. *Stress intensity factors handbook*. Pergamon Press, Oxford, UK, 1987.

- Newman, J. and Raju, I. An Empirical Stress-Intensity Factor Equation for the Surface Crack. *Engineering Fracture Mechanics*, 15(1-2):185–192, 1981.
- Niemi, E. *Structural Stress Approach to Fatigue Analysis of Welded Components*. International Institute of Welding (IIW), Doc. XIII-1819-00, IIW, 2000.
- Örjasäter, O. *Effect of plate thickness on fatigue of welded components*. IIW-YWG XIII-XV-118-93, IIW, 1995.
- Paris, P. C. *The growth of cracks due to variations in load*. PhD. Dissertation, Lehigh University, Bethlehem, Pennsylvania, U.S.A., 1960.
- Paris, P. C., Tada, H. and Donald, J. K. Service Load Fatigue Damage – A Historical Perspective. *Proceedings of Fatigue Damage of Structural Materials*, II, 1998.
- Phillips, C. E. and Heywood, R. B. The size effect in fatigue of plain and notched steel specimens loaded under reversed direct stress. In *Proceedings I. Mech. E.* 1951.
- Pook, L. and Frost, N. A fatigue crack growth theory. *Engineering Fracture Mechanics*, 9(1):53–61, March 1973.
- Portela, A., Aliabadi, M. H. and Rooke, D. P. Dual boundary element incremental analysis of crack propagation. *Computers & Structures*, 46:237–247, 1993.
- Poutiainen, I., and Marquis, G. A single-point structural stress assessment procedure for load-carrying fillet welds. *IIW document XIII-2012-04/XV-1174-04*, 2004a.
- Poutiainen, I. and Marquis, G. A fatigue assessment method based on weld stress. *International Journal of Fatigue*, 28(9):1037–1046, 2006.
- Poutiainen, I., Tanskanen, P. and Marquis, G. Finite element methods for structural hot spot stress determination – a comparison of procedures. *International Journal of Fatigue*, 26:1147–1157, 2004b.
- prEN 1993-1-9:2003. *Eurocode 3: Design of steel structure – Part 1.9: Fatigue strength of steel structures*. CEN, November 2003.
- Radaj, D. *Ermüdungsfestigkeit*. Springer-Verlag, 1995. ISBN 3-540-58348-3.
- Radaj, D. Review of fatigue strength assessment of nonwelded and welded structures based on local parameters. *International Journal of Fatigue*, 18(3):153–170, 1996.
- Radaj, D., Sonsino, C. and Flade, D. Prediction of service fatigue strength of a welded tubular joint on the basis of the notch strain approach. *International Journal of Fatigue*, 20(6):471–480, 1998.
- Radaj, D. and Sonsino, C. M. *Fatigue assessment of welded joints by local approaches*. Abington Publishing, 1998.
- Romeijn, A. *Stress and Strain concentration factors of welded multiplanar tubular joints*. Delft University Press, Delft University of Technology, The Netherlands, 1994.
- RSTAB 2003. RSTAB Version 5.11, Finite Element Software Package. Ing.-Software Dlubal GmbH, Tiefenbach, Germany, 2003.
- Schumacher, A. *Fatigue behaviour of welded circular hollow section joints in bridges*. PhD thesis EPFL n°2727, Swiss Federal Institute of Technology (EPFL), Lausanne, 2003.
- Schumacher, A. and Nussbaumer, A. Experimental study on the fatigue behavior of welded tubular k-joints for bridges. *Engineering Structures*, 28:745–755, 2006.
- Schumacher, A., Nussbaumer, A. and Hirt, M. A. Fatigue behaviour of welded CHS bridge joints: emphasis on the effect of size. In *Proceedings of the 10th international symposium on tubular structures "Tubular Structures X"*, Madrid, pp. 365–374. Balkema Publishers, 2002a.
- Schumacher, A., Nussbaumer, A. and Hirt, M. A. Modern tubular truss bridges. In *IABSE Symposium: Towards a better built environment - innovation, sustainability, information technology, Melbourne, September 11-13, 2002*. IABSE, September 2002b.
- Schumacher, A., Sturm, S., Walbridge, S., Nussbaumer, A. and Hirt, M. *Fatigue design of bridges with welded circular hollow sections*. Report ICOM 489E, Swiss Federal Institute of Technology (EPFL), Lausanne, 2003.
- Shao, Y. *Fatigue behaviour of uniplanar CHS gap k-joints under axial and in-plane bending loads*. Ph.D. thesis, Nanyang Technological University. School of Civil and Environmental Engineering, 2005.
- Shao, Y.-B. Geometrical effect on the stress distribution along weld toe for tubular T- and K-joints under axial loading. *Journal of Constructional Steel Research*, 63(10):1351–1360, October 2007.
- Shao, Y.-B., Lie, S. and Chiew, S. Effect of chord length ratio of tubular joints on stress concentration at welded region. In *12th International Symposium on Tubular Structures (ISTS 12), Shanghai, ISTS 12, 2008*. Balkema Publishers, 2008.

- Shao, Y. B. and Tjhen, L. S. Parametric equation of stress intensity factor for tubular K-joint under balanced axial loads. *International Journal of Fatigue*, 27(6):666–679, June 2005.
- Shetty, N. and Baker, M. *Fatigue Reliability of Tubular Joints in Offshore Structures: Crack Propagation Model*. Technical Report, Imperial College of Science Technology and Medicine, London, 1990.
- SIA 263. *SIA 263: Stahlbau*. Schweizerischer Ingenieur- und Architektenverein, Zürich, 2003.
- Smith, I. and Gurney, T. Changes in the fatigue life of plates with attachments due to geometrical effects. *Welding research supplement*, pp. 244s–250s, September 1986.
- Stacey, A., Barthelemy, J.-Y., Leggatt, R. and Ainsworth, R. Incorporation of Residual Stresses into the SINTAP Defect Assessment Procedure. *Engineering Fracture Mechanics*, 67:573–611, 2000.
- Susmel, L. The theory of critical distances: a review of its applications in fatigue. *Engineering Fracture Mechanics*, 75(7):1706–1724, May 2008. URL <http://dx.doi.org/10.1016/j.engfracmech.2006.12.004>.
- Tovo, R. and Livieri, P. Local and non-local approaches to fatigue of weldments: state of the art and possible developments. *Key Engineering Materials*, 348-349:529–532, September 2007.
- Tovo, R. and Livieri, P. An implicit gradient application to fatigue of complex structures. *Engineering Fracture Mechanics*, 75(7):1804–1814, May 2008. URL <http://www.sciencedirect.com/science/article/B6V2R-4N0HJH3-1/1/74cd85b3be23da2869ac5610a3acbec7>.
- van Wingerde, A. M. *The fatigue behaviour of T- and X-joints made of square hollow sections*, volume 37. Heron, 1992.
- van Wingerde, A. M., van Delft, D. R. V., Wardenier, J. and Packer, J. A. Scale Effects on the Fatigue Behaviour of Tubular Structures. *WRC Proceedings*, 1997.
- Walbridge, S. *A Probabilistic Fatigue Analysis of Post-Weld Treated Tubular Bridge Structures*. PhD thesis EPFL n°3330, Ecole polytechnique fédérale de Lausanne (EPFL), 2005.
- Wang, G. and Blom, A. A Strip Model for Fatigue Crack Growth Predictions Under General Load Conditions. 1991.
- Wardenier, J. *Hollow sections in structural applications*. CIDECT, 2001.
- Weibull, W. A Statistical Theory of the Strength of Materials. *Ingeniors Vetenskaps Akademien (Proceedings of the Royal Swedish Academy of Engineering)*, 151, 1939.
- Wilde, A. J. and Aliabadi, M. H. A 3-D Dual BEM formulation for the analysis of crack growth. *Computational Mechanics*, 23(3):250–257, April 1999.
- Wolfram, S. *Mathematica, A System for Doing Mathematics by Computer*, U.S.A. (1988). 1988.
- Xiao, Z.-G. and Yamada, K. A method of determining geometric stress for fatigue strength evaluation of steel welded joints. *International Journal of Fatigue* 26 (2004) 1277–1293, 26, 2004.
- Yamada, K. and Hirt, M. A. Fatigue Crack Propagation from Fillet Weld Toes. *Journal of the Structural Division, ASCE*, pp. 1526–1540, July 1982.
- Zhao, X. L., Herion, S., Packer, J. A. and al. *Design guide for circular and rectangular hollow section joints under fatigue loading*. CIDECT, Comité International pour le développement et l'étude de la construction tubulaire 8, TÜV-Verlag Rheinland, Köln, 2000.
- Zhao, X. L. and Packer, J. A. *Recommended fatigue design procedure for welded hollow section joints*. IIW doc. XIII-1772-99 / XV-1021-99. Abington Publ., Abington Cambridge UK, 2000.
- Zheng, X. A simple formula for fatigue crack propagation and a new method for the determination of DKth. *Engineering Fracture Mechanics*, 27(4):465–475, 1987.

Curriculum Vitæ

Luis António Costa Borges

Date of birth : 23 March 1977
Nationality : Portuguese

Education

- 2004 - Present PhD candidate
Swiss Federal Institute of Technology (EPFL), Lausanne, Switzerland
Doctoral Thesis: "Size Effects in the Fatigue Behaviour of Tubular Bridge Joints"
supervisor: Dr A. Nussbaumer
- 2001 - 2003 MSc. in Civil Engineering - Structures
University of Coimbra, Portugal
Master Thesis: "Probabilistic Evaluation of the Rotation Capacity of Steel Joints"
supervisor: Prof. L. Simões da Silva
- 1995 - 2000 Diploma in Civil Engineering
University of Coimbra, Portugal

Professional experience

- June 2004 - Present Research Engineer
Steel Structures Laboratory (ICOM)
Swiss Federal Institute of Technology (EPFL), Lausanne, Switzerland
- October 2003 - March 2004 Assistant
Department of Civil Engineering
Polytechnic School of Leiria, Portugal
- September 2000 - May 2003 Research Assistant
Department of Civil Engineering - Steel Structures
University of Coimbra, Portugal

Publications

- ◆ Borges, L., Nussbaumer, A., Advanced numerical modelling of fatigue size effects in welded CHS K-joints. In: 12th International Symposium on Tubular Structures (ISTS 12), Shanghai, ISTS 12, 2008
- ◆ Nussbaumer, A., Borges, L., Experimental determination of stress intensity factors on large-scale tubular trusses fatigue tests. In: 12th International Symposium on Tubular Structures (ISTS 12), Shanghai, ISTS 12, 2008
- ◆ Borges, L., Nussbaumer, A., Size effects in the fatigue behaviour of welded CHS bridge joints. 7th International Conference on Steel Bridges, Guimarães, Portugal, 2008

- ◆ Nussbaumer, A., Borges, L., Size effects correction factors for the fatigue strength of welded tubular joints. SOSDID - Symposium on Structural Durability in Darmstadt, Germany, 2008
- ◆ Borges, L., Schumacher, A., Nussbaumer, A. - "Size effects on the fatigue behaviour of welded CHS bridge joints" - First International Conference on Fatigue and Fracture in the Infrastructure - Bridges and Structures of the 21st Century, Philadelphia, PA, USA, 2006
- ◆ Wald, F., Simões da Silva, L., Moore, D., Lennon, T., Chadná, M., Santiago, A., Benes, M. and Borges, L. "Experimental Behaviour of a Steel Structure Under Natural Fire" - Fire Safety Journal, 2005
- ◆ Lima, L., Vellasco, P., Silva, J., Borges, L., Silva, L. - "Post-limit stiffness prediction of semi-rigid joints using genetic algorithms", Latin American Journal of Solids and Structures, 2005
- ◆ Wald, F., Simões da Silva, L., Moore D. B., Santiago, A., Benes, M., Borges, L. - "Experimental Behaviour of a steel structure under natural fire" New Steel Construction, Vol. 13 No 3, pp. 24-27, ISSN 0968-0098, Mar 2005
- ◆ Gervásio, H., Simões da Silva, L., Borges, L., "Reliability assessment of the post-limit stiffness and ductility of steel joints", J. of Constructional Steel Research Volume 60, Issues 3-5, Pages 635-648, March-May 2004
- ◆ Lima, L., Vellasco, Silva, J.G., Borges, L. "CIL01-021: Pos-limit stiffness calibration of beam-to-column joints using genetic algorithms" XXV CILAMCE, 25th Iberian Latin-American Congress on Computational Methods in Engineering Recife, November 10-12, 2004
- ◆ Santiago, A., Simões da Silva, L., Wald, F., Moore, D., Borges, L. - "Experimental behaviour of steel joints under a natural fire" - The Second International Conference on Steel & Composite Structures (ICSCS'04) Seoul, Korea, September 2-4, 2004
- ◆ Simões da Silva, L., Borges, L., Gervásio, H. - A probabilistic evaluation of the rotation capacity of End-plate beam-to-column steel joints - Connections in Steel Structures V - Amsterdam - June 3-4, 2004
- ◆ Borges, L., Lima, L., Ramires, F., Simões da Silva, L., Vellasco, P. - "NASCon: Uma ferramenta para análise avançada de ligações metálicas e mistas" - 4th Portuguese Conference of Steel and Composite Construction, Lisbon 4-5, December 2003
- ◆ Ramires, F., Borges, L., Lima, L., Simões da Silva L., Vellasco, P. - "Comportamento estrutural de ligações viga-pilar com placa de extremidade de altura parcial" - 4th Portuguese Conference of Steel and Composite Construction, Lisbon, 4-5 December 2003
- ◆ Borges, L. - "Evaluation of the Rotation Capacity of Steel Joints", Dissertação de Mestrado, Universidade de Coimbra, 2003
- ◆ Borges, L., Lima, L., Simões da Silva, L. and Vellasco, P., "An evaluation of the post-limit stiffness of beam-to-column semi-rigid joints using genetic algorithms", in Proceedings of the Ninth International Conference on Civil and Structural Engineering Computing, The Netherlands, September 2-4, 2003
- ◆ Gervásio, H., Simões da Silva, L. and Borges, L., "Reliability assessment of the post-limit stiffness and ductility of steel joints", in Proceedings of Eurosteel 2002 - 3rd European Conference on Steel Structures, pp. 1027-1038, Coimbra, Portugal, 2002

Professional affiliations

- ◆ Member of the International Association for Bridge and Structural Engineering (IABSE)
- ◆ Member of CMM, Portuguese Steelwork Association
- ◆ Registered effective member in the Portuguese Engineer Association (*Ordem dos Engenheiros - OE*)